UNIVERSITAT DE BARCELONA

Analysis of KRAS phosphorylation and KRAS effector domain as targets for cancer therapy

Débora Cabot Romero

DOCTORAL PROGRAMME IN BIOMEDICINE

SCHOOL OF MEDICINE AND HEALTH SCIENCES, UNIVERSITY OF BARCELONA

Analysis of KRAS phosphorylation and KRAS effector domain as targets for cancer therapy

Thesis presented by

Débora Cabot Romero

to qualify for the degree of Doctor in Biomedicine

by the University of Barcelona

This thesis has been performed in the Department of Biomedicine
of the School of Medicine and Health Science of University of Barcelona,
under the supervision of Prof. Neus Agell Jané and Dra. Montserrat Jaumot Pijoan.

Barcelona, July 2020

Débora Cabot

INDEX

ABBREVIATIONS

ABC: avidin-biotin complex

AML: acute myeloid leukemia

AMPK: 5' adenosine monophosphate-activated protein kinase

AP1: clathrin/adapter protein 1

APC: Adenomatous Polyposis Coli

APS: Ammonium persulfate

aPKC: atypical PKC

Arf: ADP-ribosylation factor

Arl: Arfs like proteins

ATCC: American Type Culture Collection

BIM: Bisindolylmaleimide I

BSA: Bovine Serum Albumin

BrdU: bromodeoxyuridine

CaM: Calmodulin

CaMBPs: CaM-binding proteins

CaMKII: calmodulin-dependent protein kinase II

cDNA: complementary DNA

CIMP-H: high CpG island methylator phenotype

CIMP-L: low CpG island methylator phenotype

CIN: chromosomal instability

CMS: consensus molecular subtype

co-IP: co-immunoprecipitation

CRC: colorectal cancer

Ct: cycle threshold

DAB: Diaminobenzidine

DAB2IP: Disabled-2 interacting protein

DARPins: Designed Ankyrin Repeat Proteins

DFS: Disease Free Survival

DMEM: Dulbecco's modified Eagle's medium

DMSO: dimethyl sulfoxide

DPIs: dual prenyltransferase inhibitors

DTT: Dithiothreitol

ECM: extracellular matrix

EF-hands: helix–loop–helix motifs

EGF: epidermal growth factor

EGFR: epidermal growth factor receptor

EMT: Epithelial-Mesenchymal Transition

ER: Endoplasmatic Reticulum

FBS: fetal bovine serum

FC: fold change

FDR: false discovery rate

FTase: farnesyltransferase

FTIs: FTase inhibitors

Gal-3: Galectin-3

GAP: GTPase activating protein

GDI: guanine nucleotide dissociation inhibitor

GEF: guanine exchange factors

GGTase: geranylgeranyltransferase

GGTI: GGtase inhibitor

GPCR: G protein-coupled receptors

GRB2: growth-factor-receptor-bound protein 2

GSEA: Gene set enrichment analyzes

HDAC6: histone deacetylase 6

H&E: Hematoxylin and Eosin

hnRNP: Heterogeneous nuclear ribonucleoproteins

HRP: horseradish peroxidase

HVR: hypervariable region

ICMT: isoprenylcysteine carboxyl methyltransferase

IHC: Immunohistochemistry

IPMNs: intraductal papillary mucinous neoplasm

ITS: Insulin, Transferrin and Sodium Selenite

LB: L-Broth

MAPK: mitogen-activated protein kinase

MSI: microsatellite instability

MSI-H: MSI-high

MSI-L: MSI low

MSS: MSI stable

mTORC1: mammalian target of rapamycin complex 1

mTORC2: mammalian target of rapamycin complex 2

NF1: neurofibromin

NMR: Nuclear Magnetic Resonance

NO: nitric oxide

NPM: Nucleophosmin

NSAID: non-steroidal anti-inflammatory drug

NSCLC: non-small cell lung cancer

ON: overnight

PAI-1: Plasminogen Activator Inhibitor-1

PanINs: intraepithelial neoplastic lesions

PBS: Phosphate-Buffered Saline (PBS)

PBS-T: PBS-Tween 20 (PBS-T)

PDAC: pancreatic ductal adenocarcinoma

PDEδ: phosphodiesterase 6 delta subunit

PDK1: phosphoinositide-dependent kinase 1

PFA: paraformaldehyde

PH: pleckstrin homology

PI: propidium iodide (PI)

PI3K: phosphatidylinositol-3-kinase

PIP_2: phosphatidylinositol-4,5-bisphosphate

PIP_3: phosphatidylinositol-3,4,5-triphosphate

PKB: protein kinase B

PKC: Protein Kinase C

PKG: isoform 2 of Protein Kinase G

POLε: polimerasa epsilon

PPIs: protein-protein interactions

PtdIns: phosphatidylinositol

PtdSer: phosphatidylserine

PTEN: phosphatidylinositol-3,4,5-trisphosphate 3-phosphatase.

PVDF: polyvinylidene fluoride

RASGRF: RAS guanine nucleotide releasing factors

RASGRP: RAS guanine nucleotide releasing proteins

RBD: RAS binding domains

RCE1: Ras converting enzyme 1

REB: Ras extraction buffer

RMA: Robust Multichip Average

RT: room temperature

RTKs: tyrosine kinase receptors

SDS: Sodium dodecyl sulfate

SIRT2: Sirtuin 2

SOS1: Son of sevenless 1

STK33: Serine/threonine Kinase 33

TAC: Transcriptome Analysis Console

TBK1: TANK-binding kinase 1

TBS: Tris Buffer Saline

TBS-T: TBS-Tween 20

TPA: (12-*O*-tetradecanoilforbol-13-acetate)

tPA: tissue plasminogen activator

uPA: urokinase

WB: Western Blot

WT: wild type (WT)

INTRODUCTION

1. RAS

1.1 Ras superfamily

The Ras superfamily is composed of small GTPases that act as molecular switches cycling between an active state by binding of GTP and an inactive state by hydrolysis of GTP. In the active state, they are able to bind to the effectors thereby regulating different biological processes as cell proliferation, differentiation, survival migration, polarity, morphology, adhesion and apoptosis[1,2]. The first members of RAS superfamily were identified more than forty years ago[3–6], and so far 167 human proteins have been described belonging to this category[6,7] (figure 1).

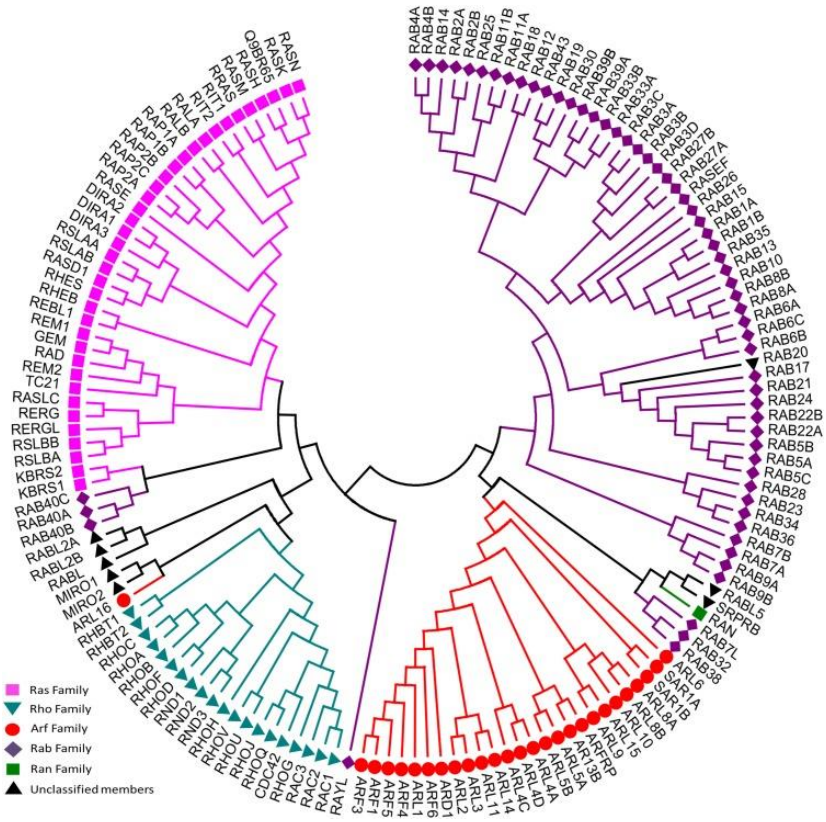

Figure 1. Evolutionary relationships of human Ras superfamily. The evolutionary history was inferred using the Neighbor-Joining method (*From Liang Qu at al, 2019)*.

1.1.1 Classification of small GTPases

According to their evolutionarily conservation at structural and functional levels, the Ras superfamily of small GTPases are divided into five major different protein families: Ras, Rho, Arf/Sar, Rab and Ran[2,7] (figure 1).

I. **Ras family:** The Ras genes family was the first identified in the 1970s after extensive studies in retroviruses isolated from rats, mice and other animals. These viruses were able to induce rapid formation of sarcoma in different infected animals and to transform cells in culture. Along the following years, these investigations led to the detection of Ras mutations in the context of carcinogenesis[2,8]. The Ras family is composed of 36 members divided into six different subfamilies: Ras, Ral, Rap, Rad, Rheb and Rit. They can be activated in response to multiple extracellular signals, regulating cell proliferation, differentiation, apoptosis and survival. Within Ras family, KRAS, HRAS and NRAS have been thoroughly studied and characterized due to their relevance in human cancer[1,6].

II. **Rho family:** The Rho family, *Ras homologous*, are small GTPases closely related to the Ras family. It is composed of 20 members which are involved in biological processes such as actin cytoskeleton organization; cell adhesion, polarity and motility; cell proliferation, survival and differentiation; cell morphology and gene expression[9,10]. The best-characterized classical Rho GTPases are RhoA, Rac1 and Cdc42 which have been well studied biochemically and have been described to contribute in cancer progression[2,11,12].

III. **Arf/Sar Family:** The ADP-ribosylation factor (Arf) family, classified in three different classes (Arfs, Arfs like proteins (Arl) and Sar1), are proteins involved in the regulation of membrane traffic, vesicular biogenesis and intracellular traffic, as well as in cytoskeletal dynamics. These proteins, in contrast to Rab family, develop different functions in several steps of vesicular trafficking such as the recruitment of coat

proteins, the formation of clathrin/adapter protein 1 (AP1) complex-associated vesicles, and the formation of the AP3-containing endosomes. Additionally, ARFs proteins play a role in the recruitment and activation of enzymes that can modify membrane lipid composition, and in the interaction with cytoskeletal factors[1,13–15].

IV. **Rab family:** The Rab family, described as Ras like protein in brain, comprises more than 60 members implicated in intracellular vesicular transport. In the endocytic and secretory pathways, Rab proteins are distributed in different cellular compartments regulating the transport between organelles. These proteins facilitate the vesicle budding from donor compartment, the vesicle motility along cytoskeletal filaments to target compartment, the fusion of vesicle in the membrane of acceptor compartment and the release of cargo[2,16]. The amplification of Rab genes, which induces overexpression of Rab proteins, is usually associated with tumorigenesis and cancer progression due to the activation of cell survival and of growth signaling pathways[17,18].

V. **Ran family:** Ran, encoded by a single ortholog in Eukaryotes, is the most abundant small GTPase in the cell. Ran-GTP is mainly accumulated in the nucleus while Ran-GDP is localized in the cytoplasm. For this reason, it is the responsible of the directionality for both nuclear export and import. Moreover, Ran is involved in the maintenance of nuclear envelope, nuclear pores and mitotic spindle assembly [1,15,19].

1.2 RAS family

The discovery of Harvey murine sarcoma virus in 1964[20] and the Kirsten murine sarcoma virus in 1967[21] together with their capacity to induce rat sarcomas (Ras) were the basis for their current genes names, *HRAS* and *KRAS*, respectively [8,22]. The cellular origin of viral *HRAS*

and *KRAS* genes was determined during 1970s and 1980s[23,24]. Moreover, it was described that these genes encoded for 21kDa proteins, which were able to bind to GTP and GDP, and were located in the plasma membrane[25–27]. Later on, the homologous human genes were found[6,22]; and *NRAS*, the third member of the mammalian RAS genes family, was discovered[28,29].

The Ras family has been extensively studied due to its implication in different biological processes and for its critical role in oncogenesis[1,6,8]. The three genes encode for a total of four RAS isoforms known as HRAS, NRAS and the alternatively spliced KRAS4A and KRAS4B (only a 10% of the total gene transcription is leaded to KRAS4A synthesis).

This thesis is focused on the study of KRAS4B which is explained in detail in *chapter 2.* Although, all Ras isoforms share common features due to a high homology in their N-terminal domains, the C-terminal hypervariable region (HVR) and the CAAX box confer specific characteristics to each RAS isoform, which determine different localization patterns and distinctive posttranslational modifications[6,30,31] (detailed in the *chapter 1.2.2 and 1.2.3*). Furthermore, it was revealed that KRAS was essential for embryonic development whereas HRAS and NRAS were dispensable[32,33]. However, this last topic is challenged, since it has been reported that HRAS and KRAS are biologically equivalent in homeostatic conditions when the locus of KRAS gene is replaced by the sequence of HRAS[34].

1.2.1 Activity cycle

All Ras superfamily and subfamily members act as molecular switches that alternate between two conformational states, a GTP-bound state (active) and GDP-bound state (inactive)[35] (figure 2). Although, the small GTPases show biochemical and functional similarity with the heterotrimeric G protein α subunits, they function as monomeric G proteins. During the GTPase cycle, the exchange of GDP to GTP induces conformational changes in the GTPases, allowing an increased affinity for the effectors[36]. However, this nucleotide exchange is the rate-limiting step in the activation of RAS proteins. Due to the

high affinity binding for GTP or GDP and the low intrinsic GTP hydrolysis and GDP/GTP exchange activities, small GTPases are tightly regulated by two groups of regulatory proteins: GTPase activating proteins (GAPs) and guanine exchange factors (GEFs). Whereas GEFs promote the formation of the active form (GTP-bound), the GAPs induce the hydrolysis of GTP accelerating the intrinsic GTPase activity and promoting the establishment of the inactive form (GDP-bound)[1,35,37] (figure 2). Different GEFs and GAPs are able to regulate the activity of the same small GTPase in different tissues or in different subcellular compartments of the same tissue[15].

Due to the fact that cellular concentration of GTP is ten times higher than the one of GDP, the GTP-bound state prevails over the GDP-bound state[38]. As previously mentioned, GEFs are the proteins responsible for the exchange of GDP for GTP. Specifically, they catalyze the dissociation of the nucleotide from the GTPases by modifying the nucleotide-binding site, thus reducing molecular affinity and allowing the release and replacement[36,39]. GEFs are regulated by protein interactions (protein-lipid interaction included), binding to second messengers and posttranslational modifications. These let them to establish specific subcellular localizations, to revert the autoinhibition by releasing the GTPase-binding site, and to induce changes in their catalytic domain[38].

As mentioned above, small GTPases show low intrinsic capacity to hydrolyze GTP to GDP and thus they require GAPs proteins to stimulate it. The action of GAPs is necessary to induce rapidly the inactive state of small GTPases when cellular conditions require it. As GEFs protein, the regulation of GAPs is tightly controlled by protein-protein and protein-lipid interactions, protein degradation, interaction with second messengers and posttranslational modifications. All these regulatory processes are involved in the translocation of GAPs to specific cell localizations, conformational changes in their catalytic domain and mechanisms that allow the release of the autoinhibition[37,38,40].

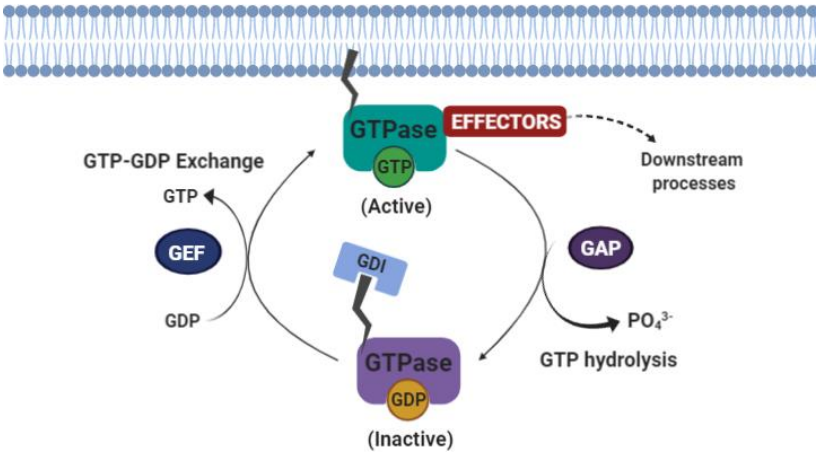

Figure 2. Schematic diagram of small GTPases activation cycle with GEFs, GAPs and GDIs.

Finally, the guanine nucleotide dissociation inhibitor (GDIs) exercise another small GTPase regulatory mechanism. These proteins have specific affinity for GDP-bound GTPases and thus, they act as negative regulators by inhibiting the GDP release. Furthermore, they can bind the lipid-modified GTPases in the cytosol, preventing their association with membranes and the interaction with their regulators or effectors[2,15,41]. GDIs are only found in Rho and Rab GTPases superfamilies.

1.2.2 Structure of Ras family

Ras isoforms, as small GTPases, share a common structural and biochemical domain in the N-terminal region, the globular domain, composed of five G-box (G1 – G5) which regulate nucleotide binding, GTP hydrolysis and interaction with effectors. Specifically, the G-domain (residues 1 –166) is divided into two different lobes: an effector lobe (residues 1 – 86) essential for interaction with effectors, and an allosteric lobe (residues 87 – 166) involved in intra-protein interactions (connecting the active site of the effector lobe to membrane-interacting residues). The effector lobe harbors the Switch I (residues 30 – 40) and Switch II (residues 60 – 76) regions which undergo conformational changes when the GTPase is activated by GTP binding[42–44]. As mentioned above, these conformational changes increase the interaction[36] with effectors and thus the subsequent signaling processes.

On the other hand, another common features of small GTPases are posttranslational modifications in the C-terminal region comprising the HVR[1](residues 166-188/9). These modifications are essential to induce association with membranes and subcellular localization, critical processes for GTPases biological functions. The C-terminal cysteine residue of the CAAX box comprised in the HVR can be recognized and modified by farnesyltransferase (FTase) and geranylgeranyltransferase (GGTase) I or II, which catalyze the addition of a farnesyl or geranylgeranyl isoprenoid, respectively. These modifications by FTase and GGTase I or II are commonly observed in the RAS and Rho/Rab families, respectively. Conversely, the ARF family lack C-terminal lipid modification but shows modifications in its N-terminal region by a myristate fatty acid. Finally, lipid posttranslational modifications and membrane binding processes are not observed in the Ran family[1,42].

The N-terminal regions of HRAS, NRAS,KRAS4A and KRAS4B, comprising the nucleotide binding catalytic globular domain, share 90-100% of homology; while the C-terminal ends, comprising the HVR , differ significantly in sequence between them (15% homology)[30,45]. The HVR can be divided into two domains: the membrane-targeting domain (anchor domain), which regulates association to membranes; and the linker domain which is the responsible for stabilizing localization to the plasma membrane. The CAAX box (C=cysteine, A=aliphatic aminoacid and X=variable amminoacid) present in the anchor domain of HVR, is common to all Ras proteins. The correct processing of the CAAX box is essential for RAS transport and association to membrane and is activated by two different targeting signals (*see more details in the next chapter*). Briefly, the C-terminal cysteine residue of all RAS isoforms is firstly modified by the FFtase. However, the second targeting signal differs between RAS isoforms. HRAS, NRAS and KRAS4A are palmitoylated on cysteine residues of HVR, while KRAS4B presents a polylysine sequence positively charged enough to reach KRAS to the cell membrane[30,45–47].

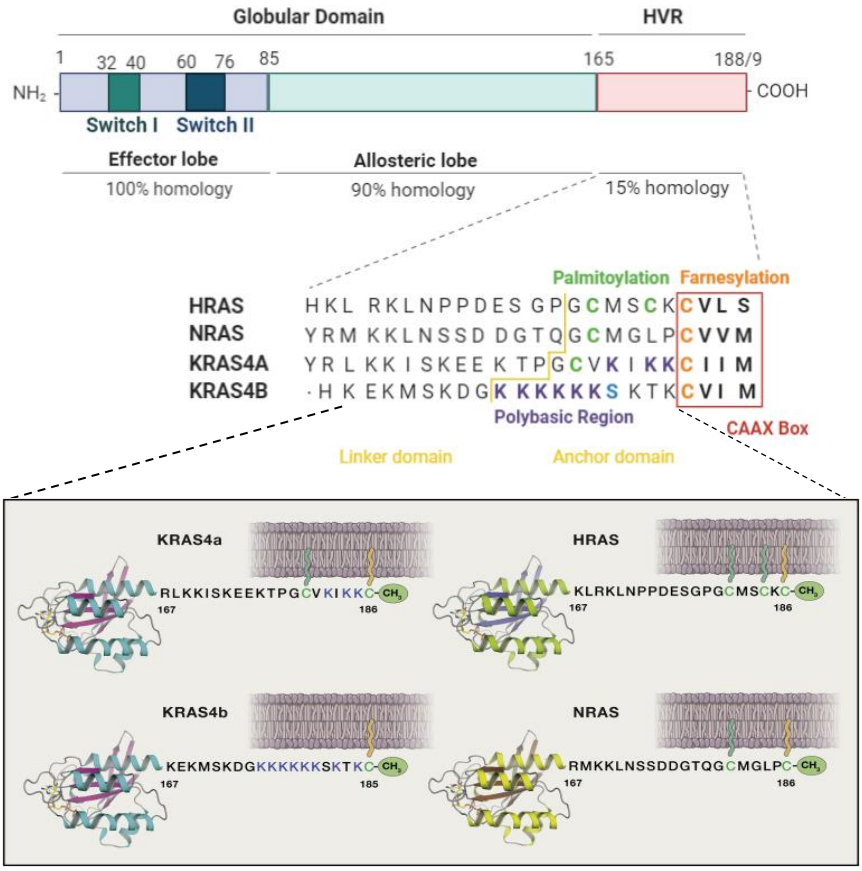

Figure 3. Structure and functional domains of RAS isoforms including posttranslational modifications. Scheme comparing functional and structural domains of the RAS isoforms (top panel). Lipid modifications of the HVR targeting RAS isoforms to the plasma membrane (bottom panel from *Simanshu DK et al, 2017*).

1.2.3 RAS posttranslational modifications: regulation of RAS trafficking to plasma membrane

As previously commented, different posttranslational modifications are necessary to traffic RAS proteins to cell membrane (figure 4)[48]. After RAS protein translation, all RAS isoforms are farnesylated in the cytosol by FTase, which adds a 15-carbon farnesyl lipid in the C-terminal cysteine of CAAX box[49,50]. The farnesylated CAAX sequence allows RAS proteins to reach to the cytosolic surface of Endoplasmatic Reticulum (ER)[51], where they are recognized by the Ras converting enzyme 1 (RCE1). Ras prenylation is a prerequisite for RCE1, an endoprotease, which removes the AAX aminoacids from farnesylated CAAX sequence[52]. After AAX cleavage, the α-Carboxyl group of farnesylated cysteine is methylated by the enzyme isoprenylcysteine carboxyl methyltransferase (ICMT) present in the cytosolic surface of ER[53]. Only the last step (methyl esterification of α-Carboxyl) of these three posttranslational modifications is reversible. Together, these three steps provide a hydrophobic region to RAS proteins that allow its insertion into cell membranes. However, plasma membrane RAS insertion requires a second signal: a palmytoilation on HRAS, NRAS and KRAS4A isoforms; and an hexalysine polybasic region in KRAS4B conferring additional hydrophobicity or electrostatic attraction, respectively[47,54].

Palmitoylation on cysteine residues in the HVR of HRAS, NRAS and KRAS4A is required for them to traffic from endomembranes to plasma membrane by the classical exocytic pathway[51,55]. Palmytoilation in RAS proteins was described 25 years ago[56]. Whereas HRAS is palmitoylated on two cysteine residues (Cys181 and Cys184), NRAS is palmitoylated only on Cys181. However, the spliced variant KRAS4A is unique among the four RAS proteins in possessing a dual second membrane targeting motif that consists of both a palmitoylated cysteine in the residue 180 and two short polybasic regions flanking this acylated cysteine[31,47,54,57,58] (figure 3). Thus, while KRAS4A is palmitoylated on Cys180 by an unknown palmitoylacyltransferase, and apparently traffics to the plasma membrane without transiting Golgi[59], HRAS and NRAS isoforms palmitoylation is conducted by DHHC9–GPC16 protein complex located in Golgi apparatus[60]. Subsequently, they are directed to plasma

membrane by vesicular transport[55]. Unlike farnesylation, palmitoylation is a reversible process under physiologic conditions[61].

Regarding to KRAS4B isoform, the second signal corresponds to polybasic region of six consecutives lysines that facilitates RAS association to-membrane by interacting with the negatively charged headgroups of phospholipids at the inner leaflet of the plasma membrane[47]. Together, the farnesyl group and the hexalysine polybasic region provide to KRAS4B enough affinity for stable association to membrane. The mechanism for trafficking KRAS to cell plasma membrane, by Golgi-independent pathway, has not been yet characterized.

Whereas the retrograde traffic of NRAS and HRAS back to the Golgi from plasma membrane occurs after depalmitoylation process[61], KRAS4B internalization from plasma membrane remains unclear (*see next chapter*). However, it has been proposed that KRAS4B can be dissociated from plasma membrane and translocated to mitochondria in part by the phosphorylation at serine 181 (within HVR) catalyzed by Protein Kinase C (PKC)[62]. KRAS phosphorylation will be discussed in the *chapter 2.1.3.1.*

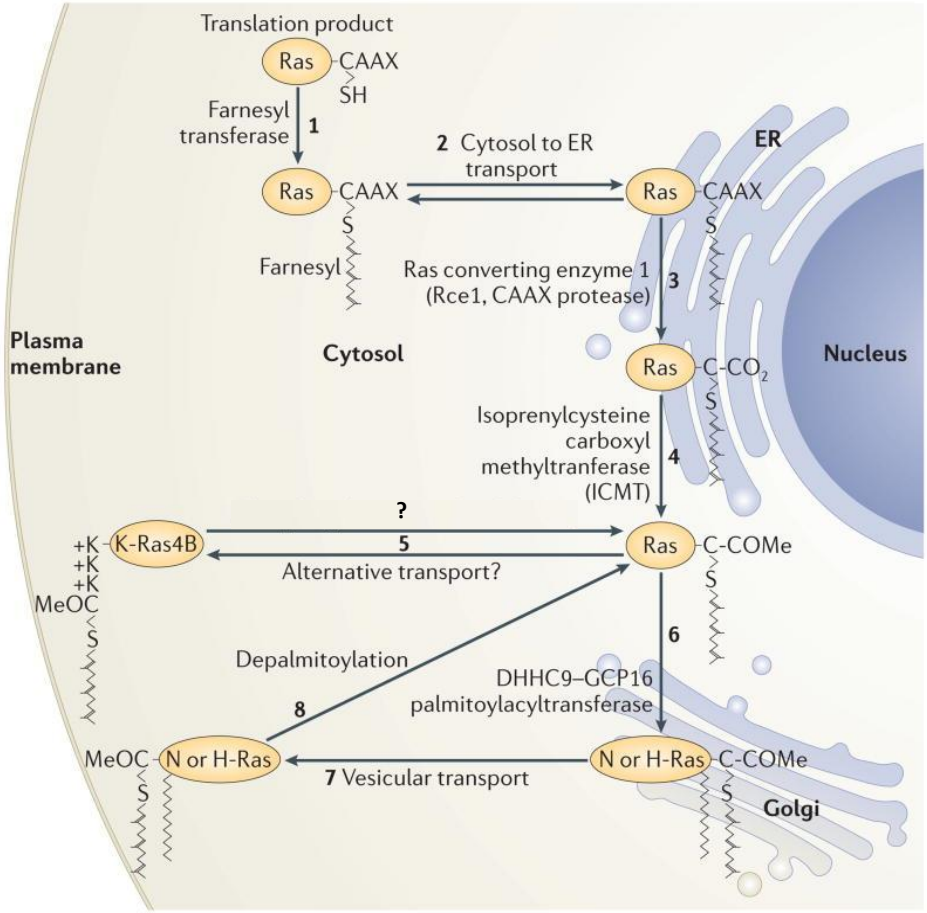

Figure 4. Ras trafficking. Ras proteins are synthesized in the cytosol. After synthesis, FTase recognizes and then farnesylates the C-terminal cysteine residue of all isoforms **(1).** Farnesylated RAS proteins are directed to ER **(2)** where the AAX aminoacids are removed from farnesylated CAAX sequence by the RCE1 endoprotease **(3)** and subsequently the α-Carboxyl group of farnesylated cysteine is methylated by ICMT **(4)**. Following that, KRAS4B is targeted to plasma membrane by uncharacterized pathway **(5),** while HRAS and NRAS are directed to Golgi where they are palmitoylated by DHHC9-GCP16 complex **(6)**. After palmitoylation, HRAS and NRAS are targeted to plasma membrane by vesicular transport **(7)**. Palmitoylation is a reversible process that allows a retrograde traffic of NRAS and HRAS back to the Golgi **(8)**, while KRAS internalization has been proposed to be induced by KRAS4B phosphorylation at serine 181 by PKC (*Adapted from Ahearn, I et al, 2012).*

1.2.4 RAS localization: plasma membrane microdomains and endomembranes

RAS isoforms are in distinct membrane microdomains where they can interact with their specific effectors and regulatory proteins. The best characterized microdomain is the liquid-ordered domain (cholesterol-dependent) known as lipid raft, composed by sphingolipids, glycosphingolipids and cholesterol[63]. In general, palmitoylated proteins are often associated with lipid rafts due to the palmitate, allowing good association to the liquid-ordered raft structure. In contrast, plasma membrane anchored proteins only by farnesyl or geranylgeranyl groups are excluded from lipid rafts[64]. Therefore, HRAS and NRAS differ from KRAS4B in their localization and distribution through membrane microdomains (raft and non-raft compartments)[45]. Conversely, the nature of KRAS4A nanoclustering is not known, but its dual membrane targeting motif (polybasic domain and palmytoilation on Cys180) would cause that it segregates laterally from other RAS[65].

KRAS4B is predominantly anchored (~85%) in non-raft regions[66], where KRAS4B GTP- and GDP-bound populations are distanced spatially. However, KRAS4B presents relative unrestricted lateral movement in the membrane[67]. In contrast, HRAS is distributed between lipid rafts and non-ordered plasma membrane, being HRAS GDP-loaded localized in lipids rafts, while HRAS GTP-loaded is predominantly located in non-rafts domains[46,66]. In the case of NRAS isoform, an intact mono-palmitoylated linker domain is necessary for a correct localization in the cell membrane[58]. In fact, NRAS distribution in the plasma membrane is opposite to that of HRAS preventing overlapping isoforms. Thus, active NRAS is stablished in lipid rafts while GDP-loaded NRAS is localized in disordered plasma membrane[68].

The differential localization of HRAS and KRAS in distinct nanoclusters has important consequences for effector interactions and activation of downstream signaling[45,69–71]. In fact, deletions of the linker region confine HRAS in lipid rafts, preventing normal segregation when GTP-loaded and thus disrupting the activation of MAPK signaling.[66,72]. In addition, since KRAS4B nanonclustering is predominately promoted by phosphatidylinositol (PtdIns) and phosphatidylserine (PtdSer) acidic lipids (components of cytosolic plasma membrane leaflet displaying high negative charge), and RAF1 selectively binds PtdSer, activated KRAS

nanoclusters recruit RAF1 to the membrane more efficiently than those of HRAS[68,73]. In fact, other studies have reported that depleting the PtdSer induces a loss of KRAS from plasma membrane and reduces the nanoclustering[74,75]. Finally, our research group has reported that KRAS phosphorylation at Ser181 regulates the localization of oncogenic KRAS in different nanocluster influencing the activation of RAS signaling transduction pathways[76]*(see chapter 2.1.3.1 for more details)*. Previously, in agreement with earlier studies, we had demonstrated that both phosphorylated and non-phosphorylated KRAS are located at plasma membrane[73,77]. Accordingly with this, a subsequent study described that KRAS phosphorylation can increase the phosphatidylinositol-4,5-bisphosphate (PIP_2) (substrate for PI3K) changing the nanocluster lipid content[78].

Regarding to endomembrane RAS localization, it has been described that HRAS isoform can also be targeted to caveolae and non-caveolar lipid rafts due to its palmytoilation sequences and CAAX motif modification[66]. Additionally, HRAS and NRAS can be de-ubiquitylated and then targeted to endocytic vesicles[79]. Finally, HRAS and NRAS can be depalmitoylated allowing their release from plasma membrane for recycling back to endomembranes. The redistribution to ER and Golgi induces that they can be repalmitoylated[61] (figure 5).

In contrast to HRAS and NRAS, KRAS4B, after CAAX sequence processing in the ER, is directly trafficked to the non-ordered plasma membrane bypassing Golgi apparatus. KRASB internalization back to endomembranes has also been proposed (figure 5). Indeed, it has been shown that several KRAS-binding proteins can modulate the rate of KRAS dissociation from plasma membrane[62,80–83]. Furthermore, KRAS recruitment on endosomes membranes is also reported. Early endosomes are enriched in PtdIns and PtdSer, thus it would be reasonable to expect that KRAS could interact with their membranes. Some studies describe that KRAS4B is present in the endocytic pathway (clathrin-dependent) for lysosomal degradation[84]; and that it is mislocalized to endosomes and more efficiently degraded by lysosomes when PtdSer recycling is inhibited[85]. Recently published data show that KRAS can be localized in endosomes independently of its activation state, and that PtdSer has an important role in this association. Therefore, this study proposed the major role of PtdSer in

the association of KRAS with endosomes and that theses organelles are appropriate cellular platforms for KRAS recruitment and where it can be funtional[86]. Following studies support this role of PtdSer in KRAS mislocalization[74].

Finally, emerging reports have described that RAS proteins and its related proteins can be localized and induce its signaling in the exosomes, and that they have a role in exosomal secretion, selection of cargo and maintenance[87].

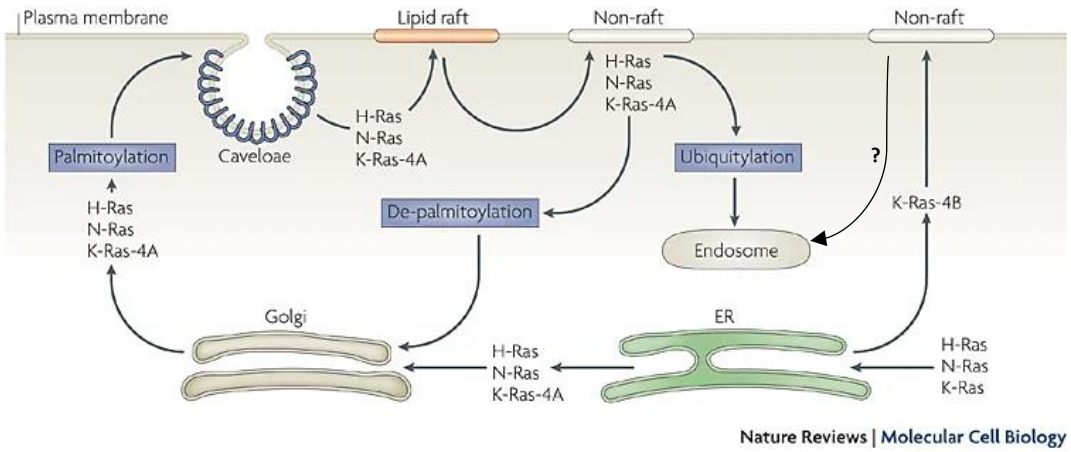

Figure 5. Recycling of Ras proteins. Farnesylated HRAS, NRAS and KRAS are directed to ER where CAAX box is correctly processed. Whereas KRAS4B is targeted immediately to plasma membrane (non-raft domains); HRAS, NRAS and KRAS4A are targeted to Golgi where they are palmitoylated and directed to plasma membrane by vesicular transport. HRAS, NRAS and KRAS4A can be distributed in lipid raft and non-raft as well as caveolae and non-caveolae lipid raft. Depalmitoylation induces an endocytic process allowing these isoforms to be directed from plasma membrane to Golgi where they are recycled. Moreover, HRAS and NRAS can be de-ubiquitylated and targeted to endocytic vesicles. The internalization of KRAS4B from plasma membrane back to endomembranes is not well known. *(Adapted from Karnoub, AE and Weinberg, RA, 2008).*

2. KRAS

The cell homologous of Kirsten transforming RAS sequences was firstly identified in 1981[4] in rat genome and was subsequently identified in mouse[88] and human genomes[5]. KRAS4B (hereinafter referred as KRAS) is a major driver of human cancers and it has been under the spotlight for more than three decades.

In recent years, emergence of new regulators either by direct interaction or by reversible posttranslational modifications have been reported to regulate KRAS functionality.

2.1 Regulators of KRAS

2.1.1 Activity cycle: GAPs and GEFs

As mentioned above, RAS proteins function as a molecular switch cycling between inactive state (GDP-bound) and active state (GTP-bound).

When RAS is found in an inactive GDP-bound state, GEFs are associated causing 10^4-fold enhancement in the GDP ejection rate[6]. Three distinctive classes of RAS-GEFS are expressed by mammals, Son of sevenless 1 (SOS1), RAS guanine nucleotide releasing factors (RASGRF) and RAS guanine nucleotide releasing proteins (RasGRP)[8,22]. RAS-GEFs families share a common domain known as REM-CDC25 (by the homology with yeast CDC25 gene), which is involved in the catalytic process[22,89]. The GEF that is usually associated with RAS and the most studied is SOS1. The α-helix of CDC25 domain of SOS1 is inserted into Switch I domain of RAS and opens the nucleotide-binding pocket. In addition, the α-helix interacts with Switch II causing a series of side-chain rearrangements. The resulting conformational modification allows GDP to dissociate from RAS and RAS nucleotide-free state is obtained. The RAS nucleotide-free state is an exceptional unstable conformation, which is stabilized by the binding of SOS1. Due to the high intracellular levels of GTP, GDP is replaced by GTP when RAS is found in its nucleotide-free state[6,41,48,90]. After that, SOS1 is released from the complex. Active RAS has been reported to be in two dynamic conformations: one of these

conformations is an “open and off”, referred as state 1, which consists of a more open active state of RAS with weak GTP-binding (allowing GAP interaction); the second conformation is the “closed and on”, known as state 2 of RAS, which regulates the signal propagation, due to that the effector proteins with RAS binding domains (RBD) are bound to Switch I and II of the effector lobe inducing downstream signaling[91].

However, this active conformation induced by GTP-binding is reversible. The intrinsic GTPase activity of RAS is slow, but can be accelerated more than ~1000-fold by GAP-binding[6]. The first RAS-GAP protein described was p120 RAS-GAP, which was characterized[92,93] after Trahey and McCormick discovered that the hydrolysis of GTP bound to normal RAS was accelerated 300-fold by a cytosolic protein, but not that of the mutant RAS proteins[94]. Few years later, a second RAS-GAP was discovered, the neurofibromin (NF1)[95–97]. Subsequently, additional RAS GAPs have been described. Nowadays, there are 14 predicted RAS GAP genes in the human genome and all present RAS binding domains[41,98]. Specifically, GAPs contain a residue, known as the arginine finger, which is responsible for GTPase reaction by inserting into the RAS active site. This arginine finger, which is conserved between all the RAS GAPs, interacts particularly with Gly12 and Gln61 residues and participates and stabilizes the cleavage reaction of the phosphate. Once the phosphate is released, the GAP is dissociated from RAS, suggesting that GAP is necessary for both cleavage and release of phosphate processes[90].

KRAS is frequently mutated in G12 and Q61 codons, therefore these mutations prevent GAPS to insert the arginine finger into the active site of KRAS protein. In this scenario, the capacity of GAPs to induce GTPase activity of KRAS is reduced by 97-99%, remaining the GTP-bound KRAS state. The constitutively active state of KRAS increases downstream signaling, being the most common cause of induction of tumorigenesis[90,99].

On the other hand, mutations in p120 RAS-GAP and NF1 have been described. However, whereas p120 RAS-GAP mutations rarely occur in human cancer, inactivation of NF1 has been observed in some cancer types. Additionally, DAB2IP, another RAS-GAP, has been reported for its implication in cancer onset and progression[89]. Therefore, RAS GAPs have

emerged as an expanding new class of tumor suppressor genes[100], and a tight regulation is necessary to maintain RAS nucleotide cycling.

Conversely, mutational activation of RAS-GEF SOS1 is not common in human cancers, however gain-of-function of this RAS-GEF has been observed in developmental disorders as Noonan Syndrome. Mutations in other RASGEFs are also rare in cancer. Nevertheless, the role of RAS-GEFs as downstream effectors of RAS has been associated with cancer[101]. Thus, as GAPs, the activity of GEFs is strictly regulated.

2.1.2 Main interactors

2.1.2.1 PDEδ

The prenyl-binding protein phosphodiesterase 6 delta subunit (PDEδ) solubilizes the cytosolic farnesylated proteins and it has been demonstrated to assist intracellular trafficking of HRAS, NRAS and KRAS, since the intramembrane exchange of farnesylated RAS to direct it to plasma membrane is a slow process. For palmitoylated RAS proteins, such as HRAS and NRAS, PDEδ has been described to facilitate the diffusion of depalmitoylated forms and to trap and concentrate them at the Golgi apparatus to be repalmitoylated. However, for KRAS isoform, the role of PDEδ is to solubilize it in order to enhance the kinetics of trapping at the plasma membrane[82]. Specifically, when KRAS is internalized by endocytic pathway, the negative charges of membranes are reduced, and it is rapidly dissociated from them creating a soluble fraction of KRAS, which can be recognized by PDEδ. The complex PDEδ-KRAS facilitates that PDEδ-solubilized KRAS can be released in the perinuclear membranes, such as those of the RE, and it can be directed to plasma membrane by vesicular transport from the RE[102]. Once the PDEδ-solubilized KRAS is bound to cell membrane by electrostatic interactions of the polybasic region, the binding site of PDEδ is not exposed allowing the dissociation of the complex and the insertion of farnesyl residue into plasma membrane[103], resulting in KRAS microdomain formation and signaling pathways activation[70].

Conversely to the role of PDEδ in maintaining a retrograde trafficking to Golgi apparatus facilitating the acylation cycle of HRAS and NRAS, PDEδ helps KRAS to maintain an anterograde trafficking to plasma membrane. However, in both cases, the cytosolic diffusion is increased by PDEδ enhancing the trapping at the right membrane compartment[82].

Since PDEδ cannot accommodate palmitoylated proteins, PDEδ inhibition selectively affects KRAS trafficking. Interfering with the solubilizing PDEδ functionality can disrupt the trafficking cycle that maintains KRAS concentration on the plasma membrane, thereby impairing KRAS downstream signaling[82,102,104]. For that reason, pharmacological targeting this interaction has been studied and different inhibitors of PDEδ have been developed in order to block KRAS signaling[105–109].

Nevertheless, some studies proposed that PDEδ can bound to palmitoylated HRAS and that overexpression of PDE6δ could regulate the rate of dissociation of both HRAS and KRAS from the plasma membrane[81,110].

2.1.2.2 Calmodulin

Calmodulin (CaM) is the most ubiquitously abundant intracellular protein and well-known as a Ca^{2+} sensor and signaling molecule. It is involved in several cellular processes such as growth, differentiation, survival, proliferation or motility. CaM is composed of a central flexible linker region (the α-helix) that connects the N- and C-terminal domains, both containing two helix–loop–helix motifs (EF-hands) able to bind one molecule of calcium each. When Ca^{2+} binds to EF hands, they change their orientation inducing the appearance of hydrophobic patches that interact with proteins known as CaM-binding proteins (CaMBPs). This binding modulates the function of these proteins and thus affects many aspects of cell regulation[111].

It has been established that Ca^{2+}- CaM is able to regulate the RAS-MAPK pathway at different levels. Specifically, our group has demonstrated that KRAS, in its GTP-bound state, is the only RAS isoform able to bind to CaM, indicating that KRAS-GTP is a CaMBP; and that this

interaction inhibits KRAS activity at low growth factor concentrations[112,113]. Previously, we showed that CaM and Ca^{2+} are able to downregulate the RAS-MAPK pathway at low serum concentrations, impairing a too-sustained response of this pathway to growth factors[114]. Moreover, we have also described that the polybasic region and the farnesyl group within the HVR of KRAS are essential for CaM interaction and thus, the requirement of both regions would explain the isoform specificity of the interaction with KRAS. The switch II region and the helix α5 (residues 151-166), inside the globular domain, are also important to the interaction between KRAS and CaM. Our results also demonstrated that CaM colocalizes with KRAS mainly at plasma membrane, while the interaction is very low in intracellular compartments[77]. Later, it was confirmed that the C-terminal domain and the linker region of CaM predominantly interact with the HVR of KRAS, whereas the weak association of N-terminal region of CaM to the globular domain of KRAS was necessary for higher affinity binding[115]. Moreover, a subsequent study confirmed these results, demonstrating the relevance of HVR (farnesylated residue) in the interaction with CaM and establishing that the hexalysine polybasic region plays an important role[116], therefore confirming the requirement of these six consecutives lysines to allow CaM to distinguish between RAS isoforms (figure 6).

Additionally, our group has demonstrated that KRAS-CaM interaction is inhibited by KRAS phosphorylation at Ser181 by PKC[77] *(detailed in the chapter 2.1.3.1)* and that this modification modulates the functionality of oncogenic and non-oncogenic KRAS[117,118]. Previously, we had already demonstrated that CaM inhibition specifically enhances KRAS activation only when PKC is active[113]. Therefore, we proposed that, by preventing KRAS phosphorylation, CaM induces a diminished signaling output.

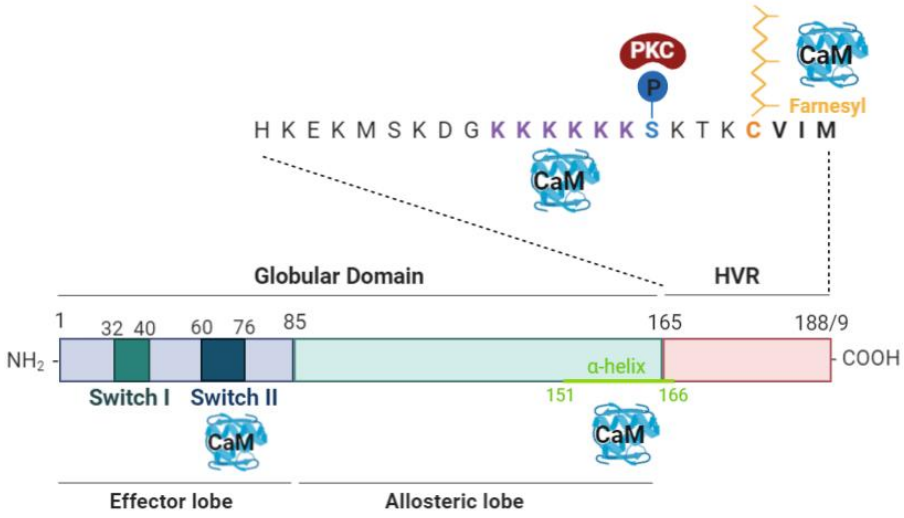

Figure 6. Regions of KRAS important for CaM binding and PKC phosphorylation.

Finally, using both conventional molecular dynamics and scaled molecular dynamics our group has described how CaM and KRAS can interact at the plasma membrane without indispensable extracting KRAS from membrane. Specifically, we have confirmed and identified that arginine 161 and 164 residues of the α-helix of KRAS seem to be responsible for the interaction with the N-terminal region of CaM. Moreover, we have also confirmed that the addition of a phosphate group at Ser181 (highly negatively charged) of KRAS induces a negative impact on CaM-KRAS interaction, preventing it. Lastly, the model proposed also demonstrates that CaM-KRAS interaction would interfere with KRAS dimerization *(see chapter 2.2.3 for more details)*, and consequently this would be another mechanism (apart from inhibiting KRAS phosphorylation) by which CaM can be negatively regulating RAS-MAPK signaling[119] (figure 7).

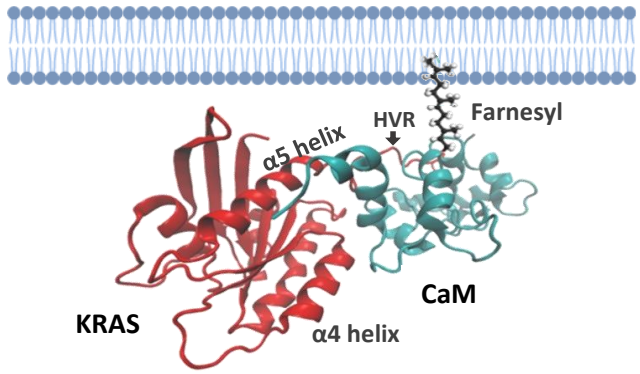

Figure 7. Proposed model of union of KRAS with CaM in the presence of plasma membrane. CaM is presented in light blue, while KRAS is shown in red and the phospholipids in dark blue. HVR, α4- and α5 helix are indicated. (*Adapted from Garrido et al, 2018).*

However, despite these results, controversial studies about diverse functional roles of CaM-KRAS interaction have been reported. It has been suggested that KRAS can be extracted from plasma membrane[81,120,121] and redirected to intracellular compartments[80] through Ca^{2+}-CaM dependent pathway. Moreover, McCormick and colleagues have reported that CaM-KRAS interaction reduces the levels of available CaM for Calmodulin-dependent protein kinase II (CaMKII) and subsequently activates the non-canonical branch of Wnt-signaling. In fact, they have described that disrupting the interaction between KRAS and CaM by KRAS phosphorylation at Ser181 induces the activation of CaMKII suppressing the non-canonical Wnt signaling and thus, the oncogenic KRAS-driven malignancy in pancreatic cancers[122]. On the other side, Nussinov et al have proposed that CaM-KRAS interaction potentially stabilizes the interaction of KRAS with PI3K, through the formation of a ternary complex (KRAS-CaM-PI3K). This complex would favor the activation of PI3K/AKT signaling rather than MAPK signaling, inducing proliferative signaling and cell migration[123–125]. Finally, it has been also described that blocking the interaction between CaM with KRAS using the CaM antagonist CBP501, a modified-peptide, inhibits human non-small cell lung cancer (NSCLC) cell migration, EGF(epidermal growth factor)-induced invasiveness, and epithelial-mesenchymal transition (EMT)[126].

Therefore, despite of the major efforts to understand the biological relevance of CaM-KRAS interaction, there are several aspects that remain still unknown.

2.1.2.3 hnRNPA2/B1

Heterogeneous nuclear ribonucleoproteins (hnRNP) are expressed in numerous human tissues and they have multiple functions such as mRNA processing and nucleic acids metabolism. These proteins participate and regulate every step of mRNA biogenesis and trafficking, including gene transcription, splicing, cytoplasm sorting, nuclear export, stabilization and translation. hnRNP family was originally proposed as a mean of transporting mRNA out of the nucleus, however it has been described that they are also essential for several cytoplasmatic functions. In fact, the interaction of some members of the hnRNPs family with plasma membrane proteins has been described[127–132]. hnRNPA2/B1 is a member of the hnRNP family identified by our group as a novel oncogenic KRAS binding protein in pancreatic ductal adenocarcinoma (PDAC) and HeLa cells. Specifically, our research team demonstrated that knocking down hnRNPA2/B1 in PDAC cells significantly reduced viability, anchorage-independent proliferation, and formation of human xenograft tumors in mice from KRAS-dependent PDAC cells. hnRNPA2/B1 knock down also increased apoptosis of these cells, inactivated AKT signaling via mTOR, and reduced interaction between KRAS and PI3K. Therefore, our data indicate that the interaction between KRAS and hnRNPA2/B1 is important for PI3K/AKT activation in KRAS-dependent PDAC cells. Furthermore, this interaction is dependent on KRAS Ser181-phosphorylation status (*see chapter 2.1.3 for more details)*[133].

2.1.2.4 Other interactors

I. **Galectin-3:** Galectin-3 (Gal-3), a β-galactoside binding protein, is a cytosolic protein which can directly interact with KRAS when it is farnesylated and GTP-loaded[134]. It has been demonstrated that the exogenous expression of Gal-3 can stabilize KRAS GTP-loading in response to EGF stimulation thus inducing downstream cell signaling [134,135]. Moreover, Gal-3 can directly regulate the formation and function of KRAS-GTP nanoclusters but not those of KRAS-GDP. In fact, when KRAS is GDP loaded, Gal-3 is

mostly localized in the cytoplasm, but when KRAS is active (GTP-bound), Gal-3 is recruited from the cytoplasm to the plasma membrane. The GTP-loading and the interaction with Gal-3 decrease KRAS dissociation from the plasma membrane. Therefore, ectopic Gal-3 expression can enhance nanoclustering formation which correlates with an increase in KRAS-GTP and signal output levels[81,136,137]. Collectively, these studies have shown the significance of the interaction between KRAS and Gal-3 modulating both the spatial distribution of KRAS protein in nanoclusters and the use of its effectors thus being a hotpot for cancer therapy.

Finally, a recent study has identified and characterized Galectin-8 as a new direct KRAS-binding protein, which can modulate RAS downstream signal transduction pathways and cell processes involved in tumorigenesis[138].

II. **Nucleophosmin and Nucleolin:** Nucleophosmin (NPM) and nucleolin are two nucleolar proteins that have been described as novel KRAS regulators. Principally, NPM binds to KRAS when it is anchored in the plasma membrane rather than to cytosolic KRAS, since the farnesyl group that blocks NPM-binding to KRAS is hidden inside the lipid bilayer. Moreover, overexpression of NPM induces an increase in nanoclustering of both GTP and GDP bound KRAS. However, while NPM acts at the plasma membrane to drive KRAS clustering, nucleolin operates in the cytoplasm, maybe as a chaperone that enables the delivery of KRAS to the plasma membrane. Therefore, although through different molecular mechanisms, both proteins stabilize KRAS at the plasma membrane leading to an increase in KRAS nanoclustering that amplifies downstream signaling like the one of the MAPK pathway[139,140].

2.1.3 Posttranslational modifications

2.1.3.1 Phosphorylation

Phosphorylation, which was described more than thirty years ago by *Ballester's* research group[141], is the most studied KRAS conditional posttranslational modification. Serine 181, encoded in exon 4, was the phosphorylation site suggested by *Ballester et al*, which was validated in the following years[62,73,117].

Although KRAS is thought to be phosphorylated by a conventional PKC, it has yet to be addressed which one of the PKC isoforms is the responsible, or even whether PKC is the only kinase able to phosphorylate KRAS at serine 181. In fact, it has recently been reported that isoform 2 of Protein Kinase G (PKG2) can also phosphorylate KRAS at serine 181 in response to activation of AMP-activated protein kinase (AMPK)[142].

The phosphorylation of KRAS has been studied intensively during the last years, and the role of this posttranslational modification in the rapid dissociation of active KRAS from the plasma membrane is still being discussed. Firstly, M. Phillip's group described that KRAS phosphorylation at Ser181 induces the translocation of KRAS to endomembranes of the ER, Golgi apparatus and mitochondria. Moreover, they evidenced that a pseudo-phosphorylated KRAS mutant (S181**D**) was able to interact with Bcl-X_L inducing apoptosis in established cell lines[62]. In agreement with this, it has also been reported that KRAS phosphorylation at Ser181 inhibited the formation of KRAS-GTP nanoclusters at plasma membrane. The insertion of negative charges in the HVR might reduce the stability of KRAS at plasma membrane decreasing nanocluster formation. Specifically, data show that phosphomimetic KRAS (S181**D**) presented lower affinity to plasma membrane and reduced clustering than non-phosphorylatable KRAS mutant (S181**A**). However, although non-phosphorylatable mutant showed increased nanoclustering capacity and recruited more RAF1 at the plasma membrane, inducing the signal output, phosphomimetic KRAS presented the highest signal output, demonstrating that RAF1 is recruited at plasma membrane, and thus the nanoclusters it formed were functional. Therefore, the study proposed that

phosphorylated KRAS achieves its maximal signal from plasma membrane nanoclusters and additional signal derived from endomembranes, such as mitochondria[73]. Therefore, both investigations coincide that KRAS phosphorylation can induce internalization of KRAS but being the phosphomimetic KRAS still mainly found at the plasma membrane. Despite these findings, it has been demonstrated that translocation of KRAS to intracellular membranes, such as endosomes, can occur independently of KRAS phosphorylation, since non-phosphorylatable KRAS can also be internalized to endosomes[84].

Regarding these results, our group has reported that KRAS phosphorylation at Ser181 regulates the localization of oncogenic KRAS at the plasma membrane. Specifically, co-clustering assay demonstrated that phosphomimetic and non-phosphorylatable KRAS mutants are segregated in different nanoclusters. This finding was validated with the phosphorylatable KRAS mutant after induction or inhibition of the phosphorylation. The differential segregation correlated with higher co-fractionation of the active form of RAF1 and p110α (catalytic subunit of PI3K) with the phosphomimetic KRAS mutant. Moreover, strong co-clustering of PI3Kp110α and phosphomimetic KRAS mutant was also demonstrated and validated after the modulation of the phosphorylation of the phosphorylatable KRAS mutant. Therefore, our data suggest that phosphorylated KRAS constitutes a preferential functional signaling platform, explaining the distinct levels of activation of RAS signaling transduction pathways of phosphorylated versus non-phosphorylated oncogenic KRAS[76] (figure 8). In agreement with this, a recent study showed that a transient and acute KRAS phosphorylation at Ser181 induced by PKG2 did not dislodge KRAS from the plasma membrane and, phosphorylated KRAS segregated to form nanoclusters that enhanced the activation of PI3K-AKT and MAPK signaling pathways[142]. Additionally, another paper supports that KRAS phosphorylation modified the nanocluster lipid content reducing PtdSer and increasing PIP_2, the lipid substrate of PI3K [78].

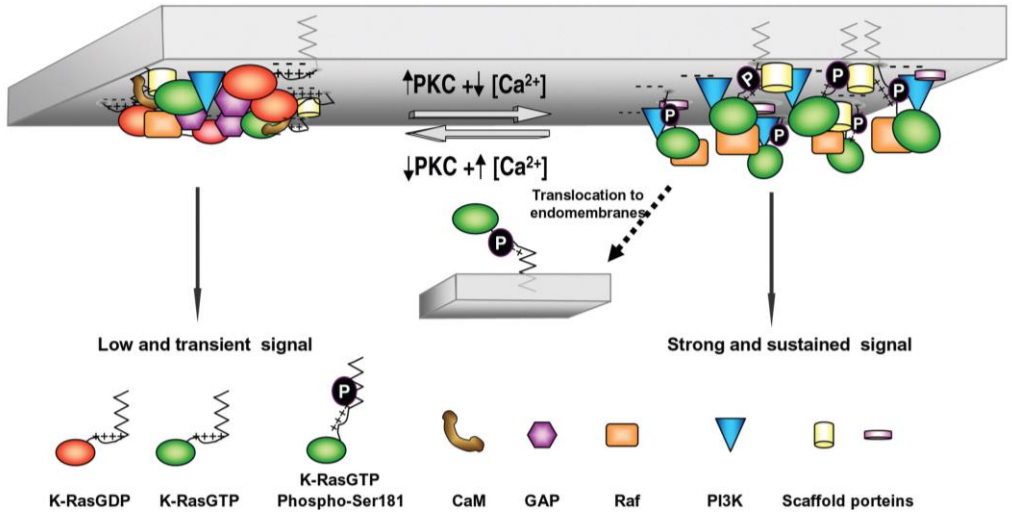

Figure 8. Diagram of the model proposed for the regulation of KRAS functionality and clustering by PKC phosphorylation. When PKC activity is low and the presence of Ca_{2+} ionophore is high, KRAS can be cycling between its GTP- and GDP-bound states depending on incoming extracellular signals. However, in this condition KRAS can interact either with GAPs leading to its inactive form (GDP-bound), or with CaM (when it is GTP-bound) preventing KRAS phosphorylation; and thus, in both cases KRAS signaling is low. Nevertheless, when calcium levels are low and PKC activity is high, CaM cannot interact with KRAS, and consequently KRAS can be phosphorylated by PKC. This modification allows KRAS to translocate to distinct nanoclusters enriched in KRAS effectors and scaffold proteins; and with different lipid content but limited GAPs. Therefore, KRAS will be sustained inducing a strong downstream signaling from the plasma membrane, and besides that it will be able to translocate to endomembranes. (*Adapted from Alvarez-Moya et al, 2011).*

In contrast, a prolonged KRAS phosphorylation by AMPK-PKG2 pathway can displace KRAS from plasma membrane and decrease oncogenic KRAS signaling[142]. However, molecular dynamics validated that the addition of this phosphate conferring a negative charge to KRAS at Ser181 was not sufficient to disrupt the interaction with the plasma membrane, suggesting alternatives scenarios whereby phosphorylated KRAS is removed from the plasma membrane, such as endosomal recicling[84,86,142]. In fact, our last data using molecular dynamics showed the relevance of this phosphorylation to prevent CaM interaction[119], which has been proposed to extract KRAS from plasma membrane[80]. Nevertheless, other study has suggested that KRAS phosphorylation could prevent the farnesyl insertion into the lipid bilayer[143].

The effect of KRAS phosphorylation at Ser181 during tumorigenesis is also still to be understood and several controversial studies have been reported. As mentioned above, M. Phillip's group demonstrated that phosphorylated KRAS in mitochondria can trigger apoptosis. Moreover, they reported that Briostatin-1, a PKC modulator, inhibits the growth of oncogenic KRAS-derived tumors *in vivo* by promoting programmed cell death[62]. In agreement with this, McCormick group, demonstrated that phosphorylated KRAS at Ser181 induces suppression of malignancy driven by oncogenic KRAS in pancreatic cancer[122].

However, in contrast to these studies, our group has demonstrated the relevance of KRAS phosphorylation at Ser181 in promoting KRAS activity and function as well as in the development of oncogenic KRAS-driven cancers.

Firstly, we demonstrated that the inhibition of CaM, under serum-limiting conditions, triggered KRAS signaling pathways only when PKC remains activated. We evidenced that an increased in active RAS induced by a CaM inhibitor was blocked by suppressing PKC activity, suggesting that RAS activation due to the inhibition of CaM is dependent on PKC at growth factor limiting conditions. Subsequently, by treating NIH3T3 cells with both a PKC activator and a CaM inhibitor we observed strong synergism in increasing KRAS activity, concluding that CaM was preventing KRAS activation by PKC[113].

Next, by using RAS exogenously expressed in COS-1 and NIH3T3 cells, we confirmed that KRAS can be phosphorylated by PKC *in vitro* and demonstrated that this phosphorylation was inhibited when CaM was added. Afterwards, we proved in NIH3T3 and HEK293 transfected cells that both non-oncogenic and oncogenic KRAS can be phosphorylated at Ser181 *in vivo*, either in the presence of growth factors or upon PKC activation, and that this phosphorylation was inhibited by CaM interaction[117].

Additionally, we reported that KRAS phosphorylation allows to maintain a sustained KRAS activity and consequently an increase in PI3K/AKT signaling under low serum conditions. In fact, we revealed that KRAS phosphorylation at Ser181 was not relevant for cell growth at serum saturating conditions, whereas this was impaired when non-phosphorylatable KRAS

mutant was expressed under serum-limiting conditions. All these data suggest that KRAS phosphorylation at S181 is necessary to drive cell proliferation under unfavorable conditions[117].

Finally, we generated clones of NIH3T3 cells stably expressing phosphorylatable, non-phosphorylatable or phosphomimetic oncogenic KRAS mutants and showed that oncogenic KRAS phosphorylation under serum limiting conditions induced increased cell growth, mobility and survival as well as high downstream signaling activation[117].

In agreement with the last results, we have established that KRAS phosphorylation at Ser181 is required for tumor growth. Specifically, we demonstrated that subcutaneous tumor growth in mice was nearly abolished when injecting cells expressing a non-phosphorylatable KRAS mutant. Additionally, the tumors presented an epithelioid appearance with significant lymphocytic infiltration. Moreover, non-phosphorylatable KRAS-derived tumors showed less activation of MAPK and PI3K/AKT signaling pathways, high levels of cleaved caspase-3 correlating with high number of apoptotic cells, and low mitotic rate. In addition, phosphorylatable KRAS-derived tumors from animals treated with two different PKC inhibitors efficiently recapitulated the growth and signaling pattern of non-phosphorylatable-derived tumors[144]. Accordingly, phosphorylation of KRAS was observed in phosphorylatable KRAS-derived tumors by Phos-Tag SDS-PAGE assay[145], but it was absent in tumor samples from animals treated with PKC inhibitors. We also detected KRAS phosphorylation in a panel of human tumor cells lines. If PKC was inhibited in these cells, they showed reduced proliferation rates, which correlated with a diminished KRAS phosphorylation. Finally, we analyzed orthotopic xenografts tumors derived from carcinomas of the exocrine pancreas and we demonstrated that KRAS is phosphorylated in human tumors. Therefore, these observations reinforce that Ser181 phosphorylation of oncogenic KRAS by PKC is required for tumorigenesis[144].

Some of these results were confirmed in subsequent analysis using a human colorectal cancer (CRC) cell line stably expressing the KRAS phosphomutants *(See background section).*

Besides that, our group evidenced that KRAS was phosphorylated in KRAS-dependent but not in KRAS-independent pancreatic cell lines; and identified hnRNPA2/B1 as a KRAS-binding protein. Interestingly, this association was dependent on KRAS phosphorylation since a phosphomimetic oncogenic KRAS mutant interacted with hnRNPA2/B1, but a non-phosphorylatable KRAS mutant did not [133]. In agreement with this, hnRNPA2/B1 was only efficiently recruited to plasma membrane when phosphomimetic KRAS mutant was expressed. These results were also confirmed in human CRC cells stably expressing KRAS phosphomutant (unpublished data). Functionally, hnRNPA2/B1–KRAS interaction was important for PI3K/AKT activation in KRAS-dependent pancreatic cells lines and for xenograft tumor growth in mice. Concluding, oncogenic KRAS phosphorylation is a requirement for HNRNPA2B1 interaction in KRAS-driven malignancies[133].

Despite phosphorylation at Ser181 is the most studied, it has been described that KRAS can be phosphorylated by Src at tyrosine 32 and 64. These residues, localized inside switch I and II regions, are important for GTP cycle and for KRAS-effectors interactions. Briefly, the study demonstrates, by nuclear magnetic resonance and mass spectrometry, that tyrosyl phosphorylation of KRAS induces conformational changes, which decrease the sensitivity of KRAS for GAP and GEF activities, thus inducing deregulation of the GTP cycle. In this scenario, tyrosine-phosphorylated KRAS in its GTP-bound form is accumulated, presenting reduced affinity for its effector RAF. However, the tyrosine phosphatase SHP2 can dephosphorylate KRAS inducing an increase in KRAS signaling. SHP2 is well stablished as a major regulator of RAS-MAPK signaling pathway, and overexpression or somatic gain-of-function mutations have been identified in several solid tumors. Therefore, the authors propose that the inhibition of SHP2 could induce accumulation of tyrosine-phosphorylated KRAS and thus, reduced RAF binding and KRAS signaling, which would suppress oncogenesis[146].

2.1.3.2 Ubiquitination

RAS proteins have been recently described to be substrates of mono- and diubiquitination. Although, at first, ubiquitination was considered as the beginning of an irreversible destruction process for ubiquitinated proteins, currently it has been recognized to serve as a reversible modification which can affect several processes such as enzyme activity, subcellular localization, and protein–protein interaction[147].

Initially, it was established that the ubiquitination of HRAS and NRAS, but not of KRAS, induced RAS internalization in endosomes and consequently, reduced MAPK signaling output[79,147]. Later, it was described that KRAS is mainly mono-ubiquitinated at lysine 147 affecting protein-protein interactions (PPIs) and upregulating KRAS activity. Indeed, this KRAS ubiquitination enhances GDP/GTP exchange increasing the fraction of KRAS bound to GTP. In addition, oncogenic KRAS ubiquitinated at lys147 favors its affinity for RAF1 and PI3K, increasing KRAS downstream signaling. Accordingly, an oncogenic KRAS mutation that prevents ubiquitination at lys147, reduces KRAS-PI3K binding, thus decreasing its tumorigenic capacity[148]. Subsequent studies supported that mono-ubiquitination at lys147 impairs GTP hydrolysis mediated by GAPs and favors the interaction of the effectors *in vitro*, as well as, in cell lysates[149,150]. Finally, another residue that is a minor site of KRAS ubiquitination is the lysine 104, but it does not seem to affect nucleotide exchange[148].

Anyway, KRAS polyubiquitination can modulate KRAS protein stability and thus, strategies to target oncogenic KRAS for ubiquitination and proteasome degradation are nowadays being studied as potential anti-cancer therapies[147].

2.1.3.3 Acetylation

Despite lysine 104 of KRAS can be ubiquitinated, it can also be acetylated. KRAS acetylation is able to attenuate KRAS oncogenic capacity by interfering with nucleotide exchange mediated by GEFs[151]. A later study described that the deacetylases HDAC6 and SIRT2 are the responsible for regulating KRAS acetylation at lysine 104 in cancer cells. Indeed, these

results suggest that inhibition of these deacetylases, which positively regulate KRAS activity, could be a new therapeutic strategy[152].

2.1.3.4 Nitrosylation

KRAS, as well as whole RAS family and other RAS-related proteins, has been described to react to free radical nitric oxide (NO) which regulates its activity. Cysteine 118, a highly conserved residue between RAS isoforms, can be nitrosylated when it is exposed to NO[48]. In fact, *S*-nitrosylation leads to increase RAS guanine nucleotide exchange, thus inducing an enhancement of RAS transduction pathways activation. However, this modification does not affect RAS structure[153–155]. A recent proteomic analysis has confirmed the endogenous KRAS nitrosylation at this site[156].

Moreover, another study shows that the sustained activation of PI3K/AKT pathway by oncogenic KRAS in cancer cells is due, at least in part, to an increased nitrosylation and activation of wild type (WT) KRAS[157]. Finally, a putative model to explain the role of Cys118 nitrosylation in modulating KRAS proteoforms signaling has been proposed for both cell lines and primary tumors[156].

2.2 Cell signaling

KRAS is activated in response to extracellular stimuli that induce its GTP-bound form. Consequently, KRAS can interact with different effectors, activating several signal transduction pathways. KRAS signaling activation can achieve by recruiting its effectors to the plasma membrane, by acting as an adaptor protein, or by direct stimulation of the intrinsic catalytic capacity of its effectors. Although KRAS can modulate several signaling pathways, the best characterized are the mitogen-activated protein kinase (MAPK) and the phosphatidylinositol-3-kinase (PI3K)/AKT pathways.

2.2.1 MAPK signaling pathway: RAF-MEK-ERK

The MAPK signaling pathway is engaged by protein tyrosine kinase receptors (RTKs) that have been stimulated by extracellular growth factors. For instance, MAPK pathway activation by KRAS can be triggered by EGF binding to the its receptor (EGFR). This induces EGFR dimerization and autophosphorylation on tyrosine residues that function as docking sites for proteins containing SH2 domains. The adaptor protein growth-factor-receptor-bound protein 2 (GRB2) can bind to EGFR through its SH2 domains, allowing the recruitment and binding of Sos1 to the plasma membrane, in this case through its SH3 domains. The EGFR-GRB2-Sos1 complex interacts then with membrane-associated KRAS, promoting KRAS activation[2,22,158] (figure 9).

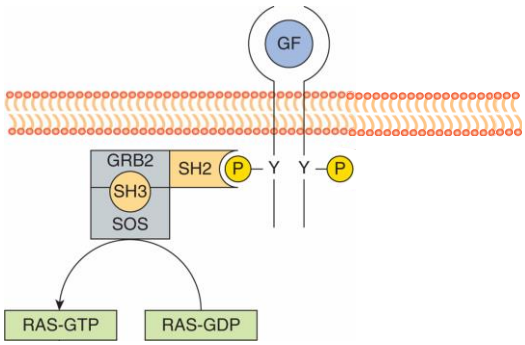

Figure 9. Diagram of RAS activation by protein tyrosine kinase receptor and the recruitment of cytoplasmatic signaling molecules. *(Modified and adapted from Basic Science of Oncology, 5th Ed).*

The first effector described to directly interact with RAS proteins was the RAF1 Ser/Thr kinase, also known as C-RAF[159–162].

There are three mammalian RAF family members encoded by three independent genes: RAF1/C-RAF, B-RAF and A-RAF. C-RAF was the first isoform to be discovered. Although all RAF isoforms are highly conserved, they differ in their activity, regulation and tissue distribution. B-RAF presents the highest activity among the isoforms due to its constitutively

phosphorylated acidic N-terminal motif. Moreover, it is considered the most oncogenic, since it has been identified to be mutated in several types of tumors, emphasizing an important role in aberrant RAF-MEK-ERK signaling in oncogenesis[163–166]. C-RAF, which plays an important role in several RASopathies, shows an intermediate kinase activity, whereas A-RAF, which is rarely observed genetically altered, is the lowest active isoform[165].

All RAF proteins share MEK1/2 kinases as substrates, which in turn can activate ERK1/2 proteins. Therefore, active GTP-loaded RAS proteins induce RAF recruitment (mainly C-RAF and B-RAF isoforms) to the plasma membrane initiating RAF activation. This process is divided at least into four steps: RAF recruitment by RAS, RAF dimerization, RAF phosphorylation and kinase activation. Once RAF is active it phosphorylates and activates MEK1/2, which in turn phosphorylates and activates ERK1/2. Finally, ERK is translocated to the nucleus where interacts with and phosphorylates nuclear transcription factors inducing several biological processes such as cell proliferation, differentiation, growth, migration and apoptosis[158,164,167,168]. To return to the basal state, several phosphorylations are necessary to attenuate RAS signaling. One of them is directed by ERK-mediated negative feedback phosphorylation of several specific residues of RAF, preventing RAS binding to RAF and disrupting RAF dimerization [163,169]. Moreover, ERK can also phosphorylates Sos1 inhibiting its interaction with GRB2 and terminating RAS activation[165] (figure 10).

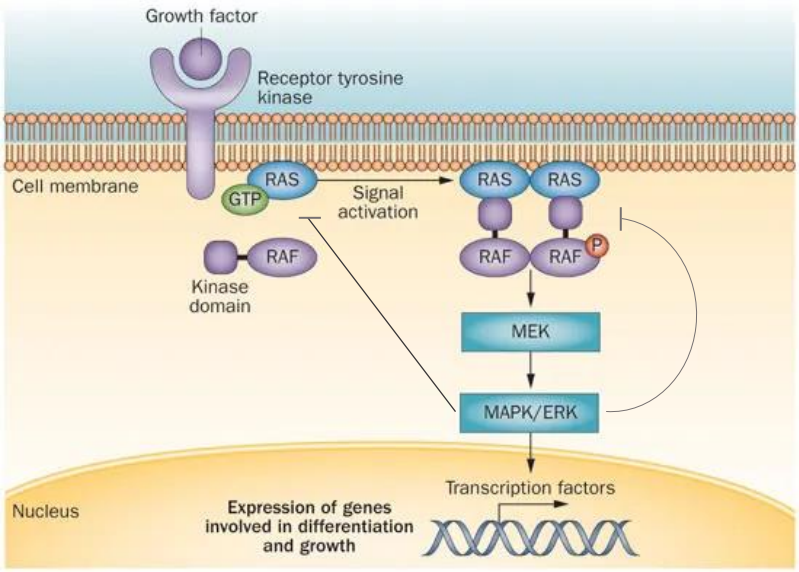

Figure 10. The MAPK signaling pathway activation by RAS proteins. *(Adapted from Gibney et al, 2013).*

Recent data show that RAF dimerization is an essential RAS-regulated event in RAF activation. It was initially observed by artificial oligomerization[170,171] and it was later confirmed when RAS was found to induce active C-RAF/B-RAF dimers[172,173]. Moreover, respective homodimers of these two isoforms were also detected under physiological conditions but their kinase activity was lower than the previous ones. Subsequent studies described that if B-RAF was catalytically impaired, it was still able to promote ERK signaling by interacting with endogenous C-RAF, suggesting that B-RAF could induce C-RAF activity independently of its intrinsic catalytic activity[174–176]. Later, it was demonstrated that phosphorylation of the acidic N-terminal domain of B-RAF was necessary to transactivate C-RAF[177], which was subsequently phosphorylated (figure 11). Summarizing, RAFs proteins are presented as autoinhibited monomers in the cytosol of quiescent cells[178] and the dimerization promoted by RAS triggers a conformational change essential to induce the activation loop in C-RAF. That allows the allosteric transactivation of one monomer by the other. Finally, RAS-dependent activation of C-RAF requires additional phosphorylations at

specific sites (S338 and Y341) of its activation loop to induce the RAF-MEK-ERK cascade[163] (Figure 10 and 11). Nevertheless, the oncogenic mutation V600E of B-RAF can mimic these activation loop, facilitating ERK signaling without RAF dimerization neither RAS activation[166].

According to these data, in a normal RAS-dependent signaling scenario, Morrison's group reported that B-RAF/C-RAF heterodimerization predominated over B-RAF and C-RAF homodimerization, inducing MEK and ERK phosphorylation cascade and activation. Moreover, they reported that RAF dimerization can be blocked using a peptide mimetic of the RAF dimerization interface, which suppress MEK activation and induces cell death in KRAS and B-RAF-driven tumor cells[179].

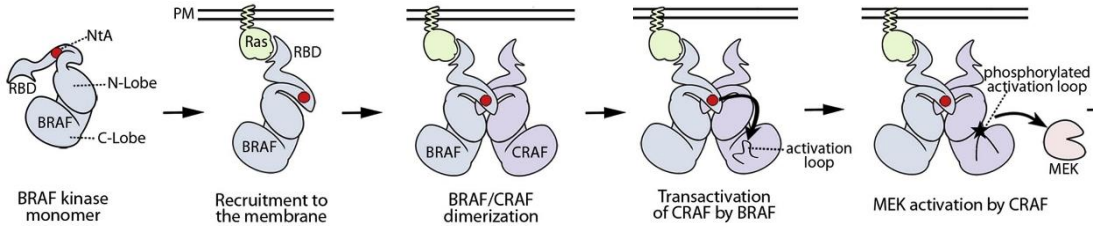

Figure 11. Model of RAF Transactivation. RAS activation induces the recruitment of B-RAF and C-RAF at the plasma membrane, promoting C-RAF/B-RAF dimerization. Transactivation of C-RAF by B-RAF is induced by the phosphorylated acidic N-terminal domain of B-RAF (red dot) that leads to the activation loop in C-RAF, which in turn is phosphorylated (black star). The phosphorylation of the activation loop of C-RAF triggers downstream RAF-MEK-ERK signaling. *(Modified and adapted from Hu et al, 2013).*

Apart from all of this, C-RAF has the highest level and affinity binding for all RAS isoforms. In fact, C-RAF, but not B-RAF, is necessary for both initiation and maintenance of KRAS-driven lung tumorigenesis[180–182]. As mentioned, the role of C-RAF in the development of KRAS-driven tumors might be kinase dependent, explaining the possible no dependence on B-RAF for tumor growth[182]. Surprisingly, recent data showed a strong selectively of B-RAF for KRAS, while low affinity for HRAS and NRAS isoforms was observed[183].

Therefore, considering these findings, it could be possible that the differential binding affinities of B-RAF and C-RAF for specific RAS family members as well as that of B-RAF/C-RAF heterodimers or respective homodimers, could influence MAPK signaling in RAS mutant tumors.

2.2.2 PI3K/AKT signaling pathway

The second best-characterized KRAS effector family is phosphatidylinositol-3-kinase (PI3K). The first evidence of the interaction between RAS and PI3K was detected in RAS transformed cells by immunoprecipitation assay[184].

Three classes of PI3K (Class I, II and III) have been identified in mammals, being Class I present at the plasma membrane by interacting with cell surface receptors. Class I PI3Ks are constituted by heterodimeric enzymes with a catalytic subunit (p110) and a regulatory subunit (p85). Physiologically, class I PI3Ks can promote the transduction of signals from RTKs, G protein-coupled receptors (GPCRs) and activated RAS[185,186]. Upon activation, the catalytic subunit of PI3K phosphorylates PIP_2 to generate phosphatidylinositol-3,4,5-triphosphate (PIP_3). This final product, PIP_3, acts as a second messenger in the cell, being the main mediator of PI3K activity. Specifically, PIP_3 constitutes a docking site for proteins containing the pleckstrin homology (PH) domain, such as phosphoinositide-dependent kinase 1 (PDK1) and protein kinase B (PKB/AKT). The translocation of these two kinases to the plasma membrane allows that PDK1 phosphorylates AKT at threonine 308, which is responsible for propagating the signal and partially activating AKT. This AKT phosphorylation is enough to activate mTORC1 that induces increased protein synthesis and cell survival. However, full activation of AKT requires a second phosphorylation at serine 473 by mTORC2. The complete activation of AKT controls several cell processes such as transcription, translation, cell cycle progression, apoptosis, autophagy, and metabolism (Figure 12). The activation loop of PI3K downstream signaling is finished when the phosphatase of PIP_3 (PTEN) dephosphorylate PIP_3 into PIP_2[186–189].

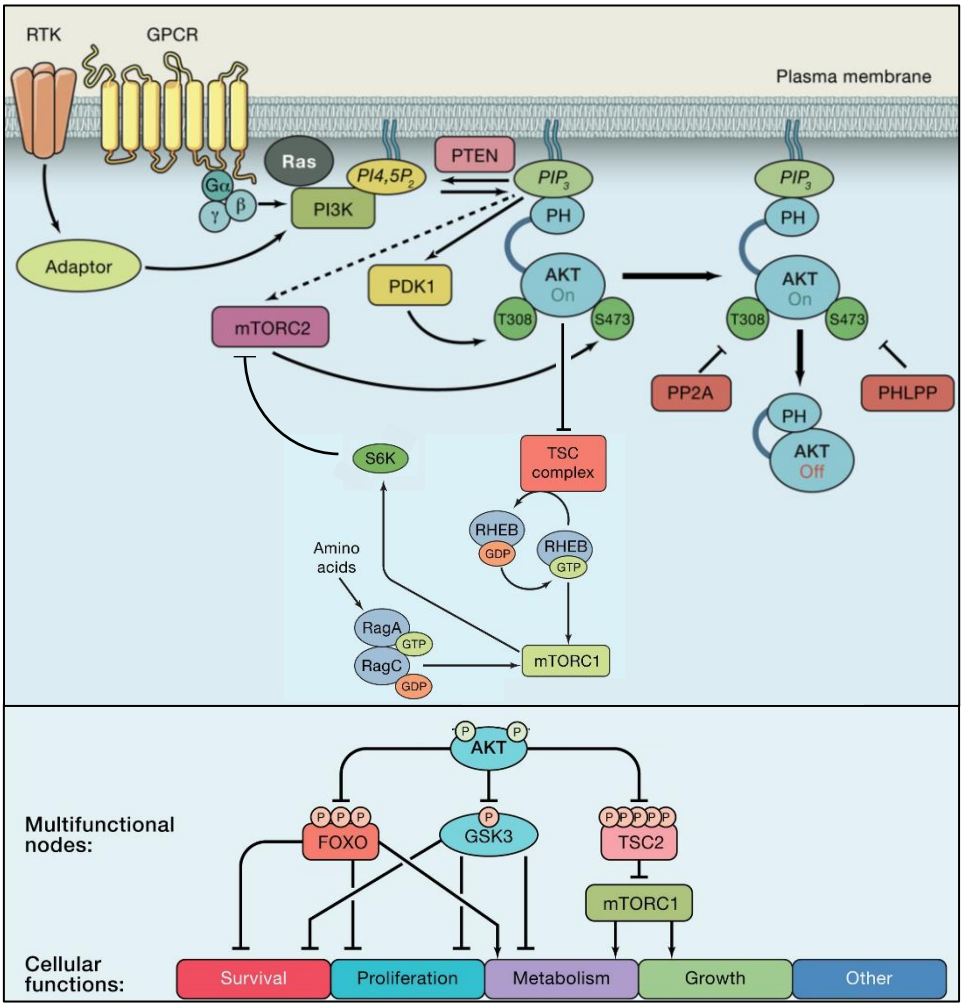

Figure 12. PI3K/AKT signaling pathway activated by RTKs, GPCRs and active RAS. Substrates and Functions of the AKT Signaling Network *(Modified and adapted from Manning et al, 2017).*

After evidencing RAS and PI3K interaction, it was demonstrated that the catalytic subunit (p110) of PI3K, which has a RAS-binding domain, was responsible for the interaction between PI3K and RAS-GTP, which contributes to RAS-driven PI3K signaling. Therefore, PI3K was considered as an important effector of RAS, promoting survival and proliferative functions[190,191].

In recent years, the requirement of the RAS-PI3K interaction in KRAS-driven malignancies has been described. Some reports showed that although several effectors of RAS were

necessary to induce tumorigenesis, only the PI3K signaling pathway seemed to be able to maintain tumor growth[192]. Subsequent studies, using a mice model expressing a mutant form of the catalytic subunit of PI3K that fails to bind RAS, exhibited that the interaction KRAS-PI3K was required to induce cell transformation *in vitro* and in lung tumor formation[193,194]. However, in contrast to the previous evidences[192], both PI3K and MAPK signaling contributions seemed to be necessary for tumor maintenance in oncogenic KRAS driven lung cancers[194]. Later, it was described that targeting PI3K pathway reduced carcinogenesis and tumor progression in oncogenic KRAS-driven PDAC. In fact, KRAS-PI3K signaling was required to induce cell plasticity, acinar cell dedifferentiation as well as tumor formation and maintenance[195]. Additionally, PI3K inhibition induced cell cycle arrest and diminished viability of CRC cells harboring mutated KRAS, suggesting that PI3K/AKT signaling was required for maintaining the growth of these cells [196].

2.2.3 KRAS dimerization

According to the current model, it is known that RAS activation allows the effector domain of RAS to interact with the RAS binding domain of RAF. The binding exposes the C-terminal catalytic domain of RAF, which is inhibited by the N-terminal regulatory domain when RAF is in the cytosol as a monomer[178], allowing RAF to interact with the downstream kinase MEK and to activate the MAPK cascade. As mentioned above, dimerization of RAF is an essential RAS-regulated process in RAF activation. In addition, RAS exists in different nanoclusters comprised of five to ten monomers, setting that aggregation of several proteins in the same nanocluster can be a key factor for signaling activation[71]. Moreover, it has been described that RAS functions as a dimer or as a higher order multimer to activate its effectors[59,197,198] (figure 13).

The first evidence of RAS dimerization was demonstrated by Santos and colleagues by radiation target analysis[199]. A subsequent study, using purified and iodinated RAS, described that monomeric RAS and a small amount of a polymeric specie can exist in equilibrium[200].

Later, it was shown that artificial dimerization of RAS could induce RAF activation, whereas monomeric RAS did not, suggesting the involvement of RAS dimerization in the activation of RAS effectors[201].

According to these studies, it was reported that farnesylated KRAS can dimerize upon binding to a synthetic membrane[202]. But a more recent analysis described that farnesylated and methylated GTP-loaded-KRAS could be purified as a monomer and remained monomeric in the lipid bilayer membranes[203], suggesting that RAS does not possess an intrinsic dimerization capacity.

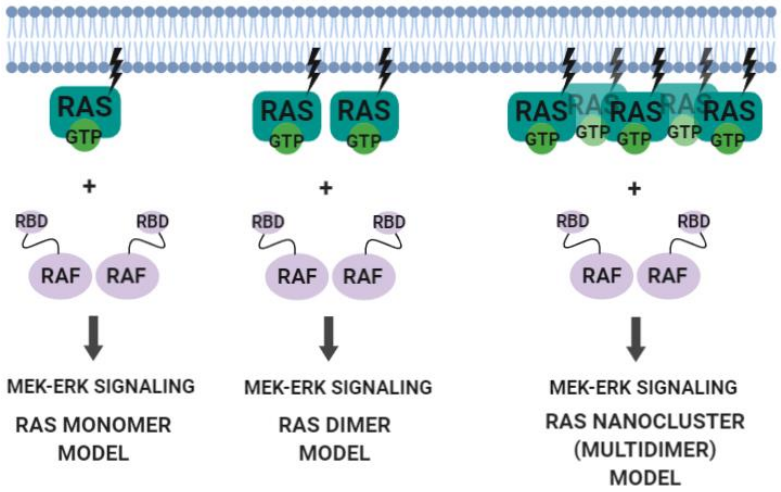

Figure 13. Model of RAS signaling through RAF dimerization. *(Modified from Chen et al, 2016).*

Nevertheless, during the last years, cell biology experiments have suggested that KRAS, as well as the other RAS isoforms, activate RAF through homodimerization. Recent super-resolution microscopy studies in cells expressing KRAS under control of a doxycycline-inducible promoter, described the presence of KRAS dimers at the plasma membrane of living cells and the coincident activation of the MAPK signaling [204]. In fact, the authors also demonstrated that forced KRAS dimerization turned out in a robust activation of ERK, concordant with the results of a previous study[201]. Recently, Nussinov and co-workers proposed two different modes of dimerization, one involving the α-helix 3 and 4, and other

requiring the β-sheet interactions of the effector binding region. But importantly, they demonstrated that dimerization requires GTP-binding, since only an active globular domain of KRAS tended to dimerize with high affinity, while GDP-loaded globular domain showed decreased affinity[205]. Other groups have studied the distinct possible surfaces of RAS that might be interacting during dimerization. Hancock and Gorfe proved that dimerization through the effector binding regions of two KRAS proteins would have low affinity[206], whereas through the α-helix 3, 4 and 5 would be suitable for dimerization[207] (figure 14). Indeed, they demonstrated reduced clustering and dimer formation in cells expressing KRAS harboring point mutations at α-helix 3 and 4 surface.

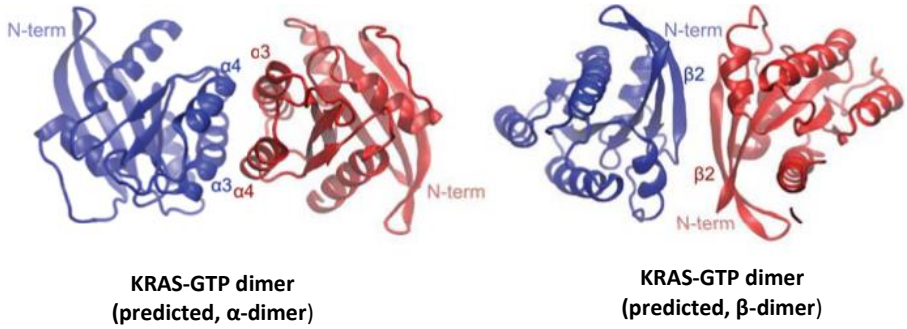

Figure 14. Potential mechanisms regulating RAS dimer formation and signaling. *(Chen at al, 2016)*

Interestingly, recent data showed that dimerization of WT KRAS with oncogenic KRAS decreased cell proliferation. However, it diminished the sensibility to MEK inhibitors in cells and in xenograft models of lung cancer, maybe by reactivation of C-RAF. Moreover, the authors demonstrated that dimerization between two oncogenic KRAS proteins was essential for activation of RAS downstream signaling, cell growth and tumor growth *in vivo*[208]. Therefore, disrupting the dimers of WT and oncogenic KRAS (restoring the sensitivity to MEK inhibitors), and impairing oncogenic KRAS dimerization could be therapeutically effective in these type of cancers harboring oncogenic KRAS[208–210] (figure 13).

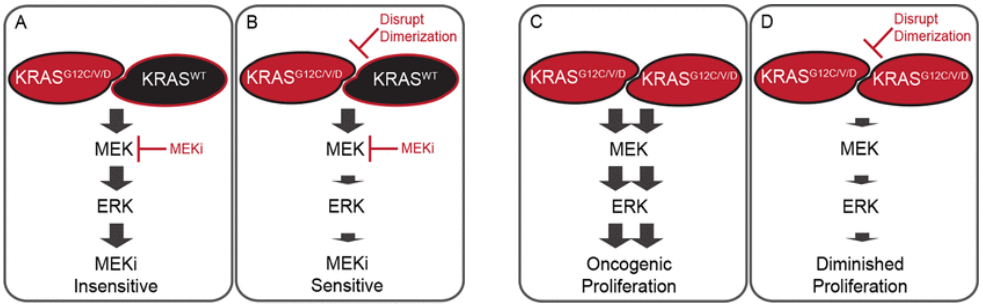

Figure 13. Disruption of KRAS dimerization improves sensitivity to MEK inhibitors and abrogates the oncogenic potential of mutant KRAS. (A) Despite the tumor-suppressive effects of WT KRAS ($KRAS^{WT}$), heterodimerization of $KRAS^{WT}$ with $KRAS^{G12C}$, $KRAS^{G12V}$, or $KRAS^{G12D}$ promotes insensitivity to MEK inhibitors (MEKi: trametinib and selumetinib). (B) Development of strategies to disrupt $KRAS^{WT}$ heterodimerization with $KRAS^{G12C}$, $KRAS^{G12V}$, or $KRAS^{G12D}$ may enhance sensitivity to MEK inhibition. (C) Homodimerization of $KRAS^{G12C}$, $KRAS^{G12V}$, or $KRAS^{G12D}$ promotes aberrant signaling and oncogenic proliferation. (D) Development of strategies to disrupt $KRAS^{G12C}$, $KRAS^{G12V}$, or $KRAS^{G12D}$ homodimerization may diminish the aberrant biological effects of oncogenic KRAS. *(Ambrogio et al, 2018 and Nabet et el, 2018)*

According to these results, a recent report have described that loss of wild-type KRAS enhances tumor fitness in KRAS mutant acute myeloid leukemia (AML) and CRC cell lines while concomitantly resulting in increased sensitivity to MEK inhibition[211]. However, it should be considered that WT RAS proteins can display either tumor promoting or tumor suppressing functions, depending on context[212].

In line with previous studies[204,205,207], it was demonstrated in living cells that dimerization of oncogenic KRAS constitutively active was through α-helix 3 and 4 and, as expected, this dimerization was enriched at the plasma membrane. The authors also demonstrated that cells expressing either α-helixes or β-sheet KRAS mutants displayed decreased MAPK signaling. However, whereas the α-interface mutation impaired ERK signaling by disrupting KRAS dimerization, the β-interface mutation abrogated KRAS signaling may be due to interference with RAF binding[213].

Although these studies suggested that RAS may indeed dimerize, the lack of an available experimental tool to block dimerization has limited the study of this mechanism. However, recent works described that a synthetic binding protein, a monobody called NS1, interacted with α-helixes 4 and 5 disrupting RAS dimerization and nanoclustering. In fact, NS1 potently inhibited RAF dimerization mediated by oncogenic RAS *in vitro*, revealing for the first time the importance of RAS self-association via α4–α5 interface as a requisite step in the activation of downstream effectors such as RAF[214]. Importantly, it was also demonstrated that NS1 interfered with RAS dimerization and nanoclustering, inhibiting specifically KRAS driven tumor development *in vivo*. The authors proved that selective expression of NS1, decreased proliferation of KRAS- but not NRAS- driven tumor cells. In fact, they reported that despite the variability observed under 2D cell culture conditions, NS1 was able to inhibit tumor growth and to reduce KRAS mutant tumors once were established. According to this, decreased RAS downstream signaling was observed[215]. However, these results were not reproducible in oncogenic NRAS-driven tumors. Finally, it was described that the small molecule BI-2852, which bound to KRAS between Switch I and II inhibiting KRAS-effectors interaction, induced the formation of a nonfunctional KRAS dimer[216,217].

Therefore, KRAS dimerization is being revealed as a new therapeutic strategy for directly targeting KRAS.

2.3 KRAS in oncogenesis

The first report that described the transformation of NIH-3T3 cells with genomic DNA from chemically transformed mouse cells was published in 1979 by Weinberg's and colleagues[218]. Later, the laboratories of Robert Weinberg, Michael Wigler and Mariano Barbacid reported the molecular cloning of human transforming genes from T24 and EJ bladder carcinoma cell lines, revealing the existence of transforming genes in human tumors cells[219–221]. Next year, Weinberg's group demonstrated that the transformation of NIH-3T3 cells reported by them four years ago was due to KRAS, being the first human oncogene to be described[222].

The first RAS mutation in human cancer tissue was identified one year later by Barbacid's group in 1984 when a mutated KRAS form was found in a tumor biopsy from a lung cancer patient, but not in his blood cells or in the normal parenchyma[223]. In the following years, mutational analyses exhibited the frequent mutation and activation of KRAS in several types of tumors such as colon[224,225], lung[226] and pancreatic[227] carcinomas. Further studies were expanded to other isoforms, demonstrating that RAS is one of the most frequently mutated oncogenes in human cancers, present in approximately 30% of all malignances.[59,228,229].

Oncogenic mutations of RAS proteins occur mainly at codons 12, 13 and 61. Replacement of glycine at codon 12 and 13 by any of the amino acids, excluding proline, prevents the interaction of arginine finger of GAPs with the active site of RAS proteins, leading to a constitutively active state. Glutamine 61 (Q61) also participates in the GTP hydrolysis mechanism, so mutations at this residue avoid both intrinsic and GAP-mediated GTP hydrolysis, by interfering with the coordination of a water molecule that is necessary for the nucleophilic attack on the γ-phosphate[99,230,231]. In fact, nuclear magnetic resonance (NMR) assay showed that G12V mutation induces a slow rate of activation. However, the reduced intrinsic GTP hydrolysis capacity and the complete resistance to GAP inactivation of RAS G12V sustain its active state. Conversely, Q61L mutant shows a slightly sensitivity to GAP inactivation but maintains an increased nucleotide exchange, leading a mostly GTP-bound state. This is extended to G13D mutation, which leads to less severe GTP hydrolysis defect but induces remarkably high nucleotide exchange[232].

Each RAS isoform shows different bias in codons mutations, being the mutations at codon 12 most frequently found in KRAS (82%), whereas codon 61 is predominantly mutated in NRAS (62%). However, HRAS presents relatively similar mutation frequencies at codons 12, 13 and 61 (27%, 25% and 40%, respectively)[229,233]. Moreover, the frequency of specific mutations also varies significantly between RAS genes, being G12D the most common mutation in KRAS, whereas Q61R and G13R are the most frequent in NRAS and HRAS isoforms, respectively. The distribution of RAS mutations is summarized in the next figure[198].

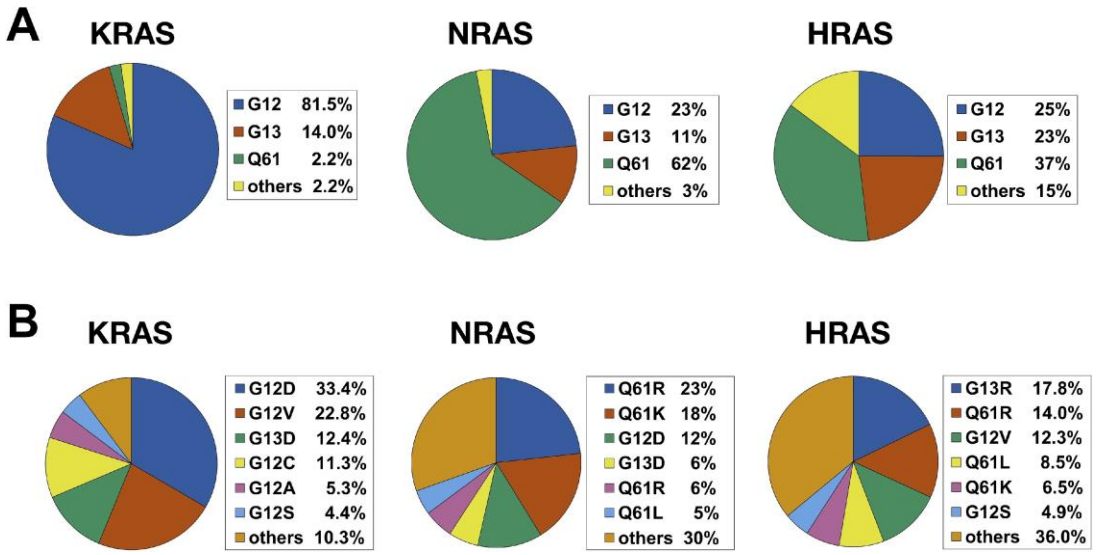

Figure 14. Distribution of RAS mutations in human tumors. (A) Frequency of mutations at codons 12,13, and 61 for each RAS allele. (B) Distribution of specific codon mutations for each RAS isoform. Data were compiled from the Catalogue of Somatic Mutations (COSMIC). *(O'Bryan, 2019)*

KRAS is found to be the most frequently mutated oncogene in human cancers. Overall, data from COSMIC data base show that the highest incidence of mutations has been detected in pancreatic cancer (57%). Relatively, high occurrence has also been discovered in malignancies of the large intestine (35%), biliary tract (28%), small intestine (17%), lung (16%), endometrium (15%) and ovary (14%)[229].

Specifically, mutated KRAS is highly detected in three of the four most lethal cancers: PDAC (97%), CRC (45%) and lung adenocarcinoma (31%). Additionally, the spectrum of mutations in KRAS also differs between cancer types. G12D and G12V occur mainly in pancreatic and colorectal cancer, while G12C is common in lung cancer[234] (figure 15).

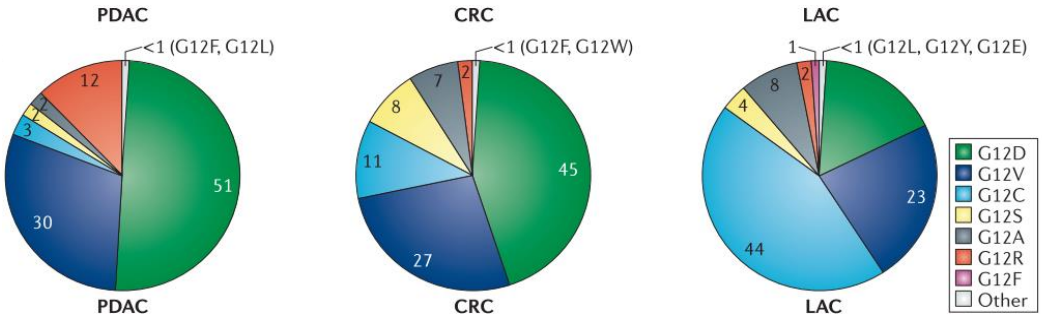

Figure 15. Frequency and distribution of RAS mutations in human cancers. *(Adapted from Cox et al, 2014)*

2.3.1 KRAS in colorectal cancer

CRC is an epithelial tumor originated in the large bowel, which evolves to adenocarcinoma, a neoplasia with glandular characteristics. From molecular and morphology studies, Fearon and Vogelstein (1990) postulated the "Adenoma- to-Adenocarcinoma" theoretical model. This model was characterized by sequential mutations in Adenomatous Polyposis Coli (APC), KRAS and p53[235]. The authors reported that during this cascade, the tumor is initiated by APC inactivation, which induces an evolution from normal mucosa to adenoma. Subsequent mutations in KRAS and p53 drive the adenoma to a more aggressive tumor (figure 16).

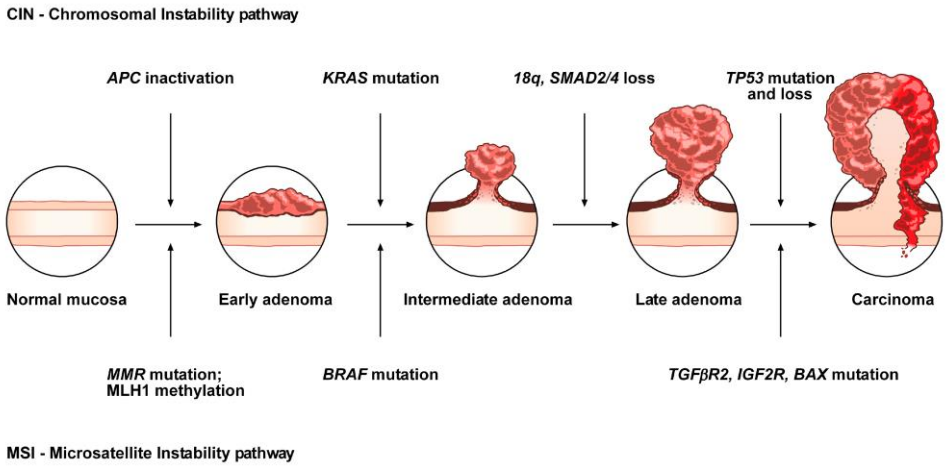

Figure 16. Conventional "Adenoma-to-Adenocarcinoma" model. The CIN pathway begins with mutations in the tumor suppressor gene APC within the normal colonic mucosa which becomes an adenoma. Subsequent additional mutations in the genes KRAS, SMAD4, and TP53, with consequent dysregulation of Wnt/β-catenin, MAPK, PI3K and TGF-β signaling pathways, promote progressivedifferentiation into adenocarcinoma. Alternatively, the MSI pathway involves an initial alteration of Wnt signaling that leads to the formation of an early adenoma. Then, BRAF mutation followed by alterations of the genes TGFBR2, IGF2R, and BAX, participate in the progression toward the intermediate and late stages. *(Adpated from De Palma et al, 2019)*

Subsequent molecular studies have allowed to identify various types of CRC. The molecular organization of CRC subgroups are based on two different mechanisms of tumorigenesis: genetic instability, which include chromosomal instability (CIN) and microsatellite instability (MSI), and epigenetic instability (figure 16 and 17). CIN, which consists of the gain or loss of all or part of the chromosome, is associated with mutations in proto-oncogenes or in tumor suppressors genes such as KRAS and p53, respectively. Whereas MSI, which affects small repetitive sequences of DNA, is associated with BRAF mutations. Depending on the frequency of mutations in these repetitive sequences, colorectal tumors can be stratified in MSI-high (MSI-H), MSI low (MSI-L) and MSI stable (MSS). CRC with CIN is classified as MSS. The second keystone, which CRC classification is based, is epigenetic instability. This is due to aberrant hypermethylation of CpG site within the promoter region of a gene. Thus, according to the frequency of CpG loci methylation, CRC can be classified into negative, low or high CpG island methylator phenotype (CIMP-L and CIMP-H, respectively) groups[236–239].

Combination of these characteristics allows to classify CRC in five molecular subgroups (figure 17). However, this categorization has presented limits due to the tumors classified in each subgroup have been considered as a homogenous entity from the therapeutic point of view. Therefore, since tumors show different drug response and distinct prognosis, four consensus molecular subtypes (CMSs) have been defined, based on a meta-analysis method of six different taxonomies followed by comprehensive multi-omic and clinical characterization[240]. These four CMSs can be separated into: CMS1 (MSI immune subtype, 14%) with a hypermutated phenotype, microsatellite instability, and strong immune activation; CMS2 (canonical subtype, 37%) with epithelial morphology, marked WNT and MYC signaling activation, and CIN; CMS3 (metabolic subtype, 13%) also with epithelial morphology, but with evident metabolic dysregulation, CIMP-L, and KRAS mutations; and CMS4 (mesenchymal subtype, 23%) with prominent TGF-β activation, stromal invasion, and angiogenesis (figure 17).

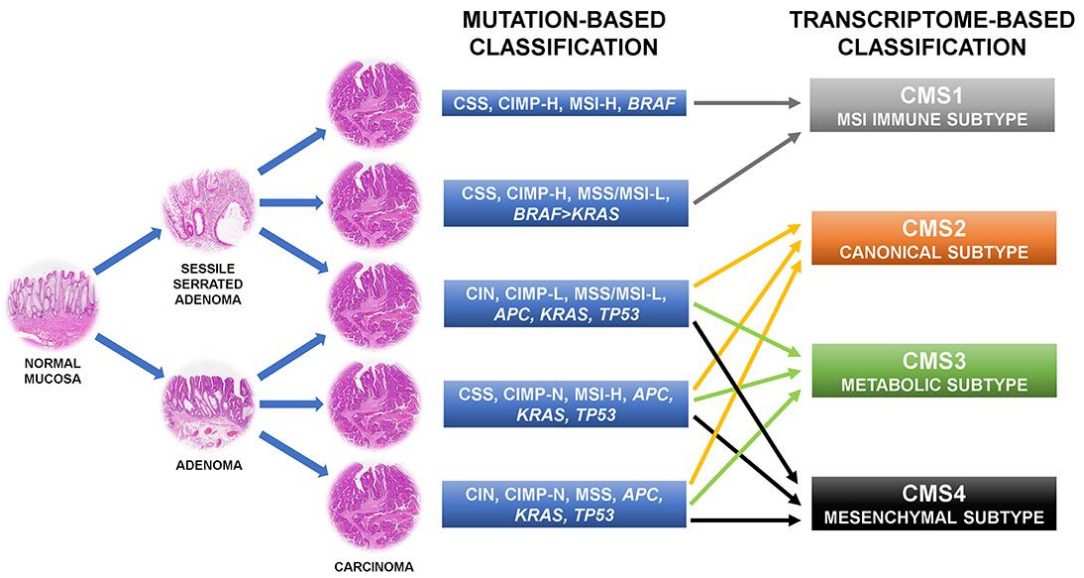

Figure 17 Diagram of CRC subgroups clasification. CRC molecular classifications recently shifted from the mutation-based toward the transcriptome-based approach because this can better describe the behavior of the tumors. CIN, chromosomal instability; CSS, chromosomal stability; CIMP-N/L/H, CpG island methylator phenotype-negative/low/high; MSS, microsatellite stability; MSI-L/H, microsatellite instability-low/high. *(Maffeis et al, 2019)*

A recent study based on a multi-omics approach examined 34 CRC cell lines frequently used, categorizing them into the four CMS subtypes[241] depending on their molecular phenotype, analyzing MSI, MSS, CIMP and POLε mutations. In general, the morphological appearance of most of the cell lines in CMS1 and all cell lines in CMS4 was mesenchymal, whereas CMS2 and CMS3 cell lines were more epithelial-like. DLD-1 and SW480 cell lines, the two colorectal cell lines used in this thesis, have been classified as CMS1 and CMS4, respectively, but both show an epithelial cell morphology in culture.

KRAS mutations have been considered to play a pivotal role both in early phases of malignant transformation of colorectal cells and in the advanced metastatic disease[238,242,243]. Although several studies about the involvement of KRAS and RAS downstream signaling pathways in CRC have been reported, how oncogenic KRAS contributes to CRC progression and tumor maintenance remains still unclear. Recent research has generated a genetically engineered mouse model of CRC harboring the most common mutations in human CRC (APC, KRAS and p53), spatially and temporally regulated. It exhibited genomic heterogeneity and disease progression from adenoma to adenocarcinoma as well as lung and liver metastases, thus reproducing human CRC[244]. This model expressing mutationally activated $KRAS^{G12D}$ in an independently controlled and reversible way, exhibited intratumoral heterogeneity comparable to human. These characteristics allowed the investigators to study the role of oncogenic KRAS signaling in noninvasive primary tumor growth, in tumor progression to metastasis, and in maintenance of the invasive and metastatic disease.

2.3.2 KRAS in pancreatic cancer

Pancreatic cancer can emerge from any cell type within the pancreas, but incidence and prognostic outcome of the disease depend on the origin of the cells. Most of pancreatic cancers are ductal adenocarcinomas, which progress in a histological defined, stepwise development. PDAC usually arises from intraepithelial neoplastic lesions (PanINs) that eventually develop into adenocarcinoma. Oncogenic KRAS mutations are present in 40% of

low-grade PanINs1 lesions, but the incidence of these mutations approximately is doubled in PanIN3 stage[245]. Other precursor lesions such as acinar-ductal-metaplasia and intraductal papillary mucinous neoplasm (IPMNs) have been observed during pancreatic cancer development[246].

Oncogenic activation of KRAS has been validated as an initiating PDAC event by using genetically engineered mouse models of inducible oncogenic $KRAS^{G12D}$. PanINs lesions were observed in these mice, although less than 10% developed to adenocarcinomas. Additional mutations such as loss of *TP53, CDKN2A, SMAD4* or *BRCA2* are required for human PDAC to progress. Thus, when an oncogenic KRAS mutation was combined with the conditional loss of one or more of these four genes, rapid development of pancreatic and metastatic cancers was observed, suggesting that additional mutations a part from that of KRAS are required to induce PDAC[245].

Numerous scientific reports have demonstrated the role of oncogenic KRAS mutations in many pancreatic cancer cell processes such as increased proliferation, survival, migration and invasion. Therefore, by using these mice models, it has been confirmed the initiating role of oncogenic KRAS in pancreatic carcinogenesis, but also the importance of multistep genetic mutations. Moreover, the roles of RAS downstream signaling, tumor microenvironment, several cofactors and inflammatory processes have been studied by using these models of pancreatic cancer[245,247,248].

Despite the efforts of scientific community to understand pancreatic cancer, this has remained a difficult cancer to treat due to the disease heterogeneity, its frequent diagnosis at advanced stages, and its metastatic nature. In addition, lack of approaches to inhibit KRAS appears to complicate targeted therapies.

2.3.3 KRAS dependency

The concept of "oncogene addiction" to highlight the apparent dependency of some cancers on a single activated oncogenic protein or signaling pathway, which maintain the malignant phenotype, has been studied during the last years in order to develop new therapies. The inactivation of this critical oncogene in cancer cells would be enough to lead to cell death. Although human cancers are predominantly induced by progressive accumulation of mutations in some genes with distinct functions, several studies performed in human cancer cell lines, in genetically engineered mouse models of human cancers, and in clinical trials involving specific molecular targeted agents, have evidenced the dependence on a single oncogene[249,250]. However, lack of a pharmacological devices to inhibit KRAS has prevented KRAS dependency to be explored *in vivo*.

Several reports, by using RNAi-based methods, have defined the KRAS addiction status of various cancer cell lines harboring mutated KRAS[251–257]. Moreover, this differential sensitivity to KRAS silencing has also been described in 3D culture assays. Indeed, it has been shown that KRAS mutant cancers are more dependent on KRAS when grown in anchorage-independent culture conditions or *in vivo* than in monolayer[254,255,257–259].

Nevertheless, correct functioning of non-mutated genes has been shown to enhance survival of many cancers, a phenomenon called non-oncogene addiction. Efforts to understand non-oncogenic RAS addiction has led to discover that non-oncogenic proteins associate with oncogenic KRAS to maintain KRAS-addicted tumorigenesis[252,260].

Therefore, research should not be only focused on directly targeting KRAS but also on targeting multiple unmutated or overexpressed proteins associated. This approach seems to be attractive for cancer therapy.

3. KRAS inhibition

Given the essential role of RAS proteins in tumor development, there has been significant interest in pharmacologically inhibiting oncogenic RAS. However, over the decades, oncogenic RAS mutants have been considered "undruggable proteins" due to two main reasons: their high affinity for GTP, rendering GTP-competitive inhibitors ineffective; and the lack of proper binding pockets for small inhibitory molecules. For these reasons several strategies have been developed to inhibit KRAS, including indirect (figure 18) and direct approaches (figure 19).

3.1 Indirect strategies

3.1.1 Inhibition of plasma membrane KRAS localization

Due to the initial perception that RAS would be complicated to inhibit, attention was first turned toward to prevent RAS association with the plasma membrane, which is critical for its biological function[31,261]. Therefore, the first drugs were directed to inhibit the enzyme FTase[50]. This is the protein responsible for farnesylating the terminal CAAX box of RAS which is essential to target RAS to the plasma membrane. Early studies demonstrated that FTase inhibitors (FTIs) could successfully prevent tumor cells growth both *in vitro* and *in vivo*, although these effects did not depend on RAS mutations[262,263]. Moreover, KRAS and NRAS association with plasma membrane was not avoided due to alternative lipidations by GGTase upon FTase inhibition[264–266]. Because of this, combined FTIs and GGtase inhibitors (GGTIs) were tested. However, although co-treatment was successful to prevent prenylation in both KRAS and NRAS in 2D cell cultures and xenograft models, the efficacy was restricted by dose limiting toxicity and thus, the clinical trials were concluded[267,268]. Additionally to the combination of FTIs and GGTIs, considerable failed efforts were focused on the development of dual prenyltransferase inhibitors (DPIs), as well as of ICMT and RCE1 inhibitors[31,233,234].

After unsuccessful results another approach to prevent RAS membrane localization was studied. As mentioned in *section 2.1*, PDEδ binds to farnesylated RAS, in order to induce either membrane association or recycling of RAS. Accordingly, pharmacological disruption of the oncogenic KRAS-PDEδ complex was assessed. The first small molecule identified for its capacity to bind to the prenyl binding pocket of PDEδ was Deltarasin[107]. This inhibitor was able to disrupt the interaction between KRAS and PDEδ, leading to KRAS mislocalization and reduced KRAS signaling as well as tumorigenic potential of PDAC cells. However, non-specific toxicities were observed, limiting its effectiveness. Therefore, a second generation PDEδ inhibitor was generated, called Deltazinone 1[106]. But although this compound was highly selective it had low membrane permeability.

Finally, Hancock and colleagues, using a chemical library, identified Fendiline, a L-type calcium channel blocker, which inhibited selectively KRAS association to the membrane but not that of HRAS and NRAS[269,270]. This compound significantly abrogated proliferation and RAS signaling in KRAS-transformed cells. Although at first it was thought Fendiline to interact with KRAS anchor region, it was later demonstrated that its effects were relatively non-specific. Thus, by inhibiting acid sphingomyelinase, PTdSer plasma membrane levels were reduced [74] and since PtdSer is important for KRAS localization, cell treatment with Fendiline induced KRAS misocalization.

3.1.2 Inhibition of KRAS effectors

The RAF/MEK/ERK cascade is the best characterized RAS effector pathway, so its inhibition has long been an attractive therapeutic target[234,261,271,272]. Targeting RAF kinase appeared to be a reasonable strategy for the treatment of KRAS mutant cancers. The first generation of RAF inhibitors (Vemurafenib, Dabrafenib, and Encorafenib) were designed to inhibit B-RAF^{V600E} for treating B-RAF-mutant melanomas[273–275]. Nevertheless, multiple mechanisms of resistance were observed, such as RTK amplification, B-RAF^{V600} amplification, KRAS or NRAS amplification or mutation, activating MEK mutations or reactivation of MAPK signaling

through alternative pathways as RAC1-dependent signaling[272]. In addition, treatment with B-RAF inhibitors in different RAS-mutant cancers cells produced a paradoxical activation of ERK signaling. In fact, the mechanism underlying this effect was the formation of active RAF dimers in cancers harboring RAS mutations[176,276–279]. To overcome the drug resistance of the first generation of RAF inhibitors, a second generation was developed[165,234]. These included pan-RAF inhibitors, and compounds designed to block or to prevent RAF dimerization. These drugs are now under consideration and may prove to be more efficacious in the long run.

Regarding to block hyperactive MAPK signaling in RAS-driven cancers, MEK and ERK have also been used as targets for drug design. Indeed, MEK inhibitors have usually been favored over RAF inhibitors in both preclinical and clinical studies. Two of these inhibitors, Trametinib and Cobimetinib, were approved for treating cancers harboring B-RAF^{V600E}. In general, their mechanism of action is by allosteric regulation as a non-ATP competitive inhibitor. Although MEK inhibitors have been suitable against B-RAF-mutant melanoma, they have only been partially effective in RAS-mutant cancers models, in part because of ERK reactivation[59,234,271,272]. So, according to the appearance of innate or acquired mechanisms of resistance to RAF or MEK inhibitors, the obvious approach was to inhibit ERK. ERK inhibitors can suppress the growth of KRAS-mutant pancreatic cancer[272] as reported in preclinical models. Although multiple drugs targeting ERK have reached the clinical phase, intrinsic and acquired resistances also occur[234,271,272].

Therefore, it could be that a combined inhibition of the MAPK cascade at multiple nodes would be more effective and less toxic in the treatment of oncogenic RAS mutant cancers.

The second-best validated class of RAS effectors is p110 catalytic subunit of class I PI3Ks. However, the PI3K pathway has not proved to be an efficient target for KRAS mutant cancers as monotherapy. Conversely, a potent synergism in the treatment with both PI3K and MAPK pathways inhibitors has been reported[234,261,272]. Accordingly, numerous clinical trials have evaluated the combined inhibition of RAF and PI3K effector signalling[261,280–282], but toxicity remains to be evaluated.

3.1.3 Synthetic lethality

As mentioned above, non-oncogenic addictions induced by RAS signaling have been achieved. For that reason, synthetic lethal strategies have been employed to screen for genes that are essential for the function of RAS in cancer cells carrying mutated RAS alleles but not in cells with WT RAS[283].

Several studies using RNAi screens in human cancer cell lines to identify synthetic lethal interactors of oncogenic KRAS has been published [234,261,272]. For example, some groups reported the STK33 and TBK1 protein kinases as synthetic lethal interactors of mutant KRAS[284,285], however subsequent studies failed to validate the functional linkage of these hits with oncogenic KRAS[286–288]. Therefore, the success of these approaches have been limited[283] until now.

3.1.4 Other approaches for RAS inhibition

In recent years, the significance of novel signaling pathways that interact with the KRAS classical ones are being evaluated to be considered for the development of new co-targeting therapies. These new approaches include targeting stem cell program, inflammation processes and immune response, metabolic pathways, oncogenic stress, or tumor microenvironment, among others[261,272,289–292].

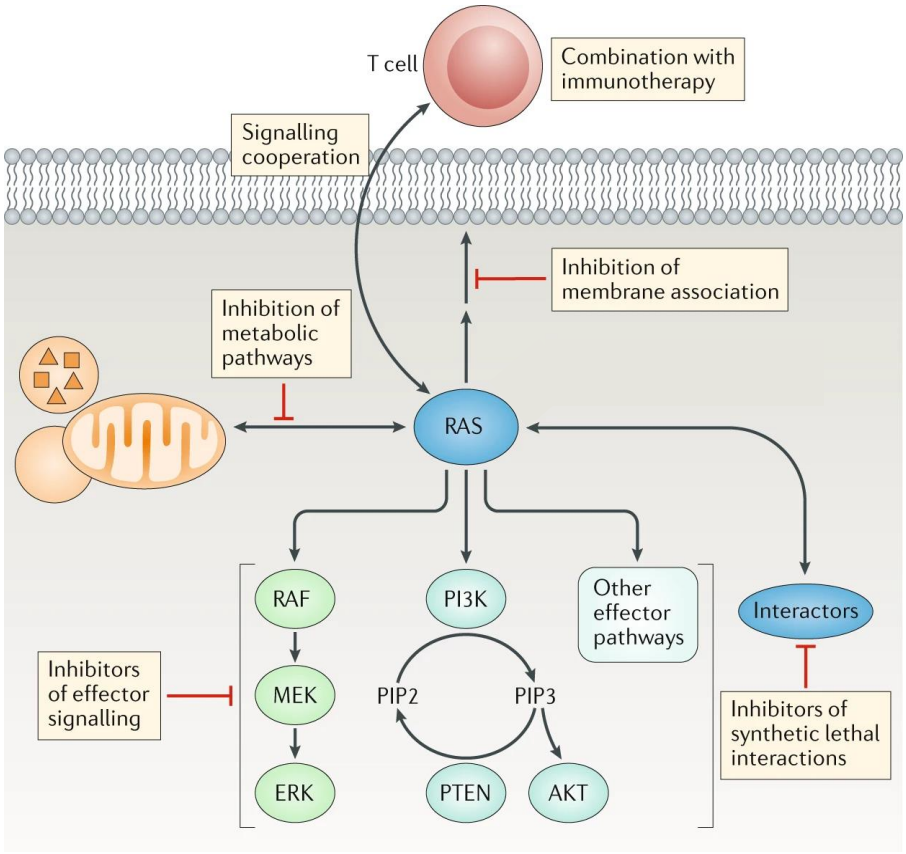

Figure 18. Indirect approaches intended to inhibit RAS function. A general overview is provided including inhibition of RAS association with the plasma membrane, inhibition of effector signaling pathways, inhibition of synthetic lethal interactions, and other more recent such as targeting tumor metabolism or immune system *(Modified from Ryan et al, 2018).*

3.2 Direct strategies

3.2.1 Preventing RAS activation: targeting GTP/GDP binding and exchange

Since KRAS leads to tumorigenicity in its GTP-bound state, some researchers have focused their efforts in preventing this activation. The first approach was to inhibit nucleotide exchange by designing drugs capable of competing with GDP in the nucleotide-binding site of RAS. Some of these GDP analogues were able to inhibit RAS-dependent cell growth, but were toxic and unstable metabolically [234]. The second strategy was to prevent SOS1 (a RAS GEF) interaction with RAS. Bar-Sagi and colleagues designed a peptide, called HBS3, based on the α-helix of SOS1 (important region for RAS binding). This peptide was able to disrupt the interaction between RAS and SOS1 diminishing GTP loading and thus downstream signaling [293]. Later, other team isolated stapled peptides based on the same region obtaining similar results. However, higher concentrations were required to inhibit the viability of KRAS-mutant cells and hence, the specify of these compounds was questioned[233,294]. In 2012, two different groups discovered small molecules that inhibited KRAS-SOS1 interaction[295,296]. One of them identified a compound, called DCAI, which bound to KRAS by the α-helix 2 and β-sheets. It was able to inhibit SOS1-mediated nucleotide exchange by disrupting KRAS-SOS1 interaction and so, preventing RAS activation in cells[296]. Independently, by using Nuclear Magnetic Resonance (NMR)-based screening the other scientists discovered small molecules that bound directly to KRAS between Switch I and II regions (same pocket as DCAI did), thus inhibiting SOS1-catalyzed KRAS activation[295]. However, in both studies the interaction between KRAS and the compounds was weak, and it was unclear whether they would have enough potency or selectivity to inhibit RAS *in vivo*.

More recently, other groups have developed new drugs that prevent nucleotide exchange by disrupting RAS-SOS1 interaction or by blocking nucleotide association[261,297]. Nevertheless, this strategy to inhibit RAS remains in debate, since usually oncogenic KRAS is constitutively GTP-bound, and these kinds of inhibitors might only be effective with WT RAS.

3.2.2 Disruption protein-protein interaction: targeting RAS-effector complexes

Despite of the mechanisms of action of the compounds described above could be advantageous to inhibit active RAS proteins, nowadays it remains controversial. For that reason, the scientific community has refocused on the search for direct RAS inhibitors. One of the strategies that is being followed is looking for drugs that can disrupt PPIs, specifically RAS binding with its effectors[198,233,298]. Three different kind of inhibitors have been used to directly target RAS proteins: (1) small molecules, (2) antibodies, and (3) peptides and peptidomimetics.

I. **Small molecules**: The first compound shown to inhibit RAS was a non-steroidal anti-inflammatory drug (NSAID) called sulindac, which was able to block RAS dependent RAF activation and reduced RAS-driven transformation *in vitro*[299]. Later, new sulindac-derived molecules targeting RAS-RAF interaction and able to reverse RAS-driven transformation were designed[300,301] . However, high concentrations for their biological effects were required, indicating a lack of potency of these compounds. Moreover, further studies suggested that the effects of NSAID on RAS signaling may arise through increased inhibitory phosphorylation of C-RAF and activation of ERK phosphatases[302]. Furthermore, another set of compounds named MCP, were shown to inhibit RAS-RAF interaction, MAPK signaling and RAS-mediated transformation[303,304]. Other researches selected, by *in silico* screening, several small molecules for their ability to block RAS (GTP-form) interaction with the RAS-binding domain of C-RAF[305]. These compounds, called Kobe 0065 and Kobe 2606, by binding to Switch I, blocked RAS-RAF interaction and inhibited also the allosteric RAS-binding site of SOS1. In cells, they decreased downstream RAS signaling, thus MEK, ERK and AKT phosphorylation. Besides, they inhibited colony formation in soft agar in several different human cancer cell lines, RAS-transformed cells proliferation and tumor growth in a xenograft mice model. Despite the promising results, these compounds were not enough potent.

Of great interest, a recent study reported several small molecules that covalently and selectively reacted and bound to the cysteine of G12C mutant form of KRAS (KRAS-

G12C), which is the most frequent RAS mutation found in NSCLC. These compounds were found to react with the GDP-bound state of KRAS-G12C. As predicted, they blocked SOS1-mediated nucleotide exchange and decreased the binding of KRAS to both B-RAF and C-RAF. Moreover, they also seemed to selectively killed cancer cells harboring KRAS G12C mutation[306]. Later, further optimization resulted in an improved inhibitor, ARS-583, whose biological effects were observed at lower concentrations than initial compounds, increasing its efficacy in mutated KRAS-G12C cells[259,307]. Together, these reports provided evidence that KRAS-G12C could cycle between active and inactive state in cells, and thus targeting its inactive GDP-bound state could sequester KRAS and exhaust the active conformation. Based on these works, an optimized small molecule, known as ARS-1620[257], was shown to bind KRAS-G12C in its GDP-bound form, trapping it in an inactive conformation. The consequences were relevant since ARS-1620, in addition to inhibiting growth of KRAS-G12C expressing cells, it prevented the development of tumor xenografts derived from cells harboring this mutation but not from KRAS-G12V mutant cells. Furthermore, ARS-1620 activity was potent in tumor xenografts derived from patients with KRAS-G12C mutant cells.

Regarding to these results, additional cysteine-reactive small molecules (as MRTX849) with high selectively for KRAS-G12C over WT KRAS and high anti-tumor potency, have been developed in pre-clinal models[308].

Other small molecules have been designed to inhibit KRAS, for instance BI-2852[216,217], cmpd2 or the pan-RAS inhibitor termed 3144[198,233]. In addition, genetic depletion of RAS mutant gene would also enable the targeting of oncogenic RAS driven cancers[261,272].

Finally, different compounds so-called Abds were selected from a chemical fragment library by using an intracellular antibody capture technology. The use of an intracellular antibody fragment disrupting RAS-effector PPI[309] is used in a competition assay to select RAS-binding compounds from a chemical fragment library that binds at a similar site. These compounds were able to bind to RAS by the region adjacent

to the effector binding site. One of them, by disrupting RAS-effector interactions of oncogenic RAS isoforms ($KRAS^{G12D}$, $NRAS^{Q61H}$ and $HRAS^{G12V}$) decreased MAPK and PI3K/AKT signaling pathways and cell viability in cancer cell lines harboring oncogenic $KRAS^{310}$.

II. **Antibodies**: As an alternative of the use of small molecules to modulate the PPIs is the use of macrobiomolecules such as antibodies. They have a large structure that allows them to recognize and interact with large protein surfaces. The monoclonal antibody Y13-259, which inhibited oncogenic HRAS-driven proliferation and cell signaling, was one of the first to be identified[311–314]. Posteriorly, the monoclonal antibody anti-p21ser against KRAS-G12S successfully, prevented oncogenic RAS-mediated transformation[315,316]. However, these compounds were limited by their capacity to enter cells. As a variation, single domains of the variable fragment of antibodies, known as intrabodies, were designed to recognize RAS GTP-loaded[317]. One of them, iDab#6, were able to bind all oncogenic RAS isoforms and abrogated their transforming potential[309]. But again, the size and poor penetrance limited its therapeutic ability. Other biological compounds such as RT11 and R11.1.6 were used to RAS targeting[318,319]. RT11 is a chimeric IgG1 antibody developed from replacing the heavy chain fragment of the cell penetrating antibody (TMab4) with the heavy chain fragment of a RAS specific antibody. It was able to inhibit growth and signaling in RAS tumor cells by preventing RAS effector association. On the other hand, R11.1.6 is a high affinity small scaffold based on the DNA binding protein sso7d, which blocked RAS-driven MAPK activation disrupting the association between GTP-bound active RAS with its effector. Nevertheless, these compounds were not able to discriminate between activated WT and mutant versions of all three RAS isoforms. A different option was to genetically engineer the antibody mimetic proteins K27 and K55 to target oncogenic KRAS. This type of molecules is known as Designed Ankyrin Repeat Proteins (DARPins). K27 and K55 inhibited KRAS nucleotide exchange and blocked

KRAS effector interactions, respectively[320]. More recently, two new DARPins were described to block KRAS dimerization as well as SOS1-mediated nucleotide exchange[321]. Unfortunately, the ability of all these antibodies to cross biological barriers was limited and thus, their therapeutic use was unsuccessful.

In the search to identify novel strategies to inhibit RAS, monobody technology has been used. Monobodies are single-domain synthetic binding proteins of approximately 95 aminoacids showing high levels of affinity and selectivity for their targets. Unlike conventional antibodies, they are insensitive to the redox potential of their environment[322]. Recently, a monobody so-called NS1, which inhibited oncogenic HRAS and KRAS signaling and transformation both *in vitro* and *in vivo*, was isolated. NS1 was able to disrupt RAS dimerization through the α4-α5 helix[214,215] *(See more details in chapter 2.2.3).*

III. **Peptidomimetics**: Considering the low capacity of antibodies to cross cell membranes, the peptides have emerged as a promising tool to modulate the biological activity of PPIs. Since they are in the middle of the chemical space between traditional small molecules and antibodies, peptides can also explore large surfaces[323,324]*(e.g HSB3 in chapter 3.2.1)*. Overall, peptides can mimic aminoacid sequences and secondary structures of natural interaction domains. These characteristics allow them to adapt to large proteins surfaces. Other advantages of peptides are easy modularity, high selectively and potency, low toxicity in humans and low accumulation in tissue. However, the poor capability to cross physiological barriers, the rapid degradation by proteolytic enzymes, rapid hepatic and renal clearance and potential immunogenicity are the major limitations for their therapeutic application[323,325–327]. For that reason, the peptidomimetics have been developed. They are peptides modified with non-natural amino acids, cyclization or having unusual peptide bonds generated to improve the stability and the permeability of the peptides in cells, and also the binding

affinity for their targets. These synthetic molecules that mimic the secondary structure of peptides have been applied to modulate PPIs in living cells[324,326,328–330].

The relevance of cyclic peptides inhibiting PPIs was demonstrated when targeting the RAS-effector interactions[331]. Subsequent screening of a combinatorial library of 5.7 million cell-permeable bicyclic peptides against oncogenic KRAS-G12V mutant discovered the cell penetrating Cyclorasin 9A5 cycloundecapeptide. This molecule disrupted the RAS-RAF interaction, inhibited MEK and AKT phosphorylation, reduced cell proliferation and induced apoptosis of lung cancer cells[332]. However, Cyclorasin 9A5 did not exhibit selectivity toward a specific RAS isoform, or WT vs mutant RAS. Later, the same group identified different bicyclic peptides that bound directly to KRAS-G12V mutant showing moderate potent cell permeability and RAS inhibitory capacity. Successive optimization allowed them to synthetize a novel potent direct RAS inhibitor, which was able to reduce RAS-RAF interaction, MAPK signaling and induced apoptotic cell death. Nevertheless, these compounds were not able to distinguish between oncogenic and WT RAS isoforms and high working concentrations were required. Despite this, the researchers developed a general strategy for synthesizing and screening combinatorial libraries of cell permeable bicyclic peptides against intracellular PPIs, such as KRAS interaction with its downstream effectors[333].

Other groups have demonstrated the importance of using peptidomimetics as a strategy to inhibit RAS proteins. Sacco et al developed peptides derived from a specific sequence of a RASGRF1 (a RAS GEF) dominant negative mutant fused to the Tat transduction domain from HIV virus that confers cell-penetrating properties. This synthetic peptide reduced nucleotide exchange and downregulated proliferation and cell signaling in KRAS transformed cells, aside from migration and invasion capacities of human urothelial cancer cells[334]. However, the potency was not determined, nor off-target effects studied. More recently, another laboratory designed a cyclic inhibitory peptide generated via disulfide bonding between two cysteine residues, the KRpep-2d. This peptidomimetic presented a remarkably selectivity for KRAS-G12D

mutant in cell-free enzyme assay as well as in cell-based assays. In fact, it inhibited cell proliferation and downregulated MAPK signaling of cancer cells expressing KRAS-G12D mutant, but not KRAS-G12C. Nevertheless, the efficacy was not enough for *in vivo* experiments[335]. In their next work the researchers revealed that this peptidomimetic bound KRAS near the Switch II region and allosterically blocked protein−protein interactions with GEFs[336]. Finally, a peptidomimetic that could inhibit KRAS prenylation and C-RAF interaction was reported. It was designed by covalent linking of the CAAX box and a compound mimicking the hexalysine domain of KRAS. This molecule was able to bind to the active pockets of FTase and GGTase, acting as a dual inhibitor of KRAS farnesylation and geranylgeranylation. This attribute allowed the peptidomimetic to inhibit KRAS association with the plasma membrane thus disrupting KRAS-C-RAF interaction[337]. Nevertheless, it showed limited activity.

According to these data, the use of peptidomimetics appears to be a good therapeutic tool, but further studies would be necessary to optimize their mechanisms of action.

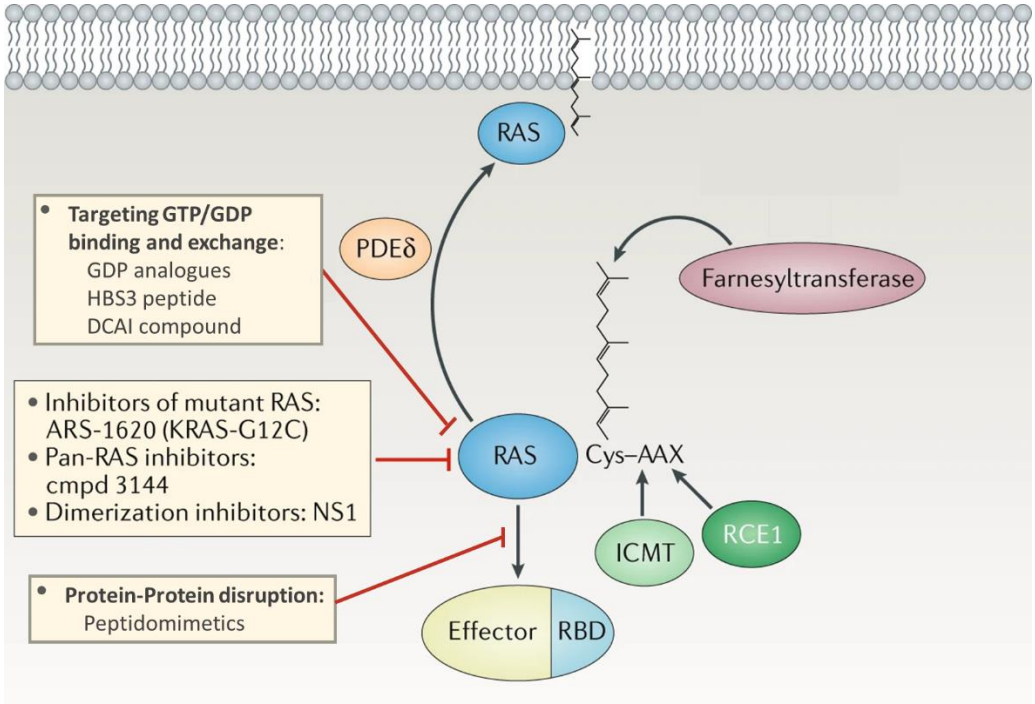

Figure 19. Therapeutic strategies for direct inhibition of RAS function. Therapeutic strategy for the direct inhibition of RAS, including inhibitors of RAS activation, inhibitors of mutant RAS, pan-RAS inhibitors, inhibitors of RAS dimerization with antibodies and inhibitors of the RAS-effectors interaction *(Modified from Ryan et al, 2018).*

BACKGROUND

As mentioned in the introduction, our group has demonstrated that KRAS phosphorylation at Ser181 by PKC enhanced different signaling pathways, being important for cellular transformation, survival, and cell proliferation. Furthermore, this phosphorylation was required for tumor growth in animal models[76,117,133,144]. Additionally, our laboratory was the first to show that KRAS can bind to CaM[77,111,112,119] and also that KRAS phosphorylation at Ser181 is inhibited by CaM[113,117].

Most recent studies of our group have been focused on investigating the relevance of KRAS phosphorylation at Ser181 specifically in colorectal cancer. The experiments were performed by using DLD-1 KO ($KRAS^{WT/-}$) CRC cancer cell lines stably overexpressing the exogenous HA-KRAS-G12V phosphorylation mutants: **S**181 (phosphorylatable mutant), S181**A** (non-phosphorylatable mutant) and S181**D** (phosphomimetic mutant) (*published data in Barceló et al, 2014 and unpublished data Paco, N et al).*

Firstly, we showed that KRAS phosphorylation enhanced cell proliferation under serum-limiting conditions (figure 20A), whereas PKC inhibition decreased KRAS phosphorylation, and reduced cell proliferation in these cells (figure 20B).

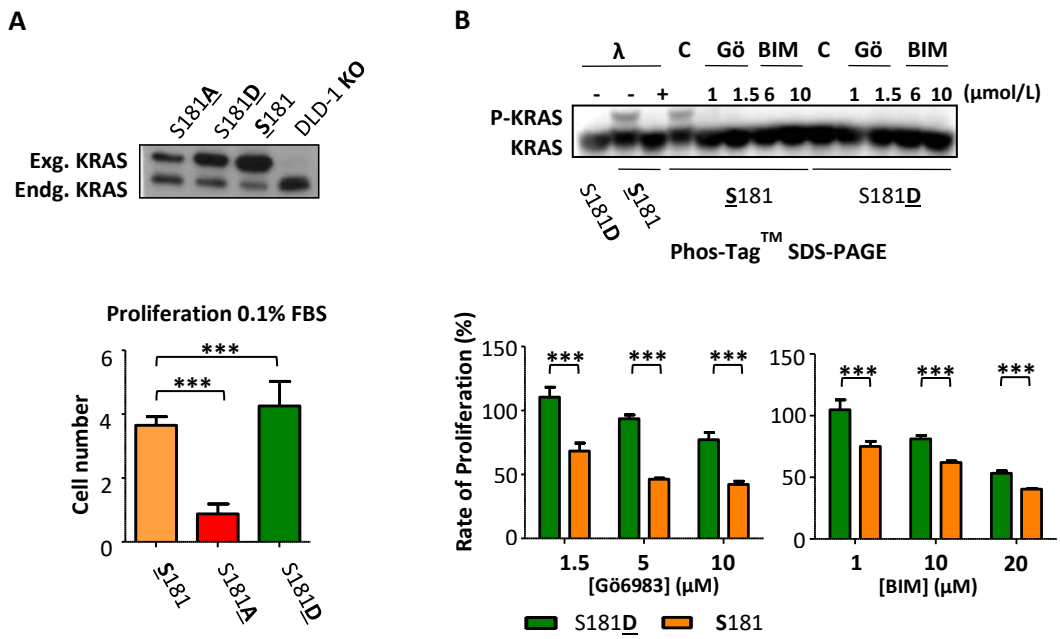

Figure 20. KRAS phosphorylation at Ser181 increases cell proliferation. (A) 3 x 10^4 DLD-$1^{KRASWT/-}$ cells stably expressing either HA-KRAS-G12V-**S**181, -S181**A** or -S181**D** were cultured under serum-limiting conditions (0.1% FBS) for 4 days and counted to evaluate the proliferation rate. Oncogenic KRAS exogenous protein levels from the different clones were analyzed by WB (upper panel). **(B)** DLD$1^{KRASWT/-}$ cells expressing HA-KRAS-G12V-**S**181 or -S181**D** were treated with the PKC inhibitors Gö6983 (Gö) and BIM for 48 hours. Columns represent the growth rate estimated by the measurement of the absorbance in an MTT assay as a function of the initial cell number. To detect KRAS phosphorylation, Phos-Tag SDS-PAGE followed by WB using anti-KRAS specific antibodies was performed with protein extracts from the **S**181 or -S181**D** mutant cells treated or not with PKC inhibitors (Gö6983 or BIM). Phosphatase λ incubation of the samples was used as a control of protein phosphorylation *(Adapted from Barceló et al, 2014)*.

By co-immunoprecipitation (co-IP) techniques, we had previously evidenced in HeLa cells that phosphorylation at Ser181 was important for the interaction of KRAS with its main effectors. Thereby, phosphomimetic KRAS mutant (S181**D**) showed higher interaction with active C-RAF and with the catalytic subunit of PI3K than the non-phosphorylatable mutant (S181**A**). (Figure 21)[76].

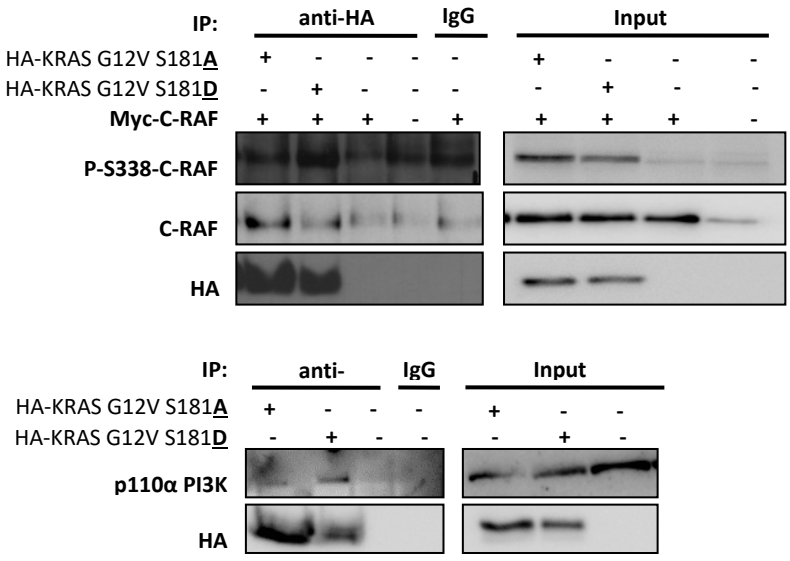

Figure 21. Oncogenic KRAS-S181D mutant shows higher interaction with C-RAF and PI3K than the S181A mutant. HeLa cells were co-transfected with myc-C-RAF and HA-KRAS-G12V-S181**A** or -S181**D** mutants (upper panel) or transfected only with HA-KRAS-G12V-S181**A** or -S181**D** mutants (lower panel), and co-IP of KRAS with C-RAF or PI3K were analyzed. IP was performed with anti-HA antibodies immobilized on agarose beads and the bound and input fractions were electrophoresed and then immunoblotted with anti-p110α PI3K, anti-C-RAF and anti P-S338-C-RAF (activating RAF phosphorylation) antibodies. *(Adapted from Barceló et al, 2013)*.

According to these results, both phosphorylatable (**S**181) and phosphomimetic (S181**D**) KRAS mutant cells presented higher expression levels of P-AKT and P-ERK than S181**A** mutant. This result indicated that KRAS phosphorylation was a requirement for PI3K/AKT and MAPK signaling pathways activation (figure 22A) (*Paco N, et al; unpublished*). Moreover, S181**D** and **S**181 KRAS mutant cells expressed lower levels of cleaved caspase compared to S181**A** clones under Adriamycin treatment, indicating that the phosphorylation at this residue confers resistance to apoptosis (figure 22B)[144].

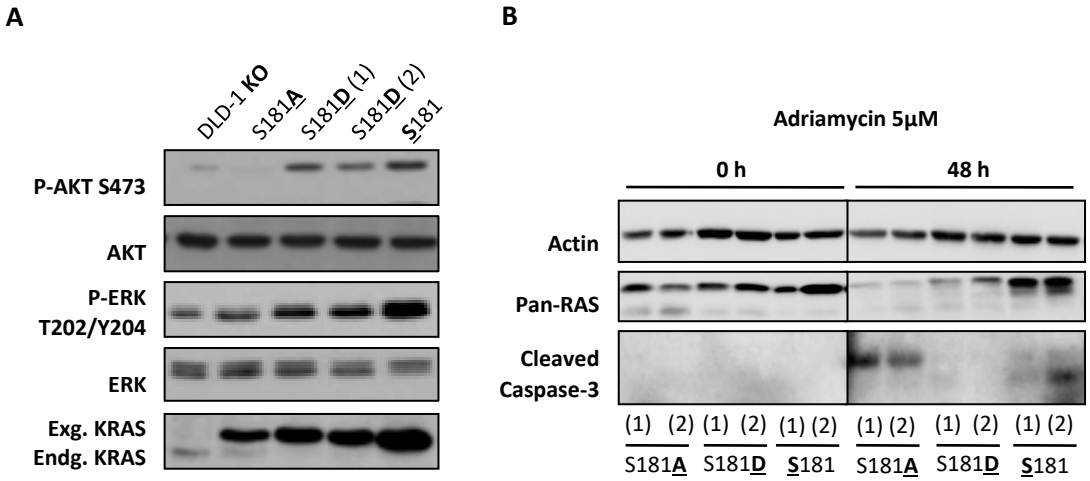

Figure 22. KRAS phosphorylation enhances MAPK and PI3K signaling pathways and confers resistance to apoptosis. (A) DLD-1$^{KRASWT/-}$ cells expressing KRAS-G12V-**S**181, -S181**A** or -S181**D** were cultured under growth factors (10% FBS) conditions**.** Total lysates from the different cell clones were analyzed by immunoblot to detect the indicated proteins (numbers correspond to different clones). **(B)** DLD-1$^{KRASWT/-}$ cells stably expressing KRAS-G12V phosphomutants were incubated with 5µM of the Adriamycin for 48 hours. Cells extracts, including cells recovered from supernatant, were immunoblotted against cleaved caspase to analyze apoptosis (numbers correspond to different clones). Actin was used as a loading control. *(Adapted from Barceló et al, 2014)*.

When analyzing the phenotype of the different clones, we detected that KRAS-S181**A** mutant cells expressed epithelial markers such as E-cadherin and Claudin, whereas both KRAS-S181**D** and -**S**181 mutants showed mesenchymal markers such as ZEB-1, Vimentin, Slug and Snail (*Paco N, et al; unpublished*) (figure 23A). These data correlated with the

images obtained by phase-contrast microscopy (figure 23B) in which all cell clones displayed mesenchymal-like morphology but being less visible in KRAS-S181**A** expressing cells. These results suggest a putative role of KRAS phosphorylation promoting the EMT in these cells.

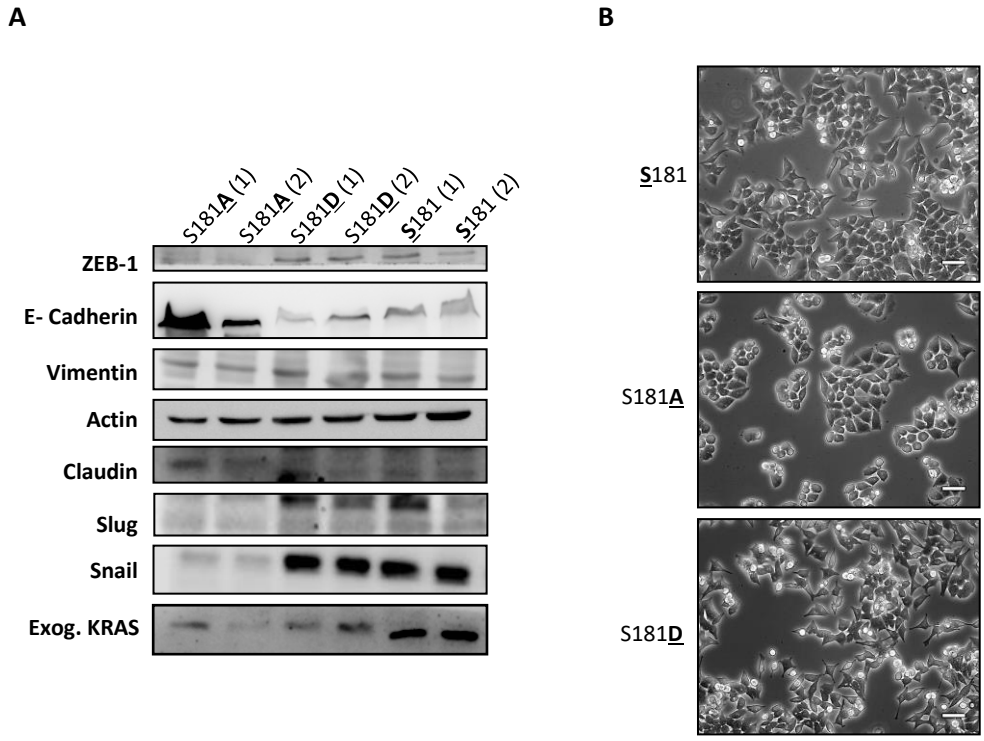

Figure 23. KRAS phosphorylation induces the expression of mesenchymal markers. (A) DLD-1$^{KRASWT/-}$ cells expressing KRAS-G12V-**S**181, -S181**A** or -S181**D** were cultured under growth factors (10% FBS) conditions**.** Cell lysates from the different clones were analyzed by immunoblot to detect the indicated proteins (numbers correspond to different clones). **(B)** phase-contrast images of DLD-1$^{KRASWT/-}$ cells stably expressing either HA-KRAS-G12V-**S**181, -S181**A** and -S181**D** are shown. All scale bars, 50µm.

Furthermore, ELISA analysis of secreted proteins by the different KRAS phosphomutant cells, showed that KRAS phosphorylation induced TGF-β1 secretion (figure 24) (*Paco N, et al; unpublished*).

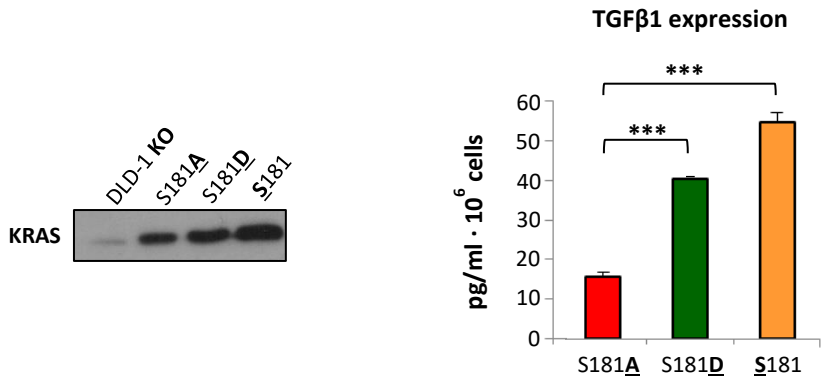

Figure 24. KRAs phosphorylation induces TGFβ1 secretion. DLD-1$^{KRASWT/-}$ cells expressing KRAS-G12V-**S**181, -S181**A** or -S181**D** were cultured under serum limiting conditions for 48 hours. Cell supernatants were collected and assayed by ELISA to detect TGF-β1 secreted to the culture medium by the cells. Data are presented by pg/mL of TGFβ secreted per million of cells. Data shown represent the mean ± SEM of independent experiments. Significant differences were assessed using one-way ANOVA and Tukey Multiple Comparisons Tests (*p-value<0.05, **p-value<0.01, ***p-value<0.001, ****p-value<0.0001). The day of sample collection for the ELISA experiment, the levels of exogenous KRAS in cells were examined by immunoblot (left panel).

Finally, our group examined the tumorigenic potential and metastatic capacity of the different KRAS phosphomutant cell lines when subcutaneously injected in nude mice. As shown in the figure 25A, KRAS-**S**181 derived-tumors were significantly larger compared to the non-phosphorylatable (S181**A**) derived-tumors[144]. No clear results were obtained regarding to KRAS-S181**D** derived-tumors. Preliminary experiments of analysis of the metastatic capacity evidenced that phosphomimetic mutant (S181**D**) cells induced a significantly elevated percentage of mice with metastasis as well as higher number of metastatic tumors in the liver compared to non-phosphorylatable mutant (S181**A**) (figure 25B) (*Paco, N et al; unpublished*). Metastatic capacity was not evaluated in cells expressing phosphorylatable mutant (**S**181) due to its expression was not comparable to that of non-phosphorylatable (S181**A**) and phosphomimetic (S181**D**) mutants.

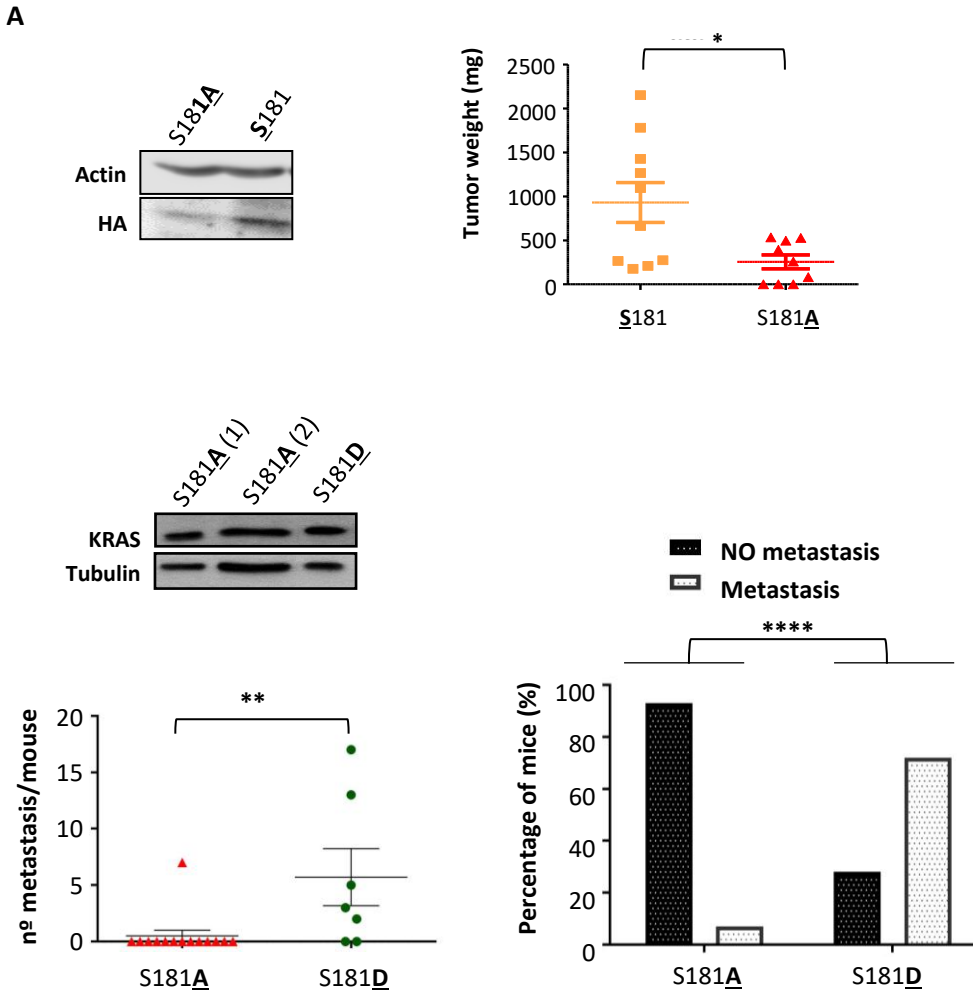

Figure 25. KRAS phosphorylation promotes tumor growth and metastasis. (A) 1 x 10^6 DLD-$1^{KRASWT/-}$ cells stably expressing either oncogenic KRAS-**S**181, or -S181**A** were injected into each flank of nude mice. At day 28 mice were euthanized and tumors were dissected, measured, weighed and processed for analysis. Oncogenic KRAS exogenous protein levels from the different cell clones were analyzed by immunoblot the day of injection into mice (left panel). Actin was used as loading control. The weight of excised tumors is showed in the right graph (each dot corresponds to a tumor). Significant differences were assessed using U Mann Whitney test (*p-value<0.05, **p-value<0.01, ***p-value<0.001, ****p-value<0.0001). **(B)** 2 x 10^6 DLD-$1^{KRASWT/-}$ cells stably expressing HA-KRAS-G12V-S181**A** or -S181**D** were injected into spleen of nude mice. Spleen was removed at the day 3 after injection, and liver was removed at day 38 after injection to evaluate the number of metastasis. Oncogenic KRAS exogenous protein levels from the different cell clones were analyzed by immunoblot the day of injection into mice (*upper left panel*). Data shows the number of metastasis in the liver of each mouse (*left graph*) and the number of mice with or without metastasis in percentage (*right panel*). Significant differences were assessed using U Mann Whitney test or Chi-square statistical analysis, respectively (*p-value<0.05, **p-value<0.01, ***p-value<0.001, ****p-value<0.0001). *(Adapted from Barceló et al, 2014)*.

Therefore, the main conclusion was that KRAS phosphorylation at S181 is involved in tumor growth and metastasis in CRC. Nevertheless, further investigations need to be done since the levels of expression of the oncogenic KRAS phosphomutants were much higher than those of the endogenous protein, and such an overexpression of the oncogenic form is not common in CRC.

HYPOTHESIS AND OBJECTIVES

Our general **hypothesis** is that the activity of oncogenic KRAS can be modulated by phosphorylation at Ser181 and that understanding the exact role of this modification will help to develop new therapies against cancers in which KRAS mutations are associated with bad prognosis. In contrast to the previous work of the group, and with the aim to reproduce more faithfully the tumor development conditions, we propose to investigate this by using colorectal cancer cell lines stably expressing exogenous HA-KRAS-G12V phosphorylation mutants at levels similar to those of endogenous KRAS.

The **objectives** of this project are the following:

1. To study the role of the phosphorylation at Ser181 of oncogenic KRAS in modulating tumoral properties of CRC cells expressing exogenous levels of oncogenic KRAS phosphorylation mutants similar to that of endogenous KRAS. To perform this objective, we will first generate from the CRC cells DLD-1 KO ($KRAS^{WT/-}$), the following stable cell lines exogenously expressing HA-KRAS-G12V-**S**181 (phosphorylatable mutant), S181**A** (non-phosphorylatable mutant) or S181**D** (phosphomimetic mutant); and next analyze:

- **I.** Activation of KRAS downstream signaling pathways: c-RAF-MEK-ERK and PI3K/AKT.
- **II.** Morphologic features and cell proliferation rates in 2D culture conditions.
- **III.** Morphologic features and growth capacity in 3D cultures conditions.
- **IV.** Gene expression patterns.
- **V.** Effects of PKC modulation on the expression of genes regulated by KRAS phosphorylation.
- **VI.** Tumor growth capacity.

2. To generate, by CRISPR technology, CRC cell lines endogenously expressing the oncogenic KRAS phosphomutants and corroborate the results obtained in objective 1.

3. To determine the efficacy and effects of treating cells with different peptidomimetics against the RAS effector domain, designed *in silico* for RAS inhibition by Iproteos technology (IPROTech).

MATERIALS AND METHODS

1. Antibodies

Table 1. Primary antibodies, commercial provider, reference and dilution used for WB.

Primary antibodies	Reference	Source	Dilution
AKT	Cell Signaling 9272	Rabbit	1:1000
CDK4	Santa Cruz sc-749	Rabbit	1:500
c-RAF	BD Transduction 610151	Mouse	1:500
E-Cadherin	Cell Signaling 3195	Rabbit	1:1000
α-E-Catenin	Biolegends 844801	Mouse	1:100
HNF4G	Proteintech 25801	Rabbit	1:500
KRAS	AbCam 196630	Rabbit	1:1000
Lamin B	Santa Cruz sc-6217	Goat	1:200
MEK	Cell Signaling 9122	Rabbit	1:1000
Neogenin 1	Proteintech 20246	Rabbit	1:500
p44/42 MAPK (ERK1,2)	Cell Signaling 9102	Rabbit	1:2000
Phospho-AKT S473	Cell Signaling 4060	Rabbit	1:1000
Phospho-AKT Thr308	Cell Signaling 4056	Rabbit	1:1000
Phospho-c-RAF S338	Cell Signaling 9427	Rabbit	1:500
Phospho-p44/42 MAPK T202/Y204	Cell Signaling 4370	Rabbit	1:2000
Phospho-MEK S221	Cell Signaling 9121	Rabbit	1:1000
Phospho-S6 ribosomal S235/236	Cell Signaling 2211	Rabbit	1:1000
PI3K p110α	Cell Signaling 4249	Rabbit	1:1000
Ras Gap120	Santa Cruz sc-63	Mouse	1:200
SERPINE1	R&D systems AF1786	Goat	1:100
S6 Ribosomal	Cell Signaling	Mouse	1:500
Trypsin	AbCam ab211491	Rabbit	1:500
α-Tubulin	Sigma-Aldrich T9026	Mouse	1:2000

Table 2. Secondary antibodies, commercial provider, reference and dilution used for WB.

Secondary antibodies	Reference	Dilution
Anti-Goat IgG (whole molecule)-Peroxidase	Sigma-Aldrich A5420	1/5000
Anti-Mouse IgG (H+L) HRP Conjugate	BioRad 170-6516	1/3000
Anti-Rabbit IgG (H+L) HRP Conjugate	BioRad 170-6515	1/3000

Table 3. Primary antibodies, commercial provider, reference and dilution used for IF or IHQ.

Primary antibodies	Reference	Source	Dilution
BrdU	AbCam ab6326	Rat	1:250
E-Cadherin	Cell Signaling 3195	Rabbit	1:200
E-Catenin	Biolegends 844801	Mouse	1:100
Integrin α6	R&D systems AF1350	Goat	1:200
Ki-67	AbCam	Rabbit	1:100
MPM2	Millipore 05-368	Mouse	1:250
Phospho-histone 3 Ser10	Millipore 06-570	Rabbit	1:100
Phalloidin Alexa Fluor 594	Invitrogen A12381	-	1:500

Table 4. Secondary antibodies, commercial provider, reference and dilution used for IF or IHQ.

Secondary antibodies	Reference	Dilution
Alexa 488 anti-mouse green	Invitrogen A21202	1:500
Alexa 647 anti-mouse red	Invitrogen A31571	1:500
Alexa 488 anti-rabbit green	Invitrogen A21206	1:500
Alexa488 anti-rat green	Invitrogen A21208	1:400
Ultra-Sensitive ABC Peroxidase Rabbit IgG staining kit	Thermo Fischer Scientific 32054	1:200

2. Reagents and Kits

Table 5. Reagents used, manufacturer and reference number.

Reagent	Reference
Acrylamide/Bis-Acrylamide (37.5: 1) 30% (w/v)	Bio Basic A0011
Aprotinin	Sigma-Aldrich A1153
APC Annexin V	BD Pharmingen 550474
Bisindolylmaleimide I (BIM)	Millipore 176504-36
Bovine Serum Albumin (BSA)	Sigma-Aldrich A7906
Bromodeoxyuridine	Sigma-Aldrich B5002
DAPI	Sigma-Aldrich D9564
DH5α cells	Life technology 18265-017
3,3'-Diaminobenzidine (DAB)	
DMEM High Glucose	Biological Industries 01-055-1A
DMSO	Sigma-Aldrich D2650
Dithiothreitol (DTT)	Sigma-Aldrich D0632
Epidermal Growth Factor (EGF)	Sigma-Aldrich E4127
Eosin Yellowish	Panreac AppliChem 251299.1606
Fetal Bovine Serum (FBS)	Biological Industries 04-007-1A
Folin-Ciocalteau	Merck 109001
F12 (HAM's) Nutrient Mixture	Biological Industries 01-0951A
GeneJet *in vitro* DNA Transfection Reagent	Signagen laboratorios SL100499
Gö6983	Sigma Aldrich G1918
HA-tag antibody crosslinked to agarose beads clone HA-7	Sigma-Aldrich A20956
Hematoxylin de Harris	Panreac AppliChem 256991.1610
Igepal CA-630 (Nonidet-P40)	Sigma-Aldrich I3021
Insulin-Transferrin-Sodium Selenite (ITS) liquid media supplement	Sigma-Aldrich I3146
Immobilon®-P transfer membranes	Merck Millipore IPVH00010
Leupeptine	Sigma-Aldrich CL-2884
L-Glutamine	Sigma-Aldrich G8540
Lipofectamine® 2000 reagent	Invitrogen 11668-019
Matrigel	Corning 356237
MEM Non-Essential Amino Acids Solution	Biological Industries 01-340-1
Mowiol	Sigma-Aldrich 81381

Paraformaldehyde (PFA)	Electron Microscopy Sciences 15710
Penicillin-Streptomycin	Biological Industries AAL-107
Phenylmethylsulfonyl fluoride (PMSF)	Sigma-Aldrich S6508
Phos-tag™	Wako Chemicals GmbH AAL-107
Ponceau	Sigma-Aldrich P7170
Precision Plus Protein™ Unstained Standards	BioRad 161-0363
pSpCas9(BB)-2A-Puro plasmid	Addgene 62988
Pyruvic Acid	Sigma-Aldrich P5280
RNase	Sigma-Aldrich R4875
SCR7 (inhibitor of NHEJ)	Sigma-Aldrich SML1546
Sodium Fluoride	Sigma-Aldrich S7920
Sodium Orthovanadate	Sigma-Aldrich S6508
TEMED	Sigma-Aldrich T9281
TPA (12-*O*-tetradecanoilforbol-13-acetate)	Calbiochem 524400
Trypsin	Gibco 15400-054
W13	Calbiochem 681636
Xylol	Panreac AppliChem 251769.2711

Table 6. Kits used, manufacturer and reference number.

Kits	Reference
cDNA reverse transcription kit	Thermo Fisher Scientific 4368814
CellTiter 96® Aqueous One Solution Cell Proliferation Assay	Promega G3580
DeadEnd Colorimetric TUNEL System	Promega G7360
EZ-ECL kit (Enhanced Chemiluminescence Detection Kit for HRP)	Biological Industries, 20-500-120
GoTaq® qPCR master mix	Promega A6001
MTT Cell Growth Assay Kit	Merck Millipore CT02
Nucleo Bond® Xtra Midi	Macherey-Nagel 740410
RNeasy Mini Kit	Qiagen 74104
Ultra-Sensitive ABC peroxidase staining kit	Thermo Fischer Scientific 32054

3. Solutions and buffers

Table 7. Solutions and buffers used in the experimental approaches and composition.

Solution	Composition
Annexin V 10X Binding Buffer	0.1 M Hepes pH 7.4, 1.4 M NaCl and 25 mM $CaCl_2$
Borate Buffer pH 8.5	100 mM $Na_2B_4O_7 \cdot 10H_2O$ pH 8.5 and 100 mM H_2BO_3
Diaminobenzidine (DAB) buffer	1 mg/ml DAB, 0.03% H_2O_2 in PBS 1X
Electrolyte buffer	25 mM Tris-HCl pH 8.3, 192 mM glycine and 0.2% SDS.
Eosin solution	1 g Eosin, 20 ml deionized H_2O and 80 ml Ethanol 96%
HCl 0.1% 2M Triton denaturing solution	2 M HCL-PBS and 0.1% Triton X-100
Hydrogen peroxide 3%	3% H_2O_2 and 30% Methanol in PBS 1X
Iodide Solution for FACS	1% Propidium Iodide and 0.1 µg/µl RNAse solution
Laemmli sample buffer 4X	30 mM phosphate buffer, 30% glycerol, 7% SDS, 0.15% DTT and 0.05% Bromophenol blue.
Phosphate-Buffered Saline (PBS)	145 mM NaCl, 6 mM Na_2HPO4, 2.5 mM NaH_2PO_4
PBS-T	0.05% Tween in PBS 1X
PBS cell culture	131 mM NaCl, 1.54 mM KH_2PO_4, 5.06 mM Na_2HPO_4
Phos-tag lysis buffer	50 mM Tris-HCl pH 8, 150 mM NaCl, 2 mM EDTA pH 8, 10% glycerol and 1% Igepal
Ponceau Protein Stain Solution	0.1% Ponceau reagent and 5% Acetic acid.
(Ras Extraction Buffer)	20 mM Tris-HCl pH 7.5, 2 mM EDTA, 100 mM NaCl, 5 mM $MgCl_2$, 1%Triton X-100, 10%glycerol
Sodium dodecyl sulfate (SDS) lysis buffer	2% SDS and 67 mM Tris-HCl (pH 6.8)
Sodium citrate 1X buffer	2 mM $C_6H_8O_7$ and 8.2 mM $Na_3C_6H_5O_7 \cdot 2H_2O$ pH 6
Solution 1 for gel preparation	0.75 M Tris-HCl pH 8.8 and 0.2% SDS.
Solution 2 for gel preparation	30% acrylamide and 0.8% bis-acrylamide
Solution 3 for gel preparation	0.25% HCl pH 6.8 and 0.2% SDS
Solution 1 for Lowry assay	2% Na_2CO_3 and 0.1 N NaOH
Solution 2 for Lowry assay	0.5% $CuSO_4$
Solution 3 for Lowry assay	1% Sodium potassium tartrate
Tris Buffer Saline (TBS)	50 mM Tris-HCl pH 7.5 and 150 mM NaCl.
TBS-T	0.05% Tween in TBS 1X
Transfer buffer	25 mM Tris-HCl pH 8.8, 192 mM glycine, 0.2% SDS and 20% ethanol or methanol.

4. Cell Culture

4.1 Cell lines and maintenance

- **DLD-1 (KRASWT/KRASG13D):** human colorectal adenocarcinoma cell line isolated by D. L. Dexter *et al.* in 1977[338]**.** DLD-1 cells have one WT allele of KRAS and one allele of KRAS carrying a G13D mutation. This cell line is dependent on KRAS under serum-limiting conditions. Besides KRAS-G13D mutation, DLD-1 cells present mutations in CRC critical genes as TP53 (S241F) and PIK3CA (E545K; D549N). Moreover, it is classified in CMS1 and has microsatellite instability (MSI) among other characteristics[241]. DLD-1 cell line was obtained from Horizon Discovery Ltd.
- **DLD-1 KO (KRASWT/-):** DLD-1 cell line with a heterozygous knockout of mutant KRAS allele. It was obtained from Horizon Discovery Ltd. (clone D-WT7, #HD105-002; http://www.horizondiscovery.com). DLD-1 KO cells were generated using the proprietary adeno-associated virus (AAV) gene targeting technology GENESIS.
- **SW480: human** colorectal adenocarcinoma cell line with a G12V mutation in both KRAS alleles. It was obtained from the American Type Culture Collection (ATCC).
- **MPANC-96:** human pancreatic tumor cell line established from a metastatic site of PDAC. This cell line has a heterozygous KRAS G12D mutation, and it is dependent on KRAS under serum-limiting conditions.
- **HPAF-II:** human pancreatic tumor cell line established from a metastatic site of PDAC. This cell line has a heterozygous KRAS G12D mutation, and it is dependent on KRAS under serum-limiting conditions.
- **PA-TU 8902:** human pancreatic tumor cell line established from a PDAC. This cell line has a heterozygous KRAS G12V mutation, and it is dependent on KRAS under serum-limiting conditions.

- **SW1990:** human pancreatic tumor cell line established from a metastatic PDAC in the spleen. This cell line has a heterozygous KRAS G12V mutation, and it is independent of KRAS at low serum conditions.
- **PA-TU 8988-T:** human pancreatic tumor cell line established from a metastatic PDAC in the liver. This cell line has a heterozygous KRAS G12V mutation, and it is independent of KRAS at low serum conditions.
- **PANC-1:** human pancreatic tumor cell line established from a PDAC. This cell line has a heterozygous KRAS G12D mutation, and it is independent of KRAS at low serum conditions.
- **HeLa:** human cervix adenocarcinoma cell line with no KRAS mutations. It was obtained from ATCC.
- **hTERT-RPE:** human retinal pigmented epithelial normal cell line immortalized with hTERT. It was obtained from ATCC.

PDAC cell lines were kindly provided by Prof. Dr. A. Kimmelman (Harvard Medical School, Boston USA).

DLD-1, DLD-1 KO and hTERT-RPE cell lines were maintained in DMEM-HAM's F12 (1:1) while PDAC, HeLa and SW480 cell lines were maintained in DMEM medium. All mediums were supplemented with 10% fetal bovine serum (FBS), 2 mM L-glutamine, 50 U/ml penicillin, 50 µg/ml streptomycin, 1 mM acid pyruvic and 1% nonessential aminoacids. The supplements were filtered before being added to the medium in order to maintain sterility. All cell lines were maintained at 37ºC and 5% partial pressure of CO_2. The manipulation of cells was performed in a laminar flow hood (Mars Safety Class 2), in sterile conditions.

4.2 Cryopreservation

In order to maintain cells during long periods, cell lines were cryopreserved in liquid nitrogen in complete medium containing 10% dimethyl sulfoxide (DMSO) as following. DMSO is a cryoprotective agent that reduces the formation of ice crystals.

Cells from 75 or 150 cm^2 cell culture flask were washed three times with Phosphate-Buffered Saline (PBS) from cell culture and 2 or 4 ml of trypsin, respectively, were added. After trypsin inactivation with complete medium, cells were detached from cell culture flask, collected in sterile canonical tubes and centrifuged at 650 g for 5 minutes at 4ºC. Then, supernatants were removed, and pellets were resuspended in 3 ml of complete medium. Three cryotubes were labeled and 0.9 ml of cell suspension was transferred to each of the three cryotubes. Following, 100 µl of DMSO was added to 1 ml final volume. Next, cryotubes were immediately shaken and transferred to dry ice. Finally, vials were stored in a liquid nitrogen container.

When required, frozen cells in cryotubes were slowly thawed by adding small volumes of fresh complete medium, and then collected in a tube containing 10 ml of fresh supplemented medium to dilute DMSO. After spinning at 650 g for 5 minutes at 4ºC, supernatants were removed, and cell pellets were resuspended in 10 ml of complete medium. Finally, cell suspensions were transferred to a 25 or 75 cm^2 cell culture flask.

4.3 Generation of stable cell lines

4.3.1 DLD-1$^{KRASWT/-}$ cells stable expressing oncogenic KRAS phosphomutants

DLD-1 KO (KRASWT/-) stable cell lines expressing either HA-KRAS-G12V-**S**181, HA-KRAS-G12V-S181**A**, or HA-KRAS-G12V-S181**D** were obtained from DLD-1 KO cells after being transfected with the specific HA-KRAS-G12V plasmids[117] (1 µg) and a puromycin resistance plasmid (pSG5A) (25 ng) in a proportion 40:1 for 24 hours, using lipofectamine 2000. The day

of transfection cells were at 80% confluence. Following, cells were seeded in p100 dishes (87 mm) and next day selected with 4 µg/ml puromycin. After selection, clones or pools were obtained and the expression levels of exogenous oncogenic KRAS phosphomutants were analyzed.

4.3.2 SW480 cells stable expressing oncogenic KRAS-S181A

SW480 cells with one oncogenic KRAS allele containing the S181**A** mutation was generated by single guide Cas9-based CRISPR technology. The PAM, guide and ssODN were chosen as previously indicated [339]. Guide was cloned in pSpCas9(BB)-2A-Puro plasmid in BbsI site. Cells (35 mm plate (p35), 80% confluence) were transfected with HA-KRAS-G12V-S181**A** plasmid (1 µg) plus the ssODN (1.25 µg) using GeneJet *in vitro* DNA Transfection Reagent. After 4 hours, SCR7 (inhibitor of NHEJ) at 1 µM final concentration was added and 20 hours later cells were seeded in a p100 plate. 24 hours later (48 hours after transfection) puromycin was added for further 24 hours at 4.25 µg/ml final concentration. Clones resistant to puromycin were collected 2 weeks later. Specific PCR primers for the modified sequence of the DNA and DNA Sanger sequencing were used to identify knock-in clones. mRNA and cDNA from the clones used in this work were obtained, and the full sequence of KRAS cDNA was checked.

Guide: TTAAGGCATACTAGTACAAG

PAM: TGG (SpCas9 3'side): On target score 56.3[340] Off target score 79.8[341]

ssODN KRAS 181A:

CTTCTATACATTAGTTCGAGAAATTCGAAAACATAAAGAAAAGATGAGCAAAGATGGTAAAAAGA
AGAAAAAGAAGGCCAAAACTAAGTGTGTAATTATGTAAATACAATTTGTACTTTTTTCTTAAGGCAT
ACTAGTACAAGTGATAATTTTTGTACATTACACTAAATTATTAGCATTTGTTTTAGCATTACCTAATT

5. Bacterial transformation

Transformation is the genetic alteration of bacterial cells resulting from the direct uptake and incorporation of exogenous DNA through the cell membrane. It is a technique employed to amplify DNA. A tube containing frozen Dh5α competent E. Coli cells was thawed for 30 minutes on ice. Next, 50 µl of cells were incubated with 0.5 µg of DNA plasmid for 30 minutes on ice; and then heat-shocked at 42ºC for 45 seconds by placing the tube in a dry bath. Immediately, cells were transferred to ice for 2 minutes. Hereinafter all steps were performed on sterile conditions (near flame). Consecutively, 0.8 ml of sterile L-Broth (LB) without antibiotics were added to the cells and incubated for 1 hour at 37ºC. After that, 100 µl of cells were plated on a LB/Agar plate containing the antibiotic for selection (plasmids used for bacterial transformation have a specific antibiotic resistance); and the rest of the cells were centrifuged at 2400 g for 30 seconds. Most of LB was removed, leaving 100 µl to resuspend the cells which were seed on a new LB/Agar plate containing antibiotic. Finally, plates were incubated upside down overnight (O.N) at 37ºC.

Next day, surviving bacterial colonies were those that had incorporated the plasmid since they were resistant to the antibiotic. Three colonies were selected and introduced in three different tubes containing 6 ml of LB with the antibiotic of selection. Then, transformed bacteria were incubated shaking at 37ºC O.N to let them grow. Finally, to maintain the cells for a longer period, 1.5 ml of bacteria were collected in a cryotube. Subsequently, 0.5 ml of glycerol (60%) were added, mixed and the cryotubes rapidly stored at -80ºC. The remaining bacterial culture (4.5 ml) was used to plasmid purification.

5.1 Plasmid purification

PureYield™ Plasmid Miniprep System (to obtain 15 µg of DNA) or NucleoBond®Xtra Midi system (to obtain until 750 µg of DNA) were used to purify the amplified plasmids from transformed bacteria. In both cases manufacturer's instructions were followed.

DNA concentration was quantified using a nanodrop (ThermoFisher Scientific), and DNA sequencing was outsourced to the Sequencing Service of CSIC-IRTA, UAB campus, CRAIG building, Bellaterra.

5.2 Cell transfection

Cells were transiently transfected following the commercial protocol of Lipofectamine™. Lipofectamine creates liposomes around the vectors which are introduced into the cells through the plasma membrane, allowing the expression of proteins of interest. Briefly, cells were cultured in p60 plates (53 mm) to be 70% confluent the day of the transfection. 15 µg of DNA and 30 µl of Lipofectamine were added into two different tubes containing 0.5 ml of non-supplemented DMEM. Then, both solutions were mixed and incubated for 20 minutes at room temperature (RT). Meanwhile, cells were washed with PBS from cell culture and 9.5 ml of DMEM (supplemented, except with antibiotics to avoid lipofectamine inhibition) was added. After that, the mixture containing DNA and Lipofectamine was poured in the cells and incubated for 6 hours. Finally, the medium was replaced by complete fresh medium, and cells were collected after 48 hours.

6. Electrophoresis and Western Blot (WB)

6.1 Sample preparation

6.1.1 Cell lysates

Cultured cells were washed three times with cold PBS and lysed in a buffer containing 67 mM Tris-HCl pH 6.8, and 2% Sodium dodecyl sulfate (SDS). Cells were collected directly by scraping. Then, samples were heated at 97ºC in a dry bath for 15 minutes and centrifuged at 10000 g for 1 minute at RT. After that, the supernatant was saved for further protein quantification.

6.1.2 Tumors

Tumors were lysed in Ras extraction buffer (REB) supplemented with a cocktail of proteases and phosphatase inhibitors (150 nM Aprotinin; 20 µM Leupeptin; 1 mM PMSF; 5 mM NaF and 0.2 mM Na_2VO_4) and with 1 mM Dithiothreitol (DTT). Initially, the tumors were placed in a tube and maintained on ice. Depending on tumors size, a range between 500 – 900 µl of REB was used. For DLD-1 KO derived tumors (very small), this volume was 200 – 250 µl. Then, tumors were disrupted and homogenized (maintained on ice) using a TissueRuptor (Qiagen). As many disruption cycles as required were applied for 30 seconds at medium speed. Some disruption cycles at full speed were necessary to complete homogenization of the samples. In order to increase the efficiency of the process the tip of the TissueRuptor was continuously stirred within the sample. Once tumor samples were complete homogenized, they were maintained for 10 minutes on ice and centrifuged at 21900 g for 10 minutes at 4ºC. Finally, the supernatant was saved for further protein quantification.

6.2 Protein quantification

In this thesis the Lowry assay for quantification of protein concentration was used. It is based on the Biuret method and consists of two reactions. In the first, peptides react with copper to form a cuprous complex under alkaline conditions. In the second one, the Folin–Ciocalteu reagent (phosphomolybdic/phosphotungstic acid) is added. This interacts with the cuprous ions and oxidizes tyrosine, tryptophan, and cysteine to produce the blue-green color heteropolymolybdenum, which absorbs light at 750 nm. The Lowry assay was performed in 96-well plates and different concentrations of Bovine Serum Albumin (BSA) (from a 1 µg/µl stock solution) as standards for calibration were used.

First, samples and standards were prepared twice as indicated in table 8. Then, the Lowry solution A was prepared following the 48:1:1 ratio of solutions 1 (2% Na_2CO_3 and 0.1 M NaOH), 2 (0.5% $CuSO_4$) and 3 (1% sodium potassium tartrate).

Table 8. Volumes required for standard curve and samples.

	BSA (µL)	Sample (µL)	Lysis buffer (µL)	H_2O (µL)
Standard curve	**0**	-	2	43
	1	-	2	42
	2	-	2	41
	4	-	2	39
	8	-	2	35
	16	-	2	27
	32	-	2	11
	40	-	2	3
Sample	**-**	2	-	43

Next, 225 µl of Lowry solution A were added to each well, mixed well by pipetting and incubated for 10 minutes at RT.

Meanwhile, the Lowry solution B was prepared following the 1:1 ratio of Folin- Ciocalteu reagent and deionized water. Next, 22.5 µl of Lowry solution B were added to each well and mixed well by pipetting. After an incubation for 30 minutes at RT, absorbance at 750 nm was measured in a multimode plate reader (Spark®, TECAN). The simple linear regression was assessed with the standards absorbance values. Finally, the average of absorbance values of each sample was interpolated, and protein concentration was calculated.

Once protein concentrations were calculated, 15 or 20 µg of protein per sample and buffer 4X were prepared for SDS-PAGE following the 3:1 ratio.

6.3 SDS Polyacrylamide Gel Electrophoresis (SDS-PAGE)

Electrophoresis is a method of separation and analysis of macromolecules and their fragments based on their size and charge. The SDS-polyacrylamide gels can be prepared at different concentrations of acrylamide, which provides different pores sizes as needed to separate proteins depending on their molecular weight (high polymer concentration for small molecules and vice versa).The SDS added to the samples, to the running buffer and to

the gels is used to negatively charge and denature proteins that are thus directed to anode when an electric field is applied. Proteins advance towards the positive pole at different speed according to their size and in this way, they physically separate one of the others.

Gels are made up of two sections, the stacking that due to its large pores allows the alignment of proteins of the loaded samples; and the resolving with the adequate size pores to let the proteins to separate according to their molecular weight. Depending on the size of the protein to be identified, gels were prepared at different acrylamide concentrations as indicate in the table 9.

Table 9. Volumes of solutions required for resolving and stacking gel preparation.

	Resolving gel				**Stacking gel**
	6%	**8%**	**10%**	**12%**	
Solution 1 (ml) 0.75M Tris-HCl pH 8.8, 0.2% SDS	5	5	5	5	-
Solution 2 (ml) 30% Acrylamide, 0.8% Bis-acrylamide	2	2.8	3.4	4	0.36
Solution 3 (ml) 0.25M Tris-HCl pH 6.8, 0.2% SDS	-	-	-	-	1.5
H_2O (ml)	3	2.2	1.6	1	1.2
Temed (µl)	14	14	14	14	7.5
Ammonium persulfate (APS) 13% (µl)	50	50	50	50	30

Once the resolving gel was prepared by adding the polymerizing agents (Temed and APS) the last, the mix was poured between the two glasses of the gel building structure. Then, 1 ml of deionized water was carefully added on top to allow acrylamide polymerization, which requires oxygen-free conditions. Next, after removing the water, the freshly prepared stacking mix was poured on top of resolving gel and the comb was inserted quickly to set up the loading wells.

Finally, the polymerized gel together with the glasses were assembled on the electrophoresis system (Mini-PROTEAN, BioRad) filled with running buffer, and the comb was removed. Samples and molecular weight marker (Precision All Blue or Low or High Range Unstained Protein Standards) were loaded into the wells using a Hamilton syringe. A constant current of 35 mA per gel was applied until the colored front of the samples reached the end of the gel. Next, the electro-transference of the proteins from the gel to a blotting membrane was performed.

6.4 Protein transfer to a blotting membrane

Once proteins were separated by their molecular weight in an SDS-gel, they were transferred to polyvinylidene fluoride (PVDF) membrane in order to perform WB.

First, since PVDF membranes are hydrophobic they were hydrated with an alcohol solution above 50% (methanol in this case) for 30 seconds, and then soaked in water and in transfer buffer for 2 minutes each. After that, gel and membrane sandwich were assembled within a gel holder cassette, stacked and placed into the transfer tank, and transferred to transfer bucket filled with buffer, as visualize in figure 26. Sponges and filter paper sheets (Whatman), used to build up pressure inside the cassette, were previously soaked in transfer buffer.

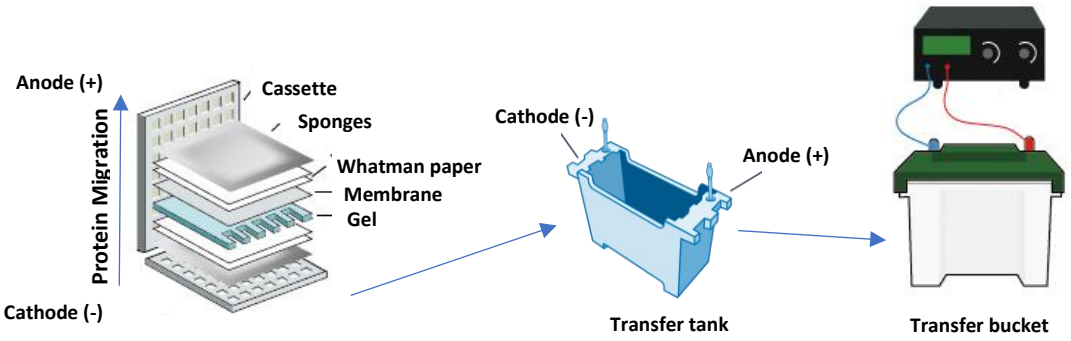

Figure 26. Diagram of protein transfer from gel to PVDF membrane. (*Adapted from https://www.creative-diagnostics.com/The-Basis-of-Western-Blot.htm*.*

Electro-transfer was performed at 70 V for 2 hours or at 20 V O.N in the refrigerator (4ºC). Finally, when transfer was finalized, membranes were dried for further analysis.

6. 5 Total protein detection: Ponceau S staining

The ponceau S staining is a sodium salt of diazo dye used to do a rapid and reversible stain to visualize proteins bands on nitrocellulose or PVDF membranes. When the membranes are washed with water the dye is removed. During this thesis, the Ponceau staining has been used to check the efficacy of the electrophoresis and protein transfer as well as if the samples were correctly loaded. Additionally, it allowed us to visualize the protein standards.

Therefore, once the membranes were dried, they were incubated with Ponceau for 1 minute at RT. Then, protein standards were marked with a pencil and the excess of staining was eliminated after several washes with distilled water.

6.6 Blocking

Since PDVF membranes has a high capacity to bind proteins, in order to avoid non-specific bindings during incubation with the antibodies, membranes must be blocked. In this thesis, membranes were saturated with a solution of BSA in Tris Buffer Saline (TBS).

After Ponceau staining, membranes were completely dried again. Next, they were rehydrated with methanol for 30 seconds, and then soaked in water and in TBS for 2 minutes each. Finally, blocking was performed by incubating the membranes in a 5% BSA solution in TBS for 1 hour at RT by shaking.

6.7 Western blot: Immunological detection

6.7.1 Hybridization with primary and secondary antibodies

In order to detect specific proteins among those transferred, the blotting membrane is incubated with primary antibodies that specifically recognize the protein of interest. Another incubation with secondary antibodies, directed to the constant domain of the primary antibodies and usually linked to a reporter enzyme, allows visualization.

So, once blocked, membranes were incubated with the primary antibodies diluted in TBS-Tween 20 (TBS-T) containing 5% of BSA O.N at 4ºC by shaking.

Next day, the excess of primary antibody was removed by washing the membrane three times for 10 minutes with TBS-T at RT by shaking. Then, membranes were incubated with secondary antibodies diluted in a solution of 2.5% of milk powder in TBS for 1 hour at RT by shaking. Finally, the excess of secondary antibody was removed by washing the membrane three times for 10 minutes with TBS-T at RT by shaking and maintained in TBS until protein visualization.

6.7.2 Chemiluminescence detection and imaging

The last step of WB is to detect the proteins of interest that have been labeled with specific antibodies. In this thesis, the reporter enzyme horseradish peroxidase coupled to the secondary antibodies was used. This catalyst oxidizes luminol when peroxide hydrogen is added, a reaction that radiates light (chemiluminescence). Protein detection was assessed by the enhanced chemiluminescence system using the ECL-EZ detection kit and light emitted was captioned and quantified with the ChemiDoc imaging system (BioRad).

7. Cell proliferation and survival assays

In order to study cell proliferation and survival different experimental approaches were followed during this thesis.

7.1 Cell proliferation assay based on crystal violet staining

Crystal violet dye interacts with DNA and proteins; thus, it allows to detect and quantify adhered cells, which corresponds to living cells at the time of staining. Since dead cells miss their adherent properties, they are lost during the staining protocol.

$3x10^4$ cells were seeded in triplicates in 12-well plates in DMEM-HAM's F12 10% FBS. Cells were washed twice with cold PBS and fixed with 0.4 ml paraformaldehyde (PFA) 4% in PBS for 15 minutes after 24, 48, 72 and 96 hours. After washing twice with PBS, cells were stained with 0.25% crystal violet in deionized water for 5 minutes. Then, cells were washed several times with distillated water to remove the excess of dye. After drying, absorbance was measured with a multimode plate reader (Spark, Tecan, Männerdorf, Switzerland) at 595 nm. The absorbance measured of wells without cells was used as a reference. Finally, proliferation ratio was calculated for each clone at 96 hours with respect to 24 hours.

7.2 Cell cycle analysis by flow cytometry

Flow cytometry allows to examine the cell cycle from different perspectives. In this thesis, the DNA content, the percentage of cells in S phase and the percentage of mitotic cells have been studied by combining propidium iodide (PI) DNA staining, bromodeoxyuridine (BrdU, thymidine analog) incorporation into DNA, and mitosis specific antibodies (MPM-2), respectively. Accordingly, cells were cultured in 35 mm plates under serum-limiting conditions for 48 hours and then, incubated with 10 μM of BrdU for 30 minutes. After that, the cell culture medium containing detached cells was transferred to a canonical tube. The attached cells remaining in the plate were washed three times with 1 ml cold PBS and then

incubated with 0.4 ml trypsin for 5 minutes. After trypsin inactivation with 1 ml DMEM-HAM's F12 10%FBS, cells were collected to the same previous tube, and centrifuged at 650 g for 5 minutes at 4ºC. Pellets were washed with 3 ml cold PBS and centrifuged at 650 g for 5 minutes at 4ºC. Finally, they were resuspended with 5 ml of cold PBS diluted 1:10 in cold ethanol 70% and kept at -20ºC for 2 hours to fix the cells. Samples can be stored at -20ºC for several months.

Fixed cells were centrifuged at 650 g for 5 minutes at 4ºC, washed with 3 ml PBS-Tween 20 (PBS-T) to remove the ethanol and centrifuged again. For DNA denaturalization, cells were incubated in 2 ml 2M HCL diluted in PBS containing 0.1% Triton X-100 for 15 minutes at RT. Then, HCL was neutralized with 4 ml borate buffer pH 8.5 and cells were centrifuged at 650 g for 5 minutes at 4ºC. The last step was repeated twice. After that, cells were washed with 3 ml PBS-T, centrifuged and incubated in 1 ml blocking solution (PBS-T containing 3% of BSA) for 1 hour at RT, in Eppendorf tubes. Next, cells were centrifuged as above and then incubated with both primary antibodies anti-BrdU (1:250) and anti-MPM2 (1:250) diluted in blocking solution for 1 hour at RT in rotation (50 µl/sample). Later, cells were centrifuged at 650 g for 5 min at RT and washed with 1 ml PBS-T. Then, they were incubated with both secondary antibodies Alexa488-conjugated anti-rat (1:400) and Alexa647-conjugated anti-mouse (1:500) protected from light for 45 minutes at RT (50 µl/sample). Finally, cells were again centrifuged and washed with 1 ml PBS-T, and then resuspended and incubated in 0.5 ml PBS containing 1% PI and 0.1 µg/µl RNAse for 30 minutes at 37ºC. Flow cytometry analysis was performed with the BD FACSCalibur™ Cell Analyzer and the data was analyzed with FlowJo software.

7.3 Cell viability assay (MTT)

MTT is a colorimetric assay that is performed to assess metabolic cell activity and therefore, cell viability. The reduction of tetrazolium dye MTT [3-(4,5-dimethylthiazol-2-yl)-2,5-diphenyltetrazolium bromide] to formazan, which depends on mitochondrial activity, allows

to reflect the percentage of viable cells. Specifically, the cell viability is observed when the MTT, a yellow compound, is reduced to formazan, a dark purple no soluble molecule, which is solubilized by adding an acidified 2-propanol solution. The absorbance of this dark compound can be detected at specific wavelength (maximum peak around 630nm). MTT assays are usually performed to test the biological effects of a drug or compound on cell viability, but in our case, it was used to analyze and compare survival between different cell lines under serum starved conditions for 48 hours.

$5x10^3$ cells were resuspended in 100 µl DMEM-HAM's F12 0.1% FBS and seeded in sextuplicate in two 96-well plates. In order to define the initial conditions, the day after seeding, cell viability was quantified in one of the plates using MTT Cell Growth Assay Kit following the manufacturer's instructions. Briefly, cells were treated with 10 µl of AB solution and incubated at 37ºC for 4 hours. Then, 100 µl isopropanol with 0,04 N HCl was added and mixed thoroughly by pipetting. Absorbance was measured at 570 nm and at 630 nm, as a reference, using a multimode plate reader (Spark, Tecan). The second plate was incubated under 0.1% FBS conditions since then for 48 hours more, and then quantified with MTT Cell Growth Assay Kit as mentioned above. The defined final conditions were relativized to the initial ones, and a cell viability ratio was obtained for each cell clone.

8. Annexin V assay

Annexin V apoptosis assay is used to determine the number of apoptotic cells within a cell population. Annexin V is a Ca^{2+} dependent phospholipid-binding protein, which binds to cells with exposed PtdSer. In the apoptotic cells PtdSer residues, which are localized in the inner layer of the plasma membrane in healthy cells, translocate to the outer layer, consequently being exposed to the external cell environment. This method takes advantage of this event and consist of incubating the cells with Annexin V conjugated with a

fluorophore (APC). The fluorescent protein will only be able to bind to apoptotic cells since are the only ones with exposed PS, thus allowing their detection.

In this thesis, cells were seeded in 35 mm plates and cultured in DMEM-HAM's F12 0.1% FBS for 48 hours. After that, the cell culture medium containing detached cells was transferred to a canonical tube. The attached cells remaining in the plate were washed three times with 1 ml cold PBS and then incubated with 0.4 ml trypsin for 5 minutes. After trypsin inactivation with 1 ml DMEM-HAM's F12 10%FBS, cells were transferred to the same previous tube, and centrifuged at 650 g for 5 minutes at 4ºC. Following, cells were resuspended (without previous permeabilization) with 0.5 ml Annexin V binding Buffer 1X (Annexin V binding buffer 10X diluted 1:10 in PBS) containing 2 µl APC Annexin V and 0.1 µg/ml PI. Cells were incubated for 15 minutes with this solution and immediately examined by flow cytometry with BD FACSCalibur™ Cell Analyzer. The data generated were analyzed with the FlowJo software.

9. Cell migration assay

The Boyden chamber assay (or transwell cell migration assay) is a method to measure the capacity of cells to move towards a chemo-attractant gradient. It is based on a chamber of two medium-filled compartments separated by a microporous membrane (8 µm pore size in this case). The cells are placed in the upper compartment and are allowed to migrate through the microporous into the lower compartment, filled with chemotactic agents.

In this thesis, previously seeding, the upper compartment was covered over night with DMEM-HAM's F12 0.1% FBS. The lower compartment was filled with 0.6 ml of DMEM-HAM's F12 10% FBS as an attractor. Next day, the medium of the upper compartment was removed and $5x10^4$ cells resuspended in 100 µl DMEM-HAM's F12 0.1% FBS were seeded. After 72 hours, nuclei of cells were stained with 5 µg/ml Hoechst for 1 hour. Hoechst was directly

added to the upper and lower compartments. Finally, cells that had moved through the membrane were visualized by SP5 confocal microscopy (Leica). Migrating cells in 4 consecutive high-power fields (objective 63X) were obtained. Cells were counted using Image J software and the mean was calculated.

10. 3D cell culture assays

10.1 Soft Agar colony formation assay

The soft agar colony formation assay is an *in vitro* method to study the capability of cells to grow independently of a solid surface (anchorage-independent growth), which is one of the main characteristics of transformed cells.

First, 1 ml 0.5% agar solution (DMEM-HAM's F12 10% FBS, agar solution 2% (previously autoclaved) in a 3:1 proportion) was evenly added in 6-wells plates. It must be taken into consideration that soft agar solution must be maintained at 45ºC before the experiment and during the preparation to avoid its solidification. In order to solidify the agar layer, the 6-wells plates were kept for 15 minutes at 4ºC and then for 10 minutes at RT. Before seeding, the plates were maintained at 37ºC in the incubators. Then, $3x10^3$ cells diluted in 1 ml of 0.3% agar solution (DMEM-HAM's F12 10% FBS, agar solution 0.6% (previously autoclaved) in a 1:1 proportion) were seeded in triplicates in the 6-well plates containing the 0.5% agar layer. Finally, the plates were placed at 37ºC in the incubator for 20 minutes and then, 1 ml DMEM-HAM's F12 10% FBS was added to each well. After 10 days, images of the colonies grown in soft agar were obtained by the MZSLIII stereomicroscope (Leica). Colonies were counted using the Image J Software.

10.2 Matrigel-based 3D cell culture *in vitro*

Matrigel is a basement membrane mixture extracted from the Engelbreth-Holm-Swarm (EHS) mouse carcinoma. This hydrogel contains the following extracellular matrix (ECM) components: laminin, collagen IV, heparan sulfate proteoglycans, entactin/nidogen, and several growth factors. It is used as *in vitro* model of 3D cell culture that better mimics the cell growth conditions *in vivo*.

3D on-top Matrigel assay was performed following the Materials and Methods protocol from Nat. Methods (figure 27)[342]. It must be taken into consideration that Matrigel and material required must be maintained at 4ºC before the experiment and during the preparation to avoid its solidification.

Before seeding, 24-wells plates were evenly covered with 120 µl of Matrigel (8.1 mg/ml and <1.5 mg/ml endotoxin) and placed at 37ºC for 30 minutes to let it to solidify. Then, plates were washed with 0.5 ml of non-supplemented medium to remove the excess of Matrigel. After that, $2.5x10^4$ cells suspended in 0.4 ml DMEM-HAM's F12 supplemented with 1% of ITS (Insulin, Transferrin and Sodium Selenite) were seeded in triplicates in the Matrigel-containing 24-well plates. Subsequently, the plates were moved at 37ºC for 30 minutes and gently waved every 5 minutes. Finally, cells were overlaid with 250 µl of a 10% solution of the same matrix diluted in DMEM-HAM's F12 supplemented with 1% of ITS. Images of the cells growing in 3D (structures defined by us as organoid-like by their similarity to the morphology of organoids) were taken with the phase-contrast microscope at day 3 and 7.

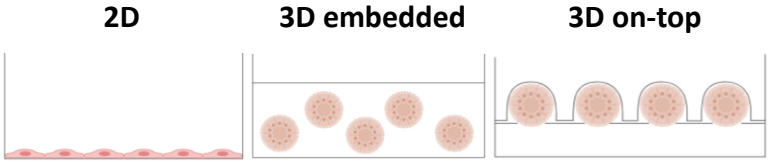

Figure 27. Scheme of cells growing on cell culture plastic (2D) (left), in the 3D embedded assay (middle), and in the 3D on-top assay (right). *Adapted from Nat. Methods protocol*[342].

10.3 Immunofluorescence of cells growing in Matrigel-based 3D cell culture

Organoid-like structures of growing cells were fixed and directly immunostained following option C of the protocol for whole-culture fixation[342]. This method was used to avoid disruption of the 3D organization of the cells during the process of extraction from Matrigel.

After seven days of being the cells growing in Matrigel, the medium was removed, and the organoid-like structures were washed twice with 0.5 ml cold PBS and fixed with 0.4 ml PFA 4% for 10 minutes at RT. Then, they were rinsed twice with 0.3 ml PBS containing 100 mM glycine for 10 minutes at RT to stop the fixation. After washing once with 1 ml PBS, they were stored in PBS O.N at 4ºC. Fixed 3D cultures may be stored at 4 °C for up to 4 days. Next day, PBS was removed, and cells were permeabilized with 0.5 ml PBS containing 0.1% of saponin for 5 minutes at RT and blocked with 0.5 ml 1% BSA-PBS for 1 hour at 37ºC. After blocking, the cells were incubated with the primary antibodies diluted in 0.4 ml PBS containing 0.1% BSA-0.02% saponin for 1 hour and 30 minutes at 37ºC. Then, the organoid-like structures were washed three times with 1 ml PBS and were incubated with the secondary antibodies diluted in 0.4 ml PBS containing 0.1% BSA-0.02% saponin for 1 hour at 37ºC. Finally, they were washed three times with 1 ml PBS and nuclei were counterstained with DAPI (1 mg/ml, 1:10000) for 5 minutes. After washing, they were covered with Mowiol mounting medium. Confocal sections of the cells were obtained with the LSM880 confocal microscope (ZEISS).

10.4 Cell invasion assay

The Boyden chamber assay is also used to analyze the invasive capacity of cells. The difference is that in this type of experiment, the upper compartment of the chamber is previously covered with Matrigel, thus cell invasiveness instead of migration capability can be tested. As mentioned above, Matrigel and material required must be maintained at 4ºC before the experiment and during the preparation of the transwells.

In this thesis, previously seeding, the upper compartment of Boyden chamber was covered with 100 µl of 1 mg/ml of Matrigel diluted in DMEM supplemented with penicillin and streptomycin and left O.N at 37ºC to let the matrix to solidify. The lower compartment was filled with 0.6 ml DMEM-HAM's F12 10% FBS (for DLD-1 cells) or DMEM 10% FBS (for SW480 cells) as an attractor.

Next day, once Matrigel was solidified the medium of upper compartment was removed. Then, $5x10^4$ (DLD-1) or $6x10^4$ (SW480) cells resuspended in 100 µl of culture medium supplemented with 0.1% FBS were seeded in the upper compartment for 72 or 48 hours, respectively. Finally, nuclei were stained with 5 µg/ml Hoechst for 1 hour. Cells that had moved through the membrane were visualized by SP5 confocal microscopy (Leica). Invading cells in 4 consecutive high-power fields (objective 63X) were obtained. Cells were counted using Image J software and the mean was calculated.

11. RNA extraction

Cells were cultured under growth factors conditions and total RNA was isolated using the RNeasy Mini Kit following manufacturer's instructions. Briefly, RNA extraction is based on disruption and homogenization of the cells with a specific buffer followed by ethanol addition to create conditions that promote selective binding of RNA to the RNeasy membrane. Then, the samples are applied to the RNeasy Mini spin column and total RNA binds to the membrane. At the end, contaminants are efficiently washed away, and RNA is eluted in RNAse-free water. All binding, wash and elution steps are performed by centrifugation. The obtained RNA was quantified using a nanodrop (Thermo Fisher Scientific).

12. Microarray analysis

Microarray analysis was performed in order to analyse gene expression of cells in 2D cell culture under growth factor conditions. To test this, cells were cultured in DMEM-HAM's F12 supplemented with 10% FBS and total RNA was isolated using the RNeasy Mini Kit following manufacturer's instructions. RNA integrity was confirmed in a Bioanalyzer 2100 (Agilent). Transcriptomes were determined on a genome wide GeneChip PrimeView Human Gene Array (Affimetrix).

12.1 Gene expression analysis

Transcriptome Analysis Console (TAC) Software (Thermo Fisher Scientific) was used to normalize raw CEL files using Robust Multichip Average (RMA) algorithm. Normalized expression values were used to determine the fold change (FC) expression between clones and its statistical significance using ebayes Anova Method (p-value). To generate lists of differentially expressed genes between clones a cut-off of FDR<0.05 or 0.01 (false discovery rate) was used as indicated in the results. Hierarchical clustering (linkage WPGMA) of proves and cell clones using expression data (Log2) was performed using Genesis programme Release 1.8.1[343]. Gene set enrichment analyzes (GSEA) were performed with the GSEA platform of the Broad Institute (http://www.broadinstitute.org/gsea)[344]. Publicly available gene sets database MSigDB version v7.0 sub collection C6 oncogenic gene sets were used. The CANCERTOOL (http://web.bioinformatics.cicbiogune.es/CANCERTOOL/)[345] web-based interface was used to analyze in the public clinical cohort GSE39582[346]: (a) correlation (Pearson's Coefficient) between the expression of different transcripts in CRC primary tumors, (b) differential expression of specific transcripts between control and CRC primary tumors and, (c) Disease Free Survival (DFS) curves.

13. Quantitative Real-Time PCR (RT-qPCR)

1 µg RNA was reversed transcribed to complementary DNA (cDNA) using the high capacity cDNA reverse transcription kit. The reversed transcription was performed following the manufacturer's instructions. Briefly, the reverse transcription master mix was prepared. Then, 1 µg RNA diluted in a final volume of 10 µl RNAse-free water was mixed with 10 µl of this master mix. Finally, the thermal cycler was applied as indicate in the table 10.

Table 10. Thermal cycler of reverse transcription followed.

Settings	Step 1	Step 2	Step 3	Step 4
Temperature	25ºC	37ºC	85ºC	4ºC
Time	10 min.	2 hours	5 min.	Forever

After reverse transcription, RT-qPCR was performed with GoTaq® qPCR master mix using the real time LightCycler® 96 (LifeScience Roche) and following the manufacturer's specifications. The GoTaq® qPCR master mix system contains a fluorescent DNA-binding dye, the BRYT Green® Dye, that exhibits greater fluorescence enhancement upon binding to double stranded DNA (dsDNA) than SYBR® Green I. Concisely, the GoTaq® qPCR reaction mix was prepared by combining primers, water and GoTaq® qPCR master mix. The primers set sequences of target genes used are indicated in the table 11. After that, 2 µl of cDNA were added to PCR real time tubes in strip with 10.5 µl of the reaction mix. Finally, the thermal cycler was applied as indicate in the table 12.

Table 11. Primer sets of target genes

Target gene	Forward sequence 5' → 3'	Reverse sequence 5' → 3'
HPRT1	TGACACTGGCAAAACAATGCA	GGTCCTTTTCACCAGCAAGCT
CTNNA1	CAGGACTCTGGCAGTTGAGA	GAGCAGGGATCATCTGCGAA
SERPINE1	CGCAACGTGGTTTTCTC	CATGCCCTTGTCATCAATC
PRSS2	CTCTGAGTTCTGGTGCCGAC	CTCCAGGCCTGTTCTTCTGG
HNF4G	ACAGAATAAGCACCAGAAG	TCACAGACATCACCAATAC
TRIB2	ATGAACATACACAGGTCTACCCC	GGGCTGAAACTCTGGCTGG
LGR5	GACTATGCCTTTGGAAACC	GGAGCCCATCAAAGCATT

(a) HPRT1, CTNNA1 and PRSS2 designed with Primer-Blast tool.
(b) SERPINE1 obtained from Mol Cancer. 2019 May;17(5):1142-1154[347].
(c) HNF4G obtained from Oncotarget. 2017 Dec 4;9(26):18018-18028[348].
(d) TRIB2 obtained from Mol Cancer. 2018 Dec 12;17(1):172[349].
(e) LGR5 obtained from Eugenia Cuesta Borràs doctoral thesis.

Table 12. Thermal cycler of RT-qPCR followed.

Settings	Step 1: Pre-incubation	Step 2: Cycles (40X)			Step 3: Melting		
Temperature	95ºC	95ºC	60ºC	72ºC	95ºC	65ºC	97ºC
Time	10 min.	30 sec.	15 sec.	30 sec.	10 sec.	60 sec.	1 sec

RT-qPCR was performed in triplicates or quadruplicates and mean cycle threshold (Ct) values were calculated for the expression analysis. HPRT1 mRNA expression was used as an internal control to normalize mRNA expression of target genes. The mRNA expression levels were calculated using 2^{-DDCt} method[350].

14. Tumor generation in mice

The day of the injection, $2x10^6$ DLD-$1^{KRASWT/-}$ cells stably expressing KRAS-G12V-**S**181, -S181**A** or S181**D** (one clone of each phosphomutant was selected) resuspended in 50 µl PBS from cell culture were subcutaneously injected into both flank of Swiss nude mice (Foxn$1^{-/-}$, defective development of the thymic epithelium). Mice were maintained in germ free environment at 25ºC, five mice per box, and kept at 12 hours light/dark cycle. They received autoclaved food pellets and water ad libitum.

Generated tumors were measured on days 12, 15, 19, 23 after injection and on the day of euthanasia, using a caliper. Mice were euthanized by cervical dislocation at day 28 after injection and tumors were harvested, weighed, measured and processed for analysis (each group = 4 tumors). The volume of the tumors was calculated using the ellipsoid volume formulas 1/2 x (L x W^2) and 1/2 x (L x W x H)[351–353].

For histology and immunohistology, tumors were immediately fixed in 4% buffered formalin solution. For WB analysis, tumors were immediately frozen with dry ice and transferred to -80ºC for long-period storage. Tumor sample preparation for WB and tumor processing for histology are detailed in the section 6.1.2 and section 14.1, respectively.

All mouse experiments were performed in accordance with protocols approved by the Animal Care and Use Committee of ICO-IDIBELL Hospitalet de Llobregat (Barcelona, Spain).

14.1 Histology of the tumors

For histological analysis, tumors were processed routinely: fixed, dehydrated and embedded in paraffin. Serial longitudinal sections of 5-6 µm-thickness were obtained.

Slide-mounted tumor sections were stained following hematoxylin and eosin routine procedure (*section 14.1.1*) to study the histological appearance. Immunohistochemistry standard protocols (*section 14.1.2*) and TUNEL assay (*section 14.1.3*) were also applied.

14.1.1 Hematoxylin and Eosin staining (H&E)

H&E staining is one of the principal techniques used in the histological analysis. This method is a combination of hematoxylin stain, which dyes cell nuclei blue , and of eosin stain which dyes the extracellular matrix and cytoplasm pink.

Once tumor sections were slide-mounted, they were incubated for 30 minutes at 60ºC; and then, were deparaffined by immersion in xylol three times for 10 minutes each. Next, the slides were rehydrated by immersion in decreasing concentrations of ethanol: 100%, 96% and 70% and distilled water for 7 minutes each.

Following, the slides were stained with hematoxylin for 5 minutes and rinsed in running water for 5 minutes to remove the excess dye. After staining, they were immersed in 1% HCL diluted in ethanol 96% for 4 seconds (to change the color tone of hematoxylin) and immediately, were rinsed in running water for 5 minutes. Then, the slides were submerged in ethanol 96% for 1 minute and stained with eosin solution (table 7), diluted in ethanol 70% in a 1:3 proportion, for 5 minutes. Next, they were immersed 4 o 5 times in distilled water and dehydrated by means of quick 4 o 5 times immersions in each increasing concentrations of ethanol: 70%, 96% and 100%. Eosin can be completely removed by ethanol; thus, a rapid dehydration of the tumor sections was performed to prevent it. Afterwards, they were immersed in xylol three times for 10 minutes each. Finally, in order to fix the stained tumor sections, a drop of DPX (resin-based slide mounting medium soluble in xylol) was added on top and immediately the coverslip was placed, taking care to leave no bubbles. The slides were dried O.N in the extractor hood.

14.1.2 Immunohistochemistry (IHC)

With the aim of analyzing cell proliferation in tumors, IHC using specific antibodies against Ki-67 and phospho-histone H3 as markers of proliferating and mitotic cells, respectively, were performed.

Once tumor sections were slide-mounted, they were incubated for 30 minutes at 60ºC; and then, were deparaffined by immersion in xylol three times of 5 minutes each. Next, the slides were rehydrated by immersion in decreasing concentrations of ethanol: three times in ethanol 100% and 96% for 5 minutes each, and once in ethanol 70% and distilled water for 5 minutes each.

After that, antigen retrieval to unmask the antigenic epitopes was performed. The most commonly antigen retrieval used is the citrate buffer method. Therefore, the slides were arranged in a pressure cooker filled with 1 l of citrate buffer pH 6.0 and incubated for 5 minutes at 95-100ºC (buffer must be boiled). Next, the pressure cooker was removed from heater, and the slides were cooled for 20 minutes at RT within the citrate buffer. Then, they were washed with distilled water for 5 minutes. In order to block the endogenous peroxidase activity, the slides were incubated in PBS containing 3% H_2O_2 solution and 30% methanol for 10 minutes at RT. Following, they were washed with distilled water for 5 minutes and with PBS-T for 10 minutes. After that, the slides were blocked with PBS-T containing 2% BSA and 20% FBS (200 µl/slide) for 2 hours in a humidified chamber at RT. Finally, blocking solution was removed and tumor sections were incubated with anti-Ki-67 (1:100) or anti-P-H3 (1:100) primary antibodies diluted in PBS (100µl/slide), O.N in a humidified chamber at 4ºC.

Next day, the slides were washed twice with PBS-T and once with PBS. Incubation with the secondary antibody was carried out using the Ultra-Sensitive ABC peroxidase staining kit following the manufacturer's instructions. The advantage of the avidin-biotin complex (ABC) system is the formation of large complexes that enhance the signal. Briefly, the tumors sections were incubated with the biotinylated secondary antibody diluted 1:200 in PBS containing a goat blocking serum (100 µl/slide) for 30 minutes in a humidified chamber at RT. After been washed twice with PBS-T and once with PBS, samples were incubated with the ABC system. The ABC system was performed by incubating the slides with the reagents A (Avidin) and B (biotinylated horseradish peroxidase (HRP)) in a 1:1 proportion diluted in PBS (100 µl/slide) for 30 minutes in a humidified chamber protected from light at RT. Then, the slides were washed twice with PBS-T and once with PBS. The signal was developed by

incubating the slides with 200 µl PBS containing 1 mg/ml DAB (Diaminobenzidine) and 0.03% H_2O_2 for 5-10 minutes. The reaction between hydrogen peroxide and DAB catalyzed by the peroxidase activity of biotin gives a brown insoluble product. DAB is a suspected carcinogen, so it must be handled with care and residues must be inactivated with bleach. After developing, the slides were washed with running water to stop the reaction and were counterstained by been submerged 4 o 5 times in hematoxylin diluted 1:10 in deionized water. Next, tumor sections were rinsed in running water and dehydrated by immersion in increasing concentrations of ethanol: once in ethanol 70%, and three times in ethanol 96% and 100% for 5 minutes each. Afterwards, they were immersed in xylol three times for 5 minutes each. Finally, a drop of DPX was added on top and immediately the coverslip was placed, taking care to leave no bubbles. The slides were dried O.N in the extractor hood.

14.1.3 TUNEL assay for apoptotic cells detection

In order to study the apoptotic cells in the tumor sections the The DeadEnd™, Colorimetric TUNEL System was performed following the manufacturer's instructions. This assay is used to detect apoptotic cells in situ at single-cell level in tissue sections or cultured cells by visualizing DNA fragmentation. The TUNEL system is based on the incorporation of biotinylated nucleotides at the 3'-OH DNA ends using the Terminal Deoxynucleotidyl Transferase recombinant enzyme (rTdT). The biotinylated nucleotides are able to bind to horseradish peroxidase-labeled streptavidin (streptavidin-HRP), which allows the nucleotides to be detected by adding the HRP substrate DAB. Using this method, apoptotic nuclei are stained dark brown and visualized with a light microscope.

Briefly, tumor slices were deparaffined and rehydrated as indicated in the section 14.1.2. Then, they were washed once with 0.85% NaCl and PBS. Next, they were fixed using PFA 4%, washed with PBS and permeabilized with 20 µg/ml of Proteinase K solution. After washing with PBS, they were fixed again with PFA 4%, washed with PBS and equilibrated with Equilibration buffer at RT. For the DNA labeling, the tumor sections were incubated with the

TdT reaction mix. The reaction was stopped by immersion of the slides in 2X SCC buffer. After washing with PBS, endogenous peroxidase activity was blocked with 0.3% H_2O_2 and the slides were washed again. Finally, samples were incubated with streptavidin-HRP, washed and developed with DAB solution. Once the DAB reaction was stopped by immersion of the slides in deionized water, a drop of DPX was added on top and immediately the coverslip was placed, taking care to leave no bubbles. Finally, they were dried O.N in the extractor hood.

14.2 Generation of metastasis in mice

The day of the injection, $2x10^6$ DLD-$1^{KRASWT/-}$ cells stably expressing KRAS-G12V-**S**181, -S181**A** or S181**D** (one clone of each phosphomutant was selected) resuspended in 50 µl PBS were injected into the spleen of Swiss nude mice (Foxn$1^{-/-}$). After three days, the spleen was removed to avoid the dissemination by hepatic portal system. Mice were regularly monitored to check the generation of metastasis in the liver.

The euthanasia of the mice by cervical dislocation was performed three months after injection. The livers were harvested, and the number of metastasis were counted. Then, the livers were processed for the histological analysis (*section 14.1*) and hematoxylin and eosin routine procedure was applied (*section 14.1.1*).

15. Analysis of peptidomimetics

The effect of treating cells with peptidomimetics against the effector domain of RAS designed by Iproteos technology to inhibit RAS, was analyzed by different biological approaches. The WB analysis was performed as indicated in the section 6.

15.1 Co-immunoprecipitation

Immunoprecipitation (IP) is a technique based on the precipitation of a protein of interest from a cell lysate by using an immune complex. This includes an antibody, which specifically recognizes and binds to that protein, coupled to agarose beads. The agarose beads are the solid substrate that allows the isolation of the system by centrifugation.

Co-IP is an IP of intact protein complexes based on using a specific antibody that targets a known protein of a complex to pull the entire protein complex and thereby identify other components of the complex. Thus, the capacity of peptidomimetics to disrupt the interaction between oncogenic KRAS and its effectors was evaluated by co-IP.

For this analysis, HeLa cells were transfected with pEF-HA-KRAS-G12V plasmid (*see section 5.2 for more details*) for 24 hours and were starved for a further 24 hours. Then, cells were incubated with the different peptidomimetics for 2 hours and EGF (50 ng/ml) for the next 10 minutes. Then, a co-IP with a monoclonal specific anti-HA antibody crosslinked to agarose beads was performed.

First, cells were washed three times with cold PBS, collected in 1 ml cold PBS by scrapping and centrifuged at 650 g for 5 minutes at 4ºC. The pellets of cells were lysed with REB buffer freshly supplemented with a cocktail of proteases and phosphatase inhibitors (150 nM aprotinin; 20 µM leupeptin; 1 mM PMSF; 5 mM NaF and 0.2 mM Na_3VO_4) and with 1 mM DTT. The volume of REB buffer added depended on the pellet size (between 500 – 800 µl). Then, the samples were maintained 10 minutes on ice and centrifuged at 21900 g for 10 minutes at 4ºC. The supernatant (soluble fraction) was kept, and protein quantification was

performed (*See section 6.2 for more details*). After quantification, 40 µg of protein per sample were separated as "input" and stored at -20ºC. Meanwhile, 50 µl per sample of monoclonal anti-HA antibody-agarose beads were washed five times with PBS by centrifugation at 600 g for 30 seconds at RT. After washing, the beads were resuspended with a volume of REB buffer equal to the initial volume taken. Next, 1000 – 2000 µg of protein (soluble fraction) per sample were collected and the volumes between them adjusted by adding REB buffer. After that, samples were incubated with the anti-HA antibody-agarose beads (50 µl per sample) for 3 hours in rotation at 4ºC; and then centrifuged at 21900 g for 2 minutes at 4ºC. The pellets containing the immunocomplexes were named as the "bound fractions", while the supernatants were kept as the "not bound" fractions. The bound fractions were washed five times with 1 ml REB buffer by centrifugation at 600 g for 30 seconds at RT. Finally, SDS-PAGE loading buffer 2X was added to the bound fraction in a 1:1 proportion and the input and not bound fractions were prepared as usual. All samples were subjected to immunoblotting with the required specific antibodies.

15.2 Cell viability assay (MTS)

The effect of the peptidomimetics in the cell viability of six pancreatic adenocarcinoma human cell lines harboring different mutations in oncogenic KRAS and one non-transformed cell line (hTERT-RPE cells) was evaluated using the CellTiter 96® Aqueous One Solution Cell Proliferation Assay. It is a colorimetric method for determining the number of viable cells in proliferation or cytotoxicity assays. The CellTiter 96® AQueous One Solution Reagent contains a novel tetrazolium compound [3-(4,5-dimethylthiazol-2-yl)-5-(3-carboxymethoxyphenyl)-2-(4-sulfophenyl)-2H-tetrazolium, inner salt; MTS] and an electron coupling reagent (phenazine ethosulfate; PES). PES has enhanced chemical stability, which allows it to be combined with MTS to form a stable solution. This advantageous "One Solution" format is an improvement and requires no volatile organic solvent to solubilize the formazan product (unlike MTT).

For this analysis, $1x10^4$ cells were resuspended in 50 µl 10% FBS-containing medium and seeded in sextuplicate in 96-well plates for 24 hours. Then, different concentrations of peptidomimetics diluted in 50 µl of 10 % FBS-containing medium were added for a further 24 hours, following the pattern shown in the figure 28. Controls were treated with DMSO diluted in the same volume. Final volume of wells was 100 µl.

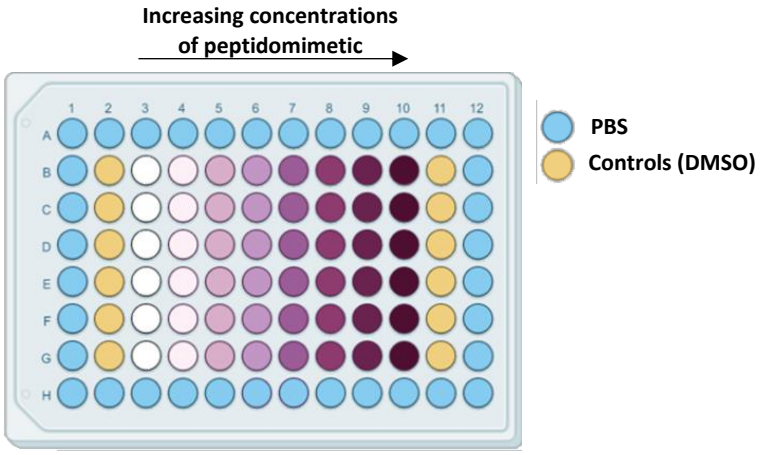

Figure 28. 96-wells plate pattern followed by the treatment.

After treatment, MTS viability assay was performed following the manufacturer's instructions. First, 20 µl CellTiter 96® AQueous One Solution Reagent were added into each well containing the 100 µl of culture medium, and then mixed by pipetting. Next, cells were incubated for 2 hours at 37ºC and the absorbance of each well was measured with a multimode plate reader (Spark, Tecan) at 490 nm. Finally, the percentage of cell viability was calculated by dividing the absorbance of each well by the average absorbance of the control wells (which had no significant deviation when Students' T-Test was applied).

16. Statistical Analysis.

Statistical analyses were performed with GraphPad Prism 8.1. Data shown represent the mean ± SEM or SD (as indicated in figure legends) of three or four independent experiments. Significant differences were assessed using one-way ANOVA with Tukey's or Dunnett's Multiple Comparisons Tests, or two-way ANOVA with Dunnett's or Sidak's multiple comparison tests; and considered when $P<0.05$.

RESULTS

SECTION 1

Study of KRAS phosphorylation at Ser181 and its relevance in colorectal cancer

CHAPTER 1

Oncogenic KRAS phosphomutants behavior in 2D cell cultures

1.1 Colorectal cancer cells stably expressing KRAS-G12V phosphomutants at endogenous levels exhibit differential epithelial morphology

In order to study the role of oncogenic KRAS phosphorylation at Ser181 in CRC, DLD-$1^{KRASWT/KRASG13D}$ cell line (named hereinafter DLD-1), which depends on the expression of the oncogenic allele of KRAS (G13D) to keep its tumorigenic properties[254,354] , was selected. The main characteristics and mutations of these cells are indicated in the materials and methods section. DLD-1 KO cell line (DLD-$1^{KRASwt/-}$) obtained from Horizon Discovery Ltd was also used. DLD-1 KO cells do not grow correctly under growth factor-limiting conditions and do not generate tumors when subcutaneously injected in mice[254,354]. Thereby, DLD-1 KO cells were stably transfected with different oncogenic KRAS phosphomutants (HA-KRAS-G12V-**S**181, HA-KRAS-G12V-S181**A** and HA-KRAS-G12V-S181**D**) to obtain and select clones of cells, which expressed these mutations at position 181 of oncogenic KRAS. Several clones of cells expressing different levels of exogenous oncogenic KRAS mutants, non-phosphorylatable (S181**A**), phosphomimetic (S181**D**) and the control phosphorylatable (**S**181) were obtained. First, the exogenous expression levels of every oncogenic KRAS phosphomutant were determined in each cell clone by WB.

With the aim of analyzing the behavior of CRC cells expressing the oncogenic KRAS phosphomutants, cell clones with an exogenous KRAS expression comparable to endogenous levels of KRAS were selected (Figure 29A). Interestingly, all KRAS phosphomutant clones presented an epithelial-like morphology, but some differences between them were observed by phase-contrast microscopy. Similarly to the original DLD-1 cell line, DLD-1 KO cells expressing oncogenic KRAS-**S**181 mutant were able to form compact clusters, in which the boundaries between the cells could barely be detected. In contrast, this cell organization did not occur in the oncogenic KRAS-S181**A** and KRAS-S181**D** cell clones (Figure 29B). Regarding to the size and shape of the cells, the non-phosphorylatable mutants were the largest while the phosphomimetic mutants were smaller and rounded.

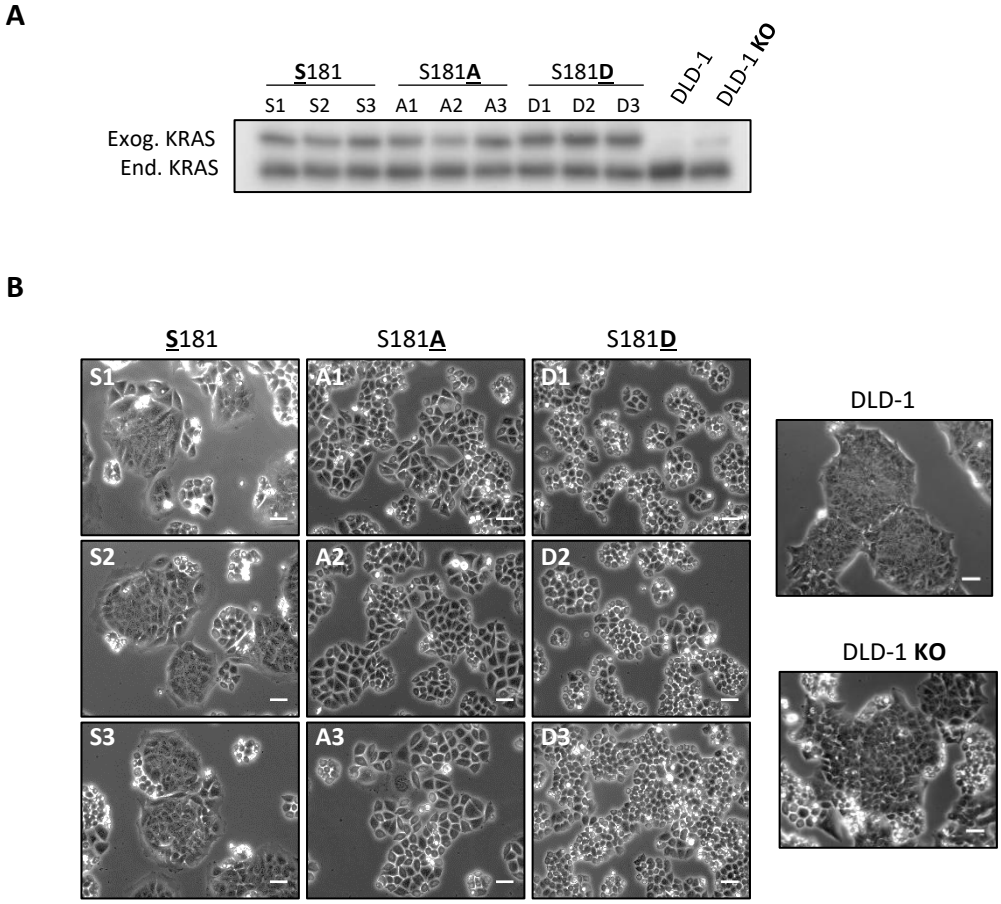

Figure 29. Stable expression of oncogenic KRAS phosphomutants in DLD-1$^{KRASwt/-}$ induces differential cell morphology. (A) WB analysis showing the clones with an exogenous expression of HA-KRAS-G12V-**S**181 (**S**181), HA-KRAS-G12V-S181**A** (S181**A**) and HA-KRAS-G12V-S181**D** (S181**D**) similar to the endogenous level of KRAS (numbers indicate different clones). (**B)** Phase-contrast images of oncogenic KRAS phosphomutants cells and DLD-1 and DLD-1 KO cell lines. All scale bars, 50µm.

Finally, it should be noted that independently of the oncogenic KRAS phosphomutant, all DLD-1 KO cells expressing high exogenous levels of oncogenic KRAS showed a mesenchymal morphology (figure 30).

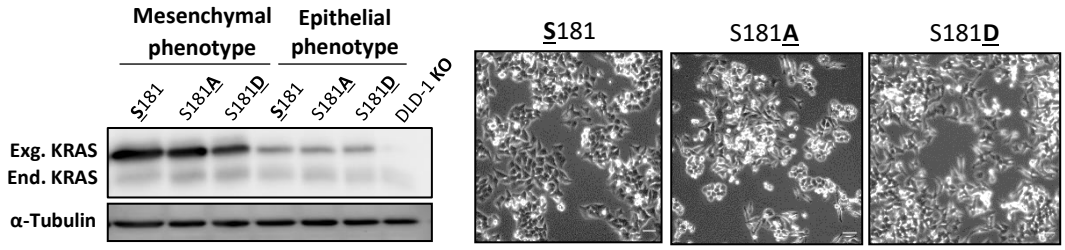

Figure 30. Stable overexpression of oncogenic KRAS phosphomutants in DLD-1$^{KRASwt/-}$ induces a mesenchymal cell phenotype. WB analysis and phase-contrast images of DLD1$^{KRASwt/-}$ cells stably expressing either HA-KRAS-G12V-**S**181, -S181**A** and -S181**D** are shown. Phosphomutants with an exogenous expression of oncogenic KRAS similar to the endogenous levels of KRAS were used as a control (left panel). KRAS phosphomutants overexpressing exogenous oncogenic KRAS compared to the endogenous levels of KRAS presented a mesenchymal cell morphology (right panel).

Therefore, KRAS phosphorylation at Ser181 was relevant to establish a specific morphology in this CRC cancer cell line.

1.2 Oncogenic KRAS expression induces cell proliferation independently of KRAS phosphorylation status at Ser181.

As specified in materials and methods section, DLD-1 cells are dependent on oncogenic KRAS for cell proliferation under growth factor-limiting conditions. In order to study if KRAS phosphorylation at Ser181 is involved in this function, we analyzed cell growth under serum-limiting conditions in the different oncogenic KRAS phosphomutants, DLD-1 and DLD-1 KO cells. As expected, DLD-1 KO cells grew less than DLD-1^{254,354}. Furthermore, DLD-1 KO cells expressing oncogenic KRAS-**S**181 were able to recover the ability to grow without serum. Surprisingly, both oncogenic KRAS-S181**A** and KRAS-S181**D** cell clones grew significantly more than DLD-1 KO cells and comparable to oncogenic KRAS-**S**181 and DLD-1 cells (Figure 31A).

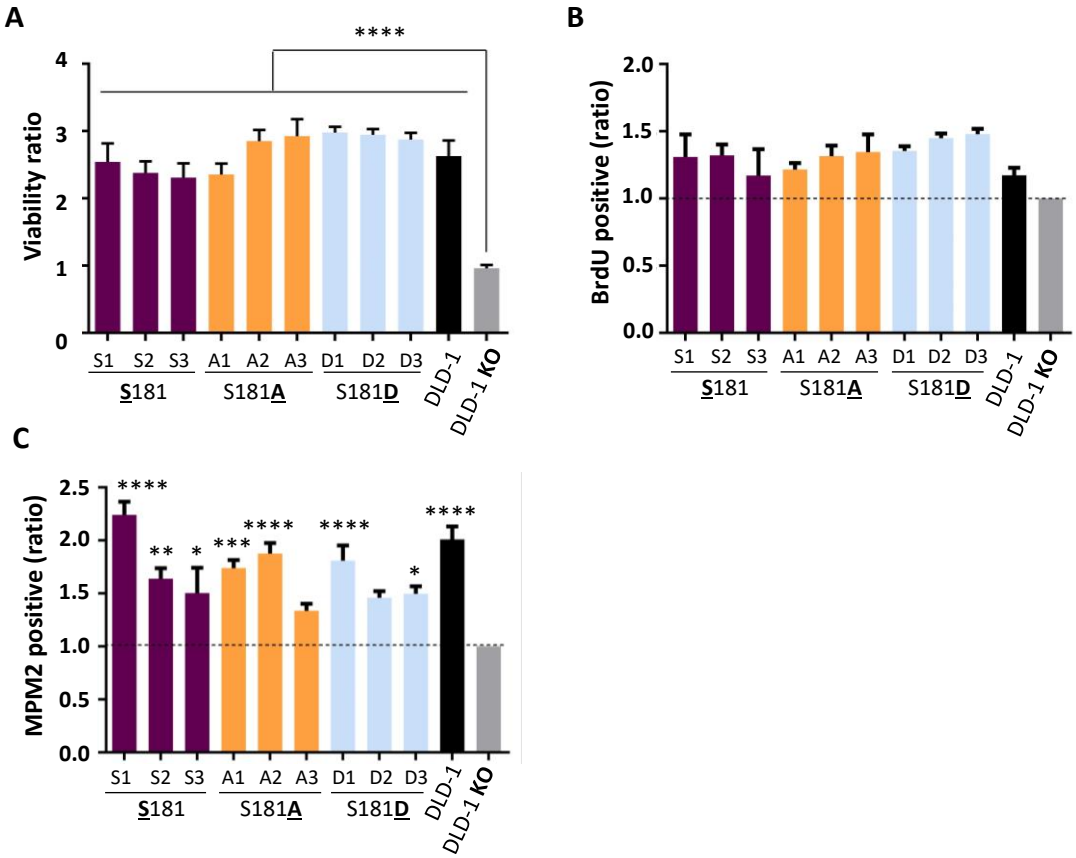

Figure 31. Oncogenic KRAS induces cell cycle entry and survival independently of KRAS phosphorylation at Ser181. (A) 5 x 10^3 DLD1$^{KRASwt/-}$ cells stably expressing either HA-KRAS-G12V-**S**181, -S181**A** or -S181**D** were cultured under serum-limiting (0.1% FBS) conditions for 48 hours to evaluate cell survival by MTT. A cell viability ratio was obtained for each clone at final conditions regarding to the initial ones. **(B-C)** Flow cytometry analysis of approximately 15000 cells was performed to analyze the S-phase population (pulse-labelled with BrdU for 30 min) and measure mitotic cells (MPM2-647 positive) from BrdU positive population. Graphs show relative ratio of each phosphomutant cells that are in S phase **(B)** and mitosis **(C)** after being 48 hours at serum-limiting conditions (0.1%FBS). Data shown represent the mean ± SEM of four independent experiments. Significant differences were assessed using one-way ANOVA and Dunnett's Multiple Comparisons Tests compared to DLD-1 KO cells (*p-value<0.05, **p-value<0.01, ***p-value<0.001, ****p-value<0.0001).

Regarding the cell cycle analysis by FACS, no significant differences in the percentage of cells that were in S phase (BrdU positive) or in mitosis (MPM2 positive) (Figure 31B and C) were observed between cells expressing the different oncogenic KRAS mutants. Also, as expected, DLD-1 KO showed less cells in S phase and a significantly diminished number of mitotic cells compared to oncogenic KRAS phosphomutants and DLD-1 cells.

These results indicated that cell cycle entry and survival under growth factor-limiting conditions was independent of oncogenic KRAS phosphorylation. Moreover, this data revealed that KRAS proteins with S181**A** or S181**D** mutations were functional, since they were able to play the same role as oncogenic KRAS-**S**181.

Surprisingly, we observed a complete tetraploid population (4n-8n peaks) in one non-phosphorylatable (S181**A**) clone and partial tetraploidies in the phosphorylatable mutant clones (**S**181). However, S181**D** clones, DLD-1 and DLD-1 KO cells presented normal diploid populations (figure 32).

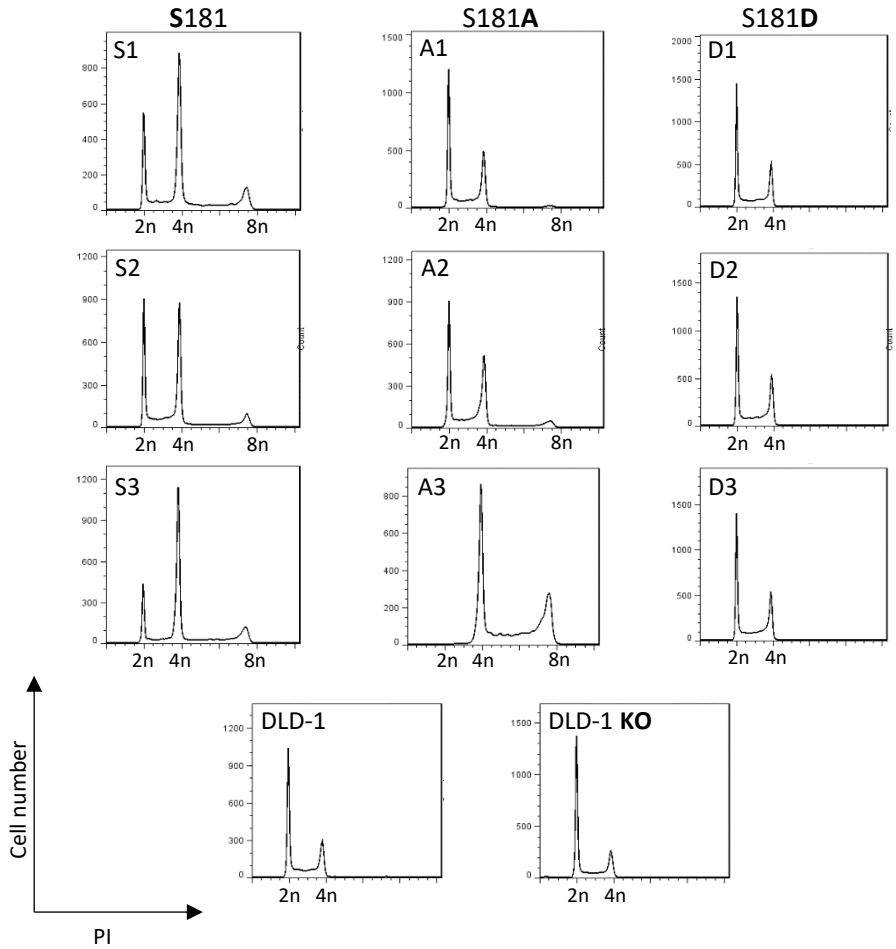

Figure 32. Non-phosphorylatable (S181A) and phosphorylatable (S181) mutant cells display higher proportion of tetraploid cells. Cell clones cultured under serum-limiting conditions (0.1%FBS) for 48 hours were incubated with propidium iodide (PI) for 30 minutes. Cell cycle profiles obtained by flow cytometry are shown.

Finally, cell proliferation at serum-saturating conditions was analyzed. Proliferation ratio related to 24 hours was calculated and no differences were observed between oncogenic KRAS mutants. Moreover, DLD-1 KO cells showed a proliferation capacity comparable to the other cell lines (figure 33), confirming that DLD-1 KO can grow under this condition independently of oncogenic KRAS[254].

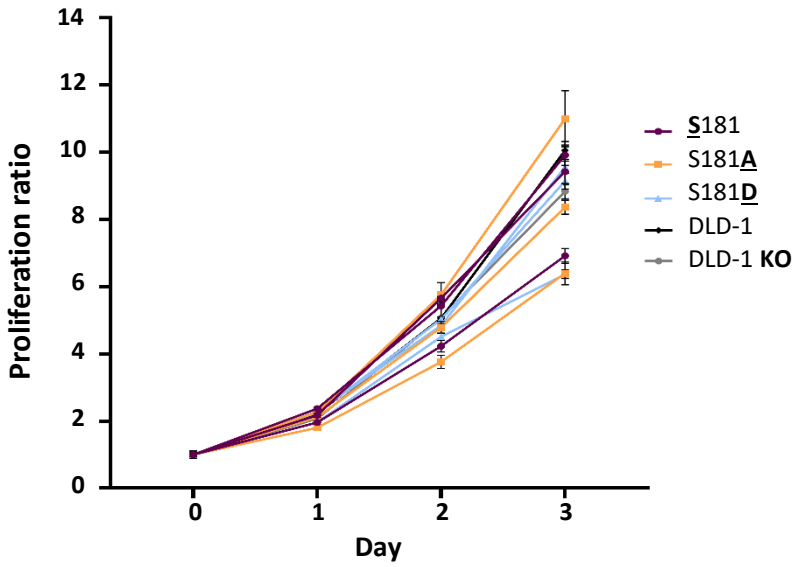

Figure 33. Cell proliferation at serum-saturating conditions is independent of oncogenic KRAS. 3 x 10^4 DLD1$^{KRASwt/-}$ cells stably expressing either HA-KRAS-G12V-**S**181, -S181**A** or -S181**D** were cultured under serum-saturating (10% FBS) conditions for 24, 48, 72 and 96 hours to evaluate cell proliferation. Cells were stained with crystal violet 0.25% and absorbance was measured. The absorbance measured in wells without cells was used as a reference. The representative graph shows the proliferation ratio calculated for each clone at 96 hours compared to 24 hours. One representative experiment is exposed. Data shown represent the mean ± SEM of three wells of each cell clone (3 cell clones of each KRAS phosphomutant). Significant differences were assessed using one-way ANOVA and Tukey's Multiple Comparisons Tests (*p-value<0.05, **p-value<0.01, ***p-value<0.001, ****p-value<0.0001). No significant differences are observed.

1.3 Oncogenic KRAS-S181D mutants exhibit reduced rates of apoptosis at growth factor-limiting conditions

Since oncogenic KRAS phosphomutants did not show differences between them regarding cell proliferation, we analyzed whether KRAS phosphorylation is involved in apoptosis at serum-limiting conditions. In order to study the apoptosis rates, Annexin V apoptosis assay was performed. Interestingly, all cell clones expressing KRAS-S181**D** mutant showed significantly less apoptotic cells than oncogenic KRAS-**S**181 cell clones and DLD-1 and DLD-1 KO cells, while variability was observed in oncogenic KRAS-S181**A** cells (figure 34).

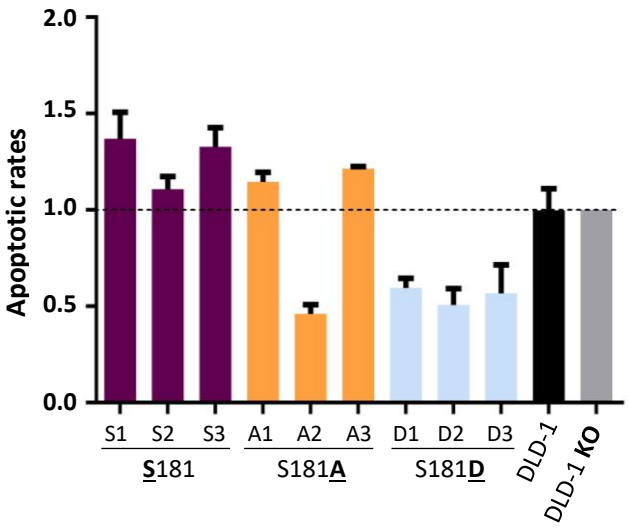

Statistical analysis

Clones	D1	D2	D3
S1	***	****	****
S2	**	***	**
S3	***	****	****
A1	**	***	***
A2	n.s	n.s	n.s
A3	***	****	***
DLD-1	*	**	*
DLD-1 KO	*	**	*

Figure 34. DLD-1$^{KRASwr/-}$ cells expressing oncogenic KRAS-S181D mutant shows less rate of apoptotic cells at serum-limiting conditions. DLD1$^{KRASwt/-}$ cells stably expressing either HA-KRAS-G12V-**S**181 -S181**A**, or -S181**D** were cultured under serum-limiting (0.1% FBS) conditions for 48 hours. Annexin V apoptosis assay was performed as described in materials and methods. Flow cytometry analysis of approximately 30000 cells was performed. Total apoptotic cells were calculated by adding the number of cells Annexin +/PI+ and the cells Annexin +/PI- determined by FACS. Data shown represent the mean ± SEM of three independent experiments. Significant differences were assessed using one-way ANOVA and Dunnett's Multiple Comparisons Tests compared to each clone of S181**D** (*p-value<0.05, **p-value<0.01, ***p-value<0.001, ****p-value<0.0001).

1.4 KRAS-G12V phosphomutants modulate c-RAF-MEK-ERK and PI3K/AKT cell signaling independently of KRAS phosphorylation status at Ser181

The best studied signal transduction pathways regulated by KRAS are c-RAF-MEK-ERK1,2 and PI3K/AKT. As it is known, oncogenic KRAS can activate them independently of external growth factors, inducing a continuous ERK1,2 and AKT signaling. However, due to the existence of diverse positive and negative feedback loops, overexpression of phosphatases, or the rewiring of some other routes, contradictory results have been described in tumor cells[355]. Therefore, we wanted to analyze if phosphorylation at Ser181 of KRAS was involved in the activation of these transduction pathways regulated by the oncogene.

Regarding the oncogenic KRAS expressing cell lines cultured under growth factors conditions, signaling did not dramatically differ between them (figure 35A). Surprisingly, under serum-starved conditions, DLD-1 KO cells exhibited higher levels of P-AKT and P-ERK than oncogenic KRAS phosphomutants or DLD-1 cells (figure 35B). This result was also observed, albeit to a lower extent, in cells cultured at serum-saturating conditions (figure 35A). Intriguingly, although DLD-1 KO cells exhibited high levels of AKT activation, the degree of S6 phosphorylation (downstream PI3K/AKT effector), was reduced under growth factors-limiting conditions (figure 35B), while this did not occur at serum saturating conditions (figure 35A). Conversely, no clear differences were observed in c-RAF and MEK activation in DLD-1 KO cells under both conditions (figure 35A and B). However, cells expressing oncogenic KRAS-**S**181 and -S181**D** showed slightly higher levels of P-RAF and P-MEK under serum starvation (figure 35B).

Therefore, according to these results, the main conclusion was that the levels of activation of ERK and AKT in cells expressing the different oncogenic KRAS phosphomutants were similar to the ones of DLD-1 cells under both conditions, independently of the status of KRAS phosphorylation. Thus, KRAS phosphorylation is not involved in the activation of ERK and AKT under restrictive or saturated serum conditions. Denote that P21 was expressed in DLD-KO cells growing in serum-saturating and serum-limiting conditions (figure 35A and B).

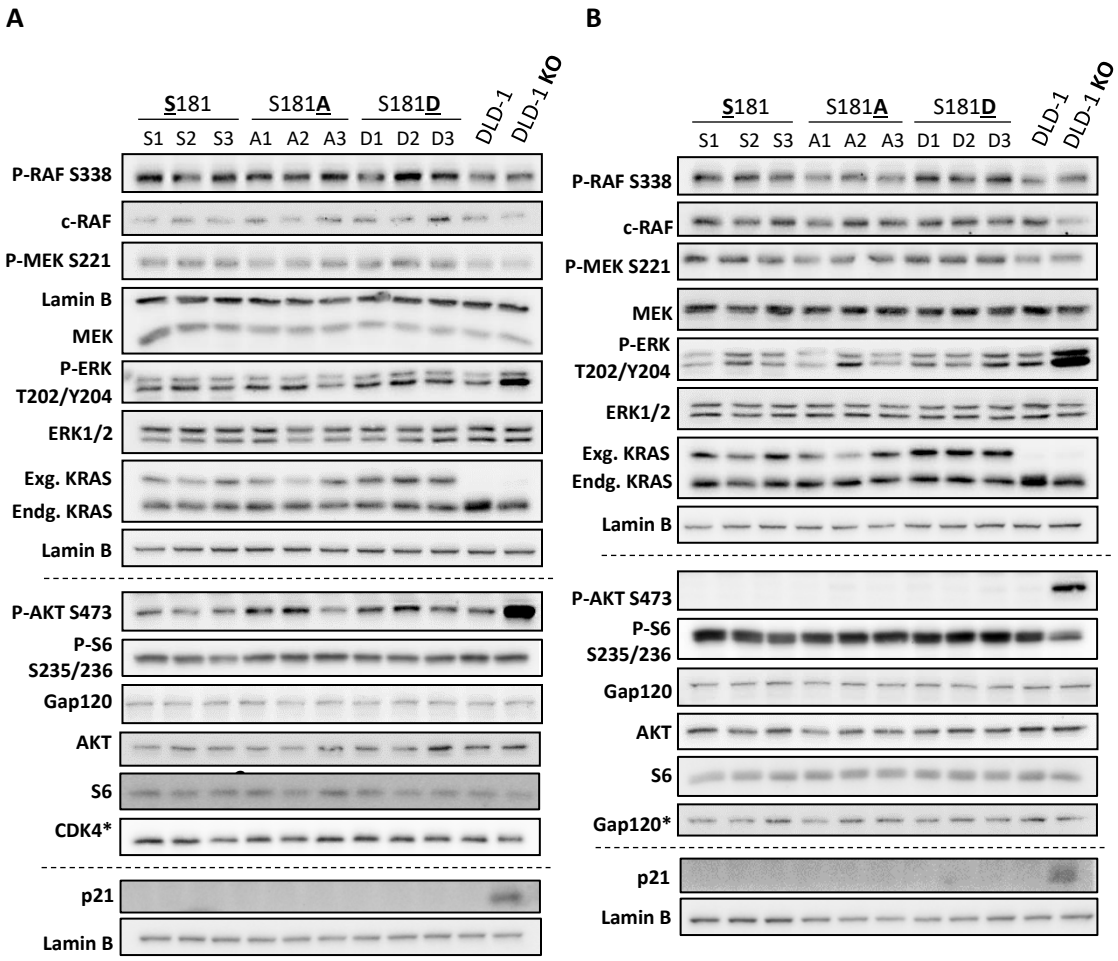

Figure 35. Activation of c-RAF-MEK-ERK1,2 and PI3K/AKT transduction pathways are independent of KRAS phosphorylation at Ser181. DLD-1$^{KRASwt/-}$ cells expressing HA-KRAS-G12V phosphomutants were cultured under growth factors (10% FBS) conditions **(A)**, and under starved conditions (0%FBS) **(B)**. Total lysates from the different cell clones were analyzed by WB to detect the indicated proteins (numbers indicate different clones). Lamin B and Gap120 were used as loading controls of phosphoproteins and p21. *CDK4 and *Gap120 was used as loading controls of total proteins.

As previously described, EGF is one of the main activators of KRAS signaling in epidermal cells. In order to investigate how the oncogenic KRAS phosphomutants might respond to EGF, cells were serum starved and then EGF stimulated. As an initial experiment to

determine the required time of EGF exposure to stimulate c-RAF/MEK/ERK and PI3K/AKT signaling pathways, DLD-1 cells were treated with EGF for 5, 10, 20 and 60 minutes. As shown in figure 36A, the highest levels of P-AKT and P-ERK were detected between the first 5-10 minutes. For that reason, the following experiments were performed by incubating the cells with EGF for 10 minutes.

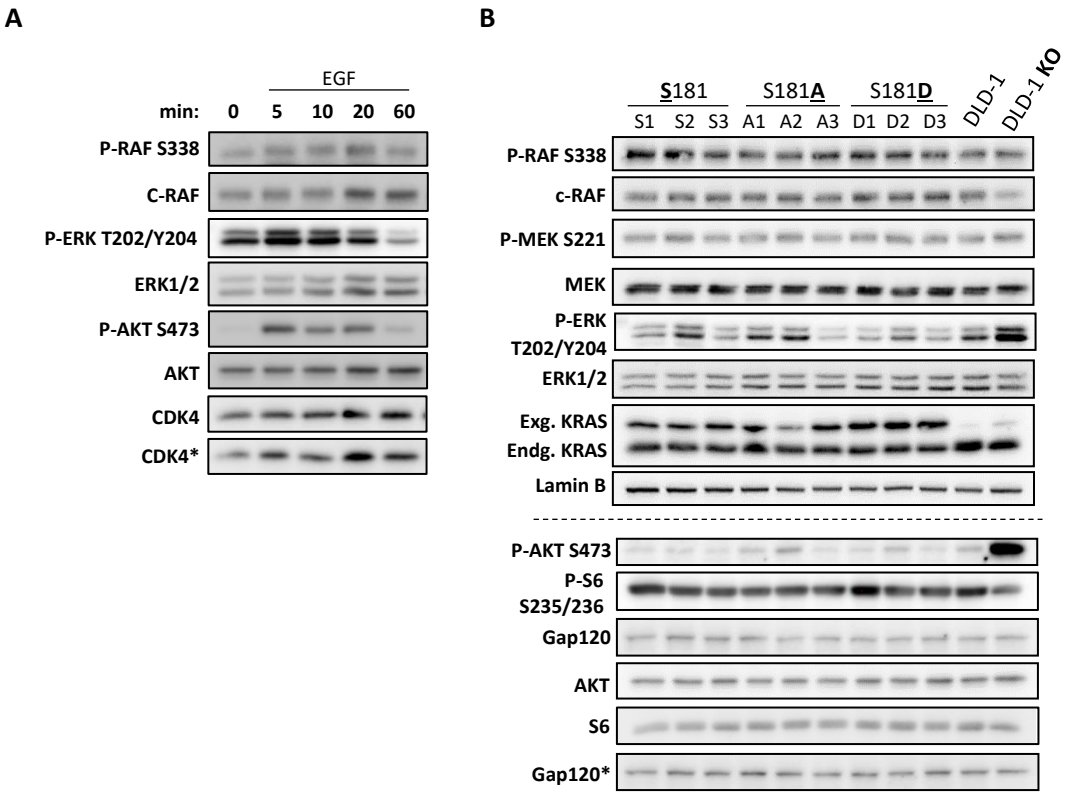

Figure 36. Oncogenic KRAS phosphomutants respond to EGF stimulation. (A) DLD-1 cells were cultured under starved conditions for 24 hours followed by EGF stimulation (50ng/ml) for 5, 10, 20 minutes and 1 hour**.** Total lysates were analyzed by WB to detect the indicated proteins. CDK4 was used as a loading control. **(B)** DLD-$1^{KRASwt/-}$ cells expressing HA-KRAS-G12V phosphomutants were cultured under starved conditions for 24 hours followed by EGF stimulation (50ng/ml) for 10 minutes. Total lysates from the different cell clones were analyzed by WB to detect the indicated proteins (numbers indicate different clones). Lamin B, CDK4 and GAP-120 were used as loading controls of phosphoproteins. CDK4* and Gap120* were used as loading control of total proteins.

Unexpectedly, all cell clones showed similar or reduced levels of P-ERK and P-AKT when compared to DLD-1 cells after EGF addition. However, in the same condition, DLD-1 KO cells exhibited the highest levels of ERK1,2 and AKT activation and the lowest of P-S6 (figure 36B), in agreement with what was observed in the previous serum stimulation experiments.

Accordingly, the effect of oncogenic KRAS on the activation of c-RAF-MEK-ERK1,2 and PI3K/AKT signaling pathways was independent of KRAS Ser181 phosphorylation in these CRC cell lines. In addition, these data confirm that our oncogenic KRAS phosphorylation mutants were functional proteins.

1.5 Oncogenic KRAS phosphomutants show a reduced cell migration capacity independently of KRAS phosphorylation status at Ser181

In order to determine if KRAS phosphorylation at Ser181 could be involved in cell migration and invasive capacity, the phosphomutant clones of KRAS as well as DLD-1 and DLD-1 KO cells were cultured in Boyden chambers covered without or with Matrigel. Cells were seeded in the upper compartment of Boyden chambers under growth factors-limiting conditions and attracted to the lower compartment using culture medium supplemented with 10%FBS. After 72 hours, the number of migrating and invading cells, which were able to move through the membrane, were counted. The migration capacity of all cell lines was very low, but surprisingly, all oncogenic KRAS phosphomutants presented even significant less migration capacity compared to DLD-1 and DLD-1 KO cells (figure 37A). Regarding to cell invasive capacity, although variability was observed in all oncogenic KRAS phosphomutants, KRAS-S181**D** cells showed higher number of invading cells compared to KRAS-**S**181 and KRAS-**S**181A cell clones. However, the differences were not significant (figure 37B).

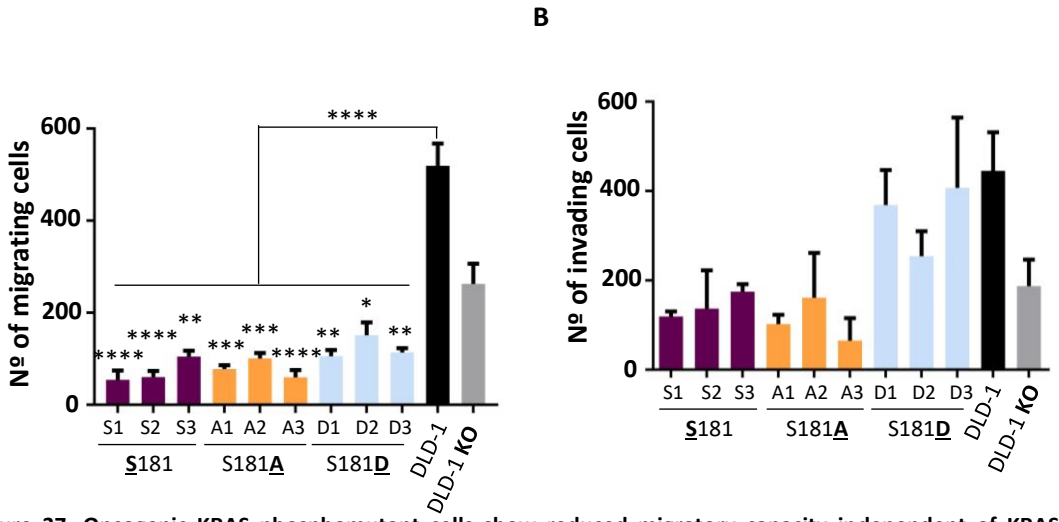

Figure 37. Oncogenic KRAS phosphomutant cells show reduced migratory capacity independent of KRAS phosphorylation at Ser181; and invasiveness of all DLD-1 derived cells is low. 5 x 10^4 DLD-$1^{KRASwt/-}$ cells stably expressing oncogenic KRAS phosphomutants were seeded in the upper compartment of Boyden chambers, covered without **(A)** or with Matrigel **(B),** under serum-limiting conditions (0.1%FBS). In the lower compartment, medium supplemented with 10%FBS as an attractor was added. After 72 hours, cells were stained with Hoechst and images were obtained by confocal microscopy. The number of migrating cells **(A)** and invading cells **(B)** were calculated as the number of cells counted in the lower compartment divided by the number of areas counted. Data shown represent the mean ± SEM of three independent experiments. Significant differences in migration assay were assessed using one-way ANOVA and Dunnett's Multiple Comparisons Tests compared to DLD-1, and DLD-1 KO cells (the last indicated by asterisks in each phosphomutant) **(A).** Significant differences in invasion assay were assessed using one-way ANOVA and Tukey's Multiple Comparisons **(B)** (*p-value<0.05, **p-value<0.01, ***p-value<0.001, ****p-value<0.0001)**.**

According to these results, we concluded that cell migration capability is independent of KRAS phosphorylation status at Ser181 in these CRC cells.

Finally, since the invading capacity of the original DLD-1 cell line is very low, this function was subsequently studied in another CRC cell line with high capacity to induce the epithelial-mesenchymal transition and, consequently, to promote invasive cells (*See chapter 5*).

CHAPTER 2

Oncogenic KRAS phosphomutants behavior in 3D extracellular matrix cultures

2.1 Colorectal cancer cells expressing KRAS-G12V phosphomutants present differential organoid morphology

Considering that one of the roles of oncogenic KRAS is to allow cell growth under non-adherent conditions, and the distinct epithelial morphology observed in CRC cells expressing different oncogenic KRAS phosphomutants, we proceeded to study how these cells lines proliferate and organize in 3D cell culture conditions.

First, the number and morphology of colonies formed in soft agar were analyzed. As expected, DLD-1 KO cells established low number of colonies. Again, in spite of the variability observed between clones, all oncogenic KRAS phosphomutants cells showed significantly higher capacity to grow in non-adherent conditions when compared to DLD-1 KO cells (figure 38A). However, the morphology of the colonies was different between the cells expressing the distinct oncogenic KRAS phosphomutants. While phosphorylatable mutant (**S**181) formed compact spheres with undistinguished boundaries between the cells, the phosphomimetic (S181**D**) and non-phosphorylatable (S181**A**) mutants presented disaggregated spheres (figure 38B).

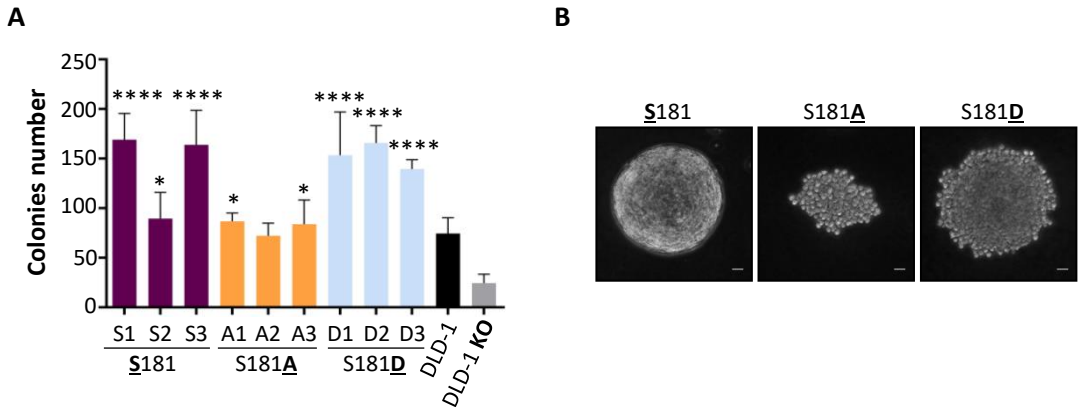

Figure 38. Oncogenic KRAS phosphomutant clones show high growth capacity under non-adherent conditions and different colony morphology. (A) 3x10^3 DLD-1$^{KRASwt/-}$ cells stably expressing either KRAS-G12V-**S**181, -S181**A**, or -S181**D** were seeded in p35 wells covered with an Agar solution as described in materials and methods section. The colonies with an area or surface greater than 1000 µm were counted. The mean of the number of colonies is shown in the graph. One representative experiment is exposed. Data shown represent the mean ± SEM of three wells of each cell clone. Significant differences were assessed using one-way ANOVA and Dunnett's

Multiple Comparisons Tests compared to DLD-1 KO cells (*p-value<0.05, **p-value<0.01, ***p-value<0.001, ****p-value<0.0001)**.** (**B)** After 10 days, images of colonies grown in soft agar were obtained by phase contrast stereomicroscopy (Leica MZSLIII). Scale bars, 50µm.

Since colonies from different oncogenic KRAS phosphomutants showed morphological differences in soft agar, phosphomutants growth in Matrigel-based 3D cultures was analyzed. Again, DLD-1 KO cells formed the smallest cellular aggregates. Interestingly, all cell clones of oncogenic KRAS-**S**181 mutant generated organized and structured glandular aggregates with a central hollow; while phosphomimetic (S181**D**) and non-phosphorylatable (S181**A**) mutants showed disorganized and branched aggregates, being the structures of KRAS-S181**D** the least aggregated (figure 39).

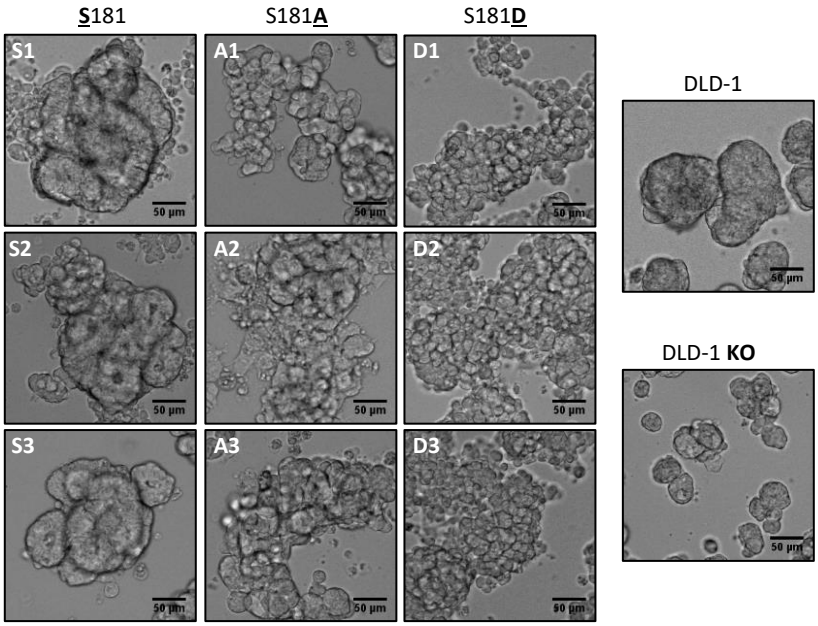

Figure 39. Oncogenic KRAS phosphorylation/dephosphorylation cycle at Ser181 is necessary to induce an epithelial organized structure. 2.5 x 10^4 $DLD1^{KRASwt/-}$ cells stably expressing either HA-KRAS-G12V-**S**181, -S181**A**, or -S181**D** were cultured on top of a thin basement membrane extract (Matrigel) overlaid on a dilute solution of the same matrix (3D on-top Matrigel assay) under ITS conditions. Phase-contrast images of phosphomutants cells grown for seven days were obtained and compared. All scale bars, 50µm.

2.2 Oncogenic KRAS-S181 mutants show epithelial polarized glandular morphology

Since we observed differential proliferation and organization of the cells expressing distinct oncogenic KRAS phosphomutants in Matrigel-based 3D cultures, we proceeded to determine the degree of polarization of these structures analyzing specific markers of cell polarity. Therefore, adherent junctions and basal cell membranes were detected by immunostaining with antibodies against E-Cadherin and alpha-6-Integrin, respectively. Polarized actin was evidenced with fluorescent Phalloidin to point apical cell membranes, and nuclei were counterstained with DAPI. As it can be observed in the confocal images, KRAS-**S**181 expressing cells displayed epithelial glandular morphology of polarized cells with a central hollow lumen. Thus, alpha-6-integrin was observed in the basal membrane of the cells, while polymerized actin was localized in the apical membrane, near the lumen, reminding a microvilli containing structure. Finally, E-cadherin was detected in the contacts established between cells. Conversely, these markers indicated that cells expressing oncogenic KRAS-S181**A** and -S181**D** formed disorganized and depolarized aggregates (figure 40).

Therefore, the evidences obtained in the soft agar and Matrigel-based 3D cultures experiments suggest that the lack of a correct phosphorylation/dephosphorylation cycle at Ser181 of oncogenic KRAS impairs proper polarization of cells and consequently, the growth of an epithelial organized structure.

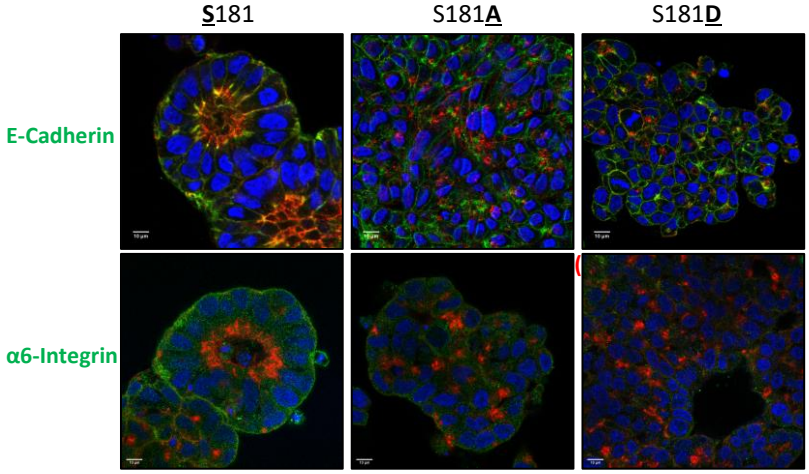

Figure 40. Oncogenic KRAS phosphorylation/dephosphorylation cycle at Ser181 induces an epithelial glandular structure of polarized cells. After seven days growing in Matrigel-based 3D cultures, the organoid like structures of oncogenic KRAS phosphomutants were fixed and immunostained against E-Cadherin (adherent junctions, green) andα-6 integrin (basal cell membrane marker, green). Polymerized actin was detected with Phalloidin (apical cell marker, red) and nuclei were counterstained with DAPI (blue). Images were obtained by confocal microscopy. All scale bars, 10µm.

CHAPTER 3

Role of oncogenic KRAS phosphomutants in tumor growth

3.1 Oncogenic KRAS-S181 mutant expression in colorectal cancer cells induces increased tumor growth capacity

In order to evaluate the tumor growth capacity of the different oncogenic KRAS phosphomutant cells, DLD-1 KO cells expressing the phosphorylatable (**S**181), non-phosphorylatable (S181**A**) and phosphomimetic (S181**D**) mutants were subcutaneously injected into both flanks of nude mice. The day of injection, the expression levels of KRAS phosphomutants were corroborated (figure 41A). Tumor growth was monitored over time and tumor weight was measured the day of euthanasia (28 days after injection).

As expected, DLD-1 KO cells formed few tumors and minor tumors (almost imperceptible macroscopically). Accordingly, our results validated that DLD-1 CRC cells depend on oncogenic KRAS to generate tumors[354]. Interestingly, KRAS-**S**181 derived-tumors had a significantly higher weight compared to the non-phosphorylatable (S181**A**) and phosphomimetic (S181**D**) mutants (figure 41B), and they also presented significantly higher tumor volume (figure 41C).

Therefore, our data suggest that tumor growth capacity of these CRC cells was dependent on a correct phosphorylation/dephosphorylation cycle of oncogenic KRAS at Ser181.

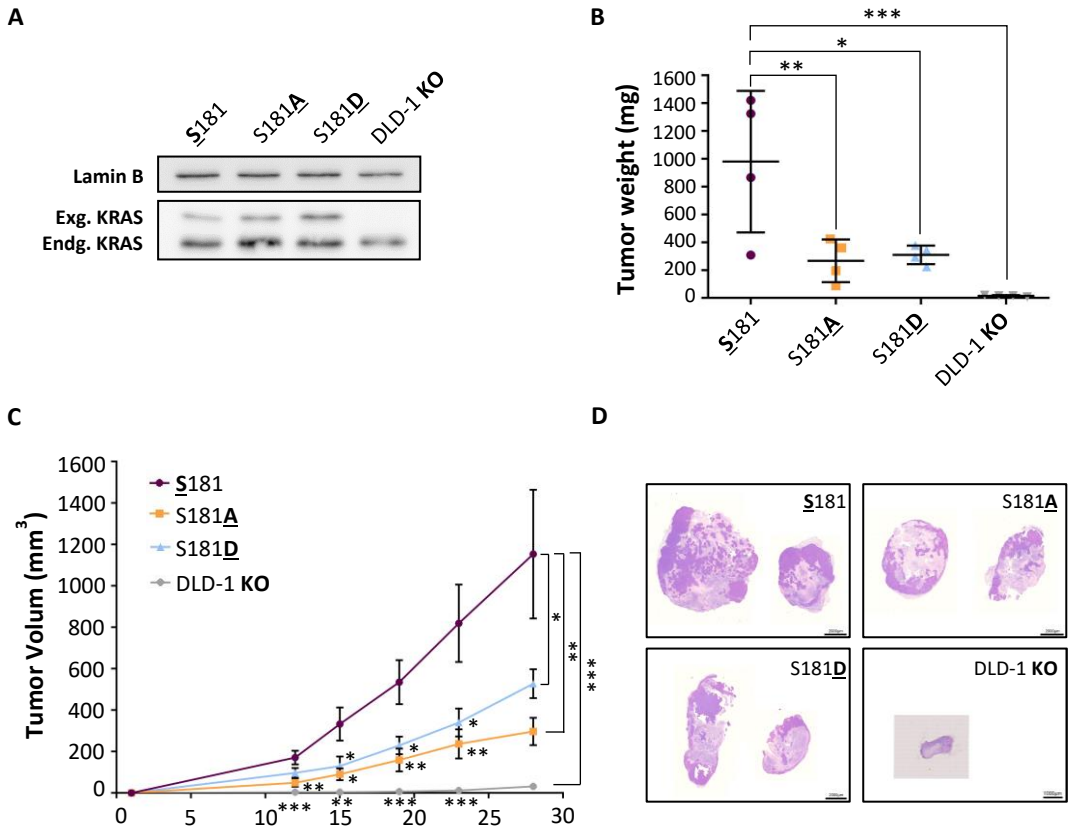

Figure 41. Oncogenic KRAS phosphorylation at Ser181 is necessary for tumor growth. DLD-1$^{KRASwt/-}$ cells stably expressing either oncogenic KRAS-**S**181, -S181**A** or -S181**D** were injected into each flank of nude mice (each group n=4 tumors). At day 28 mice were euthanized and tumors were dissected, measured, weighed and processed for analysis. **(A)** Exogenous KRAS protein levels from the different phosphomutants cell clones were analyzed by WB the day of injection into mice. Lamin B was used as loading control. **(B)** The weight of excised tumors is showed in the graph (each dot corresponds to a tumor). **(C)** The four tumors of each phosphomutant were measured, and tumor volumes calculated at days 12, 15, 19, 23 and the day of euthanasia. Data shown represent the mean ± SD **(B)** or ± SEM **(A)** of four tumors of each phosphomutant. Significant differences were assessed using one-way ANOVA and Dunnett's Multiple Comparisons Tests regarding to **S**181-derived tumor (*p-value<0.05, **p-value<0.01, ***p-value<0.001, ****p-value<0.0001). **(D)** Histology of tumors was analyzed by H&E staining. Slide scan and morphometric analysis were performed. The panels show the lowest magnification images. Scale bars of **S**181, S181**A** and S181**D**-derived tumors, 2000µm. Scale bar of DLD-1 KO derived tumor, 1000µm.

3.2 c-RAF-MEK-ERK and PI3K/AKT signaling pathways activation in oncogenic KRAS derived tumors is independent of KRAS phosphorylation at Ser181

In order to determine the activation status of c-RAF-MEK-ERK1,2 and PI3K/AKT signal transduction pathways, tumors derived from DLD-1 KO cells expressing different oncogenic KRAS phosphomutants were processed for WB analysis. Interestingly, all oncogenic KRAS derived-tumors showed lower expression levels of P-ERK and P-AKT than DLD-1 KO derived-tumors. No differences were observed in c-RAF and S6 phosphorylation (figure 42).

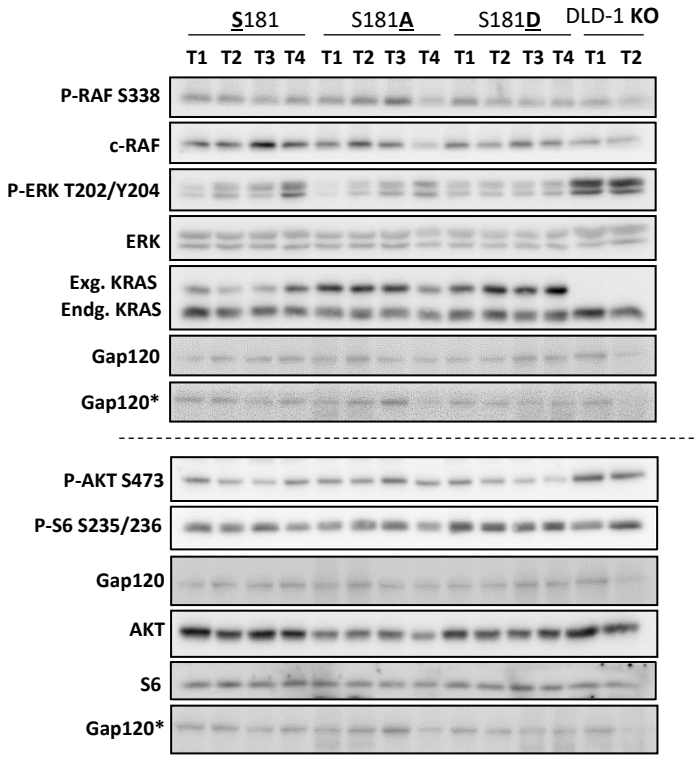

Figure 42. Oncogenic KRAS expression reduces ERK and AKT phosphorylation regardless of Serine 181 mutation. Total cell lysates of representative excised tumors were immunoblotted to detect the indicated proteins (numbers indicate different tumors). GAP120 was used as loading control of phosphoproteins and c-RAF. *Gap120 was used as loading control of total proteins and P-RAF.

Therefore, in tumors, as previously observed in 2D cell cultures, oncogenic KRAS expression reduced c-RAF-MEK-ERK and PI3K/AKT signaling pathways independently of phosphorylation status of KRAS at Ser181.

3.3 Oncogenic KRAS phosphomutants derived tumors show differential glandular morphology

The histology of the tumors was determined by H&E staining. Strikingly, the morphological differences observed between the histological sections of oncogenic KRAS phosphomutants derived tumors were similar to the differences observed in 3D cell culture assays. While oncogenic KRAS phosphorylatable derived-tumors exhibited epithelial and glandular morphology organized around blood vessels, the oncogenic KRAS-S181**A** and -S181**D** derived-tumors showed a disorganized glandular structure with smaller and collapsed blood vessels (figure 43A).

After studying the morphological features of the tumors, TUNEL assays and IHC to detect Ki-67 and P-H3 were performed to determine apoptosis, cell proliferation and mitotic index, respectively. As it can be observed in figure 43B, all tumors, regardless of the type of mutation at Ser181 of KRAS, presented an area of proliferating cells (Ki-67 positive) as well as an area of apoptotic and necrotic cells (TUNEL positive) comparable between them. Regarding the mitotic index, the cells positive for P-H3 were counted in the proliferating areas of the tumors but no differences were observed (figure 43C).

Thus, all the data suggest that the lack of a correct phosphorylation/dephosphorylation cycle of oncogenic KRAS at Ser181 interferes with the proper organization of cells around the blood vessels and consequently, with the growth of the tumor.

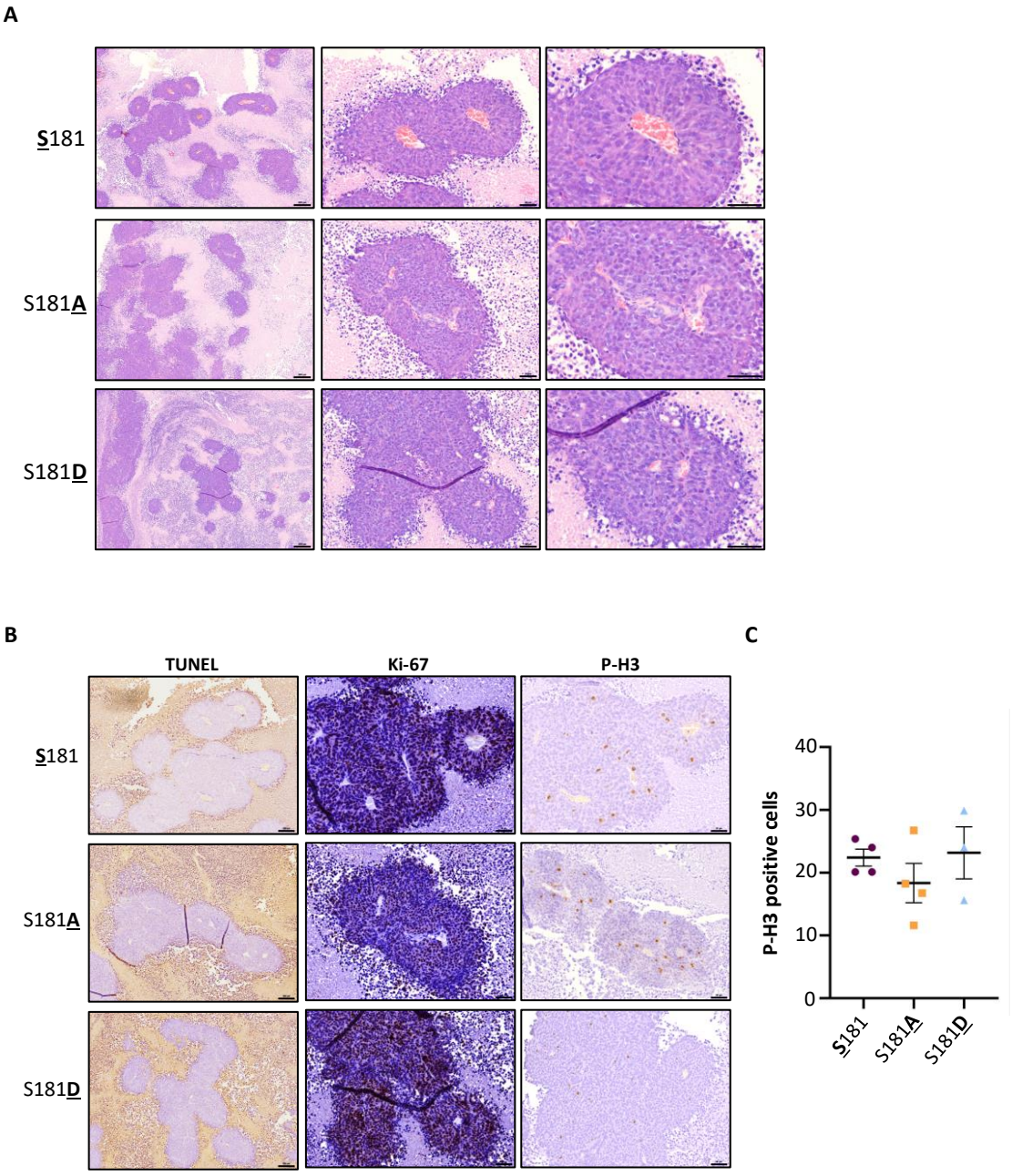

Figure 43. KRAS-G12V-S181- derived tumors show different glandular morphology and similar apoptotic and proliferating areas to KRAS-G12V-S181A and S181D-derived tumors. (A) Histology of tumors was analyzed by Hematoxylin-Eosin staining. The panels show from left to right the lowest to highest magnification images. Scale bars of lowest magnification, 200µm. Scale bars of highest magnifications, 50µm. **(B)**. TUNEL assay and immunohistochemistry of Ki-67 and P-H3 were performed in the tumor sections. Scale bars of tumor sections stained for TUNEL, 100µm. Scale bars of tumors sections stained for Ki-67 or P-H3, 50µm. **(A and B)** Slide scan and morphometric analysis were performed. **(C)**. The number of mitosis in the proliferating areas of the tumors

was counted in minimum 8 consecutive fields (x400) and the average was calculated. The mitotic index for each phosphomutant is shown in the graph (each dot corresponds to a tumor). Data shown represent the mean ± SEM of three or four tumors of each phosphomutant. Significant differences were assessed using one-way ANOVA and Tukey's Multiple Comparisons Tests (*p-value<0.05, **p-value<0.01, ***p-value<0.001, ****p-value<0.0001).

3.4 Colorectal cancer cells expressing oncogenic KRAS phosphomutants do not induce metastatic tumors

Once the effect of oncogenic KRAS phosphomutants in tumor growth was evaluated, we set out to determine the metastatic capacity of the phosphorylatable (**S**181), non-phosphorylatable (S181**A**) and phosphomimetic (S181**D**) mutant cells.

DLD-1 KO cells expressing different KRAS-G12V phosphomutants were injected into spleen of nude mice. Spleen was removed at day 3. After 3 months of injection, the liver was extracted in order to evaluate the number of metastases.

Unexpectedly, none of the oncogenic KRAS phosphomutants were able to induce liver tumors under the conditions evaluated. Considering that DLD-1 CRC cell line shows low metastatic capacity[356,357], we are planning to either analyze liver metastasis for a longer period of time, or to use other CRC cell line with higher invasive capacity.

CHAPTER 4

Differential gene expression pattern in colorectal cancer cells according to the KRAS phosphorylation status of Ser181 and its regulation by PKC

4.1 KRAS phosphorylation at Ser181 regulates gene expression profile of colorectal cancer cells

Gene expression profile of CRC cells expressing the different oncogenic KRAS phosphomutants was performed in order to understand the differences observed in the morphology and behavior of cells growing in 2D cell culture.

As shown in the clustering analysis, cells expressing different oncogenic KRAS phosphomutants presented differential gene expression patterns between them, while differences between clones expressing the same phosphomutant were minimal. However, phosphomimetic mutant (S181**D**) exhibited the highest differences when compared to phosphorylatable (**S**181) and non-phosphorylatable (S181**A**) mutants (figure 44A). When oncogenic KRAS phosphomimetic (S181**D**) and phosphorylatable (**S**181) mutants were compared, 40 genes were found to be differentially expressed, while only 9 genes were differentially expressed otherwise between non-phosphorylatable (S181**A**) and phosphorylatable mutants (**S**181) (figure 44B and table 13). Surprisingly, although we could not observe strong differences between phosphomimetic (S181**D**) and non-phosphorylatable (S181**A**) mutants regarding 3D cell cultures and tumor growth capacity, the comparison of gene expression between oncogenic KRAS-S181**D** and -S181**A** mutants showed the maximum differences (figure 44B and C and table 13).

Although phosphorylatable (**S**181) mutant showed more genes differentially expressed with phosphomimetic (S181**D**) than non-phosphorylatable (S181**A**) mutant, the few differences existing in gene expression pattern between oncogenic KRAS-**S**181 and KRAS-S181**A** mutants support the hypothesis that KRAS should be phosphorylated in a fraction of cell population being relevant to regulate the gene expression.

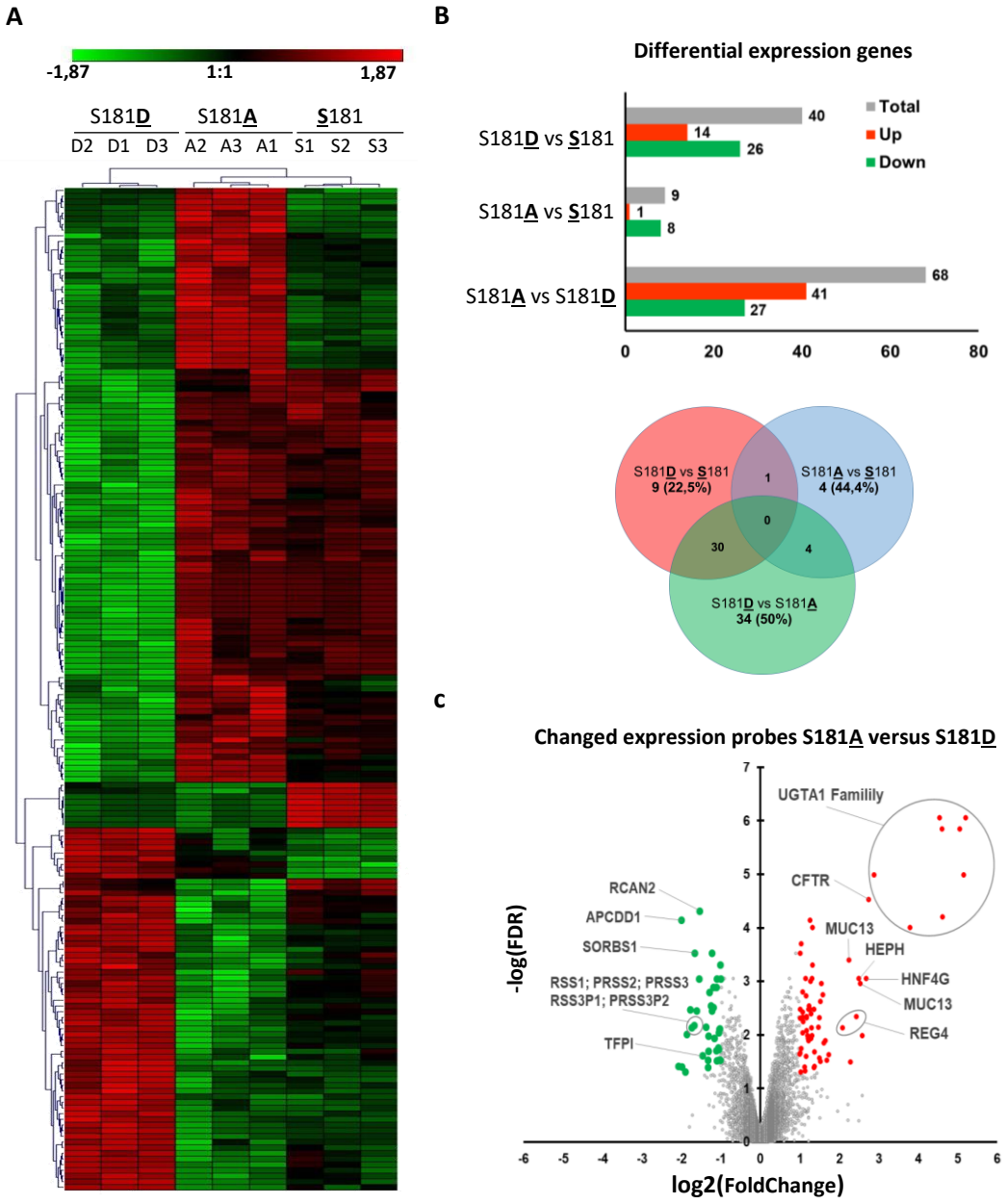

Figure 44. Status of oncogenic KRAS phosphorylation at Ser181 has an impact in gene expression profile. (A) Average linkage WPGMA Clustering of genes and clones that had a significantly different expression (FDR<0.01) in at least one of the conditions (**S**181; S181**A** or S181**D**)**.** Intensities were normalized for each gene and the scale corresponds to log2**. (B)** Differentially expressed probes were pooled in genes to determine the number of genes differentially expressed. Number of genes (upper graph) and Venn diagram (lower graph) differentially expressed (FDR<0.05 and a FC>2) between the phosphomutant groups. **(C)** Volcano plot showing genes differentially expressed when comparing S181**A** with S181**D** expressing cells. Gens with FDR<0.05 are colored: red upregulated and green down regulated. The name of genes interest is indicated

Table 13. Differential expressed genes (FDR<0.05; FC>2)

S181**D** vs **S**181		S181**A** vs **S**181		S181**A** vs S181**D**	
Upregulated	**Downregulated**	**Upregulated**	**Downregulated**	**Upregulated**	**Downregulated**
APCDD1	ALCAM	**NEO1**	**CTNNA1**	ALCAM	APCDD1
C6orf15	ANGPT1		MX2	ANKH	C6orf15
C6orf52	C1orf21		PLK4	ATP10D	CHRNA1
CHRNA1	CAT		PRSS1[b]	C1orf21	COL4A1
CYP26B1	CFTR		**PRSS2[c]**	C4BPB	CYFIP2
GPR161	CLDN2		**SERPINE1**	CFTR	GPR161
HBB	**CTNNA1**		SLC46A1	CLCN5	HAS2
ID4	CXCL3		TFPI	CLIC5	ID4
OXGR1	DAPK1			CXCL3	KIT
PCSK5	FAM46A			DAPK1	MKX
RCAN2	HEPH			DPP4	MX2
SORBS1	**HNF4G**			FAM46A	OXGR1
SUGCT	MUC13			HEPH	PLA2G7
TRIB2	NFIX			HNF4G	PMEPA1
	NPNT			HS3ST3B1	PPP2R2C
	OLFML3			IFI30	PRSS1[b]
	PIP5K1B			MUC13	PRSS2[c]
	PKIB			NFIX	PTK7
	PLBD1			NPNT	RCAN2
	REG4			OLFML3	S100A4
	RNASE4			PI3	SNCAIP
	SAMD9			PIP5K1B	SORBS1
	SEMA5A			PKDCC	SOX4
	SLC9A2			PKIB	SUGCT
	TCF4			PLBD1	TFPI
	UGT1A[a]			PLCL2	TGFB2
				PTPRR	TNFRSF19
				REG4	
				RGS2	
				SAMD9	
				SBSPON	
				SCEL	
				SDHAF3	
				SEMA5A	
				SLC6A20	
				SLC9A2	
				TCF4	
				TRNP1	
				UGT1A[a]	
				ZIC2	
				ZIC5	

(a) UGT1A1; UGT1A10; UGT1A3; UGT1A4; UGT1A5; UGT1A6; UGT1A7; UGT1A8; UGT1A9

(b) PRSS1; PRSS2; PRSS3P1; PRSS3P2

(c) PRSS2; PRSS3; PRSS3P2

When we studied the differentially expressed genes in oncogenic KRAS-S181**D** versus KRAS-**S**181 mutants, we observed that genes related to enterocyte differentiation as *HNF4G*, *HEPH*, *MUC13* and *UGT1A* were downregulated in the phosphomimetic mutant (S181**D**) (figure 45A). Therefore, these results suggest that oncogenic KRAS phosphorylation at Ser181 could be promoting a de-differentiation program. Moreover, GSEA analysis demonstrated that oncogenic KRAS-S181**D** compared to KRAS-**S**181 and KRAS-S181**A** mutants showed an expression signature similar to the one of the DLD-1 cell line which up-regulates *LEF1*, a gene related to WNT signaling pathway and pluripotency[358] (figure 45B). Finally, phosphomimetic mutant (S181**D**) also presented an increased expression of *TRIB2*, which has recently been proposed as oncogene in CRC due to its expression could inhibit cell senescence[349].

Regarding the comparative analysis between oncogenic KRAS-S181**A** and KRAS-**S**181 mutants, *NEO1*, which codifies for neogenin1, was the only gene upregulated more than 2-fold in cells expressing the non-phosphorylatable KRAS (S181**A**) (figure 45A). Neogenin1, a cell surface receptor involved in cell locomotion and EMT, has recently been described as tumor suppressor in CRC[359]. Interestingly, the expression levels of *PRSS1,2,3* (codifying for different isoforms of trypsin) and *SERPINE1* (codifying for PAI-I) genes, which are involved in cell invasion, ECM remodeling and vascular co-option[360–364], were reduced more than 2-fold in cells expressing oncogenic KRAS-S181**A** mutant (figure 45A).

Last, *CTNNA1*, codifying for α-E-Catenin, was the only gene whose expression was reduced in both oncogenic KRAS-S181**A** and KRAS-S181**D** mutants compared to KRAS-**S**181 expressing cells (figure 45A). α-E-Catenin is involved in cell-to cell adhesion and polarization of cells[365–367]. Hence, the lack of α-E-Catenin could be accounting for the impaired organization and polarization of phosphomimetic (S181**D**) and non-phosphorylatable (S181**A**) mutant cells in 3D cultures as well as in tumor growth.

A

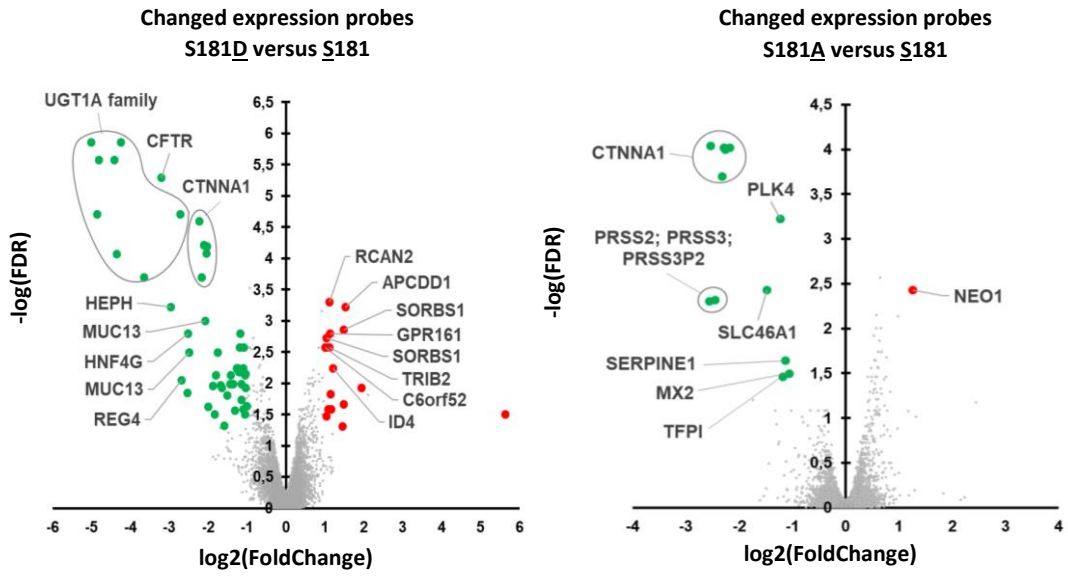

B

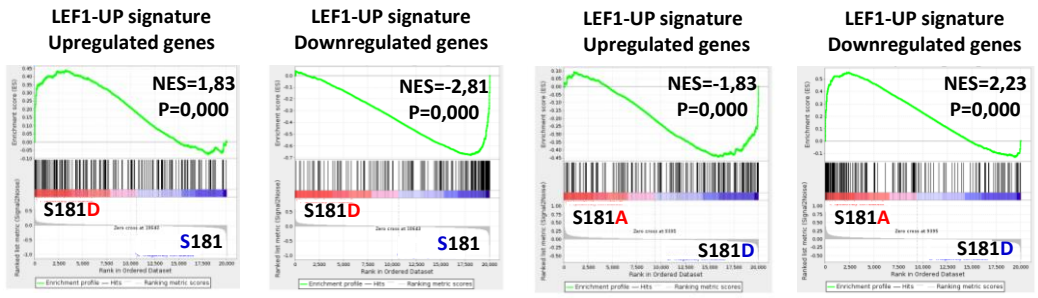

Figure 45. KRAS phosphorylation status at Ser181 induces differential gene expression. (A) Volcano plot showing genes differentially expressed when comparing S181**D** (left graph) or S181**A** (right graph) with **S**181 mutants. Gens with FDR<0.05 are colored: red upregulated and green down regulated. The name of genes interest is indicated. **(B)** GSEA plot showing enrichment of the indicated gene set in the expression profile of S181**D** versus **S**181 and S181**A** versus S181**D** cells. NES, normalized enrichment score; P, p-value.

In order to corroborate the data obtained by microarray analysis, RT-qPCR and WB were performed. As shown in the graphs of figure 46, relative mRNA levels of *CTNNA1* (decreased in S181**A** and S181**D**), *SERPINE1* and *PRSS2* (decreased in S181**A**), *HNF4G* (reduced in S181**D**) and *TRIB2* (increased in S181**D**) in cells expressing the KRAS-G12V phosphomutants, were validated.

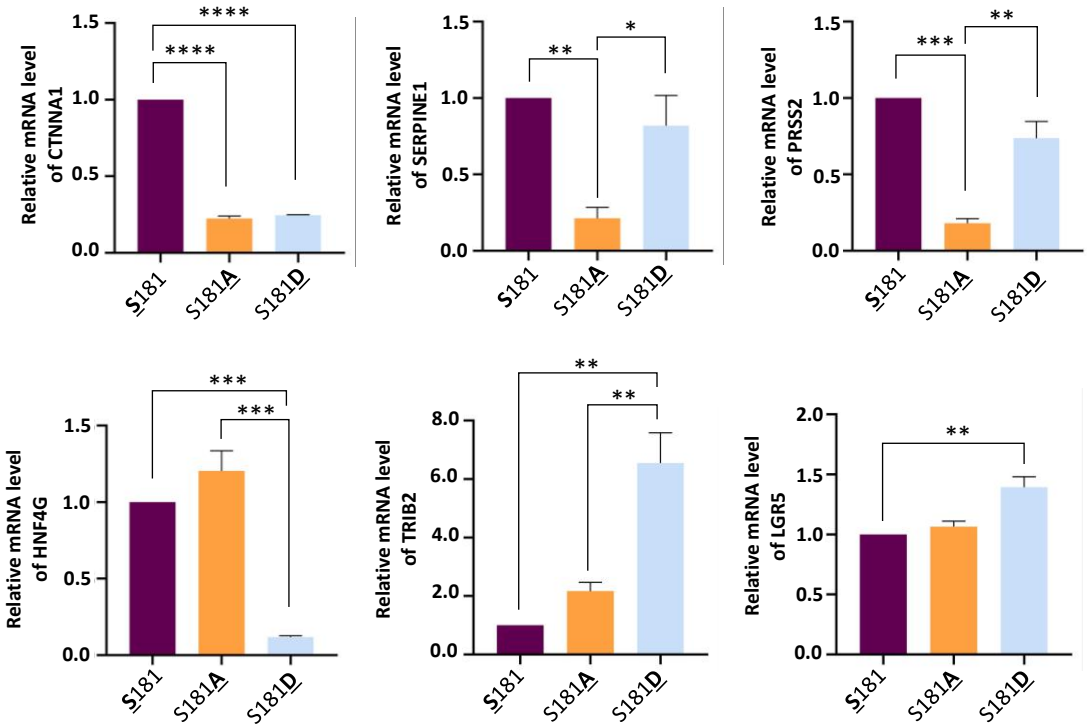

Figure 46. Differential gene expression of KRAS phosphomutants is corroborated by RT-qPCR. RNA extraction from DLD-1$^{KRASwt/-}$ cells stably expressing KRAS-G12V-**S**181, -S181**A** or -S181**D** was carried out and cDNA was obtained from 1µg of total RNA. Real Time qPCR was performed. *HPRT1* mRNA expression was used as an internal control to normalize *CTNNA1*, *SERPINE1*, *PRSS2*, *HNF4G* and *TRIB2* mRNA expression. Normalized expression of *CTNNA1*, *SERPINE1*, *PRSS2*, *HNF4G* and *TRIB2* are presented relative to **S**181 mutant. Data shown represent the mean ± SEM of three independent experiments (**S**181, S181**A** and S181**D** indicate the average of three different KRAS-G12V-**S**181, -S181**A** or -S181**D** cell clones). Significant differences were assessed using one-way ANOVA and Tukey's Multiple Comparisons Tests (*p-value<0.05, **p-value<0.01, ***p-value<0.001, ****p-value<0.0001).

Moreover, due to the results of GSEA indicating that cells expressing the phosphomimetic oncogenic KRAS were related to pluripotent cells, we thought it would be interesting to analyze RNA expression of *LGR5*, a cancer stem cell marker[368,369]. Significantly, it was increased in oncogenic KRAS-S181**D** cells (figure 46).

Regarding WB analysis, the reduced expression levels of HNF4G and increased levels of neogenin1 were confirmed in oncogenic KRAS-S181**D** and KRAS-S181**A** expressing cells**,** respectively (figure 47A); also, the diminished expression levels of trypsin were validated in the non-phosphorylatable mutant (S181**A**) derived tumors (figure 47B).

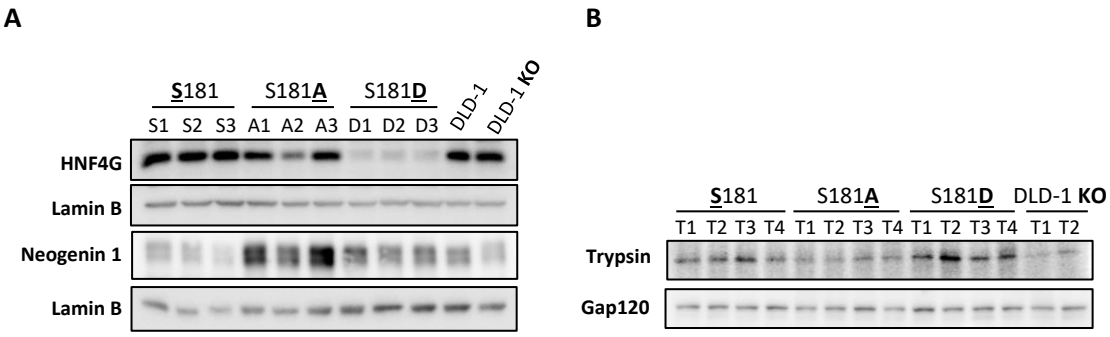

Figure 47. Corroboration of protein expression levels of differentially expressed genes (A) DLD-1$^{KRASwt/-}$ cells stably expressing KRAS phosphomutants were harvested and extracts were immunoblotted using the specified antibodies (numbers indicate different clones). Lamin B was used as loading control. **(B)** Total cell lysates of representative excised tumors were immunoblotted to detect the specified proteins (numbers indicate different tumors). GAP120 was used as loading control.

As mentioned above, organization and polarization in cells expressing oncogenic KRAS-S181**A** and KRAS-S181**D** could be impaired by the reduced *CTNNA1* gene expression. For this reason, we checked the protein levels of α-E-catenin in the oncogenic KRAS phosphomutant cells as well as in tumors derived from these cell clones. Additionally, subcellular localization of α-E-catenin was also studied.

Strikingly, the expression levels of α-E-catenin were undetectable by WB in cells expressing non-phosphorylatable and phosphomimetic mutants (figure 48A). This protein was also not observed in oncogenic KRAS-S181**A** and KRAS-S181**D** derived-tumors (figure 48B).

Finally, immunofluorescence experiments performed with phosphorylatable mutant KRAS-**S**181 cells growing in 3D conditions (Matrigel) showed α-E-Catenin to be localized mainly in the contact areas between cells but also at the plasma membrane. As expected, α-E-Catenin was not detected in cells expressing KRAS-S181**A** and KRAS-S181**D** mutants (figure 48C) under the same conditions**.**

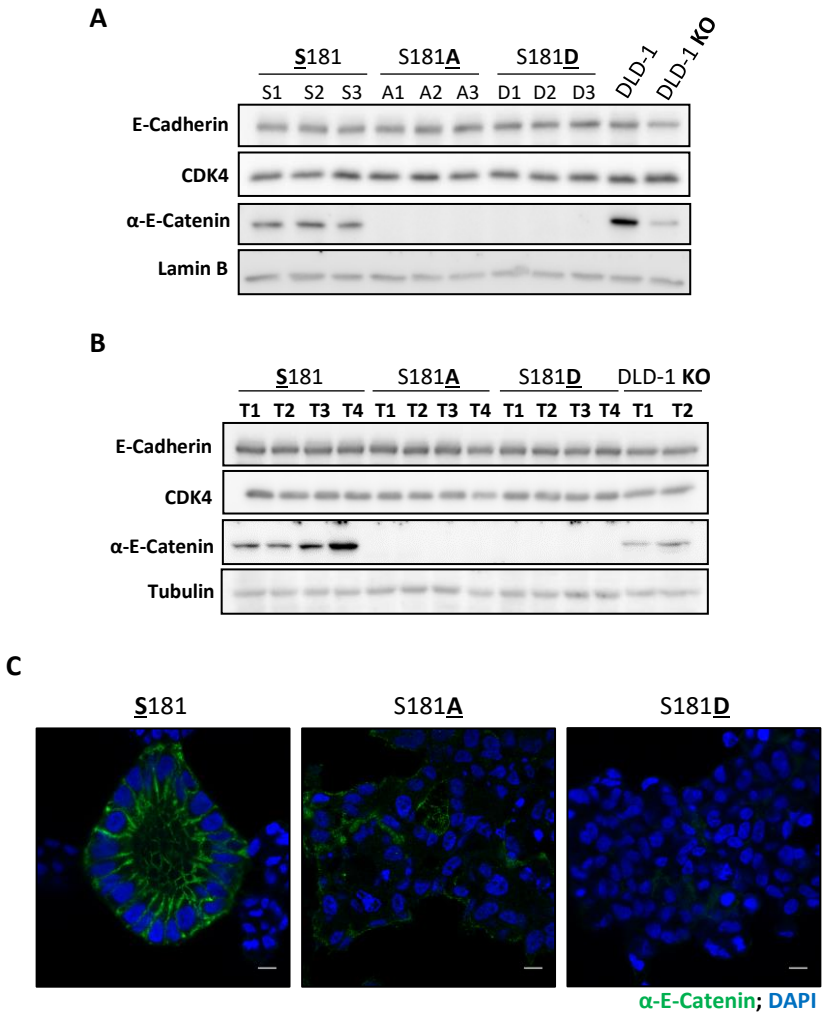

Figure 48. Oncogenic KRAS phosphorylation/dephosphorylation cycle at Ser181 regulates cell polarization. (A) DLD-1$^{KRASwt/-}$ cells stably expressing KRAS phosphomutants were harvested and extracts were immunoblotted using the specified antibodies (numbers indicate different clones). Lamin B and CDK4 were used as loading controls. **(B)** Total cell lysates of representative excised tumors were immunoblotted to detect the specified proteins (numbers indicate different tumors). CDK4 and α-tubulin were used as loading controls. **(C)** DLD-1$^{KRASwt/-}$ cells stably expressing oncogenic KRAS-**S**181, -S181**A** or -S181**D** cultured on top of a thin basement membrane extract (Matrigel) overlaid on a dilute solution of the same matrix, were extracted and immunostained using antibodies against α-E-Catenin (green) and nuclei counterstained with DAPI. All scale bars, 10µm

All in all, these results evidence that a correct phosphorylation/dephosphorylation cycle of oncogenic KRAS at Ser181 is necessary to induce the expression of α-E-Catenin and consequently to regulate cell polarization and 3D organization.

4.2 PKC activity controls the expression of genes differentially regulated by oncogenic KRAS phosphorylation

Due to the variations of the gene expression and phenotypic characteristics described above, we decided to evaluate whether the differential gene expression pattern exhibited by the oncogenic KRAS phosphomutants was dependent on the status of phosphorylation at Ser181 of oncogenic KRAS; or was a consequence of the long-adaptation time of the cells to the expression of a phosphomimetic (S181**D**) or a non-phosphorylatable (S181**A**) oncogenic KRAS mutants.

In order to answer this question, we modulated PKC activity to regulate the phosphorylation status of KRAS at Ser181 of cell clones expressing the phosphorylatable mutant **S**181. To this end, cells were treated with PKC inhibitors (BIM I and Gö6983) or with the PKC activator (TPA) and a CaM inhibitor (W13), since CaM's binding to KRAS blocks PKC dependent KRAS phosphorylation[113,117]. An initial experiment to define the doses and an adequate time of treatment to inhibit or activate PKC was performed using the oncogenic KRAS phosphorylatable **S**181 cell clone S1. Expression levels of P-MARKS and P-ERK (downstream effectors of PKC and KRAS signaling pathways, respectively) were analyzed to check the efficacy of the treatments.

As shown in figure 49A, TPA+W13 treatment was able to activate MARKS and ERK during at least 24 hours in these cells. Regarding the treatments with PKC inhibitors BIM and Gö6983, no differences in basal levels of MARKS and ERK phosphorylation were observed. Nevertheless, cells needed to be treated for at least 36 hours with BIM or Gö6983 to hinder further PKC activation and phosphorylation of both MARKS and ERK when adding TPA+W13 to the system (figure 49B). Taking this into account, it was established that the condition to induce PKC dependent phosphorylation was TPA+W13 treatment for 24 hours, and the condition to suppress PKC dependent phosphorylation was PKC inhibitor treatment for 48 hours.

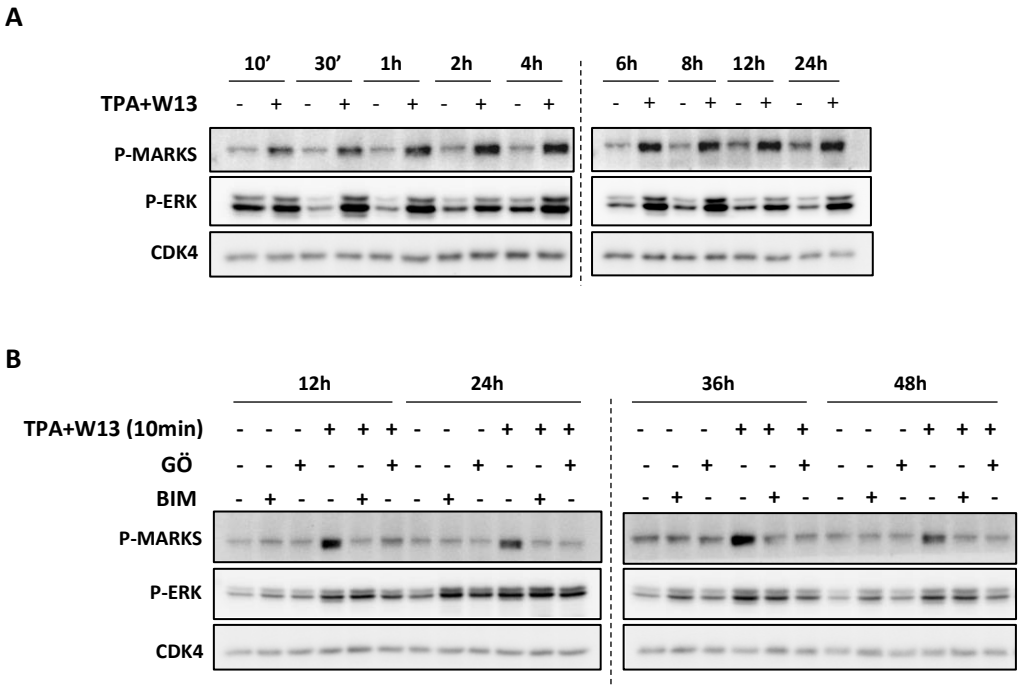

Figure 49. PKC activation or inhibition by treatment of oncogenic KRAS phosphorylatable mutant cells with TPA+W13 or BIM/Gö6983, respectively. DLD-1$^{KRASwt/-}$ cells expressing oncogenic KRAS **S**181 mutant (cell clone S1), cultured at growth factors conditions, were treated with TPA (0.1µM) and W13 (10µg/ml) for 10 and 30 minutes and 1, 2, 4, 6, 8, 12 and 24 hours **(A)** or with BIM (5µM) or GÖ6983 (2µM) during 12, 24, 36 and 48 hours. After treating the cells with PKC inhibitors, TPA+W13 were added for 10 min to check PKC activation **(B).** All cells were lysed, and extracts were immunoblotted using the indicated antibodies. CDK4 was used as loading control.

Results showed that mRNA expression levels of *SERPINE1* and *PRSS2* (low in S181**A** mutant) were reduced when oncogenic KRAS-**S**181 expressing cells were treated with PKC inhibitors, indicating that KRAS phosphorylation could be inducing the expression of these genes (figure 50A). On the other hand, *HNF4G* mRNA expression levels (which were low in phosphomimetic mutant (S181**D**) cells) were diminished after treating oncogenic KRAS-**S**181 expressing cells with TPA + W13, demonstrating that phosphorylation of KRAS could be downregulating the expression of this gene (figure 50B).

However, *CTNNA1* mRNA expression was slightly increased under both treatments (upper graphs of figure 23A and B), suggesting that the low expression of *CTNNA1* in cells expressing

oncogenic KRAS-S181**A** and KRAS-S181**D** could be an adaptation of these cell clones to the lack of KRAS phosphorylation/dephosphorylation cycle at Ser181.

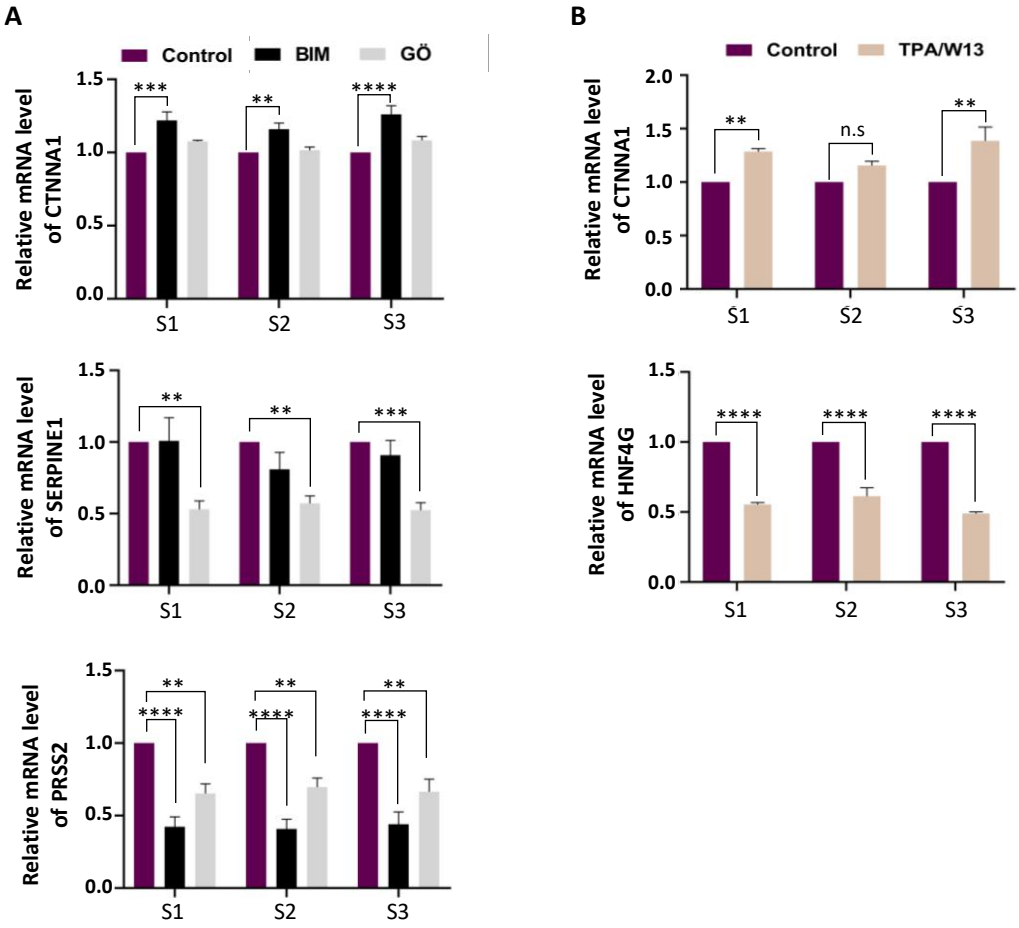

Figure 50. Pharmacological PKC activation or inhibition modifies gene expression regulated by oncogenic KRAS phosphorylation at S181. A) DLD-1$^{KRASwt/-}$ cells stably expressing KRAS-G12V- **S**181 were treated with PKC inhibitors BIM (5µM) or Gö6983 (2µM) for 48 hours. **B)** DLD-1$^{KRASwt/-}$ cells stably expressing KRAS-G12V- **S**181 were treated with PKC activator TPA (0.1µM) plus CaM inhibitor W13 (10µg/µL) for 24 hours. **(A and B)** RNA extraction was carried out and cDNA was obtained from 1µg of total RNA. Real Time quantitative PCR was performed. *HPRT1* mRNA expression was used as an internal control to normalize *CTNNA1*, *SERPINE1*, *PRSS2* and *HNF4G* mRNA expression. Normalized expression is presented relative to control of each KRAS-G12V-**S**181 clone (numbers indicate different cell clones). Data shown represent the mean ± SEM of four independent experiments. Significant differences were assessed using two-way ANOVA and Tukey's Multiple Comparisons (*p-value<0.05, **p-value<0.01, ***p-value<0.001, ****p-value<0.0001).

4.3 Gene expression in human colorectal cancer is similar to oncogenic KRAS phosphorylation signature

Since oncogenic KRAS phosphomutants showed different gene expression patterns we analyzed KRAS phosphorylation and dephosphorylation gene expression signature in human colorectal tumors. To do so, the public clinical cohort used was the GSE39582 dataset[346].

Firstly, expression of genes belonging to non-phosphorylatable oncogenic KRAS signature (KRAS-S181**A**: genes differentially expressed between KRAS-G12V-S181**A** vs KRAS-G12V-**S**181) and of genes belonging to phosphomimetic oncogenic KRAS signature (KRAS-S181**D**: genes differentially expressed between KRAS-G12V-S181**D** vs KRAS-G12V-**S**181) were analyzed in this public data set of CRC samples. Correlation analysis (Pearson's Coefficient) between the expression of different transcripts in CRC primary tumors showed that: (a) the upregulated or the downregulated genes belonging to the same signature (KRAS-S181**A** or KRAS-S181**D**) compared between them, were positively correlated; (b) upregulated versus repressed genes within the same signature (KRAS-S181**A** or KRAS-S181**D**) were negatively correlated; and (c) a negative correlation was observed in the comparative analysis between KRAS-S181**A** and KRAS-S181**D** signatures (Figure 51A). These data suggest that these genes are co-regulated by an upstream event that is most probably dependent on KRAS phosphorylation status.

After that, gene expression of normal tissue was compared to the one of tumor samples by analyzing the same public cohort. The analysis showed that gene expression of colorectal tumors was more similar to the KRAS phosphorylation signature (KRAS-S181**D**) than to the non-phosphorylated one (KRAS-S181**A**) (figure 51B).

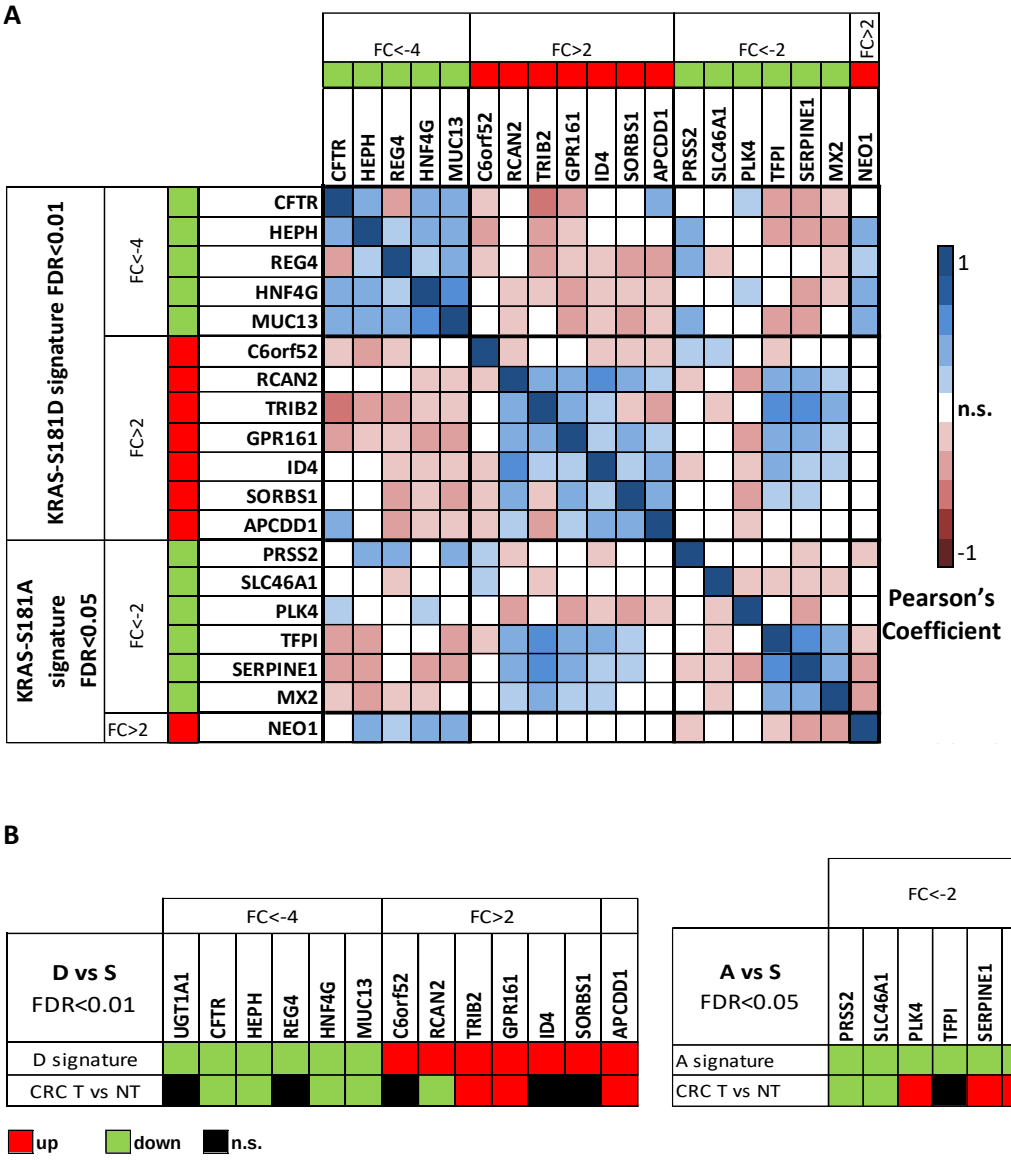

Figure 51. Expression of oncogenic KRAS-S181D and KRAS-S181A signature in human CRC primary tumors and normal colon. (A) Correlation matrix (Pearson's Coefficient) between the expression of genes belonging to KRAS-S181**A** and KRAS-S181**D** signatures analyzed in human CRC primary tumors (GSE39582). The KRAS-S181**D** signature was restricted (FC<-4 or FC>2) in order to have a similar number of genes in each one. UGT1A1-10 and CTNNA1 are excluded from the analysis (the first because is a group of genes and the second because it belongs to both signatures). Correlation is considered when p-value P<0.01 (student T-test). **(B)** Color-map showing relative expression of genes belonging to KRAS-S181**A** and KRAS-S181**D** signatures in CRC human primary tumors (CRC T) versus normal tissue (NT) (GSE39582). Differences were considered when p-value P<0.01.

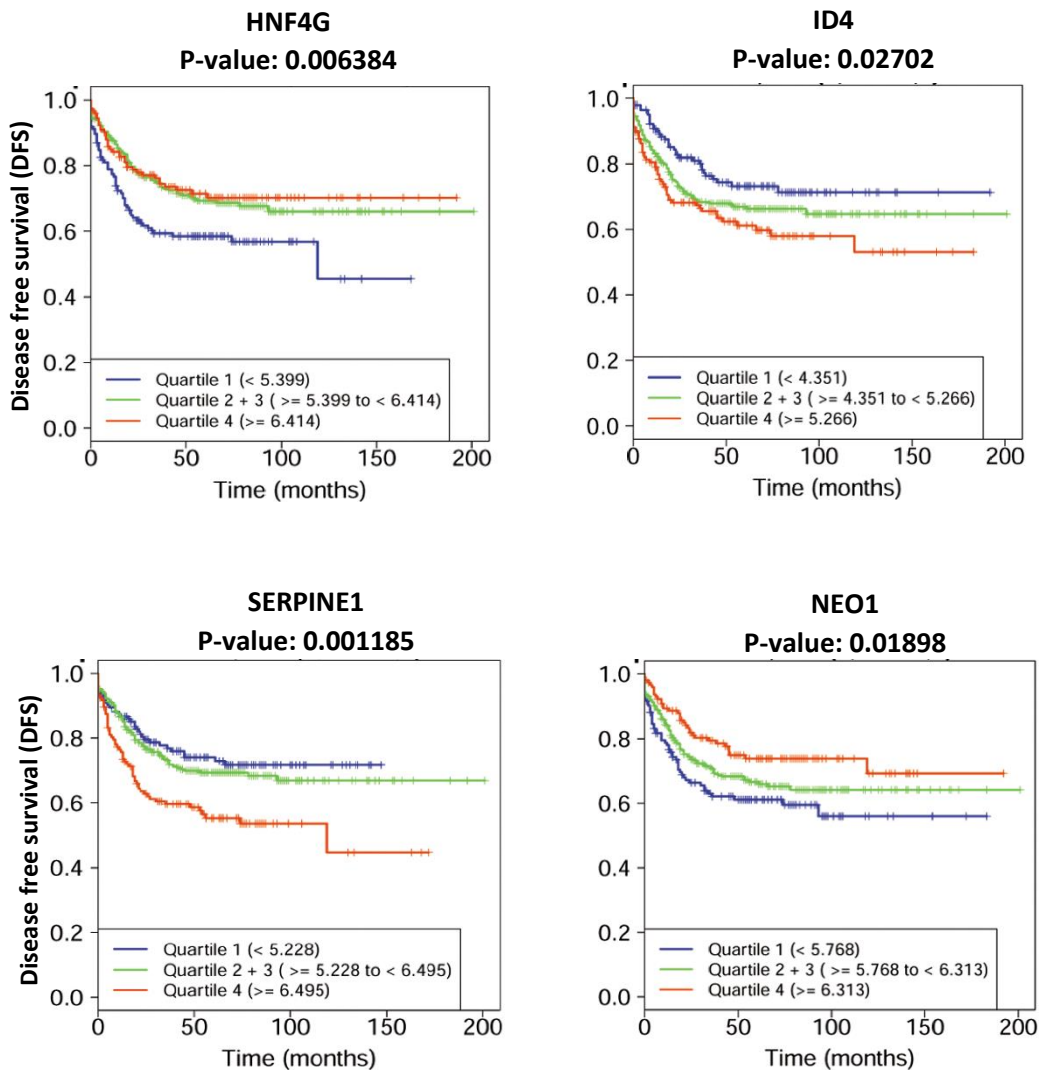

Figure 52. Gene expression of phosphomimetic oncogenic KRAS signature is similar to gene expression in human CRC. DFS Kaplan-Meyer curves using the same public cohort used in figure 24. Each curve represents the percentage (Y-axis) of the population that exhibits recurrence of the disease along time (X-axis, in months) for each indicated quartile.

Finally, DFS was analyzed for different genes belonging to KRAS-S181**A** and KRAS-S181**D** signatures. The analysis showed that patients with tumors with low expression of *HNF4G* (gene downregulated in KRAS-S181**D** signature) or with high expression of *ID4* (gene overexpressed in KRAS-S181**D** signature) presented shorter DFS. Conversely, patients that

exhibit tumors with overexpressed *NEO1* (gene highly expressed in KRAS-S181**A** signature) or with repressed *SERPINE1* (gene downregulated in KRAS-S181**A** signature) showed longer DFS (figure 52).

Summarizing all data, we conclude that gene expression signature of phosphomimetic oncogenic KRAS is more similar to human CRC gene expression, than to the one of the non-phosphorylatable form, correlating with a lower DFS, and suggesting that KRAS phosphorylation at Ser181 is important to CRC development.

CHAPTER 5

Role of KRAS phosphorylation at Ser181 in cell invasion

The invasive capacity of DLD-1 KO cells expressing the different oncogenic KRAS phosphomutants (*analyzed in Chapter 1*) was independent of the status of KRAS phosphorylation at Ser181, although a slight non-significant increase was observed in the phosphomimetic mutant. However, as mentioned above, DLD-1 cell line presents low capacities for migration and invasion due to a scarce ability to perform epithelial-mesenchymal transition[241,254,356]. For this reason, DLD-1 was not a good model to study invasive capacity of cells in CRC. Therefore, we chose the SW480 CRC cell line (KRAS-G12V-**S**181), which has high EMT potential to evaluate whether KRAS phosphorylation at Ser181 regulates the invasive capacity of cells. In this case, instead of generating stable clones expressing phosphomutants, we generated by CRISPR a S181**A** mutation in one of the alleles of oncogenic KRAS.

As shown in figure 53A, the invasive capacity of SW480 cells with S181**A** mutation was significantly reduced when compared to SW480 cell line (KRAS-G12V-**S**181). Moreover, mRNA levels of *SERPINE1*, a gene involved in vascular co-option and invasion, were also reduced in these cells (figure 53B), suggesting that KRAS phosphorylation was modulating the invasive capacity of cells in CRC.

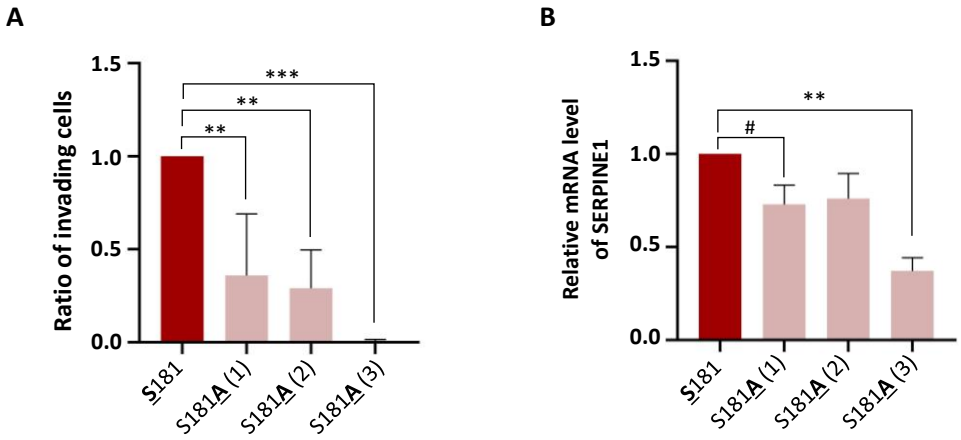

Figure 53. KRAS phosphorylation at Ser181 modulates the invasion capacity in SW480 cell line. (A) SW480 cells (**S**181) or SW480 with S181**A** mutation (numbers indicate different clones) were seeded in the upper compartment of Boyden chambers covered with Matrigel under serum limiting conditions (0.1%FBS). In the lower compartment, medium supplemented with 10%FBS was added as an attractor. After 48 hours, cells were stained with Hoechst and images were obtained by confocal microscopy. The number of invading cells was calculated as the number of cells counted in the lower compartment divided by the number of areas counted**.**

Data show the invading cell ratio and represent the mean ± SEM of three independent experiments. Significant differences were assessed using one-way ANOVA and Dunnett's Multiple Comparisons Tests compared to SW480 cell line (**S**181) (*p-value<0.05, **p-value<0.01, ***p-value<0.001, ****p-value<0.0001). **(B)** RNA extraction from SW480 cells (**S**181) and SW480 cells with S181**A** mutation carried out and cDNA was obtained from 1µg of total RNA. Real Time qPCR was performed. *HPRT1* mRNA expression was used as an internal control to normalize *SERPINE1* mRNA expression. The normalized expression of *SERPINE1* is relative to SW480 cell line (**S**181). Data shown represent the mean ± SEM of four independent experiments. Significant differences were assessed using one-way ANOVA and Dunnett's Multiple Comparisons Tests compared to SW480 cell line (**S**181) (*p-value<0.05, **p-value<0.01, ***p-value<0.001, ****p-value<0.0001). # significant differences using unpaired t test.

Finally, we proceeded to prove if the differences in gene expression observed when comparing DLD-1 KO stably expressing oncogenic KRAS-S181**A** and **S**181 phosphomutants, were also present when SW480 cell lines were analyzed. Low expression levels of *SERPINE1* and *CTNNA1* were also observed in at least 2 of the 3 clones of SW480 cells with S181**A** mutation (figure 53B and figure 54A and B). Furthermore, increased protein levels of Neogenin1 were also corroborated in these cells by WB analysis (figure 54B).

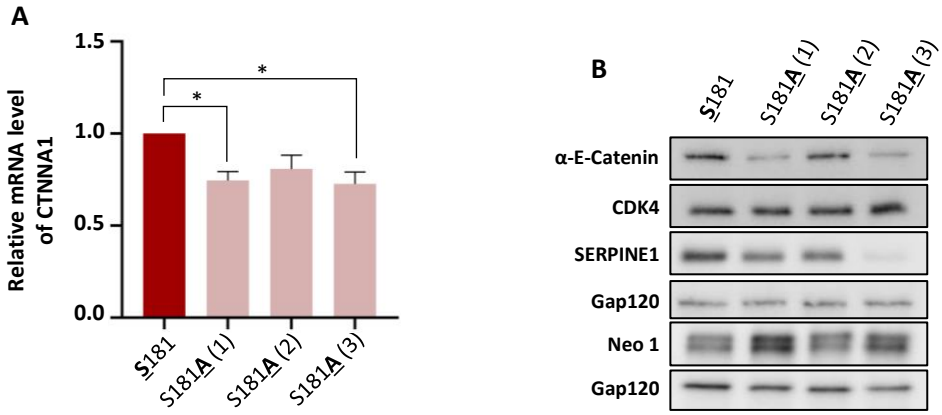

Figure 54. Differential gene expression pattern of non-phosphorylatable versus phosphorylatable mutant is corroborated in SW480 cell line with S181A mutation. (A) RNA extraction from SW480 cells (**S**181) and SW480 cells with S181**A** mutation were carried out and cDNA was obtained from 1µg of total RNA. Real Time qPCR was performed. *HPRT1* mRNA expression was used as an internal control to normalize *CTNNA1* mRNA expression. The normalized expression of *CTNNA1* is relative to SW480 cells (**S**181). Data shown represent the mean ± SEM of four independent experiments. Significant differences were assessed using one-way ANOVA and Dunnett's Multiple Comparisons Tests compared to SW480 cells (**S**181) (*p-value<0.05, **p-value<0.01, ***p-value<0.001, ****p-value<0.0001). **(B)** Cellular extract from SW480 cells were obtained and immunoblotted to detect the indicated proteins. Gap120 and CDK4 were used as loading controls

SECTION 2

Biological analysis of peptidomimetics for RAS inhibition

CHAPTER 6

Searching for KRAS inhibitors

In silico results presented in this chapter have been obtained by IPROTEOS team and they have been explained in detail in Josep Rivas Santos' Doctoral Thesis

6.1 Background

As mentioned in the introduction section, an effective direct therapy against oncogenic RAS has not yet been obtained. However, different strategies to inhibit RAS proteins indirectly have been developed, for example: to block RAS localization at the plasma membrane, to inhibit downstream effectors of RAS, to interfere with RAS-dependent metabolism of cancer cells, or to interfere with oncogenic RAS interactors[59,234,272,370,371]. Nevertheless, unclear results have been obtained with these experimental approaches. For that reason and taking advantage of methodological advances, the scientific community has focused again on the search for direct RAS inhibitors. At present, one of the strategies that is being followed is to search for drugs able to disrupt the interaction of RAS with its effectors[198,233,298].

Modulation of PPIs has been studied intensely due to the large number of PPIs involved in the cell machinery[372]. However, because of the nature of the PPIs, regulation of these interactions is complicated. PPIs have commonly been regarded as undruggable due to the contact surface area between proteins is larger than the contact area needed for small molecules binding. Moreover, many of these interactions do not present obvious pockets where a small molecule can properly interact and accommodate[297]. As an alternative to the use of small molecules to modulate PPIs, the application of biologics molecules such as antibodies is being explored. Antibodies present a larger structure than small molecules, which allows them to recognize and interact with extended protein surfaces. However, this feature limits the capacity of antibodies to cross biological barriers and thus their therapeutic use. Considering these data, peptides, whose chemical space is between those of traditional small molecules and antibodies, have emerged as a promising tool to modulate PPIs biological activity[323,324,328]. This is also due to their capacity to mimic aminoacid sequences and secondary structures of the protein domains of the natural interactions[327]. Besides that, other advantages of using peptides are their adaptability to large protein surfaces, easy modularity, low toxicity and size (which limits accumulation in tissue)[325,326]. Nonetheless, the poor capability to cross physiological barriers and the rapid degradation by proteolytic enzymes are often major limitations for their clinical applications[326,373].

For all these reasons, peptides modified with non-natural amino acids, cyclization or with unusual peptide bonds, known as peptidomimetics, have been developed and applied to modulate PPIs. These modifications allow to improve stability and permeability of the peptides in cells as well as their binding affinity with their targets[326,328].

6.2 Generation of peptidomimetics of RAS effector domain by Iproteos technology

The peptidomimetics able to prevent the interaction of RAS proteins with their effectors (used in this thesis) were designed *in silico* applying the Iproteos technology, and synthesized, purified and quantified by IPROTEOS team. Iproteos was founded in 2012 with the aim of applying peptidomimetic novel structures to target intracellular PPIs of therapeutic interest. Iproteos proprietary technology, IPROTech, consist of a set of algorithms addressed to design and develop permeable peptidomimetic structures to inhibit intracellular PPIs with large affinity and selectivity. This computational approach to generate peptidomimetics is an alternative to other more tedious experimental techniques, like using antibody fragments intracellularly for the identification of hot spots on the protein surface and to develop potential therapeutics[310]. Once the computational evaluation of PPI is completed, compounds proposed as more active are synthesized and characterized in terms of permeability, stability and potential activity versus the desired protein target. In the company website, *www.iproteos.com*, more information about Iproteos and IPROtech can be found.

In order to design and engineer the peptidomimetics used in this project, the identification of RAS pharmacophore sites was carried out. Afterwards, the identification of peptidomimetics was based on the screening of a virtual library of 80000 tri- and tetra-peptidomimetics against the identified hot spots of the protein (step 1 and 2); *in silico*

prediction of the permeability of the identified hits (step 3); and synthesis and *in vitro* evaluation of the most promising candidates (step 4) (figure 55).

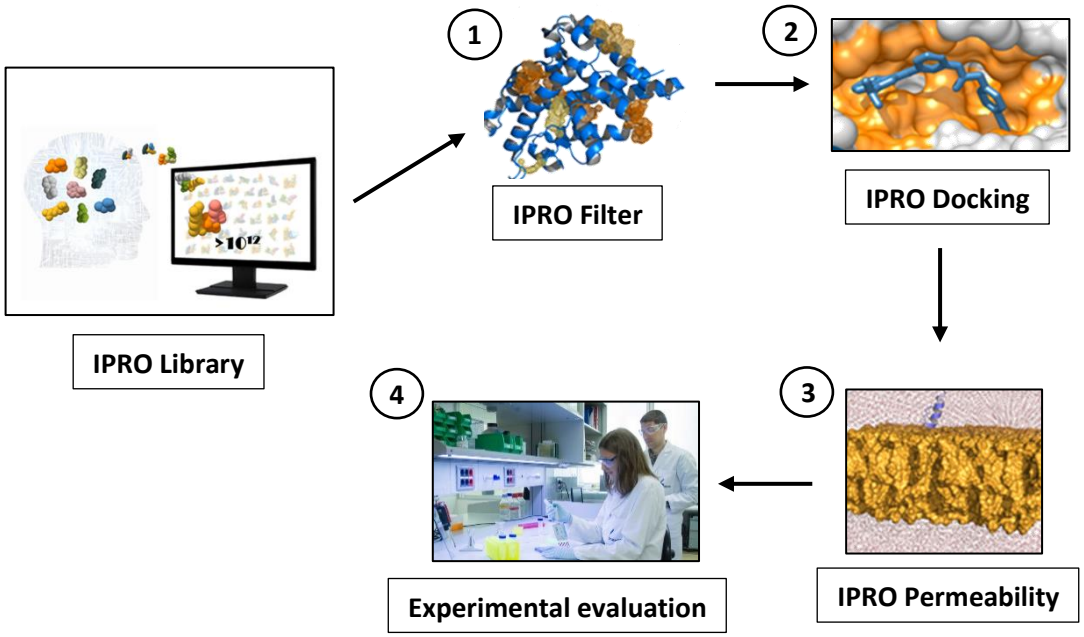

Figure 55. Scheme of the steps of Iproteos technology adapted from the company website. Screening of peptidomimetic virtual library (IPRO library) is carried out. Then, the identification of peptides is based in computational tools (IPRO filter, IPRO docking and IPRO permeability). Finally, the selected compounds are synthetized and evaluated. This process is repeated until a good candidate is obtained.

CHAPTER 7

Effect of the peptidomimetics in RAS signaling and pancreatic cancer cells viability

7.1 The peptidomimetics reduce the activation of RAS transduction pathways in non-transformed cells

In order to study whether the peptidomimetics against the effector domain of RAS (designed by Iproteos technology to inhibit RAS) were able to interfere with the activation of KRAS downstream signaling, hTERT-RPE starved cells (non-transformed cells) were treated with 9 different peptidomimetics followed by EGF stimulation.

First, we checked the solubility of the peptides when cells were cultured under growth factors limiting conditions. As it can be observed in the phase-contrast microscope images, peptidomimetics 4, 6, 7 and 9 (P4, P6, P7 and P9) generated aggregates in the cell culture medium, being those of the P6 the largest (they could be macroscopically visualized). Moreover, although P4, P5 and P9 induced massive cell death, P5 was the most efficient (figure 56). Therefore, P5 and P6 were discarded from the analysis.

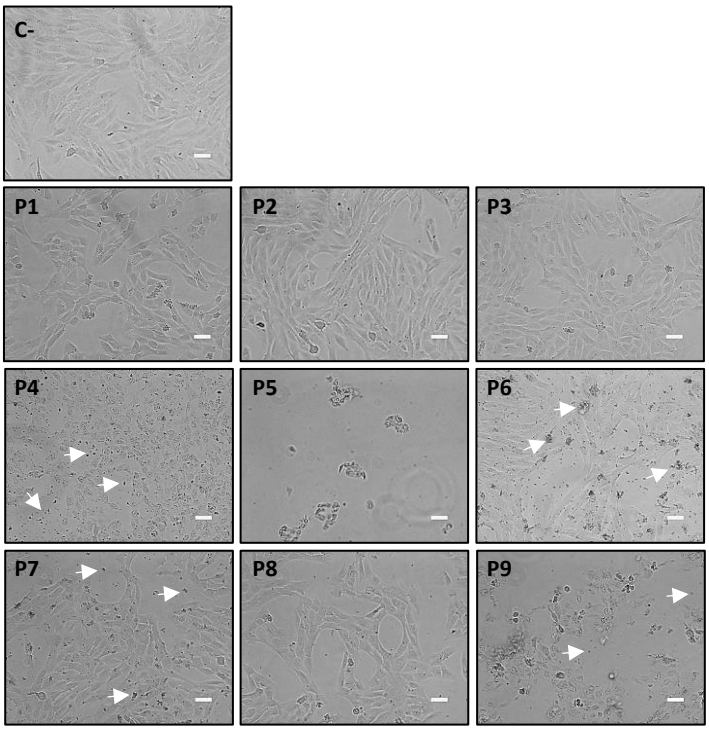

Figure 56. The peptidomimetics show different solubility. hTERT-RPE starved cells were incubated with 50µM of the indicated peptidomimetics for 2 hours. Phase-contrast microscope images were obtained. Arrows indicates the aggregates. All scale bars, 50µm.

Consecutively, extracts from cells treated with the indicated peptidomimetics and then EGF stimulated were analyzed by WB using antibodies against the active and total forms of the main KRAS downstream signaling proteins. Cells incubated with P1, P2, P3, P4 and P8 were not able to activate c-RAF and ERK in response to EGF. Additionally, AKT activation was reduced in cells treated with P1, P3, P4, P7 and P8 (figure 57). Considering these data, P1, P3 and P8 were able to decrease both c-RAF-MEK-ERK1,2 and the PI3K/AKT signaling pathways, thus being the most effective peptidomimetics. P4 was not considered (grey color) since not enough protein for WB analysis could be obtained due to cell death.

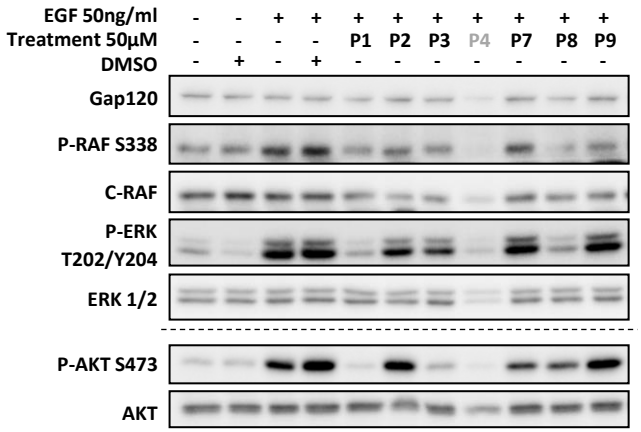

Figure 57. The peptidomimetics reduce endogenous downstream RAS signaling. hTERT-RPE cultured under starved conditions were incubated with 50 µM of the indicated peptidomimetics for 2 hours and the levels of activation of the c-RAF-MEK-ERK1,2 and PI3K/AKT pathways after EGF stimulation for 10 minutes were studied by WB. Specific antibodies against the active phosphorylated and total proteins were used. GAP120 was used as a loading control.

After that, we determined whether P1, P3 and P8 were able to reduce the activation of c-RAF-MEK-ERK1,2 and PI3K/AKT signaling pathways at lower concentrations. Data showed that P1 was able to decrease AKT activation already at 10µM, while P3 and P8 inhibited AKT activation at 25 and 50µM, respectively. ERK activation was disrupted at 50µM for the three peptidomimetics (figure 58).

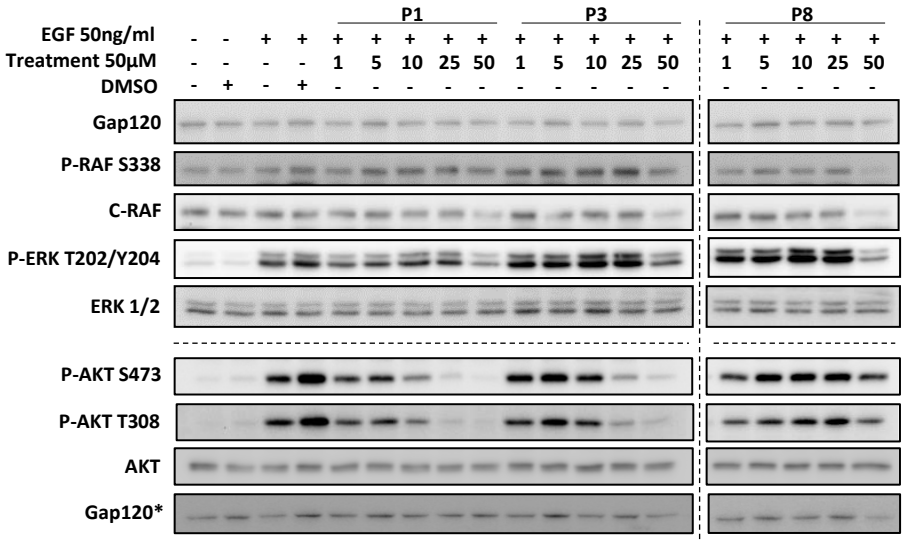

Figure 58. P1 decreases PI3K/AKT signaling at lower concentrations. hTERT-RPE cultured under starved conditions were treated with the indicated peptidomimetics in a range from 1, 5, 10, 25 and 50 µM for 2 hours followed by 10 minutes of EGF stimulation. Antibodies against the specific phosphorylated and non-phosphorylated proteins were incubated to determine the activation of the signaling pathways. Gap120 was used as a loading control.

Finally, as we observed that P1 inhibited PI3K/AKT signaling pathway at lower concentrations than the others, we evaluated whether P1 was able to maintain this inhibition during longer time of EGF stimulation. WB analysis showed that P1 prevented AKT activation after EFG addition at least for 60 minutes (figure 59).

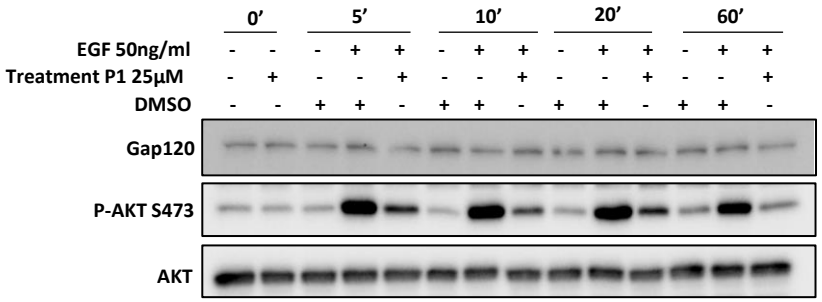

Figure 59. P1 prevents the PI3K/AKT signaling pathway activation during an extended EGF stimulation. hTERT-RPE cultured under starved conditions were treated with the P1 at 25µM for 2 hours followed by 5, 10, 20 and 60 minutes of EGF addition. Antibodies against the specific phosphorylated and non-phosphorylated proteins were incubated to determine the activation of the PI3K/AKT signaling pathway. Gap120 was used as a loading control.

Therefore, we concluded that P1 was the most efficient peptidomimetic in inhibiting KRAS downstream signaling in non-transformed cells.

7.2 Oncogenic KRAS-effector protein-protein interaction is impaired by the treatment of cells with the peptidomimetics

Since peptidomimetics were designed *in silico* to interact with RAS effector domain and we observed that peptidomimetics 1, 3 and 8 were able to decrease RAS downstream signaling, we investigated if the interaction between oncogenic KRAS and its two main effectors, c-RAF and PI3K, was disrupted by the treatment with these compounds. In order to analyze this interaction, serum starved HeLa cells were transfected with pEF-HA-KRAS-G12V expression plasmid (for 48 hours) before being treated with the peptidomimetics and EGF. Then, immunoprecipitation with anti-HA antibodies immobilized on agarose beads, which allowed isolation of protein complexes by centrifugation, was performed.

As an initial experiment to determine the dose of treatment necessary to disrupt RAS-effector interaction, cells were incubated with increasing concentrations of P1. Immunoprecipitation assay showed that P1 treatment reduced the interaction of oncogenic KRAS with c-RAF and PI3K effectors at 100µM compared to control (DMSO) (figure 60).

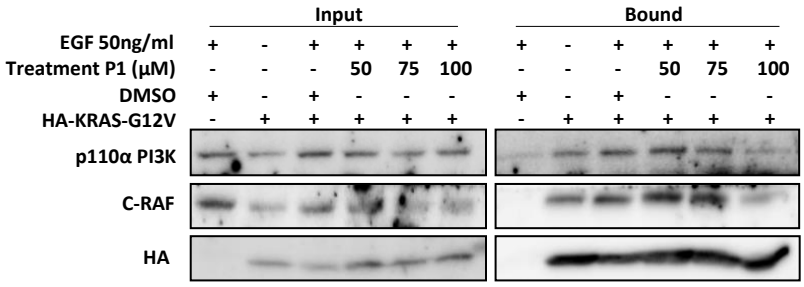

Figure 60. P1 disrupts oncogenic KRAS interaction with c-RAF and PI3K effectors. Co-immunoprecipitation of HA-KRAS-G12V with c-RAF or with PI3K were analyzed in starved HeLa cells expressing HA-KRAS-G12V after being incubated with P1 (in a range from 50, 75 and 100 µM) for 2 h, and EGF stimulated for 10 min. IP was performed with anti-HA antibodies immobilized on agarose beads and the bound and input fractions were incubated with anti-p110α PI3K and anti-C-RAF antibodies.

Following this result, we tested the effect of peptidomimetics 3 and 8 under the same conditions. Results shown in figure 61 indicate that the most efficient peptide to disrupt oncogenic KRAS binding to both effectors was P1, while P3 and P8 were only able to disrupt KRAS interaction with p110α PI3K.

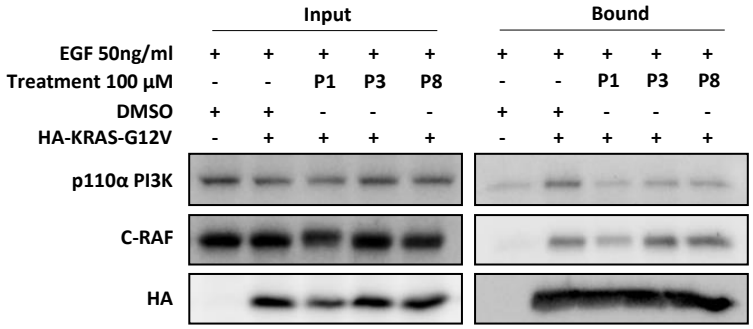

Figure 61. The peptidomimetics 3 and 8 only disrupt oncogenic KRAS binding with PI3K effector. Co-immunoprecipitation of HA-KRAS-G12V with c-RAF or with PI3K was analyzed in starved HeLa cells expressing HA-KRAS-G12V after being incubated with P1, P3 and P8 for 2 hours at 100µM and EGF stimulated for 10 minutes. IP was performed using anti-HA antibodies immobilized on agarose beads, and the bound and input fractions were incubated with anti-p110α PI3K and anti-C-RAF antibodies.

Considering the biological assays presented until now, the main conclusion was that the P1 was the most efficient peptidomimetic to reduce oncogenic KRAS interaction with its effectors PI3K and c-RAF, and as consequence, it affects negatively downstream RAS signaling pathways. Therefore, we chose the peptidomimetic P1 to be *in silico* modified with the objective of improving its inhibitory capacity.

7.3 Peptidomimetic 1.3 reduces downstream RAS signaling and KRAS effector binding capacity

A total of four compounds derived from P1 were obtained by Iproteos technology and were studied under the same conditions as the previous peptidomimetics. Therefore, hTERT-RPE

cells were treated with the new compounds P1.1, P1.2, P1.3 and P1.4 followed by EGF stimulation. P1.2 and P1.3 diminished the activation of c-RAF, ERK and AKT by EGF, being peptidomimetic 1.3 the most effective, even when compared to peptidomimetic 1 (P1). Conversely, no differences were observed in downstream RAS signaling when cells were treated with P1.1 and P1.4 (figure 62A).

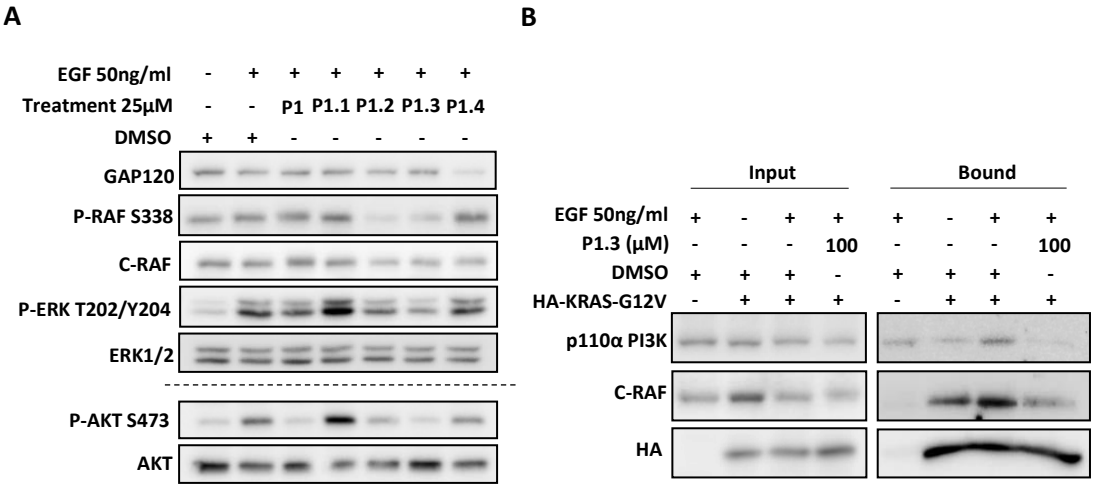

Figure 62. P1.3 disrupts oncogenic KRAS interaction with c-RAF and PI3K effectors thus regulating downstream RAS signaling. (A) hTERT-RPE cells cultured under starved conditions were incubated with 25µM of the indicated peptidomimetics derived from P1 for 2 hours followed by EGF stimulation for 10 minutes. Cells extracts were immunoblotted with the indicated antibodies. Gap120 was used as a loafing control. **(B)** Co-immunoprecipitation of HA-KRAS-G12V with c-RAF or with PI3K was analyzed in starved HeLa cells transfected with HA-KRAS-G12V after being incubated with P1.3 for 2 hours and EGF stimulated for 10 minutes. The HA antibodies immobilized on agarose beads were used to immunoprecipitation of complexes of proteins. The bounds and inputs fractions were immunoblotted using the c-RAF and p110α PI3K antibodies.

Regarding the immunoprecipitation assay, P1.3 was able to disrupt oncogenic KRAS interaction with its effectors c-RAF and PI3K (figure 62B). Therefore, these results suggested that the P1.3, derived from P1, was a good candidate to inhibit RAS signaling in cancer cells expressing oncogenic KRAS.

7.4 Viability of pancreatic cancer cells is impaired by treatment with peptidomimetic P1.3

Once P1.3 was stablished as the most promising compound due to its high capacity to inhibit oncogenic KRAS binding to effectors and to reduce activation of downstream RAS signaling, P1.3 impact on cell viability was evaluated by MTS assay. To asses this, six pancreatic adenocarcinoma human cell lines harboring different mutations in oncogenic KRAS and one non-transformed cell line (hTERT-RPE cells) were used.

Remarkably, dose-response experiments showed that P1.3 was able to reduce cell viability with an IC_{50} of 20-23µM in all tumor cells. However, less than 10% of the normal cells were affected at this concentration (figure 63).

Therefore, we concluded that P1.3 treatment killed pancreatic tumor cells expressing oncogenic KRAS selectively, since normal cells were not affected.

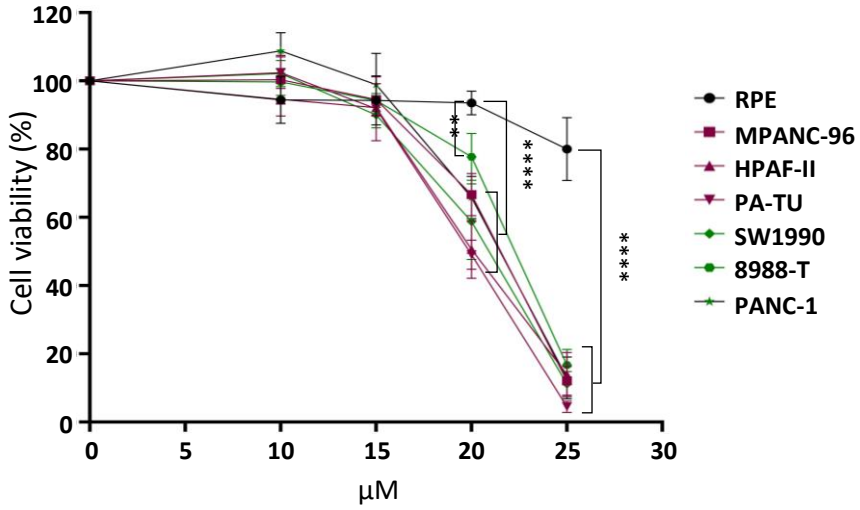

Figure 63. P1.3 reduces pancreatic adenocarcinoma cells viability. 1x10^4 cells belonging to 6 different pancreatic cancer and one normal cell lines were cultured at serum saturating conditions in individual wells of a 96-wells plate. After 24 hours, cells were treated with P1.3 at 10, 15, 20 and 25µM for further 24 hours. MTS viability assay was performed following the manufacturer's specifications and absorbance was measured at 490 nm. The representative graph shows the percentage of cell viability calculated by dividing the absorbance of each well by the average absorbance of the control wells. Statistical analysis was performed with GraphPad Prism 8.1. The mean ± SD of six wells are shown. Significant differences were assessed using one-way ANOVA and Dunnett's Multiple Comparisons Tests and considered when $P<0.05$ compared to RPE cell line (normal cells).

7.5 Peptidomimetic P1.3 does not regulate downstream RAS signaling in pancreatic cancer cells

Since viability of pancreatic cancer cells was reduced by P1.3 treatment, we next evaluated whether P1.3 was decreasing RAS signaling in these cell lines. In order to reproduce the conditions of MTS assay, pancreatic cancer and normal cells were treated with 25µM of P1.3 under growth factors saturated conditions. After 3 hours, activation of c-RAF-MEK-ERK1,2 and PI3K/AKT signaling pathways were analyzed by WB.

Despite the variability observed between cell lines, cell treatment with P1.3 was not able to reduce the basal levels of P-RAF, P-ERK, P-AKT and P-S6 (figure 64).

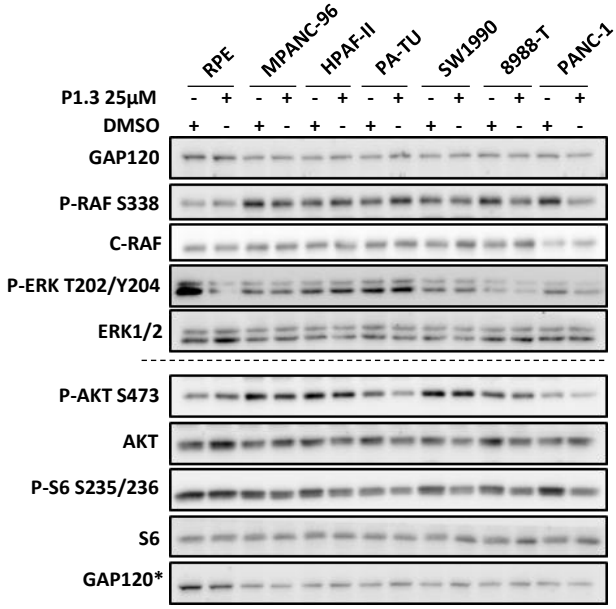

Figure 64. RAS signaling pathways are not modified by P1.3 in pancreatic cancer cells. Cells were cultured at growth factors saturated conditions (10%FBS) for 24 hours and treated for 3 hours with the drug. After that, total lysates from the different cell lines were analyzed by immunoblot to detect the indicated proteins. Gap120 was used as a loading control.

Considering these results, it is possible that downstream RAS signaling in pancreatic cancer cells might not have been analyzed under the adequate conditions. Therefore, cell signaling under growth factors-limiting conditions plus EGF stimulation (as previous experiments), or after a longer treatment time with P1.3, if the experiment is performed at serum saturating conditions, will need to be evaluated.

Therefore, the main conclusion drawn from all data presented is that IPROtech technlogy allowed us to obtain, in a quick and cost-effective manner, the compound P1.3, which efficiently inhibited the interaction of oncogenic KRAS with its effectors in cells. In addition, from an interesting therapeutic point of view, P1.3 showed high selectivity in killing pancreatic cancer cells expressing oncogenic KRAS versus non-transformed epithelial cells.

DISCUSSION

Activating point mutations that render RAS proteins insensitive to the extracellular signals are crucial steps in the development of most of the cancers, being oncogenic KRAS the most prevalent in human malignancies[198,231,374]. Oncogenic KRAS is able to interact with different effectors, activating several signal transduction pathways. Among those, the best characterized are the c-RAF-MEK-ERK and the PI3K/AKT pathways. KRAS signaling activation can be achieved by recruiting its effectors to the plasma membrane, by acting as an adaptor protein, or by direct stimulation of the intrinsic catalytic capacity of its effectors.

Unfortunately, despite numerous advances in diverse direct and indirect approaches to inhibit oncogenic KRAS have been reported, there is still no selective treatment for KRAS driven cancers[198,261,272].

On the one hand, since oncogenic mutations often maintains fully active GTP-loaded KRAS, which in turn can sustain cell signaling constitutively active, any modification capable of altering its oncogenic signaling was not initially expected. Nevertheless, in recent years, emergence of new regulators either by direct interaction or by conditional posttranslational modifications have been reported to modulate KRAS phenotype. In this way, monoubiquitination at Lys147[148–150], acetylation at Lys104[151,152], nitrosylation at Cys118[153–157] and phosphorylation at Ser181[62,76,117,122,144] were lately reported to substantially regulate KRAS oncogenic activity, being phosphorylation at Ser181 by PKC[141] the most studied. Thus, interfering with this posttranslational modification may open up a new therapeutic opportunity, but first, the relevance of this phosphorylation in the maintenance of the tumorigenic properties of stablished cancer cells must be demonstrated.

Considering these findings, in the present thesis, we investigated the impact of KRAS phosphorylation at Ser181 on its oncogenic activity at distinct levels. The studies performed to date have mainly used non-transformed cell lines, therefore, the role of KRAS phosphorylation at Ser181 in initial cell transformation[62,122,144] has been analyzed so far. In this project, we used DLD-1 cells, which are oncogenic KRAS dependent and have been shown to be a good model for the study of CRC[241,375]. This has allowed us to investigate the

contribution of oncogenic KRAS phosphorylation in the maintenance of the tumoral properties of cancer cells.

With this premise, we exogenously expressed oncogenic KRAS with different mutations at Ser181 in a genetically modified DLD-1 cell line (DLD-1 KO). These cells have the endogenous oncogenic KRAS allele deleted (KRASWT/-) avoiding the potential interference of the endogenous oncogene in the experiments. Furthermore, unlike our previous study[144], we selected cell clones with exogenous oncogenic KRAS expression at levels comparable to those of the endogenous KRAS WT thus preventing effects due only to oncogenic KRAS overexpression such as the induction of a mesenchymal phenotype[376].

On the other hand, one of the strategies that is widely being followed to inhibit RAS is to search for drugs able to disrupt RAS interactions with other proteins, among them its effectors[198,233,298]. For that reason, peptidomimetics have emerged as a promising tool to modulate the biological activity of PPIs, since they can explore large protein surfaces and have an improved binding affinity for their targets[323,324] compared with the traditional peptides.

Accordingly, in the present thesis, we studied whether different peptidomimetics of the effector domain of RAS, designed by the Iproteos technology to inhibit RAS, were able to interfere with oncogenic KRAS activity. The cancer model selected for this research was the PDAC, which is a highly metastatic disease with a high mortality rate[245]. Considering that, the effect on cell viability of treating PDAC cells with the most promising compounds was evaluated.

I. Oncogenic KRAS induces cell proliferation and modulates ERK and AKT activation in 2D cell cultures regardless of phosphorylation at Ser181

Based on these considerations, we proceeded to investigate the role of KRAS phosphorylation at Ser181 in a model of CRC to assess its potential as a therapeutic target. To begin with, we analyzed extensively the DLD-1 KO cell line stably expressing oncogenic KRAS with different mutations at Ser181 (KRAS-G12V-**S**181, KRAS-G12V-S181**A** and KRAS-G12V-S181**D**) grown in 2D cultures.

We have evidenced that all oncogenic KRAS phosphomutants show an epithelial-like morphology. But whereas oncogenic KRAS-**S**181 clones form compact clusters, in which the boundaries between the cells are barely perceptible, KRAS-S181**A** and KRAS-S181**D** mutants do not achieve this type of cell organization. Despite morphological differences, we report that cell cycle entry and survival under growth factors limiting conditions, which are dependent on oncogenic KRAS expression, are independent of the phosphorylation status of the oncogene. Furthermore, all oncogenic KRAS phosphomutants recover the growth capacity of the DLD-1 KO cells under serum starvation, indicating that they are functional proteins. In agreement with other studies[254], cell proliferation of DLD-1 KO at serum saturating conditions is not affected. All these findings indicate that the signaling pathways responsible for cell survival under growth factors limiting conditions are independent of the phosphorylation status of oncogenic KRAS.

In view of these results, we investigated whether phosphorylation at Ser181 of oncogenic KRAS was important for the regulation of c-RAF-MEK-ERK1,2 and PI3K/AKT signaling pathways. Surprisingly, under serum starved conditions, DLD-1 KO cells display the highest basal levels of P-AKT and P-ERK and the lowest of P-S6. Conversely, the levels of activation of ERK, AKT and S6 in cells expressing the different oncogenic KRAS phosphomutants are reduced, and similar to the ones of DLD-1 cells. A part from in this work, as exposed above, we had previously demonstrated that exogenously expressed oncogenic KRAS phosphomutants were functional proteins, which were GTP-loaded and able to bind to RBD of RAF[76,117]. Therefore, the reduced activation of these KRAS downstream signaling when

expressing oncogenic KRAS phosphomutants seems surprising. Nevertheless, it has been reported in DLD-1 and other CRC cells that although the presence of oncogenic KRAS led to an increase in GTP-loaded KRAS, this did not entail an increase in downstream signaling[254]. Insufficiency may arise due to the complex coordinated regulation of kinases, phosphatases, scaffolds, and cofactors required for activation of c-RAF-MEK-ERK1,2 [163] and PI3K/AKT pathways[188], and also to negative feedbacks effects. Moreover, a comparative analysis of different oncogenic KRAS mutants expressed at near-physiologic levels performed in human MCF10A isogenic cells lines, showed an overall modest downstream signaling activation[376]. More recently, it has been demonstrated that in CRC cell lines expressing different oncogenic RAS mutants, despite displaying significant RAS activation, the downstream outputs were minimal in the absence of growth factors inputs, due in part to the existence of negative feedback-loops[355]. Indeed, this report also proposed that mutant RAS is unable to activate RAF under serum starvation, arguing that additional growth factor signaling is required for RAF activation. In agreement with these data, all oncogenic KRAS phosphomutants are able to respond to EGF stimulation with very low increase of P-ERK and P-AKT resembling to those of DLD-1 cells. Once more, DLD-1 KO cells present the highest levels of activation. Taking into account all this information, it seems that the scarce signaling activation under basal (0%FBS) or EFG stimulation conditions in cells expressing oncogenic KRAS may be important for them to prevent cytotoxic stress, low viability, cell death or senescence[283]. Moreover, it is rational to propose that the high levels of signaling activation observed in DLD-1 KO cells under starved conditions, could be one of the reasons for their low proliferation rates. According to this, we detect an increase in the amount of the cell cycle inhibitor P21Cip1 in these cells. Denote that P21 is also enhanced in DLD-1 KO cells under growth factor conditions, due to ERK signaling activation. However, this increase is not enough to diminish cell proliferation, maybe due to the activation of additional signaling pathways.

Finally, although DLD-1 KO cells exhibit high AKT activation under growth factor limiting conditions, the levels of its downstream protein PS6 are low. One possible explanation is

that aminoacids, which might be low in this situation, are also required for proper activation of MTORC1, which is responsible for the activation of S6K, which in turn phosphorylates S6. On the other hand, MTORC1 can negatively regulate RTK receptors, thus decreasing the signaling. Moreover, it is known that S6K decreases the mTORC2-dependent phosphorylation of AKT S473. Therefore, a high AKT activation would induce a high MTORC1 stimulation that in turn negatively would regulate RTK signaling, decreasing S6K activation and thus S6 phosphorylation. Consequently, S6K could not inhibit MTORC2 and the phosphorylation of AKT S473 would be sustained, maintaining this activation loop[188] (figure 65).

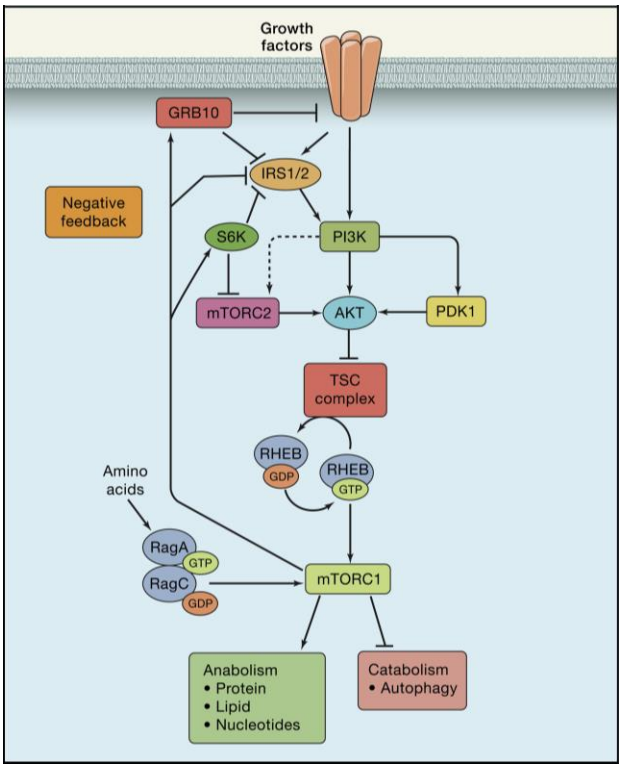

Figure 65. The PI3K-mTOR signaling pathway, depicting downstream functions and feedback regulation. *(Adapted from Manning et al, 2017)*

Besides all these reasons, it should be noted that oncogenic KRAS phosphomutant cell clones maintain WT KRAS allele, and it has been shown that WT RAS proteins can display tumor suppressing functions depending on context[212].

Surprisingly, these results seem opposed to those of our previous work using also DLD-1 cells in which we observed that KRAS phosphorylation increased cell proliferation, the interaction of oncogenic KRAS with its effectors and enhanced c-RAF-MEK-ERK1,2 and PI3K/AKT signaling pathways (*See background for more details*). However, we used CRC cells stably overexpressing oncogenic KRAS phosphomutants, and despite amplification of RAS is observed in some tumors, it is also true that overexpression can have distorting effects on signaling networks[376,377].

Therefore, according to the exposed results related to cell growth and signaling, we conclude that in these CRC cells the effect of the constitutively expression of oncogenic KRAS on the activation of final effectors of main KRAS signaling pathways is independent of the phosphorylation status at Ser181. However, these findings confirm that all KRAS phosphomutant constructs used in the experiments produce functional oncogenic KRAS proteins, since all are able to recover the growth of DLD-1 KO cells at serum-starving conditions and activated the cell signaling in similar way to the original DLD-1 cells.

II. Oncogenic KRAS phosphorylation at Ser181 induces invasive cell phenotype

Further, to determine potential divergences in migration and invasion capacities between cells expressing the different oncogenic KRAS phosphomutants, we used an alternative CRC model to the DLD-1 cells. As mentioned, DLD-1 cell line presents low migration and invasion capacities caused by a scarce ability to perform epithelial-mesenchymal transition[241,254,356]. For that reason, we choose the SW480 CRC cell line to perform this analysis, since they are a commonly used Wnt-active cell line with EMT potential[241,378]. The comparation of the invasive capacities of SW480 cells (**S**181) versus SW480 cells with S181**A** mutation (generated by CRISPR) demonstrates that, in CRC, oncogenic KRAS phosphorylation is involved in cell invasion. Moreover, these data correlate with the low expression levels of *SERPINE1* detected in the S181**A** mutant cells. This gene is related to mesenchymal phenotype[376,379] and encodes for PAI-1, an essential inhibitor of tissue plasminogen activator (tPA) and urokinase (uPA). The cleavage of plasminogen (inactive precursor) by tPA or uPA produces the active protein plasmin, which is responsible for ECM degradation (figure 66). Thus, it is plausible to consider PAI-1 as an antitumor factor to block tumor progression. However, despite showing anticancer effects in several tumors, like pancreatic cancer, emerging investigations on *SERPINE1* have favored its important implications in cell migration, invasion and tumor vascularization.

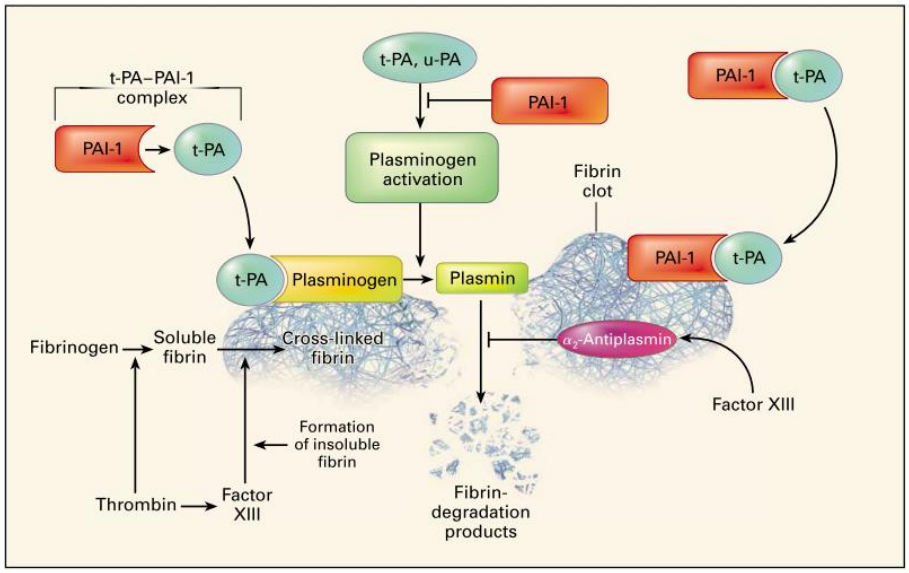

Figure 66. Activation and inhibition of the Fibrinolytic Pathway by t-PA, u-PA and PAI-1. *(Lasminogen et al, 2000).*

Apart from being a uPA inhibitor, PAI-1 can interfere with uPA-receptor (uPAR)/vitronectin binding. Vitronectin is an ECM component responsible for uPA-mediated tumor cell adhesion to the ECM[380]. In the presence of vitronectin, both integrins and uPA-occupied uPAR interact with vitronectin facilitating cell adhesion. However, vitronectin contains partially overlapping binding sites for uPAR and PAI-1[381] (figure 67A). Thus, when PAI-1 is present at elevated concentrations, it can bind to vitronectin preventing the reattachment of cells to the ECM[382]. Blocking reattachment to the vitronectin-matrix could initiate a motile phenotype leading cells to migrate onto alternative stromal ECM proteins[381] (figure 67B). Therefore, a critical balance of uPA, uPAR, and PAI-1 is the prerequisite for efficient focal proteolysis, migration and hence subsequent tumor invasion and metastasis. Based on these data, tumor promoting roles of PAI-1 have been described in some cancer types[360]. Indeed, it has been reported that *SERPINE1* is enhanced in CRC and this is associated with metastasis (lymph node, liver), vascular invasion and poor survival rates[362,383–385]. More recently,

enhanced expression of *SERPINE1* in CRC cells has been proposed as a predictor of CRC invasiveness, progression, and overall survival[361].

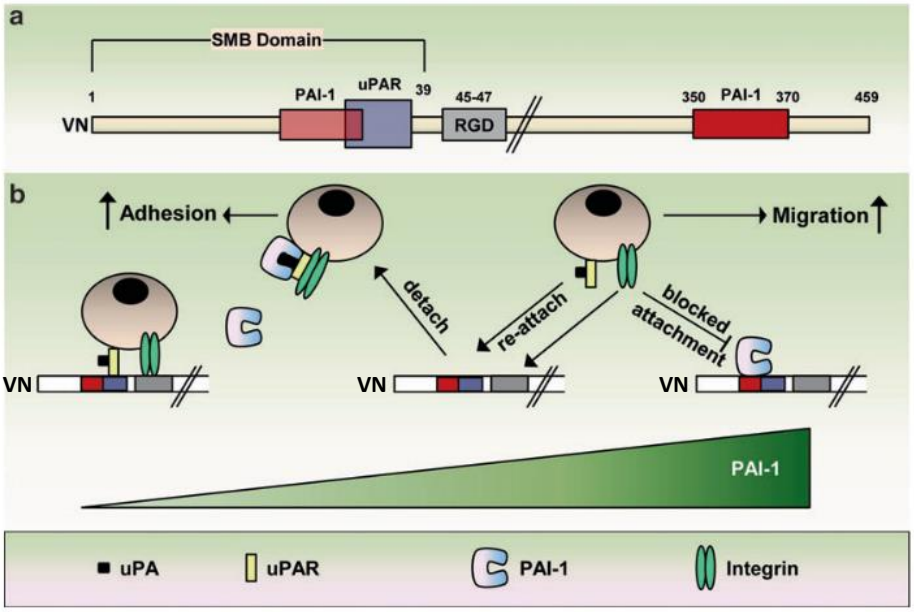

Figure 67. SERPINE1 regulates cell adhesion by modulating the binding of cell adhesion receptors to the ECM protein vitronectin (VN). *(Czekay et al, 2016).*

Consequently, our results showing that *SERPINE1* expression is low in the non-phosphorylatable (S181**A**) oncogenic KRAS cell clones compared to those in the phosphorylatable (**S**181) and phosphomimetic (S181**D**) mutant cells; and the low invasiveness capacity of CRC cells with oncogenic KRAS harboring a S181**A** mutation, support the implication of oncogenic KRAS phosphorylation in the regulation of cell invasion in CRC. Accordingly, we have evidenced that CRC patients, which tumors express low levels of *SERPINE1* present good survival rates.

III. Oncogenic KRAS phosphorylation at Ser181 induces a differential gene expression pattern related to tumor progression

Interestingly, despite oncogenic KRAS phosphomutants did not show great differences in cell growth and signaling activation between them in 2D cell cultures, the transcriptional analysis at basal conditions demonstrates that these CRC cells expressing different oncogenic KRAS phosphomutants present differential gene expression patterns.

First, an important point of our transcriptional analysis is that the existence of differentially expressed genes between oncogenic KRAS-**S**181 and KRAS-S181**A** mutants indicates that KRAS is phosphorylated in a fraction of the cell population, this being relevant to regulate gene expression. We show that differential gene expression is mainly found in genes involved in cell migration, invasion and metastasis, such as *SERPINE1* (codifying for PAI-1) and *PRSS2* (codifying for trypsin) genes, which are downregulated in KRAS-S181**A** cells**.** As mentioned above, low levels of *SERPINE1* correlates with a decreased cell invasive capacity. Besides, this is associated with a good overall survival. Additionally, we have found that non-phosphorylatable (S181**A**) oncogenic KRAS-derived tumors show a decreased expression of trypsin, which has been implicated in tumor growth, invasion and metastasis[363,364,386,387]. Conversely, *NEO1*, codifying for neogenin1, is upregulated in CRC cells expressing oncogenic KRAS-S181**A** mutant. Neogenin1 was originally identified as an axon guidance receptor. Apart from that, this protein has recently been related with epithelial morphogenesis events such as the maintenance of adherent junctions or regulation of EMT, exhibiting a possible involvement of neogenin1 in inhibiting neoplastic processes. Indeed, it has been reported that *NEO1* is downregulated in different CRC cancer cell lines and in most CRC and adenomas[388,389], whereas it is highly expressed during colon crypt maturation[388]. Other report described that *NEO1* downregulation affected cell-matrix interactions, and together with the decrease of *NEO1* expression in metastatic cells, may suggest a role of this protein as a tumor suppressor in colon cancer metastasis[390]. Neogenin1 has also been referred as a key component of the actin nucleation machinery regulating adherent junction stability and tension[391]. In fact, it has recently been demonstrated that a downregulation of *NEO1*

expression in Caco-2 cells (CRC cell line) could disrupt adherent junctions and reduce stress fibers. Furthermore, the effects of *NEO1* knockdown induced a mislocalization of E-cadherin in DLD-1 cells and a mesenchymal phenotype in SW480 and RKO cells[359].

All these findings combined with the low invasiveness of the non-phosphorylatable (S181**A**) oncogenic KRAS expressing cells, suggest that KRAS phosphorylation is important to regulate metastasis in CRC. Unexpectedly, none of the oncogenic KRAS phosphomutants were able to induce liver tumors under the conditions evaluated. Therefore, considering that DLD-1 CRC cells show scarce ability to perform the epithelial-mesenchymal transition, it would be reasonable to analyze liver metastasis for a longer period of time or perform the experiment with the SW480 cell lines with oncogenic KRAS harboring S181**A** or S181**D** mutations.

Additionally, differences in gene expression induced by phosphomimetic (S181**D**) oncogenic KRAS suggest that phosphorylation of KRAS promotes an undifferentiated cellular state related to cancer progression. The reduced expression of genes such as *HNF4G*[392], *HEPH*, *UGTA1* and *MUC13*[393–395], and GSEA indicating that these cells have an expression profile closely to the one observed upon *LEF1* upregulation, associates KRAS phosphorylation with pluripotency.

We have focused on *HNF4G*, which has been described as a major driver of enterocyte-specific gene expression patterns in intestinal organoids[392]. HNF4 family of transcription factors, which includes *HNF4A* and *HNF4G*, are implicated in the development of gastrointestinal epithelium. Whereas *HNF4A* is expressed in the development and maturation of stomach, small intestine and colon epitheliums; *HNF4G* is only expressed in the developing and mature colon[396]. Recent report has described a strong potential of *HNF4G* to induce an enterocyte-specific epigenome and transcriptome in WT intestinal organoids[392]. Indeed, loss of *HNF4G* induces a decrease in enterocyte-specific gene expression. Additionally, the lack of *HNF4G* is associated with an increase in differentiated secretory cells, indicating that it is also required to maintain a balance between secretory and absorptive cells. In agreement, other report has described *HNF4G* as a master regulator of colon-specific genes[397]. More recently, it has been showed that *HNF4G* stabilizes

enterocyte cell identity[398]. The authors have also reported that *HNF4A* and *HNF4G* factors are required to maintain Lgr5 intestinal stem cells in WT organoids via their role in promoting β-oxidation. This fact guarantees the renewal of stem cells[399]. Their data suggest that, in absence of *HNF4G*, stem cells fails to renew and instead contribute to a population of proliferating cells. Therefore, whereas *HNF4G* expression is required to enterocyte differentiation in intestinal organoids, it is one of the most downregulated transcription factors in cancer stem cells, characterized by Lgr5 expression[392]. This suggest that *HNF4G* is playing a role in gene regulation even in transformed cancer cells. In this thesis, we demonstrate that oncogenic KRAS-S181**D** cells present lower *HNF4G* expression and higher Lgr5 expression than the other oncogenic KRAS phosphomutants. Therefore, the studies exemplified above together with our results support the hypothesis that KRAS phosphorylation is involved in pluripotency and in stablishing the undifferentiated cellular state required for tumor initiation and progression. Conversely, other work described that oncogenic KRAS phosphorylation can suppress tumor initiation[122]. The authors reported that oncogenic KRAS-S181**A** can regulate Fzd8-mediated non-canonical Wnt/Ca^{2+} signaling and sequential canonical Wnt/β-catenin signaling through CaM kinase activity, promoting KRAS-driven malignancy. As known, canonical Wnt/β-catenin pathway is activated in stem cells. Furthermore, it has been evidenced that Lgr5 is a Wnt target gene expressed in intestinal stem cells[368,400,401]. Therefore, these data would indicate that non-phosphorylatable oncogenic KRAS mutant would be showing a tumor initiating cell phenotype. Nevertheless, this study was carried out on a different cell model overexpressing the oncogenic KRAS phosphomutants, which can lead to distorting effects on the wide variety of signaling networks.

Thus, our results verifying that oncogenic KRAS-S181**D** mutant cells show high expression levels of Lgr5, and an expression profile closely to the one observed upon *LEF1* upregulation (Wnt target gene) suggest that KRAS phosphorylation is required for tumor initiation. In agreement with all these, our analysis of public data from patients indicates that gene expression in human CRC is more similar to the phosphomimetic than to the non-

phosphorylatable oncogenic KRAS signature. Therefore, all these findings support the hypothesis that KRAS phosphorylation is important for human CRC development.

Despite all these evidences, surprisingly, tumor growth is impaired in phosphomimetic oncogenic KRAS mutant cells. However, the lack of a well-structured perivascular cell organization, which is required for tumor nutrition, can be one of the reasons for the tumor growth impairment. According to this, we have identified that *CTNNA1* is the only gene whose expression decreases in either S181**A** or S181**D** oncogenic KRAS-expressing cells compared with KRAS-**S**181. Interestingly, the product of *CTNNA1*, α-E-catenin, is involved in cell-to-cell adhesion, a characteristic that we find to be impaired in cells expressing either the S181**A** or the S181**D** mutants of oncogenic KRAS (*explained in detail in the next section of discussion*).

Finally, another important point emerged from our transcriptional analysis is that the differential expression of some of the genes can be reverted by activation or inhibition of PKC. Indeed, we have demonstrated that pharmacologically inhibiting PKC, reduces the expression levels of *SERPINE1* and *PRSS2* in the phospho/dephosphorylatable (**S**181) oncogenic KRAS mutant cells, phenocopying the levels detected in S181**A** cells. Otherwise, PKC activation induces a decrease of *HNF4G* expression levels in **S**181 clones, phenocopying the ones of S181**D** cells. For these reasons, we conclude that KRAS phosphorylation is regulating gene expression in this CRC cell line.

IV. The phosphorylation cycle of oncogenic KRAS at Ser181 induces tumor growth

Finally, to complete our investigation about which is the functionality of the phosphorylation of oncogenic KRAS at Ser181, we studied whether this modification was required for tumor growth.

Initially, we analyzed how these phosphomutant cell lines proliferate and organize under 3D cell culture conditions. When they grow in soft agar, although there is variability between clones, all oncogenic KRAS phosphomutant cells have a significantly higher capacity to form colonies than DLD-1 KO cells. However, some differences in cellular aggregation and organization are observed between the distinct oncogenic KRAS phosphomutants. The divergences are more evident in cells grown in Matrigel. Cells expressing a phosphorylatable oncogenic KRAS (**S**181) are the only ones able to form glandular-like structures with polarized cells. Interestingly, it has been described that in the apical domain of epithelial cells an atypical PKC (aPKC) activity is required for appropriate maintenance of cell polarization[402]. Accordingly, it is possible that phosphorylation of KRAS in the apical domain and dephosphorylation of KRAS in the basolateral domain might be necessary to achieve cell polarization. Intriguingly, both oncogenic KRAS-S181**A** and KRAS-S181**D** expressing clones present a lack of cell aggregation and polarization correlating with a reduced expression of α-E-catenin. Inside cells, α-E-catenin is known to play a pivotal role in cell–cell adhesion, forming the cadherin-catenin core complex that is essential for tissue organization. In fact, α-E-catenin facilitates F-actin attachments to reinforce the adherent junctions[365,403] (figure 68). Despite this, α-E-catenin performs other functions such as regulation of cell motility and polarity[404].

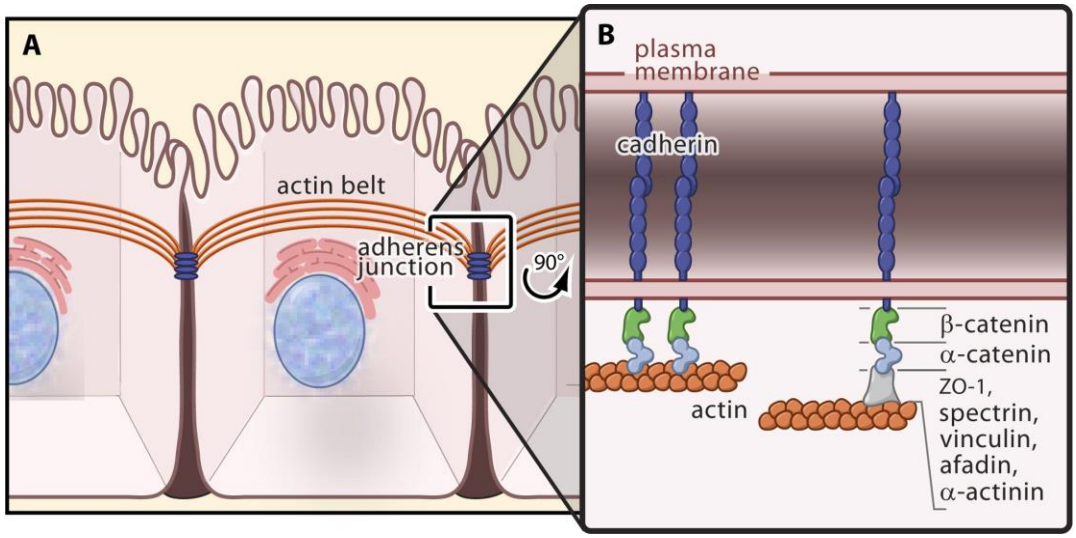

Figure 68. The cadherin-catenin core complex in adherent junctions. *(Gates et al, 2005).*

Recent reports described that lack of α-E-catenin induced a loose aggregation phenotype composed of disorganized cells with round morphology without obvious cell-cell adhesion[367,405]. These results were observed in different CRC cell lines including DLD-1. For all these evidences, the lack of this protein may be one of the reasons for the loss of intercellular adhesions; and for the inability of phosphomimetic and non-phosphorylatable KRAS expressing cells to organize a well-polarized epithelium in Matrigel. This fact could argue that the mutation of serine to aspartic acid does not properly mimics phosphorylation (being this mutant then similar to a non-phosphorylatable one), but this is unlikely to be the case, since we find a high number of genes differentially expressed between oncogenic KRAS-S181**A** and KRAS-S181**D** cells.

On the other hand, two different subpopulations have been characterized in the DLD-1 cell line. These two cell populations grow either as compact cell clusters or as groups of single cells in 3D cell cultures, which correlate with α-E-catenin expression or with its lack of

expression, respectively[367,405]. Thereby, one might think that the differences in the levels of α-E-catenin observed between the oncogenic KRAS phosphomutants is due to the selection of one or the other subpopulation of DLD-1 cells when selecting the clones, thus showing the cell clones a proper or impaired glandular-like structures regardless the status of KRAS phosphorylation. In order to clarify this important point, we have analyzed the expression of α-E-catenin of all the clones obtained in our experiments, regardless the levels of expression of the oncogenic KRAS phosphomutants. Data not shown indicate that all clones expressing the phospho/dephosphorylatable KRAS (**S**181) express α-E-catenin. In contrast, the most of the non-phosphorylatable (S181**A**) and phosphomimetic (S181**D**) KRAS expressing clones show low levels of α-E-catenin expression, being these imperceptible in some of them. Therefore, we conclude that a cycle of KRAS phosphorylation at Ser181 is required to regulate α-E-catenin expression in these cells, and in consequence for them to achieve polarized glandular-like structures in 3D.

After that, in order to evaluate tumor growth, cells expressing the different oncogenic KRAS phosphomutants were subcutaneously injected into nude mice. Interestingly, subcutaneous tumor growth is strongly impaired in KRAS-S181**A**-expressing cells, supporting our previous study[144], but also, in KRAS-S181**D**-expressing cells. Based on the gene expression data presented here and the results obtained with NIH3T3 fibroblasts[144], it is surprising that the phosphomimetic mutant does not support tumor growth. However, as mentioned, the lack of a well-organized perivascular organization of the cells observed in oncogenic KRAS-S181**D** and KRAS-S181**A** tumors might be preventing tumor nutrition and consequently tumor development. Accordingly, α-E-catenin is not detected in either oncogenic KRAS-S181**A** or KRAS-S181**D** tumors. Thus, expression of α-E-catenin might be also important to maintain certain cell polarity in colorectal tumors, promoting tumor growth. It is important to stress that cell polarity in CRCs is disrupted but not completely lost[406–408]. Although α-E-catenin has been considered as a tumor suppressor, emerging evidence suggests dual roles for this protein in colon cancer. Indeed, it has been demonstrated that α-E-catenin has an essential role in intestinal adenoma formation[409]. Additionally, an analysis of common

insertion sites has revealed many hundreds of candidate cancer drivers, including *CTNNA1* gene[410]. This has been studied performing an insertional mutagenesis in mice with somatic or germline mutation in *APC* to create a comprehensive catalog of new candidate drivers of intestinal tumorigenesis.

Taking into consideration these findings, one might think that inducing either complete KRAS phosphorylation or dephosphorylation would be a good therapeutic strategy. Indeed, both PKC inhibitors and activators haven been shown to reduce tumor growth induced by oncogenic KRAS[122,144]. Nevertheless, we have demonstrated that KRAS dephosphorylation also reduces cell invasion and gene expression related to invasiveness/metastatic phenotype; whereas KRAS phosphorylation enhances undifferentiated and pluripotent cell phenotype.

As a summary of all the results included in this thesis, a final model is shown (figure 69). We propose that phosphorylation of KRAS at Ser181 in the apical cell domain and dephosphorylation in the basolateral domain may be required to polarize and organize the cells around blood vessels, promoting tumor development. Since aPKCs have a role in cell polarization and have been described as tumor promoters in KRAS-driven cancer[411], we suggest a possible involvement of aPKCs phosphorylating KRAS during the cell polarization process. In support of this idea, α-E-Catenin is only found expressed in the phosphorylatable oncogenic KRAS mutant cells to achieve cell polarization, maintaining tumor growth. Consequently, a permanent state of KRAS phosphorylation or dephosphorylation induces disruption of cell polarization resulting in loss of organization of the cells around the blood vessels, which correlates with lack of α-E-catenin expression. As a final output of all this, tumor growth becomes compromised. However, in order to induce EMT promoting cell invasion and metastasis, some tumor cells are able to disrupt their cell organization. In fact, loss and reduction of α-E-catenin expression have been associated with an invasiveness phenotype[405,412–414]. Since phosphomimetic oncogenic KRAS mutant cells also express low levels of *HNF4G* and high levels of the *LGR5* stem cell marker, they have an undifferentiated and pluripotent phenotype suggesting that the phosphorylation at Ser181 of oncogenic

KRAS has a role in the acquisition of a tumor initiating cell phenotype. Surprisingly, oncogenic KRAS phosphomimetic-derived tumors shows an increase of HNF4G expression levels (Data not shown). However, it should be noted that *HNF4G* has also been associated with stem cell maintenance and renewal in vivo[399]. So, it is possible that these cells need to recover certain expression levels of HNF4G to completely achieve their tumorgenicity. This fact would maintain the stem cell populations, which would allow phosphorylated oncogenic KRAS to initiate a metastatic niche. Otherwise, being that the non-phosphorylatable oncogenic KRAS mutant show reduced α-E-catenin expression, low cell invasion capacity correlating with low levels of *SERPINE1* and *PRSS2,* and high levels of *NEO1;* suggest a role closely to tumor suppressor. In fact, we demonstrate a reduction of trypsin levels in oncogenic KRAS non-phosphorylated-derived tumors.

Finally, the analysis of the public data indicating that gene expression in human CRC is more similar to the phosphomimetic than to the non-phosphorylatable oncogenic KRAS signature, validates our model. Thus, these evidences together with our previous observations[117,133,144], suggest that inhibiting KRAS phosphorylation would be a good therapeutic strategy against CRC

Therefore, we conclude that CRC cells depend on KRAS phosphorylation cycle at Ser181 to maintain their tumorigenic properties.

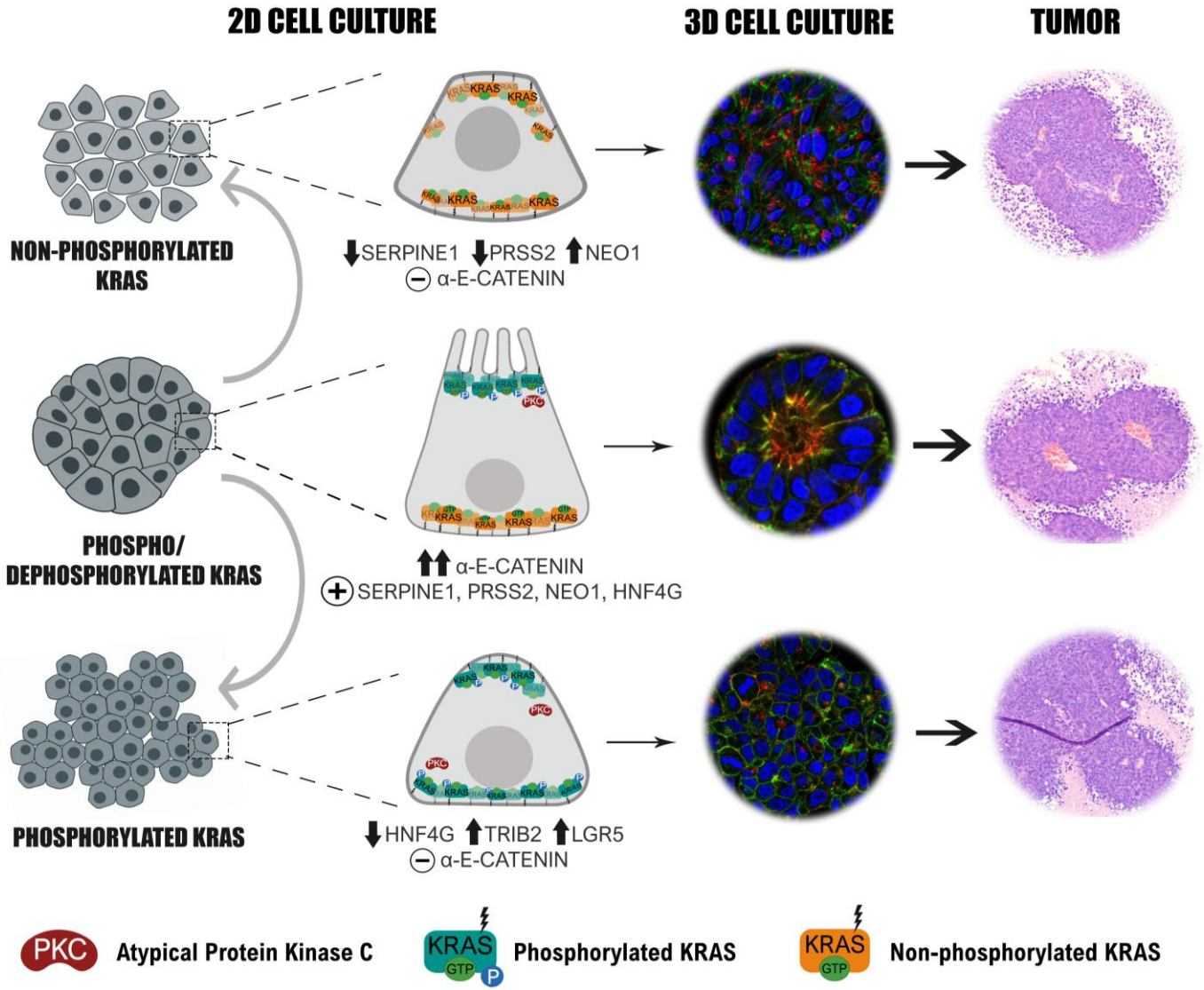
2D CELL CULTURE
3D CELL CULTURE
TUMOR
NON-PHOSPHORYLATED KRAS
⬇SERPINE1 ⬇PRSS2 ⬆NEO1
⊖ α-E-CATENIN
PHOSPHO/ DEPHOSPHORYLATED KRAS
⬆⬆ α-E-CATENIN
⊕ SERPINE1, PRSS2, NEO1, HNF4G
PHOSPHORYLATED KRAS
⬇HNF4G ⬆TRIB2 ⬆LGR5
⊖ α-E-CATENIN
PKC Atypical Protein Kinase C
KRAS GTP P Phosphorylated KRAS
KRAS GTP Non-phosphorylated KRAS

Figure 69. Hypothetical model of the role of KRAS phosphorylation cycle at Ser181 to maintain the tumorigenic properties of CRC cells.

V. The peptidomimetics against the RAS effector domain designed by Iproteos technology reduce oncogenic KRAS activity and cell viability

RAS is a well-known therapeutic target involved in many cancer diseases. Iproteos technology have been able to generate an accurate docking model and to design potent inhibitors that can disrupt the interactions of RAS with their effectors.

Initially, we have evaluated the effect of treating cells with nine different peptidomimetics, designed *in silico* by Iproteos team, in the activation of KRAS downstream signaling pathways. We have identified 3 hits able to reduce KRAS downstream signaling in non-transformed cells that have been growing under growth factors-limiting conditions and EGF stimulated. Moreover, they disrupt the interaction of oncogenic KRAS with its effectors. One of them, the peptidomimetic P1, is the most efficient. After these promising results, P1 was chosen to be *in silico* modified with the objective to improve its inhibitory capacity. After optimization, four peptidomimetics derived from P1 were obtained. In this second evaluation, we have determined that the peptidomimetic P1.3 is also able to reduce the interaction between oncogenic KRAS and its effectors, and as consequence, negatively affecting downstream RAS signaling pathways more efficiently than P1. Therefore, P1.3 seems to be a good candidate to inhibit RAS signaling in cancer cells expressing oncogenic KRAS. However, despite the variability, P1.3 is not able to reduce the basal levels of signaling activity downstream of RAS in a set of pancreatic cancer cell lines harboring different mutations in oncogenic KRAS. It should be considered that downstream RAS signaling in these pancreatic cancer cells might not have been analyzed under the adequate culture conditions (10% FBS). Therefore, we propose to evaluate cell signaling under growth factors-limiting conditions plus EGF stimulation (like in the experiments performed in non-transformed cell lines), or after a longer treatment time with P1.3, if the experiment is carried out at serum saturating conditions. In addition, it might be required to treat pancreatic cancer cells with higher concentrations of the inhibitor than those which are effective for the normal cells.

Alternatively, we analyzed whether the most promising peptidomimetics tested were able to discriminate between tumor and normal cells. For that reason, P1 and its derivative analogous P1.3 were evaluated in a cell survival assay under serum-saturating conditions. To assess this, a set of six pancreatic cancer cell lines harboring different mutations in oncogenic KRAS and one non-transformed cell line (hTERT-RPE) were used. Data indicate that although P1 is unable to kill cells, either tumor or normal cells, P1.3 efficiently discriminates between healthy and cancer cells. We have demonstrated that P1.3 is capable of causing cell death of all the tumor cell lines tested at the range of concentrations between 20-25μM. However, less than 10% of the normal cells are affected at these concentrations. These evidences suggest that P1.3 is able to selectively reduce cell viability of tumor cells growing under growth factors conditions, but c-RAF-MEK-ERK and PI3K/AKT pathways are not responsible for survival under those conditions.

According to these results, the use of this peptidomimetic emerges as a good therapeutic tool, but further studies are necessary to be done to optimize its mechanism of action. Several reports have demonstrated that different cell-permeable bicyclic peptides against oncogenic KRAS-G12V are able to reduce RAS-RAF interaction, MAPK signaling and induced apoptotic cell death. However, high concentrations were required and these compounds could not distinguish between oncogenic and WT RAS isoforms[332,333]. Other groups have also corroborate the importance of peptidomimetics to inhibit RAS proteins[334,335,337]. But, again, its potency or its off-target effects have not been determined, and its activity has found to be limited.

Accordingly, the main conclusion drawn from all data presented in this thesis, is that the Iproteos technology has allowed to design, in a quick and cost-effective manner, the compound P1.3 that efficiently inhibits the interaction of oncogenic KRAS with its effectors. Furthermore, it negatively affects downstream KRAS signaling in non-transformed cells. Besides, from the therapeutic point of view, P1.3 shows high selectivity killing pancreatic cancer cells expressing oncogenic KRAS versus normal cells. Nevertheless, the impact of the present project will be determined once the bioavailability of P1.3 has been assessed along

with its pharmacokinetic properties. Therefore, more experiments will be conducted in the near future in order to reach the preclinical phase. Additionally, P1.3 will be optimized during the process in order to improve its inhibitory capacity.

CONCLUSIONS

I. The phosphorylation cycle of oncogenic KRAS at Ser181 does not affect cell growth and the main KRAS downstream signaling pathways of colorectal cancer cells in 2D culture conditions.

II. The phosphorylation cycle of oncogenic KRAS at Ser181 induces an epithelial polarized glandular morphology of colorectal cancer cells growing in 3D extracellular matrix cultures.

III. The phosphorylation cycle of oncogenic KRAS at Ser181 is necessary to induce tumor growth of colorectal cancer cells.

IV. The phosphorylation cycle of oncogenic KRAS at Ser181 regulates cell invasion of colorectal cancer cells.

V. The phosphorylation cycle of oncogenic KRAS at Ser181 regulates gene expression pattern of colorectal cancer cells.

a. KRAS phosphorylation induces genes related to undifferentiated phenotype.

b. Lack of KRAS phosphorylation downregulates genes related to cell migration and invasion capacities.

VI. Gene expression signature of KRAS phosphorylation at Ser181 is related to gene expression of human colorectal cancer.

VII. The peptidomimetic P1.3 is the most efficient compound inhibiting the main KRAS downstream signaling pathways in non-transformed cells.

VIII. The peptidomimetic P1.3 is a promising lead compound which induces an elevated rate of cell death in pancreatic tumor cells.

REFERENCES

1. Wennerberg, K., Rossman, K. L. & Der, C. J. The Ras superfamily at a glance. *J. Cell Sci.* **118**, 843–846 (2005).

2. Goitre, L., Trapani, E., Trabalzini, L. & Retta, S. F. The ras superfamily of small GTPases: The unlocked secrets. *Methods in Molecular Biology* vol. 1120 1–18 (2014).

3. Stehelin, D., Varmus, H. E., Bishop, J. M. & Vogt, P. K. DNA related to the transforming gene(s) of avian sarcoma viruses is present in normal avian DNA. *Nature* **260**, 170–173 (1976).

4. DeFeo, D. *et al.* Analysis of two divergent rat genomic clones homologous to the transforming gene of Harvey murine sarcoma virus. *Proc. Natl. Acad. Sci. U. S. A.* **78**, 3328–3332 (1981).

5. Chang, E. H., Gonda, M. A., Ellis, R. W., Scolnick, E. M. & Lowy, D. R. Human genome contains four genes homologous to transforming genes of Harvey and Kirsten murine sarcoma viruses. *Proc. Natl. Acad. Sci. U. S. A.* **79**, 4848–4852 (1982).

6. Karnoub, A. E. & Weinberg, R. A. Ras oncogenes: Split personalities. *Nature Reviews Molecular Cell Biology* vol. 9 517–531 (2008).

7. Rojas, A. M., Fuentes, G., Rausell, A. & Valencia, A. The Ras protein superfamily: Evolutionary tree and role of conserved amino acids. *Journal of Cell Biology* vol. 196 189–201 (2012).

8. Malumbres, M. & Barbacid, M. RAS oncogenes: The first 30 years. *Nature Reviews Cancer* vol. 3 459–465 (2003).

9. Heasman, S. J. & Ridley, A. J. Mammalian Rho GTPases: New insights into their functions from in vivo studies. *Nature Reviews Molecular Cell Biology* vol. 9 690–701 (2008).

10. Hodge, R. G. & Ridley, A. J. Regulating Rho GTPases and their regulators. *Nat. Rev. Mol. Cell Biol.* **17**, 496–510 (2016).

11. Vega, F. M. & Ridley, A. J. Rho GTPases in cancer cell biology. *FEBS Letters* vol. 582 2093–2101 (2008).

12. Haga, R. B. & Ridley, A. J. Rho GTPases: Regulation and roles in cancer cell biology. *Small GTPases* vol. 7 207–221 (2016).

13. Donaldson, J. G. & Jackson, C. L. ARF family G proteins and their regulators: Roles in membrane transport, development and disease. *Nature Reviews Molecular Cell Biology* vol. 12 362–375 (2011).

14. Jackson, C. L. & Bouvet, S. Arfs at a Glance. *J. Cell Sci.* **127**, 4103–4109 (2014).

15. Reiner, D. J. & Lundquist, E. A. Small GTPases *. (2016) doi:10.1895/wormbook.1.67.2.

16. Zerial, M. & McBride, H. Rab proteins as membrane organizers. *Nature Reviews Molecular Cell Biology* vol. 2 107–117 (2001).

17. Li, G. Rab GTPases, Membrane Trafficking and Diseases. *Curr. Drug Targets* **12**, 1188–1193 (2011).

18. Krishnan, P. D. G., Golden, E., Woodward, E. A., Pavlos, N. J. & Blancafort, P. Rab gtpases: Emerging oncogenes and tumor suppressive regulators for the editing of survival pathways in

cancer. *Cancers* vol. 12 259 (2020).

19. Cavazza, T. & Vernos, I. The RanGTP pathway: From nucleo-cytoplasmic transport to spindle assembly and beyond. *Frontiers in Cell and Developmental Biology* vol. 3 82 (2016).

20. Harvey, J. J. An unidentified virus which causes the rapid production of tumours in mice [33]. *Nature* vol. 204 1104–1105 (1964).

21. Kirsten, W. H. & Mayer, L. A. Morphologic responses to a murine erythroblastosis virus. *J. Natl. Cancer Inst.* **39**, 311–335 (1967).

22. Cox, A. D. & Der, C. J. Ras history: The saga continues. *Small GTPases* **1**, 2–27 (2010).

23. Scolnick, E. M., Rands, E., Williams, D. & Parks, W. P. *Studies on the Nucleic Acid Sequences of Kirsten Sarcoma Virus: a Model for Formation of a Mammalian RNA-Containing Sarcoma Virus*. *JOURNAL OF VIROLOGY* http://jvi.asm.org/ (1973).

24. Scolnick, E. M. & Parks, W. P. *Harvey Sarcoma Virus: A Second Murine Type C Sarcoma Virus with Rat Genetic Information*. *JOURNAL OF VIROLOGY* vol. 1 http://jvi.asm.org/ (1974).

25. Scolnick, E. M., Papageorge, A. G. & Shih, T. Y. Guanine nucleotide-binding activity as an assay for src protein of rat-derived murine sarcoma viruses. *Proc. Natl. Acad. Sci. U. S. A.* **76**, 5355–5359 (1979).

26. Willingham, M. C., Pastan, I., Shih, T. Y. & Scolnick, E. M. Localization of the src gene product of the Harvey strain of MSV to plasma membrane of transformed cells by electron microscopic immunocytochemistry. *Cell* **19**, 1005–14 (1980).

27. Shih, T. Y., Weeks, M. O., Young, H. A. & Scolnick, E. M. Identification of a sarcoma virus-coded phosphoprotein in nonproducer cells transformed by Kirsten or Harvey murine sarcoma virus. *Virology* **96**, 64–79 (1979).

28. Hall, A., Marshall, C. J., Spurr, N. K. & Weiss, R. A. Identification of transforming gene in two human sarcoma cell lines as a new member of the ras gene family located on chromosome 1. *Nature* **303**, 396–400 (1983).

29. Shimizu, K. *et al.* Three human transforming genes are related to the viral ras oncogenes. *Proc. Natl. Acad. Sci. U. S. A.* **80**, 2112–2116 (1983).

30. Prior, I. A. & Hancock, J. F. Ras trafficking, localization and compartmentalized signalling. *Seminars in Cell and Developmental Biology* vol. 23 145–153 (2012).

31. Cox, A. D., Der, C. J. & Philips, M. R. Targeting RAS membrane association: Back to the future for anti-RAS drug discovery? *Clin. Cancer Res.* **21**, 1819–1827 (2015).

32. Koera, K. *et al.* K-Ras is essential for the development of the mouse embryo. *Oncogene* **15**, 1151–1159 (1997).

33. Esteban, L. M. *et al.* Targeted Genomic Disruption of H-ras and N-ras, Individually or in Combination, Reveals the Dispensability of Both Loci for Mouse Growth and Development. *Mol. Cell. Biol.* **21**, 1444–1452 (2001).

34. Drosten, M. *et al.* H-Ras and K-Ras oncoproteins induce different tumor spectra when driven

by the same regulatory sequences. *Cancer Res.* **77**, 707–718 (2017).

35. Bourne, H. R., Sanders, D. A. & McCormick, F. The GTPase superfamily: conserved structure and molecular mechanism. *Nature* **349**, 117–127 (1991).

36. Vetter, I. R. & Wittinghofer, A. The guanine nucleotide-binding switch in three dimensions. *Science* vol. 294 1299–1304 (2001).

37. Cherfils, J. & Zeghouf, M. Regulation of small GTPases by GEFs, GAPs, and GDIs. *Physiological Reviews* vol. 93 269–309 (2013).

38. Bos, J. L., Rehmann, H. & Wittinghofer, A. GEFs and GAPs: Critical Elements in the Control of Small G Proteins. *Cell* vol. 129 865–877 (2007).

39. Cherfils, J. & Chardin, P. GEFs: Structural basis for their activation of small GTP-binding proteins. *Trends in Biochemical Sciences* vol. 24 306–311 (1999).

40. Bernards, A. & Settleman, J. GAP control: Regulating the regulators of small GTPases. *Trends in Cell Biology* vol. 14 377–385 (2004).

41. Gray, J. L., von Delft, F. & Brennan, P. E. Targeting the Small GTPase Superfamily through Their Regulatory Proteins. *Angew. Chemie Int. Ed.* (2020) doi:10.1002/anie.201900585.

42. Colicelli, J. Human RAS superfamily proteins and related GTPases. *Science's STKE : signal transduction knowledge environment* vol. 2004 re13–re13 (2004).

43. Johnson, C. W. *et al.* The small GTPases K-Ras, N-Ras, and H-Ras have distinct biochemical properties determined by allosteric effects. *J. Biol. Chem.* **292**, 12981–12993 (2017).

44. Mo, S. P., Coulson, J. M. & Prior, I. A. RAS variant signalling. *Biochemical Society Transactions* vol. 46 1325–1332 (2018).

45. Hancock, J. F. RAS PROTEINS: DIFFERENT SIGNALS FROM DIFFERENT LOCATIONS. *Nat. Rev. | Mol. CELL Biol.* **4**, 3 (2003).

46. Hancock*, I. A. P. and J. F. Compartmentalization of Ras proteins. *J Cell Sci.* **114**, 1603–8 (2001).

47. Hancock, J. F., Paterson, H. & Marshall, C. J. A polybasic domain or palmitoylation is required in addition to the CAAX motif to localize p21ras to the plasma membrane. *Cell* **63**, 133–139 (1990).

48. Ahearn, I. M., Haigis, K., Bar-Sagi, D. & Philips, M. R. Regulating the regulator: post-translational modification of RAS. *Nat. Rev. Mol. Cell Biol.* **13**, 39–51 (2012).

49. Casey, P. J., Solski, P. A., Der, C. J. & Buss, J. E. p21ras is modified by a farnesyl isoprenoid. *Proc. Natl. Acad. Sci. U. S. A.* **86**, 8323–8327 (1989).

50. Reiss, Y., Goldstein, J. L., Seabra, M. C., Casey, P. J. & Brown, M. S. Inhibition of purified p21ras farnesyl:protein transferase by Cys-AAX tetrapeptides. *Cell* **62**, 81–88 (1990).

51. Choy, E. *et al.* Endomembrane trafficking of ras: The CAAX motif targets proteins to the ER and Golgi. *Cell* **98**, 69–80 (1999).

52. Boyartchuk, V. L., Ashby, M. N. & Rine, J. Modulation of ras and a-factor function by carboxyl-terminal proteolysis. *Science (80-.).* **275**, 1796–1800 (1997).

53. Dai, Q. *et al.* Mammalian prenylcysteine carboxyl methyltransferase is in the endoplasmic reticulum. *J. Biol. Chem.* **273**, 15030–15034 (1998).

54. Hancock, J. F., Magee, A. I., Childs, J. E. & Marshall, C. J. All ras proteins are polyisoprenylated but only some are palmitoylated. *Cell* **57**, 1167–1177 (1989).

55. Apolloni, A., Prior, I. A., Lindsay, M., Parton, R. G. & Hancock, J. F. H-ras but Not K-ras Traffics to the Plasma Membrane through the Exocytic Pathway. *Mol. Cell. Biol.* **20**, 2475–2487 (2000).

56. Buss, J. E. & Sefton, B. M. *Direct Identification of Palmitic Acid as the Lipid Attached to p2lras*. *MOLECULAR AND CELLULAR BIOLOGY* vol. 6 http://mcb.asm.org/ (1986).

57. Hancock, J. F., Cadwallader, K., Paterson, H. & Marshall, C. J. A CAAX or a CAAL motif and a second signal are sufficient for plasma membrane targeting of ras proteins. *EMBO J.* **10**, 4033–4039 (1991).

58. Laude, A. J. & Prior, I. A. Palmitoylation and localisation of RAS isoforms are modulated by the hypervariable linker domain. *J. Cell Sci.* **121**, 421–427 (2008).

59. Simanshu, D. K., Nissley, D. V & Mccormick, F. RAS Proteins and Their Regulators in Human Disease. *Cell* **170**, 17–33 (2017).

60. Swarthout, J. T. *et al.* DHHC9 and GCP16 constitute a human protein fatty acyltransferase with specificity for H- and N-Ras. *J. Biol. Chem.* **280**, 31141–31148 (2005).

61. Rocks, O. *et al.* An acylation cycle regulates localization and activity of palmitoylated ras isoforms. *Science (80-.).* **307**, 1746–1752 (2005).

62. Bivona, T. G. *et al.* PKC regulates a farnesyl-electrostatic switch on K-Ras that promotes its association with Bcl-XL on mitochondria and induces apoptosis. *Mol. Cell* **21**, 481–493 (2006).

63. Simons, K. & Ikonen, E. *Functional rafts in cell membranes*. *Nature © Macmillan Publishers Ltd* vol. 387 (1997).

64. Melkonian, K. A., Ostermeyer, A. G., Chen, J. Z., Roth, M. G. & Brown, D. A. Role of lipid modifications in targeting proteins to detergent-resistant membrane rafts. *J. Biol. Chem.* **274**, 3910–3917 (1999).

65. Zhou, Y. & Hancock, J. F. Ras nanoclusters: Versatile lipid-based signaling platforms. *Biochimica et Biophysica Acta - Molecular Cell Research* vol. 1853 841–849 (2015).

66. Prior, I. A. *et al.* GTP-dependent segregation of H-ras from lipid rafts is required for biological activity. *Nat. Cell Biol.* **3**, 368–375 (2001).

67. Niv, H., Gutman, O., Henis, Y. I. & Kloog, Y. Membrane interactions of a constitutively Active GFP-Ki-Ras 4B and their role in signaling evidence from lateral mobility studies. *J. Biol. Chem.* **274**, 1606–1613 (1999).

68. Parker, J. A. & Mattos, C. The Ras-Membrane Interface: Isoform-specific Differences in The Catalytic Domain. *Mol. Cancer Res.* **13**, 595–603 (2015).

69. Plowman, S. J., Muncke, C., Parton, R. G. & Hancock, J. F. H-ras, K-ras, and inner plasma membrane raft proteins operate in nanoclusters with differential dependence on the actin cytoskleton. *Proc. Natl. Acad. Sci. U. S. A.* **102**, 15500–15505 (2005).

70. Weise, K. *et al.* Membrane-Mediated Induction and Sorting of K-Ras Microdomain Signaling Platforms. *J. Am. Chem. Soc* **133**, 880–887 (2011).

71. Abankwa, D., Gorfe, A. A. & Hancock, J. F. Ras nanoclusters: Molecular structure and assembly. *Semin. Cell Dev. Biol.* **18**, 599–607 (2007).

72. Jaumot, M., Yan, J., Clyde-Smith, J., Sluimer, J. & Hancock, J. F. The linker domain of the Ha-Ras hypervariable region regulates interactions with exchange factors, Raf-1 and phosphoinositide 3-kinase. *J. Biol. Chem.* **277**, 272–278 (2002).

73. Plowman, S. J., Ariotti, N., Goodall, A., Parton, R. G. & Hancock, J. F. Electrostatic Interactions Positively Regulate K-Ras Nanocluster Formation and Function. *Mol. Cell. Biol.* **28**, 4377–4385 (2008).

74. Cho, K. *et al.* Inhibition of acid sphingomyelinase depletes cellular phosphatidylserine and mislocalizes K-Ras from the plasma membrane. *Mol. Cell. Biol.* **36**, MCB.00719-15 (2015).

75. Zhou, Y. *et al.* Signal Integration by Lipid-Mediated Spatial Cross Talk between Ras Nanoclusters. *Mol. Cell. Biol.* **34**, 862–876 (2014).

76. Barceló, C. *et al.* Oncogenic K-ras segregates at spatially distinct plasma membrane signaling platforms according to its phosphorylation status. *J. Cell Sci.* **126**, 4553–4559 (2013).

77. Lopez-Alcalá, C. *et al.* Identification of essential interacting elements in K-Ras/calmodulin binding and its role in K-Ras localization. *J. Biol. Chem.* **283**, 10621–31 (2008).

78. Zhou, Y. *et al.* Lipid-Sorting Specificity Encoded in K-Ras Membrane Anchor Regulates Signal Output. *Cell* **168**, 239-251.e16 (2017).

79. Jura, N., Scotto-Lavino, E., Sobczyk, A. & Bar-Sagi, D. Differential modification of Ras proteins by ubiquitination. *Mol. Cell* **21**, 679–687 (2006).

80. Fivaz, M. & Meyer, T. Reversible intracellular translocation of KRas but not HRas in hippocampal neurons regulated by Ca2+/calmodulin. *J. Cell Biol.* **170**, 429–441 (2005).

81. Bhagatji, P., Leventis, R., Rich, R., Lin, C. J. & Silvius, J. R. Multiple cellular proteins modulate the dynamics of K-ras association with the plasma membrane. *Biophys. J.* **99**, 3327–3335 (2010).

82. Chandra, A. *et al.* The GDI-like solubilizing factor PDEδ sustains the spatial organization and signalling of Ras family proteins. *Nat. Cell Biol.* **14**, 148–158 (2012).

83. Philips, M. R. *Ras hitchhikes on PDE6δ*. *Nature Publishing Group* (2012) doi:10.1038/ncb2429.

84. Lu, A. *et al.* A clathrin-dependent pathway leads to KRas signaling on late endosomes en route to lysosomes. *J. Cell Biol.* **184**, 863–879 (2009).

85. Cho, K. J. *et al.* Staurosporines disrupt phosphatidylserine trafficking and mislocalize ras proteins. *J. Biol. Chem.* **287**, 43573–43584 (2012).

86. Gelabert-Baldrich, M. *et al.* Dynamics of KRas on endosomes: Involvement of acidic phospholipids in its association. *FASEB J.* **28**, 3023–3037 (2014).

87. Sexton, R. E., Mpilla, G., Kim, S., Philip, P. A. & Azmi, A. S. Ras and exosome signaling. *Seminars in Cancer Biology* vol. 54 131–137 (2019).

88. Ellis, R. W., DeFeo, D., Furth, M. E. & Scolnick, E. M. Mouse cells contain two distinct ras gene mRNA species that can be translated into a p21 onc protein. *Mol. Cell. Biol.* **2**, 1339–1345 (1982).

89. Rubio, I., Hennig, A., Esparza-Franco, M. A., Ladds, G. & Markwart, R. Ras activation revisited: role of GEF and GAP systems. *Biol. Chem* **396**, 831–848 (2015).

90. Mattox, T. E., Chen, X., Maxuitenko, Y. Y., Keeton, A. B. & Piazza, G. A. Exploiting RAS Nucleotide Cycling as a Strategy for Drugging RAS-Driven Cancers. *Int. J. Mol. Sci.* **21**, 141 (2019).

91. Geyer, M. *et al.* Conformational transitions in p21(ras) and in its complexes with the effector protein Raf-RBD and the GTPase activating protein GAP. *Biochemistry* **35**, 10308–10320 (1996).

92. Trahey, M. *et al.* Molecular cloning of two types of GAP complementary DNA from human placenta. *Science (80-.).* **242**, 1697–1700 (1988).

93. Vogel, U. S. *et al.* Cloning of bovine GAP and its interaction with oncogenic ras p21. *Nature* **335**, 90–93 (1988).

94. Trahey, M. & Mccormick, F. A cytoplasmic protein stimulates normal N-ras p21 GTPase, but does not affect oncogenic mutants. *Science (80-.).* **238**, 542–545 (1987).

95. Ballester, R. *et al.* The NF1 locus encodes a protein functionally related to mammalian GAP and yeast IRA proteins. *Cell* **63**, 851–859 (1990).

96. Martin, G. A. *et al.* The GAP-related domain of the neurofibromatosis type 1 gene product interacts with ras p21. *Cell* **63**, 843–849 (1990).

97. Xu, G. *et al.* The neurofibromatosis type 1 gene encodes a protein related to GAP. *Cell* **62**, 599–608 (1990).

98. Bernards, A. GAPs galore! A survey of putative Ras superfamily GTPase activating proteins in man and Drosophila. *Biochimica et Biophysica Acta - Reviews on Cancer* vol. 1603 47–82 (2003).

99. Scheffzek, K. *et al.* The Ras-RasGAP complex: Structural basis for GTPase activation and its loss in oncogenic ras mutants. *Science (80-.).* **277**, 333–338 (1997).

100. Maertens, O. & Cichowski, K. An expanding role for RAS GTPase activating proteins (RAS GAPs) in cancer. *Adv. Biol. Regul.* **55**, 1–14 (2014).

101. Vigil, D., Cherfils, J., Rossman, K. L. & Der, C. J. Ras superfamily GEFs and GAPs: Validated and tractable targets for cancer therapy? *Nature Reviews Cancer* vol. 10 842–857 (2010).

102. Schmick, M. *et al.* KRas localizes to the plasma membrane by spatial cycles of solubilization,

trapping and vesicular transport. *Cell* **157**, 459–471 (2014).

103. Weise, K. *et al.* Dissociation of the K-Ras4B/PDEδ complex upon contact with lipid membranes: Membrane delivery instead of extraction. *J. Am. Chem. Soc.* **134**, 11503–11510 (2012).

104. Dharmaiah, S. *et al.* Structural basis of recognition of farnesylated and methylated KRAS4b by PDEd. *Proc. Natl. Acad. Sci. U. S. A.* **113**, E6766–E6775 (2016).

105. Martín-Gago, P. *et al.* A PDE6δ-KRas Inhibitor Chemotype with up to Seven H-Bonds and Picomolar Affinity that Prevents Efficient Inhibitor Release by Arl2. *Angew. Chemie Int. Ed.* **56**, 2423–2428 (2017).

106. Papke, B. *et al.* Identification of pyrazolopyridazinones as PDEδ inhibitors. *Nat. Commun.* **7**, 1–9 (2016).

107. Zimmermann, G. *et al.* Small molecule inhibition of the KRAS–PDEδ interaction impairs oncogenic KRAS signalling. *Nature* **497**, 638–642 (2013).

108. Klein, C. H. *et al.* PDEδ inhibition impedes the proliferation and survival of human colorectal cancer cell lines harboring oncogenic KRas. *Int. J. Cancer* **144**, 767–776 (2019).

109. Siddiqui, F. A. *et al.* PDE6D Inhibitors with a New Design Principle Selectively Block K-Ras Activity. *ACS Omega* **5**, 832 (2020).

110. Nancy, V., Callebaut, I., Marjou, A. El & De Gunzburg, J. The δ subunit of retinal rod cGMP phosphodiesterase regulates the membrane association of Ras and Rap GTpases. *J. Biol. Chem.* **277**, 15076–15084 (2002).

111. Agell, N., Bachs, O., Rocamora, N. & Villalonga, P. Modulation of the Ras/Raf/MEK/ERK pathway by Ca(2+), and calmodulin. *Cell. Signal.* **14**, 649–54 (2002).

112. Villalonga, P. *et al.* Calmodulin binds to K-Ras, but not to H- or N-Ras, and modulates its downstream signaling. *Mol. Cell. Biol.* **21**, 7345–54 (2001).

113. Villalonga, P. *et al.* Calmodulin prevents activation of Ras by PKC in 3T3 fibroblasts. *J. Biol. Chem.* **277**, 37929–35 (2002).

114. Bosch, M., Gil, J., Bachs, O. & Agell, N. Calmodulin inhibitor W13 induces sustained activation of ERK2 and expression of p21(cip1). *J. Biol. Chem.* **273**, 22145–22150 (1998).

115. Abraham, S. J., Nolet, R. P., Calvert, R. J., Anderson, L. M. & Gaponenko, V. The hypervariable region of K-Ras4B is responsible for its specific interactions with calmodulin. *Biochemistry* **48**, 7575–83 (2009).

116. Wu, L.-J., Xu, L.-R., Liao, J.-M., Chen, J. & Liang, Y. Both the C-Terminal Polylysine Region and the Farnesylation of K-RasB Are Important for Its Specific Interaction with Calmodulin. *PLoS One* **6**, e21929 (2011).

117. Alvarez-Moya, B., López-Alcalá, C., Drosten, M., Bachs, O. & Agell, N. K-Ras4B phosphorylation at Ser181 is inhibited by calmodulin and modulates K-Ras activity and function. *Oncogene* **29**, 5911–5922 (2010).

118. Alvarez-Moya, B., Barceló, C., Tebar, F., Jaumot, M. & Agell, N. CaM interaction and Ser181 phosphorylation as new K-Ras signaling modulators. *Small GTPases* **2**, 99–103 (2011).

119. Garrido, E., Lázaro, J., Jaumot, M., Agell, N. & Rubio-Martinez, J. Modeling and subtleties of K-Ras and Calmodulin interaction. *PLOS Comput. Biol.* **14**, e1006552 (2018).

120. Sidhu, R. S., Clough, R. R. & Bhullar, R. P. Ca2+/calmodulin binds and dissociates K-RasB from membrane. *Biochem. Biophys. Res. Commun.* **304**, 655–660 (2003).

121. Sperlich, B., Kapoor, S., Waldmann, H., Winter, R. & Weise, K. Regulation of K-Ras4B Membrane Binding by Calmodulin. *Biophys. J.* **111**, 113–122 (2016).

122. Wang, M.-T. *et al.* K-Ras Promotes Tumorigenicity through Suppression of Non-canonical Wnt Signaling. *Cell* **163**, 1237–1251 (2015).

123. Nussinov, R. *et al.* The key role of calmodulin in KRAS-driven adenocarcinomas. *Molecular Cancer Research* vol. 13 1265–1273 (2015).

124. Nussinov, R. *et al.* Calmodulin and PI3K Signaling in KRAS Cancers. *Trends in Cancer* vol. 3 214–224 (2017).

125. Nussinov, R., Zhang, M., Tsai, C. J. & Jang, H. Calmodulin and IQGAP1 activation of PI3Kα and Akt in KRAS, HRAS and NRAS-driven cancers. *Biochimica et Biophysica Acta - Molecular Basis of Disease* vol. 1864 2304–2314 (2018).

126. Saito, N., Mine, N., Kufe, D. W., Von Hoff, D. D. & Kawabe, T. CBP501 inhibits EGF-dependent cell migration, invasion and epithelial-to-mesenchymal transition of non-small cell lung cancer cells by blocking KRas to calmodulin binding. *Oncotarget* **8**, 74006–74018 (2017).

127. He, Y. & Smith, R. Nuclear functions of heterogeneous nuclear ribonucleoproteins A/B. *Cell. Mol. Life Sci.* **66**, 1239–56 (2009).

128. Van Seuningen, I., Ostrowski, J., Bustelo, X. R., Sleath, P. R. & Bomsztyk, K. The K protein domain that recruits the interleukin 1-responsive K protein kinase lies adjacent to a cluster of c-Src and Vav SH3-binding sites. Implications that K protein acts as a docking platform. *J. Biol. Chem.* **270**, 26976–85 (1995).

129. Bustelo, X. R., Suen, K. L., Michael, W. M., Dreyfuss, G. & Barbacid, M. Association of the vav proto-oncogene product with poly(rC)-specific RNA-binding proteins. *Mol. Cell. Biol.* **15**, 1324–1332 (1995).

130. Iervolino, A. *et al.* hnRNP A1 nucleocytoplasmic shuttling activity is required for normal myelopoiesis and BCR/ABL leukemogenesis. *Mol. Cell. Biol.* **22**, 2255–66 (2002).

131. Bajenova, O. *et al.* Surface expression of heterogeneous nuclear RNA binding protein M4 on Kupffer cell relates to its function as a carcinoembryonic antigen receptor. *Exp. Cell Res.* **291**, 228–41 (2003).

132. Shilo, A. *et al.* Splicing factor hnRNP A2 activates the Ras-MAPK-ERK pathway by controlling A-Raf splicing in hepatocellular carcinoma development. *RNA* **20**, 505–15 (2014).

133. Barceló, C. *et al.* Ribonucleoprotein HNRNPA2B1 interacts with and regulates oncogenic KRAS in pancreatic ductal adenocarcinoma cells. *Gastroenterology* **147**, 882-892.e8 (2014).

134. Elad-Sfadia, G., Haklai, R., Balan, E. & Kloog, Y. Galectin-3 augments K-ras activation and triggers a ras signal that attenuates ERK but not phosphoinositide 3-kinase activity. *J. Biol. Chem.* **279**, 34922–34930 (2004).

135. Shalom-Feuerstein, R., Cooks, T., Raz, A. & Kloog, Y. Galectin-3 regulates a molecular switch from N-Ras to K-Ras usage in human breast carcinoma cells. *Cancer Res.* **65**, 7292–7300 (2005).

136. Shalom-Feuerstein, R. *et al.* K-Ras Nanoclustering Is Subverted by Overexpression of the Scaffold Protein Galectin-3. *Cancer Res* **68**, 6608–6624 (2008).

137. Ashery, U. *et al.* Spatiotemporal organization of Ras signaling: Rasosomes and the galectin switch. *Cell. Mol. Neurobiol.* **26**, 471–495 (2006).

138. Meinohl, C. *et al.* Galectin-8 binds to the Farnesylated C-terminus of K-Ras4B and Modifies Ras/ERK Signaling and Migration in Pancreatic and Lung Carcinoma Cells. *Cancers (Basel).* **12**, 30 (2019).

139. Inder, K. L. *et al.* Nucleophosmin and nucleolin regulate K-ras plasma membrane interactions and MAPK signal transduction. *J. Biol. Chem.* **284**, 28410–28419 (2009).

140. Inder, K. L., Hill, M. M. & Hancock, J. F. Nucleophosmin and nucleolin regulate K-Ras signaling. *Commun. Integr. Biol.* **3**, 188–190 (2010).

141. Ballester, R., Furth, M. E. & Rosen, O. M. Phorbol ester- and protein kinase C-mediated phosphorylation of the cellular Kirsten ras gene product. *J. Biol. Chem.* **262**, 2688–95 (1987).

142. Cho, K. *et al.* AMPK and Endothelial Nitric Oxide Synthase Signaling Regulates K-Ras Plasma Membrane Interactions via Cyclic GMP-Dependent Protein Kinase 2. *Mol. Cell. Biol.* **36**, 3086–3099 (2016).

143. Jang, H. *et al.* Mechanisms of membrane binding of small GTPase K-Ras4B farnesylated hypervariable region. *J. Biol. Chem.* **290**, 9465–9477 (2015).

144. Barceló, C. *et al.* Phosphorylation at ser-181 of oncogenic KRAS is required for tumor growth. *Cancer Res.* **74**, 1190–1199 (2014).

145. Barceló, C. *et al.* Detection of Phospho-KRAS by Electrophoretic Mobility Change in Human Cell Lines and in Tumor Samples from Nude Mice Grafts. *BIO-PROTOCOL* **5**, (2015).

146. Kano, Y. *et al.* Tyrosyl phosphorylation of KRAS stalls GTPase cycle via alteration of switch I and II conformation. *Nat. Commun.* **10**, 224 (2019).

147. Dohlman, H. G. & Campbell, S. L. Regulation of large and small G proteins by ubiquitination. *J. Biol. Chem.* **294**, 18613–18623 (2019).

148. Sasaki, A. T. *et al.* Ubiquitination of K-Ras enhances activation and facilitates binding to select downstream effectors. *Sci. Signal.* **4**, ra13 (2011).

149. Baker, R. *et al.* Site-specific monoubiquitination activates Ras by impeding GTPase-activating protein function. *Nat. Struct. Mol. Biol.* **20**, 46–52 (2013).

150. Hobbs, G. A., Gunawardena, H. P., Baker, R., Chen, X. & Campbell, S. L. Site-specific

monoubiquitination activates Ras by impeding GTPase-activating protein function. *Small GTPases* **4**, 186–192 (2013).

151. Yang, M. H. *et al.* Regulation of RAS oncogenicity by acetylation. *Proc. Natl. Acad. Sci. U. S. A.* **109**, 10843–8 (2012).

152. Yang, M. H. *et al.* HDAC6 and SIRT2 regulate the acetylation state and oncogenic activity of mutant K-RAS. *Mol. Cancer Res.* **11**, 1072–1077 (2013).

153. Williams, J. G., Pappu, K. & Campbell, S. L. Structural and biochemical studies of p21RAS S-nitrosylation and nitric oxide-mediated guanine nucleotide exchange. *Proc. Natl. Acad. Sci. U. S. A.* **100**, 6376–6381 (2003).

154. Heo, J. & Campbell, S. L. Mechanism of p21 Ras S-Nitrosylation and Kinetics of Nitric Oxide-Mediated Guanine Nucleotide Exchange †. *Biochemistry* **43**, 2314–2322 (2004).

155. Raines, K. W., Bonini, M. G. & Campbell, S. L. Nitric oxide cell signaling: S-nitrosation of Ras superfamily GTPases. *Cardiovasc. Res.* **75**, 229–239 (2007).

156. Ntai, I. *et al.* Precise characterization of KRAS4b proteoforms in human colorectal cells and tumors reveals mutation/modification cross-talk. *Proc. Natl. Acad. Sci. U. S. A.* **115**, 4140–4145 (2018).

157. Lim, K. H., Ancrile, B. B., Kashatus, D. F. & Counter, C. M. Tumour maintenance is mediated by eNOS. *Nature* **452**, 646–649 (2008).

158. Guo, Y. *et al.* ERK/MAPK signalling pathway and tumorigenesis (Review). *Exp. Ther. Med.* **19**, 1997 (2020).

159. Moodie, S. A., Willumsen, B. M., Weber, M. J. & Wolfman, A. Complexes of Ras·GTP with Raf-1 and mitogen-activated protein kinase kinase. *Science (80-.).* **260**, 1658–1661 (1993).

160. Warne, P. H., Vician, P. R. & Downward, J. Direct interaction of Ras and the amino-terminal region of Raf-1 in vitro. *Nature* **364**, 352–355 (1993).

161. Zhang, X. F. *et al.* Normal and oncogenic p21ras proteins bind to the amino-terminal regulatory domain of c-Raf-1. *Nature* **364**, 308–313 (1993).

162. Vojtek, A. B., Hollenberg, S. M. & Cooper, J. A. Mammalian Ras interacts directly with the serine/threonine kinase raf. *Cell* **74**, 205–214 (1993).

163. Lavoie, H. & Therrien, M. Regulation of RAF protein kinases in ERK signalling. *Nat. Rev. Mol. Cell Biol.* **16**, 281–298 (2015).

164. Matallanas, D. *et al.* Raf family kinases: Old dogs have learned new tricks. *Genes and Cancer* vol. 2 232–260 (2011).

165. Degirmenci, U., Wang, M. & Hu, J. Targeting Aberrant RAS/RAF/MEK/ERK Signaling for Cancer Therapy. *Cells* **9**, 198 (2020).

166. Davies, H. *et al. Mutations of the BRAF gene in human cancer*. www.nature.com/nature (2002).

167. Raman, M., Chen, W. & Cobb, M. H. Differential regulation and properties of MAPKs. *Oncogene* vol. 26 3100–3112 (2007).

168. Roux, P. P. & Blenis, J. ERK and p38 MAPK-Activated Protein Kinases: a Family of Protein Kinases with Diverse Biological Functions. *Microbiol. Mol. Biol. Rev.* **68**, 320–344 (2004).

169. Dougherty, M. K. *et al.* Regulation of Raf-1 by direct feedback phosphorylation. *Mol. Cell* **17**, 215–224 (2005).

170. Farrar, M. A., Alberola-Ila, J. & Perlmutter, R. M. Activation of the Raf-1 kinase cascade by coumermycin-induced dimerization. *Nature* **383**, 178–181 (1996).

171. Luo, Z. *et al.* Oligomerization activates c-Raf-1 through a Ras-dependent mechanism. *Nature* **383**, 181–185 (1996).

172. Weber, C. K., Slupsky, J. R., Andreas Kalmes, H. & Rapp, U. R. Active ras induces heterodimerization of cRaf and BRaf. *Cancer Res.* **61**, 3595–3598 (2001).

173. Rushworth, L. K., Hindley, A. D., O'Neill, E. & Kolch, W. Regulation and Role of Raf-1/B-Raf Heterodimerization. *Mol. Cell. Biol.* **26**, 2262–2272 (2006).

174. Wan, P. T. C. *et al.* Mechanism of activation of the RAF-ERK signaling pathway by oncogenic mutations of B-RAF. *Cell* **116**, 855–867 (2004).

175. Garnett, M. J., Rana, S., Paterson, H., Barford, D. & Marais, R. Wild-type and mutant B-RAF activate C-RAF through distinct mechanisms involving heterodimerization. *Mol. Cell* **20**, 963–969 (2005).

176. Heidorn, S. J. *et al.* Kinase-Dead BRAF and Oncogenic RAS Cooperate to Drive Tumor Progression through CRAF. *Cell* **140**, 209–221 (2010).

177. Hu, J. *et al.* Allosteric Activation of Functionally Asymmetric RAF Kinase Dimers. *Cell* **154**, 1036–1046 (2013).

178. Nan, X. *et al.* Single-molecule superresolution imaging allows quantitative analysis of RAF multimer formation and signaling. *Proc. Natl. Acad. Sci. U. S. A.* **110**, 18519–18524 (2013).

179. Freeman, A. K., Ritt, D. A. & Morrison, D. K. Effects of Raf Dimerization and Its Inhibition on Normal and Disease-Associated Raf Signaling. *Mol. Cell* **49**, 751–758 (2013).

180. Blasco, R. B. R. B. *et al.* C-Raf, but Not B-Raf, Is Essential for Development of K-Ras Oncogene-Driven Non-Small Cell Lung Carcinoma. *Cancer Cell* **19**, 652–663 (2011).

181. Karreth, F. A., Frese, K. K., DeNicola, G. M., Baccarini, M. & Tuveson, D. A. C-Raf is required for the initiation of lung cancer by K-Ras G12D. *Cancer Discov.* **1**, 128–136 (2011).

182. Sanclemente, M. *et al.* c-RAF Ablation Induces Regression of Advanced Kras/Trp53 Mutant Lung Adenocarcinomas by a Mechanism Independent of MAPK Signaling. *Cancer Cell* **33**, 217-228.e4 (2018).

183. Terrell, E. M. *et al.* Distinct Binding Preferences between Ras and Raf Family Members and the Impact on Oncogenic Ras Signaling. *Mol. Cell* **76**, 872-884.e5 (2019).

184. Aoki, M. & Fujishita, T. Oncogenic Roles of the PI3K/AKT/mTOR axis. in *Current Topics in Microbiology and Immunology* vol. 407 153–189 (2017).

185. Zhao, L. & Vogt, P. K. Class I PI3K in oncogenic cellular transformation. *Oncogene* vol. 27 5486–5496 (2008).

186. Martini, M., De Santis, M. C., Braccini, L., Gulluni, F. & Hirsch, E. PI3K/AKT signaling pathway and cancer: An updated review. *Ann. Med.* **46**, 372–383 (2014).

187. Asati, V., Mahapatra, D. K. & Bharti, S. K. PI3K/Akt/mTOR and Ras/Raf/MEK/ERK signaling pathways inhibitors as anticancer agents: Structural and pharmacological perspectives. *Eur. J. Med. Chem.* **109**, 314–341 (2016).

188. Manning, B. D. & Toker, A. AKT/PKB Signaling: Navigating the Network. *Cell* **169**, 381–405 (2017).

189. Bossler, F., Hoppe-Seyler, K. & Hoppe-Seyler, F. PI3K/AKT/mTOR Signaling Regulates the Virus/Host Cell Crosstalk in HPV-Positive Cervical Cancer Cells. *Int. J. Mol. Sci.* **20**, 2188 (2019).

190. Rodriguez-Viciana, P. *et al.* Phosphatidylinositol-3-OH kinase direct target of Ras. *Nature* **370**, 527–532 (1994).

191. Rodriguez-Viciana, P., Warne, P. H., Vanhaesebroeck, B., Waterfield, M. D. & Downward, J. Activation of phosphoinositide 3-kinase by interaction with Ras and by point mutation. *EMBO J.* **15**, 2442–2451 (1996).

192. Lim, K. H. & Counter, C. M. Reduction in the requirement of oncogenic Ras signaling to activation of PI3K/AKT pathway during tumor maintenance. *Cancer Cell* **8**, 381–392 (2005).

193. Gupta, S. *et al.* Binding of Ras to Phosphoinositide 3-Kinase p110α Is Required for Ras- Driven Tumorigenesis in Mice. *Cell* **129**, 957–968 (2007).

194. Castellano, E. *et al.* Requirement for Interaction of PI3-Kinase p110α with RAS in Lung Tumor Maintenance. *Cancer Cell* **24**, 617–630 (2013).

195. Eser, S. *et al.* Selective requirement of PI3K/PDK1 signaling for kras oncogene-driven pancreatic cell plasticity and cancer. *Cancer Cell* **23**, 406–420 (2013).

196. Fernandes, M. S. *et al.* Specific inhibition of p110α subunit of PI3K: Putative therapeutic strategy for KRAS mutant colorectal cancers. *Oncotarget* **7**, 68546–68558 (2016).

197. Philips, M. R. & Der, C. J. Seeing is believing: Ras dimers observed in live cells. *Proceedings of the National Academy of Sciences of the United States of America* vol. 112 9793–9794 (2015).

198. O'Bryan, J. P. & O'Bryan, J. P. Pharmacological targeting of RAS: Recent success with direct inhibitors. *Pharmacol. Res.* **139**, 503–511 (2019).

199. Santos, E., Nebreda, A. R., Bryan, T. & Kempner, E. S. Oligomeric structure of p21 ras proteins as determined by radiation inactivation. *J. Biol. Chem.* **263**, 9853–9858 (1988).

200. Chataway, T. K. & Barritt, G. J. Studies on the iodination of a ras protein and the detection of ras polymers. *Mol. Cell. Biochem.* **137**, 75–83 (1994).

201. Inouye, K., Mizutani, S., Koide, H. & Kaziro, Y. Formation of the Ras dimer is essential for Raf-1 activation. *J. Biol. Chem.* **275**, 3737–3740 (2000).

202. Dementiev, A. K-Ras4B lipoprotein synthesis: Biochemical characterization, functional properties, and dimer formation. *Protein Expr. Purif.* **84**, 86–93 (2012).

203. Chung, J. K. *et al.* K-Ras4B Remains Monomeric on Membranes over a Wide Range of Surface Densities and Lipid Compositions. *Biophys. J.* **114**, 137–145 (2018).

204. Nan, X. *et al.* Ras-GTP dimers activate the Mitogen-Activated Protein Kinase (MAPK) pathway. *Proc. Natl. Acad. Sci. U. S. A.* **112**, 7996–8001 (2015).

205. Muratcioglu, S. *et al.* GTP-Dependent K-Ras Dimerization. *Structure* **23**, 1325–1335 (2015).

206. Sayyed-Ahmad, A., Cho, K. J., Hancock, J. F. & Gorfe, A. A. Computational Equilibrium Thermodynamic and Kinetic Analysis of K-Ras Dimerization through an Effector Binding Surface Suggests Limited Functional Role. *J. Phys. Chem. B* **120**, 8547–8556 (2016).

207. Prakash, P. *et al.* Computational and biochemical characterization of two partially overlapping interfaces and multiple weak-affinity K-Ras dimers. *Sci. Rep.* **7**, (2017).

208. Ambrogio, C. *et al.* KRAS Dimerization Impacts MEK Inhibitor Sensitivity and Oncogenic Activity of Mutant KRAS. *Cell* **172**, 857-868.e15 (2018).

209. Nabet, B. & Gray, N. S. It Takes Two To Target: A Study in KRAS Dimerization. *Biochemistry* **57**, 2289–2290 (2018).

210. Lin, Y. J. & Haigis, K. M. Brother's Keeper: Wild-Type Mutant K-Ras Dimers Limit Oncogenesis. *Cell* vol. 172 645–647 (2018).

211. Burgess, M. R. *et al.* KRAS Allelic Imbalance Enhances Fitness and Modulates MAP Kinase Dependence in Cancer. *Cell* **168**, 817-829.e15 (2017).

212. Zhou, B., Der, C. J. & Cox, A. D. The role of wild type RAS isoforms in cancer. *Semin. Cell Dev. Biol.* **58**, 60–69 (2016).

213. Muratcioglu, S. *et al.* Oncogenic K-Ras4B Dimerization Enhances Downstream Mitogen-activated Protein Kinase Signaling. *J. Mol. Biol.* **432**, 1199–1215 (2020).

214. Spencer-Smith, R. *et al.* Inhibition of RAS function through targeting an allosteric regulatory site. *Nat. Chem. Biol.* **13**, 62–68 (2017).

215. Khan, I., Spencer-Smith, R. & O'Bryan, J. P. Targeting the α4–α5 dimerization interface of K-RAS inhibits tumor formation in vivo. *Oncogene* **38**, 4426–4426 (2019).

216. Kessler, D. *et al.* Drugging an undruggable pocket on KRAS. *Proc. Natl. Acad. Sci.* **116**, 15823–15829 (2019).

217. Tran, T. H. *et al.* The small molecule BI-2852 induces a nonfunctional dimer of KRAS. *Proceedings of the National Academy of Sciences of the United States of America* vol. 117 3363–3364 (2020).

218. Shih, C., Shilo, B. Z., Goldfarb, M. P., Dannenberg, A. & Weinberg, R. A. Passage of phenotypes

of chemically transformed cells via transfection of DNA and chromatin. *Proc. Natl. Acad. Sci. U. S. A.* **76**, 5714–5718 (1979).

219. Shih, C. & Weinberg, R. A. Isolation of a transforming sequence from a human bladder carcinoma cell line. *Cell* **29**, 161–169 (1982).

220. Goldfarb, M., Shimizu, K., PERcho, M. & Wigler, M. Isolation and preliminary characterization of a human transforming gene from T24 bladder carcinoma cells. *Nature* **296**, 404–409 (1982).

221. Pulciani, S. *et al.* Oncogenes in human tumor cell lines: Molecular cloning of a transforming gene from human bladder carcinoma cells. *Proc. Natl. Acad. Sci. U. S. A.* **79**, 2845–2849 (1982).

222. Parada, L. F. & Weinberg, R. A. Presence of a Kirsten murine sarcoma virus ras oncogene in cells transformed by 3-methylcholanthrene. *Mol. Cell. Biol.* **3**, 2298–2301 (1983).

223. Santos, E. *et al.* Malignant activation of a K-ras oncogene in lung carcinoma but not in normal tissue of the same patient. *Science (80-.).* **223**, 661–664 (1984).

224. Forrester, K., Allmoguera, C., Perucho, M., Han, K. & Grizzle, W. E. Detection of high incidence of K-ras oncogenes during human colon tumorigenesis. *Nature* **327**, 298–303 (1987).

225. Bos, J. L. *Review ras Oncogenes in Human Cancer: A Review1*. *CANCER RESEARCH* vol. 49 (1989).

226. Rodenhuis, S. *et al.* Mutational Activation of the K-ras Oncogene. *N. Engl. J. Med.* **317**, 929–935 (1987).

227. Almoguera, C. *et al.* Most human carcinomas of the exocrine pancreas contain mutant c-K-ras genes. *Cell* **53**, 549–554 (1988).

228. Haigis, K. M. KRAS Alleles: The Devil Is in the Detail. *Trends in Cancer* **3**, 686–697 (2017).

229. Murugan, A. K., Grieco, M. & Tsuchida, N. RAS mutations in human cancers: Roles in precision medicine. *Semin. Cancer Biol.* **50**, 23–35 (2019).

230. Buhrman, G., Holzapfel, G., Fetics, S. & Mattos, C. Allosteric modulation of Ras positions Q61 for a direct role in catalysis. *Proc. Natl. Acad. Sci. U. S. A.* **107**, 4931–4936 (2010).

231. Pylayeva-Gupta, Y., Grabocka, E. & Bar-Sagi, D. RAS oncogenes: weaving a tumorigenic web. (2011) doi:10.1038/nrc3106.

232. Smith, M. J., Neel, B. G. & Ikura, M. NMR-based functional profiling of RASopathies and oncogenic RAS mutations. *Proc. Natl. Acad. Sci. U. S. A.* **110**, 4574–4579 (2013).

233. Khan, I., Rhett, J. M. & O'Bryan, J. P. Therapeutic targeting of RAS: New hope for drugging the "undruggable". *Biochim. Biophys. Acta - Mol. Cell Res.* **1867**, (2020).

234. Cox, A. D., Fesik, S. W., Kimmelman, A. C., Luo, J. & Der, C. J. Drugging the undruggable RAS: Mission Possible? *Nat. Rev. Drug Discov.* **13**, 828–851 (2014).

235. Fearon, E. R. & Vogelstein, B. A genetic model for colorectal tumorigenesis. *Cell* vol. 61 759–767 (1990).

236. Pino, M. S. & Chung, D. C. The Chromosomal Instability Pathway in Colon Cancer.

Gastroenterology **138**, 2059–2072 (2010).

237. Okugawa, Y., Grady, W. M. & Goel, A. Epigenetic Alterations in Colorectal Cancer: Emerging Biomarkers. *Gastroenterology* **149**, 1204-1225.e12 (2015).

238. Maffeis, V., Nicolè, L. & Cappellesso, R. RAS, Cellular Plasticity, and Tumor Budding in Colorectal Cancer. *Front. Oncol.* **9**, 1255 (2019).

239. De Palma, F. *et al.* The Molecular Hallmarks of the Serrated Pathway in Colorectal Cancer. *Cancers (Basel).* **11**, 1017 (2019).

240. Guinney, J. *et al.* The consensus molecular subtypes of colorectal cancer. *Nat. Med.* **21**, 1350–1356 (2015).

241. Berg, K. C. G. *et al.* Multi-omics of 34 colorectal cancer cell lines - a resource for biomedical studies. *Mol. Cancer* **16**, 116 (2017).

242. Han, C.-B., Li, F., Ma, J.-T., Zou, W. & Zou, H.-W. Concordant KRAS Mutations in Primary and Metastatic Colorectal Cancer Tissue Specimens: A Meta-Analysis and Systematic Review. *Cancer Invest.* **30**, 741–747 (2012).

243. Steele, C. W., Whittle, T. & Smith, J. J. Review: KRAS mutations are influential in driving hepatic metastases and predicting outcome in colorectal cancer. *Chinese Clin. Oncol.* **8**, 9 (2019).

244. Boutin, A. T. *et al.* Oncogenic Kras drives invasion and maintains metastases in colorectal cancer. *Genes Dev.* **31**, 370–382 (2017).

245. Mann, K. M., Ying, H., Juan, J., Jenkins, N. A. & Copeland, N. G. KRAS-related proteins in pancreatic cancer. *Pharmacol. Ther.* **168**, 29–42 (2016).

246. Distler, M., Aust, D., Weitz, J., Pilarsky, C. & Grützmann, R. Precursor Lesions for Sporadic Pancreatic Cancer: PanIN, IPMN, and MCN. (2014) doi:10.1155/2014/474905.

247. Buscail, L., Bournet, B. & Cordelier, P. Role of oncogenic KRAS in the diagnosis, prognosis and treatment of pancreatic cancer. *Nature Reviews Gastroenterology and Hepatology* vol. 17 153–168 (2020).

248. Arner, E. N., Du, W. & Brekken, R. A. Behind the Wheel of Epithelial Plasticity in KRAS-Driven Cancers. *Frontiers in Oncology* vol. 9 1049 (2019).

249. Weinstein, I. B. & Joe, A. Oncogene addiction. *Cancer Research* vol. 68 3077–3080 (2008).

250. Torti, D. & Trusolino, L. Oncogene addiction as a foundational rationale for targeted anti-cancer therapy: promises and perils. *EMBO Mol. Med.* **3**, 623–636 (2011).

251. Singh, A. *et al.* A Gene Expression Signature Associated with 'K-Ras Addiction' Reveals Regulators of EMT and Tumor Cell Survival. *Cancer Cell* **15**, 489–500 (2009).

252. Singh, A. & Settleman, J. Oncogenic K-ras 'addiction' and synthetic lethality. *Cell Cycle* vol. 8 2676–2678 (2009).

253. Sunaga, N. *et al.* Knockdown of oncogenic KRAS in non-small cell lung cancers suppresses tumor growth and sensitizes tumor cells to targeted therapy. *Mol. Cancer Ther.* **10**, 336–346

(2011).

254. Vartanian, S. *et al.* Identification of mutant K-Ras-dependent phenotypes using a panel of isogenic cell lines. *J. Biol. Chem.* **288**, 2403–2413 (2013).

255. Mccormick, F. KRAS as a Therapeutic Target. *Clin Cancer Res* **21**, (2015).

256. McDonald, E. R. *et al.* Project DRIVE: A Compendium of Cancer Dependencies and Synthetic Lethal Relationships Uncovered by Large-Scale, Deep RNAi Screening. *Cell* **170**, 577-592.e10 (2017).

257. Janes, M. R. *et al.* Targeting KRAS Mutant Cancers with a Covalent G12C-Specific Inhibitor. *Cell* **172**, 578-589.e17 (2018).

258. Fujita-Sato, S. *et al.* Enhanced MET translation and signaling sustains K-Ras-driven proliferation under anchorage-independent growth conditions. *Cancer Res.* **75**, 2851–2862 (2015).

259. Patricelli, M. P. *et al.* Selective inhibition of oncogenic KRAS output with small molecules targeting the inactive state. *Cancer Discov.* **6**, 316–329 (2016).

260. Nagel, R., Semenova, E. A. & Berns, A. Drugging the addict: non-oncogene addiction as a target for cancer therapy. *EMBO Rep.* **17**, 1516–1531 (2016).

261. Saliani, M., Jalal, R. & Ahmadian, M. R. From basic researches to new achievements in therapeutic strategies of KRAS-driven cancers. (2019) doi:10.20892/j.issn.2095-3941.2018.0530.

262. George Njoroge, F. *et al.* (+)-4-[2-[4-(8-chloro-3,10-dibromo-6,11-dihydro-5H-benzo[5,6]cyclohepta[1,2-b]pyridin-11(R)-yl)-1-piperidinyl]-2-oxo-ethyl]-1-piperidinecarboxamide (SCH-66336): A very potent farnesyl protein transferase inhibitor as a novel antitumor agent. *J. Med. Chem.* **41**, 4890–4902 (1998).

263. David W. End, 1 Gerda Smets, Alison V. Todd, Tanya L. Applegate, Caroline J. Fuery, Patrick Angibaud, Marc Venet, Gerard Sanz, Herve Poignet, Stacy Skrzat, Ann Devine, Walter Wouters, and C. B. Farnesyl transferase inhibitors induce apoptosis of Ras-transformed cells denied substratum attachment. *Cancer Res.* **61**, 131–137 (2001).

264. Whyte, D. B. *et al.* K- and N-Ras are geranylgeranylated in cells treated with farnesyl protein transferase inhibitors. *J. Biol. Chem.* **272**, 14459–14464 (1997).

265. Rowell, C. A., Kowalczyk, J. J., Lewis, M. D. & Garcia, A. M. Direct demonstration of geranylgeranylation and farnesylation of Ki-Ras in vivo. *J. Biol. Chem.* **272**, 14093–14097 (1997).

266. James, G. L., Goldstein, J. L. & Brown, M. S. Polylysine and CVIM sequences of K-RasB dictate specificity of prenylation and confer resistance to benzodiazepine peptidomimetic in vitro. *J. Biol. Chem.* **270**, 6221–6226 (1995).

267. Lane, K. T. & Beese, L. S. Structural biology of protein farnesyltransferase and geranylgeranyltransferase type I. *Journal of Lipid Research* vol. 47 681–699 (2006).

268. Berndt, N., Hamilton, A. D. & Sebti, S. M. Targeting protein prenylation for cancer therapy.

Nature Reviews Cancer vol. 11 775–791 (2011).

269. van der Hoeven, D. *et al.* Fendiline Inhibits K-Ras Plasma Membrane Localization and Blocks K-Ras Signal Transmission. *Mol. Cell. Biol.* **33**, 237–251 (2013).

270. Cho, K. jin, van der Hoeven, D. & Hancock, J. F. Inhibitors of K-ras plasma membrane localization. in *Enzymes* vol. 33 249–265 (Academic Press, 2013).

271. Samatar, A. A. & Poulikakos, P. I. Targeting RAS-ERK signalling in cancer: Promises and challenges. *Nature Reviews Drug Discovery* vol. 13 928–942 (2014).

272. Ryan, M. B. & Corcoran, R. B. Therapeutic strategies to target RAS-mutant cancers. *Nat. Rev. Clin. Oncol.* **15**, 709–720 (2018).

273. Lee, J. T. *et al.* PLX4032, a potent inhibitor of the B-Raf V600E oncogene, selectively inhibits V600E-positive melanomas. *Pigment Cell Melanoma Res.* **23**, 820–827 (2010).

274. Blokhin, N. *et al.* Dabrafenib in BRAF-mutated metastatic melanoma: a multicentre, open-label, phase 3 randomised controlled trial. *Lancet* **380**, 358–65 (2012).

275. Li, Z. *et al.* Encorafenib (LGX818), a potent BRAF inhibitor, induces senescence accompanied by autophagy in BRAFV600E melanoma cells. *Cancer Lett.* **370**, 332–344 (2016).

276. Callahan, M. K. *et al.* Progression of RAS-Mutant Leukemia during RAF Inhibitor Treatment. *N Engl J Med* **367**, 2316–2337 (2012).

277. Oberholzer, P. A. *et al. RAS* Mutations Are Associated With the Development of Cutaneous Squamous Cell Tumors in Patients Treated With RAF Inhibitors. *J. Clin. Oncol.* **30**, 316–321 (2012).

278. Poulikakos, P. I., Zhang, C., Bollag, G., Shokat, K. M. & Rosen, N. RAF inhibitors transactivate RAF dimers and ERK signalling in cells with wild-type BRAF. *Nature* **464**, 427–430 (2010).

279. Hatzivassiliou, G. *et al.* RAF inhibitors prime wild-type RAF to activate the MAPK pathway and enhance growth. *Nature* **464**, 431–435 (2010).

280. Engelman, J. A. *et al.* Effective use of PI3K and MEK inhibitors to treat mutant Kras G12D and PIK3CA H1047R murine lung cancers. (2008) doi:10.1038/nm.1890.

281. Britten, C. D. PI3K and MEK inhibitor combinations: Examining the evidence in selected tumor types. *Cancer Chemotherapy and Pharmacology* vol. 71 1395–1409 (2013).

282. Junttila, M. R. *et al.* Modeling targeted inhibition of MEK and PI3 kinase in human pancreatic cancer. *Mol. Cancer Ther.* **14**, 40–47 (2015).

283. Downward, J. RAS synthetic lethal screens revisited: Still seeking the elusive prize? *Clinical Cancer Research* vol. 21 1802–1809 (2015).

284. Scholl, C. *et al.* Synthetic Lethal Interaction between Oncogenic KRAS Dependency and STK33 Suppression in Human Cancer Cells. *Cell* **137**, 821–834 (2009).

285. Barbie, D. A. *et al.* Systematic RNA interference reveals that oncogenic KRAS-driven cancers require TBK1. *Nature* **462**, 108–112 (2009).

286. Babij, C. *et al.* STK33 kinase activity is nonessential in KRAS-dependent cancer cells. *Cancer Res.* **71**, 5818–5826 (2011).

287. Luo, T. *et al.* STK33 kinase inhibitor BRD-8899 has no effect on KRAS-dependent cancer cell viability. *Proc. Natl. Acad. Sci. U. S. A.* **109**, 2860–2865 (2012).

288. Muvaffak, A. *et al.* Evaluating TBK1 as a therapeutic target in cancers with activated IRF3. *Mol. Cancer Res.* **12**, 1055–1066 (2014).

289. Luo, J., Solimini, N. L. & Elledge, S. J. Principles of Cancer Therapy: Oncogene and Non-oncogene Addiction. *Cell* vol. 136 823–837 (2009).

290. Dias Carvalho, P., Machado, A. L., Martins, F., Seruca, R. & Velho, S. Targeting the Tumor Microenvironment: An Unexplored Strategy for Mutant KRAS Tumors. *Cancers (Basel).* **11**, 2010 (2019).

291. Najumudeen, A. K. *et al.* Cancer stem cell drugs target K-ras signaling in a stemness context. *Oncogene* **35**, 5248–5262 (2016).

292. Zhang, Y., Ma, J.-A., Zhang, H.-X., Jiang, Y.-N. & Luo, W.-H. Cancer vaccines: Targeting KRAS-driven cancers. *Expert Rev. Vaccines* **19**, 163–173 (2020).

293. Patgiri, A., Yadav, K. K., Arora, P. S. & Bar-Sagi, D. An orthosteric inhibitor of the Ras-Sos interaction. *Nat. Chem. Biol.* (2011) doi:10.1038/nCHeMBIO.612.

294. Leshchiner, E. S. *et al.* Direct inhibition of oncogenic KRAS by hydrocarbon-stapled SOS1 helices. *Proc. Natl. Acad. Sci. U. S. A.* **112**, 1761–1766 (2015).

295. Sun, Q. *et al.* Discovery of Small Molecules that Bind to K-Ras and Inhibit Sos-Mediated Activation. *Angew. Chemie Int. Ed.* **51**, 6140–6143 (2012).

296. Maurer, T. *et al.* Small-molecule ligands bind to a distinct pocket in Ras and inhibit SOS-mediated nucleotide exchange activity. *Proc. Natl. Acad. Sci. U. S. A.* **109**, 5299–5304 (2012).

297. Ostrem, J. M. L. & Shokat, K. M. Direct small-molecule inhibitors of KRAS: from structural insights to mechanism-based design. *Nat. Rev. Drug Discov.* **15**, 771–785 (2016).

298. Lu, S., Jang, H., Gu, S., Zhang, J. & Nussinov, R. Drugging Ras GTPase: A comprehensive mechanistic and signaling structural view. *Chemical Society Reviews* vol. 45 4929–4952 (2016).

299. Herrmann, C. *et al.* Sulindac sulfide inhibits Ras signaling. *Oncogene* **17**, 1769–1776 (1998).

300. Müller, O. *et al.* Identification of Potent Ras Signaling Inhibitors by Pathway-Selective Phenotype-Based Screening. *Angew. Chemie Int. Ed.* **43**, 450–454 (2004).

301. Waldmann, H. *et al.* Sulindac-Derived Ras Pathway Inhibitors Target the Ras–Raf Interaction and Downstream Effectors in the Ras Pathway. *Angew. Chemie Int. Ed.* **43**, 454–458 (2004).

302. Pan, M. R., Chang, H. C. & Hung, W. C. Non-steroidal anti-inflammatory drugs suppress the ERK signaling pathway via block of Ras/c-Raf interaction and activation of MAP kinase phosphatases. *Cell. Signal.* **20**, 1134–1141 (2008).

303. Kato-Stankiewicz, J. *et al.* Inhibitors of Ras/Raf-1 interaction identified by two-hybrid screening revert Ras-dependent transformation phenotypes in human cancer cells. *Proc. Natl. Acad. Sci. U. S. A.* **99**, 14398–14403 (2002).

304. González-Pérez, V. *et al.* Genetic and functional characterization of putative Ras/Raf interaction inhibitors in C. elegans and mammalian cells. *J. Mol. Signal.* **5**, 2 (2010).

305. Shima, F. *et al.* In silico discovery of small-molecule Ras inhibitors that display antitumor activity by blocking the Ras-effector interaction. *Proc. Natl. Acad. Sci. U. S. A.* **110**, 8182–8187 (2013).

306. Ostrem, J. M., Peters, U., Sos, M. L., Wells, J. A. & Shokat, K. M. K-Ras(G12C) inhibitors allosterically control GTP affinity and effector interactions. *Nature* **503**, 548–551 (2013).

307. Lito, P., Solomon, M., Li, L. S., Hansen, R. & Rosen, N. Cancer therapeutics: Allele-specific inhibitors inactivate mutant KRAS G12C by a trapping mechanism. *Science (80-.).* **351**, 604–608 (2016).

308. Hallin, J. *et al.* The KRAS G12C Inhibitor MRTX849 Provides Insight toward Therapeutic Susceptibility of KRAS-Mutant Cancers in Mouse Models and Patients. *Cancer Discov.* **10**, 54–71 (2020).

309. Tanaka, T., Williams, R. L. & Rabbitts, T. H. Tumour prevention by a single antibody domain targeting the interaction of signal transduction proteins with RAS. *EMBO J.* **26**, 3250–3259 (2007).

310. Quevedo, C. E. *et al.* Small molecule inhibitors of RAS-effector protein interactions derived using an intracellular antibody fragment. *Nat. Commun.* **9**, (2018).

311. Furth, M. E., Davis, L. J., Fleurdelys, B. & Scolnick, E. M. *Monoclonal Antibodies to the p21 Products of the Transforming Gene of Harvey Murine Sarcoma Virus and of the Cellular ras Gene Family*. *JOURNAL OF VIROLOGY* vol. 43 http://jvi.asm.org/ (1982).

312. Mulcahy, L. S., Smith, M. R. & Stacey, D. W. Requirement for ras proto-oncogene function during serum-stimulated growth of NIH 3T3 cells. *Nature* **313**, 241–243 (1985).

313. Lacal, J. C. & Aaronson, S. A. *Monoclonal Antibody Y13-259 Recognizes an Epitope of the p21 ras Molecule Not Directly Involved in the GTP-Binding Activity of the Protein*. *MOLECULAR AND CELLULAR BIOLOGY* vol. 6 http://mcb.asm.org/ (1986).

314. Cardinale, A., Lener, M., Messina, S., Cattaneo, A. & Biocca, S. The mode of action of Y13-259 scFv fragment intracellularly expressed in mammalian cells. *FEBS Lett.* **439**, 197–202 (1998).

315. Clark, R., Wong, G., Arnheim, N., Nitecki, D. & McCormick, F. Antibodies specific for amino acid 12 of the ras oncogene product inhibit GTP binding. *Proc. Natl. Acad. Sci. U. S. A.* **82**, 5280–5284 (1985).

316. Feramisco, J. R. *et al.* Transient reversion of ras oncogene-induced cell transformation by antibodies specific for amino acid 12 of ras protein. *Nature* **314**, 639–642 (1985).

317. Tanaka, T., Lobato, M. N. & Rabbitts, T. H. Single domain intracellular antibodies: A minimal

fragment for direct in vivo selection of antigen-specific intrabodies. *J. Mol. Biol.* **331**, 1109–1120 (2003).

318. Shin, S. M. *et al.* Antibody targeting intracellular oncogenic Ras mutants exerts anti-tumour effects after systemic administration. *Nat. Commun.* **8**, 1–14 (2017).

319. Kauke, M. J. *et al.* An engineered protein antagonist of K-Ras/B-Raf interaction. *Sci. Rep.* **7**, 1–9 (2017).

320. Guillard, S. *et al.* Structural and functional characterization of a DARPin which inhibits Ras nucleotide exchange. *Nat. Commun.* **8**, 1–11 (2017).

321. Bery, N. *et al.* KRAS-specific inhibition using a DARPin binding to a site in the allosteric lobe. *Nat. Commun.* **10**, 1–11 (2019).

322. Sha, F., Salzman, G., Gupta, A. & Koide, S. Monobodies and other synthetic binding proteins for expanding protein science. *Protein Sci.* **26**, 910–924 (2017).

323. Henninot, A., Collins, J. C. & Nuss, J. M. The Current State of Peptide Drug Discovery: Back to the Future? *Journal of Medicinal Chemistry* vol. 61 1382–1414 (2018).

324. Qian, Z., Dougherty, P. G. & Pei, D. Targeting intracellular protein–protein interactions with cell-permeable cyclic peptides. *Current Opinion in Chemical Biology* vol. 38 80–86 (2017).

325. Higueruelo, A. P., Jubb, H. & Blundell, T. L. Protein-protein interactions as druggable targets: recent technological advances. (2013) doi:10.1016/j.coph.2013.05.009.

326. Nevola, L. & Giralt, E. Modulating protein-protein interactions: The potential of peptides. *Chem. Commun.* **51**, 3302–3315 (2015).

327. Mabonga, L., Abidemi, & & Kappo, P. Protein-protein interaction modulators: advances, successes and remaining challenges. *Biophys. Rev.* **11**, 559–581 (2019).

328. Robertson, N. & Spring, D. Using Peptidomimetics and Constrained Peptides as Valuable Tools for Inhibiting Protein–Protein Interactions. *Molecules* **23**, 959 (2018).

329. Jiang, H. *et al.* Peptidomimetic inhibitors of APC-Asef interaction block colorectal cancer migration. *Nat. Chem. Biol.* **13**, 994–1001 (2017).

330. Kanthala, S. P. *et al.* A peptidomimetic with a chiral switch is an inhibitor of epidermal growth factor receptor heterodimerization. *Oncotarget* **8**, 74244–74262 (2017).

331. Wu, X., Upadhyaya, P., Villalona-Calero, M. A., Briesewitz, R. & Pei, D. Inhibition of Ras-effector interactions by cyclic peptides. *Medchemcomm* **4**, 378–382 (2013).

332. Upadhyaya, P. *et al.* Inhibition of Ras Signaling by Blocking Ras-Effector Interactions with Cyclic Peptides. *Angew. Chemie Int. Ed.* **54**, 7602–7606 (2015).

333. Trinh, T. B., Upadhyaya, P., Qian, Z. & Pei, D. Discovery of a Direct Ras Inhibitor by Screening a Combinatorial Library of Cell-Permeable Bicyclic Peptides. *ACS Comb. Sci.* **18**, 75–85 (2016).

334. Sacco, E. *et al.* Novel RasGRF1-derived Tat-fused peptides inhibiting Ras-dependent proliferation and migration in mouse and human cancer cells. *Biotechnol. Adv.* **30**, 233–243

(2012).

335. Sakamoto, K. *et al.* K-Ras(G12D)-selective inhibitory peptides generated by random peptide T7 phage display technology. *Biochem. Biophys. Res. Commun.* **484**, 605–611 (2017).

336. Sogabe, S. *et al.* Crystal Structure of a Human K-Ras G12D Mutant in Complex with GDP and the Cyclic Inhibitory Peptide KRpep-2d. *ACS Med. Chem. Lett.* **8**, 732–736 (2017).

337. Tsubamoto, M. *et al.* A Guanidyl-Based Bivalent Peptidomimetic Inhibits K-Ras Prenylation and Association with c-Raf. *Chem. – A Eur. J.* **25**, 13531–13536 (2019).

338. Tibbetts, L. M., Chu, M. Y., Hager, J. C., Dexter, D. L. & Calabresi, P. Chemotherapy of cell-line-derived human colon carcinomas in mice immunosuppressed with antithymocyte serum. *Cancer* **40**, 2651–9 (1977).

339. Ran, F. A. *et al.* Genome engineering using the CRISPR-Cas9 system. *Nat. Protoc.* **8**, 2281–2308 (2013).

340. Sullender, M. *et al.* Optimized sgRNA design to maximize activity and minimize off-target effects of CRISPR-Cas9. *Nat. Biotechnol.* **34**, 184–191 (2015).

341. Hsu, P. D. *et al.* DNA targeting specificity of RNA-guided Cas9 nucleases. *Nat. Biotechnol.* **31**, 827–832 (2013).

342. Lee, G. Y., Kenny, P. A., Lee, E. H. & Bissell, M. J. Three-dimensional culture models of normal and malignant breast epithelial cells. **4**, 359 (2007).

343. Gogarten, S. M. *et al.* GWASTools: an R/Bioconductor package for quality control and analysis of genome-wide association studies. *Bioinformatics* **28**, 3329–3331 (2012).

344. Subramanian, A. *et al.* Gene set enrichment analysis: A knowledge-based approach for interpreting genome-wide expression profiles. *Proc. Natl. Acad. Sci. U. S. A.* **102**, 15545–15550 (2005).

345. Cortazar, A. R. *et al.* Cancertool: A visualization and representation interface to exploit cancer datasets. *Cancer Res.* **78**, 6320–6328 (2018).

346. Marisa, L. *et al.* Gene Expression Classification of Colon Cancer into Molecular Subtypes: Characterization, Validation, and Prognostic Value. *PLoS Med.* **10**, e1001453 (2013).

347. Humphries, B. A. *et al.* Plasminogen Activator Inhibitor 1 (PAI1) Promotes Actin Cytoskeleton Reorganization and Glycolytic Metabolism in Triple-Negative Breast Cancer. **17**, 1142–1154 (2019).

348. Wang, J. *et al.* Expression of HNF4G and its potential functions in lung cancer. *Oncotarget* **9**, 18018–18028 (2018).

349. Hou, Z. *et al.* TRIB2 functions as novel oncogene in colorectal cancer by blocking cellular senescence through AP4/p21 signaling. *Mol cancer* **17**, 172 (2018).

350. Livak, K. J. & Schmittgen, T. D. Analysis of Relative Gene Expression Data Using Real-Time Quantitative PCR and the 2 C T Method. *METHODS* **25**, 402–408 (2001).

351. Euhus, D. M., Hudd, C., Laregina, M. C. & Johnson, F. E. Tumor measurement in the nude mouse. *J. Surg. Oncol.* **31**, 229–234 (1986).

352. Fiennes, A. G. T. W. Growth rate of human tumour xenografts measured in nude mice by in vivo cast modelling. *Br. J. Surg.* **75**, 23–24 (1988).

353. Tomayko, M. M. & Reynolds, C. P. Determination of subcutaneous tumor size in athymic (nude) mice. *Cancer Chemother. Pharmacol.* **24**, 148–154 (1989).

354. Shirasawa, S., Furuse, M., Yokoyama, N. & Sasazuki, T. Altered growth of human colon cancer cell lines disrupted at activated Ki-ras. *Science (80-.).* **260**, 85–88 (1993).

355. Hood, F. E. *et al.* Isoform-specific Ras signaling is growth factor dependent. *Mol. Biol. Cell* **30**, 1108–1117 (2019).

356. Yamamoto, H. *et al.* Overexpression of MT1-MMP is insufficient to increase experimental liver metastasis of human colon cancer cells. *Int. J. Mol. Med.* **22**, 757–761 (2008).

357. Kato, H. *et al.* High expression of PRL-3 promotes cancer cell motility and liver metastasis in human colorectal cancer: A predictive molecular marker of metachronous liver and lung metastases. *Clin. Cancer Res.* **10**, 7318–7328 (2004).

358. Santiago, L., Daniels, G., Wang, D., Deng, M. & Lee, P. *Wnt signaling pathway protein LEF1 in cancer, as a biomarker for prognosis and a target for treatment*. *Am J Cancer Res* vol. 7 (2017).

359. Chaturvedi, V., Fournier-Level, A., Cooper, H. M. & Murray, M. J. Loss of Neogenin1 in human colorectal carcinoma cells causes a partial EMT and wound-healing response. *Sci. Rep.* **9**, (2019).

360. Li, S. *et al.* Plasminogen activator inhibitor-1 in cancer research. *Biomed. Pharmacother.* **105**, 83–94 (2018).

361. Liang, Y., Zhang, C., Ma, M.-H. & Dai, D.-Q. Identification and prediction of novel non-coding and coding RNA-associated competing endogenous RNA networks in colorectal cancer. *World J. Gastroenterol.* **24**, 5259–5270 (2018).

362. Mazzoccoli, G. *et al.* ARNTL2 and SERPINE1: potential biomarkers for tumor aggressiveness in colorectal cancer. *J Cancer Res Clin Oncol* **138**, 501–511 (2012).

363. Soreide, K., Janssen, E., Körner, H. & Baak, J. Trypsin in colorectal cancer: molecular biological mechanisms of proliferation, invasion, and metastasis. *J. Pathol.* **209**, 147–156 (2006).

364. Yamamoto, H. *et al.* Association of trypsin expression with tumour progression and matrilysin expression in human colorectal cancer. *J. Pathol.* **199**, 176–184 (2003).

365. Takeichi, M. Dynamic contacts: rearranging adherens junctions to drive epithelial remodelling. *Nat. Rev. Mol. Cell Biol.* **15**, 397–410 (2014).

366. Harris, T. J. C. & Tepass, U. Adherens junctions: From molecules to morphogenesis. *Nature Reviews Molecular Cell Biology* vol. 11 502–514 (2010).

367. Förster, S., Hehlgans, S., Rödel, F., Otto, B. & Cordes, N. Differential effects of α-catenin on the invasion and radiochemosensitivity of human colorectal cancer cells. *Int. J. Oncol.* **52**,

1117–1128 (2018).

368. Barker, N. *et al.* Identification of stem cells in small intestine and colon by marker gene Lgr5. *Nature* **449**, (2007).

369. Kemper, K. *et al.* Monoclonal antibodies against Lgr5 identify human colorectal cancer stem cells. *Stem Cells* **30**, 2378–2386 (2012).

370. Stephen, A. G., Esposito, D., Bagni, R. G. & McCormick, F. Dragging ras back in the ring. *Cancer Cell* vol. 25 272–281 (2014).

371. Papke, B. & Der, C. J. Drugging RAS: Know the enemy. *Science* vol. 355 1158–1163 (2017).

372. De Las Rivas, J. & Fontanillo, C. Protein–Protein Interactions Essentials: Key Concepts to Building and Analyzing Interactome Networks. *PLoS Comput. Biol.* **6**, e1000807 (2010).

373. Ran, X. & Gestwicki, J. E. Inhibitors of protein–protein interactions (PPIs): an analysis of scaffold choices and buried surface area. *Current Opinion in Chemical Biology* vol. 44 75–86 (2018).

374. Prior, I. A., Lewis, P. D. & Mattos, C. A comprehensive survey of ras mutations in cancer. *Cancer Res.* **72**, 2457–2467 (2012).

375. Mouradov, D. *et al.* Colorectal cancer cell lines are representative models of the main molecular subtypes of primary cancer. *Cancer Res.* **74**, 3238–3247 (2014).

376. Stolze, B., Reinhart, S., Bulllinger, L., Fröhling, S. & Scholl, C. Comparative analysis of KRAS codon 12, 13, 18, 61, and 117 mutations using human MCF10A isogenic cell lines. *Sci. Rep.* **5**, 1–9 (2014).

377. Sarkisian, C. J. *et al.* Dose-dependent oncogene-induced senescence in vivo and its evasion during mammary tumorigenesis. *Nat. Cell Biol.* **9**, 493 (2007).

378. Sánchez-Tilló, E. *et al.* ZEB1 promotes invasiveness of colorectal carcinoma cells through the opposing regulation of uPA and PAI-1. *Clin. Cancer Res.* **19**, 1071–1082 (2013).

379. Charafe-Jauffret, E. *et al.* Gene expression profiling of breast cell lines identifies potential new basal markers. *Oncogene* **25**, 2273–2284 (2006).

380. Harbeck, N. *et al.* Clinical Relevance of the Plasminogen Activator Inhibitor Type1 – a Multifaceted Proteolytic Factor. *Oncol. Res. Treat.* **24**, 238–244 (2001).

381. Czekay, R.-P., Simone, T. M. & Higgins, P. J. SerpinE1. in *Encyclopedia of Signaling Molecules* 1–11 (Springer New York, 2016). doi:10.1007/978-1-4614-6438-9_101828-1.

382. Deng, G., Curriden, S. A., Hu, G., Czekay, R.-P. & Loskutoff, D. J. Plasminogen activator inhibitor-1 regulates cell adhesion by binding to the somatomedin B domain of vitronectin. *J. Cell. Physiol.* **189**, 23–33 (2001).

383. Sakakibara, T. *et al.* Plasminogen activator inhibitor-1 as a potential marker for the malignancy of colorectal cancer. *Br. J. Cancer* **93**, 799–803 (2005).

384. Chen, H. *et al.* Silencing of plasminogen activator inhibitor-1 suppresses colorectal cancer

progression and liver metastasis. *Surg. (United States)* **158**, 1704–1713 (2015).

385. Alamo, P. *et al.* Higher metastatic efficiency of KRas G12V than KRas G13D in a colorectal cancer model. *FASEB J.* **29**, 464–476 (2015).

386. Williams, S. J., Gotley, D. C. & Antalis, T. M. Human trypsinogen in colorectal cancer. *Int. J. Cancer* **93**, 67–73 (2001).

387. Xie, Y. *et al.* The levels of serine proteases in colon tissue interstitial fluid and serum serve as an indicator of colorectal cancer progression. *Oncotarget* **7**, 32592–32606 (2016).

388. Li, V. S. W. *et al.* Frequent Inactivation of Axon Guidance Molecule RGMA in Human Colon Cancer Through Genetic and Epigenetic Mechanisms. *Gastroenterology* **137**, 176–187 (2009).

389. Bujko, M. *et al.* Expression changes of cell-cell adhesion-related genes in colorectal tumors. *Oncol. Lett.* **9**, 2463–2470 (2015).

390. Barderas, R. *et al.* In-depth characterization of the secretome of colorectal cancer metastatic cells identifies key proteins in cell adhesion, migration, and invasion. *Mol. Cell. Proteomics* **12**, 1602–1620 (2013).

391. Lee, N. K. *et al.* Neogenin recruitment of the WAVE regulatory complex maintains adherens junction stability and tension. *Nat. Commun.* **7**, 1–13 (2016).

392. Lindeboom, R. G. *et al.* Integrative multi-omics analysis of intestinal organoid differentiation. *Mol. Syst. Biol.* **14**, e8227 (2018).

393. Brookes, M. J. *et al.* Modulation of iron transport proteins in human colorectal carcinogenesis. *Gut* **55**, 1449–1460 (2006).

394. Hu, D. G., Mackenzie, P. I., McKinnon, R. A. & Meech, R. Genetic polymorphisms of human UDP-glucuronosyltransferase (UGT) genes and cancer risk. *Drug Metab. Rev.* **48**, 47–69 (2016).

395. Maher, D. M., Gupta, B. K., Nagata, S., Jaggi, M. & Chauhan, S. C. Mucin 13: Structure, function, and potential roles in cancer pathogenesis. *Mol. Cancer Res.* **9**, 531–537 (2011).

396. Watt, A. HNF4: A central regulator of hepatocyte differentiation and function. *Hepatology* **37**, 1249–1253 (2003).

397. Lee, S. *et al.* Network Inference Analysis Identifies SETDB1 as a Key Regulator for Reverting Colorectal Cancer Cells into Differentiated Normal-Like Cells. *Mol. Cancer Res.* **18**, 118–129 (2020).

398. Chen, L. *et al.* A reinforcing HNF4–SMAD4 feed-forward module stabilizes enterocyte identity. *Nat. Genet.* **51**, 777–785 (2019).

399. Chen, L. *et al.* HNF4 Regulates Fatty Acid Oxidation and Is Required for Renewal of Intestinal Stem Cells in Mice. *Gastroenterology* **158**, 985-999.e9 (2020).

400. Haegebarth, A. & Clevers, H. Wnt signaling, Lgr5, and stem cells in the intestine and skin. *American Journal of Pathology* vol. 174 715–721 (2009).

401. Barker, N. *et al.* Crypt stem cells as the cells-of-origin of intestinal cancer. *Nature* (2009) doi:10.1038/nature07602.

402. Román-Fernández, A. & Bryant, D. M. Complex Polarity: Building Multicellular Tissues Through Apical Membrane Traffic. *Traffic* **17**, 1244–1261 (2016).

403. Maiden, S. L. & Hardin, J. The secret life of α-catenin: Moonlighting in morphogenesis. *J. Cell Biol.* **195**, 543–552 (2011).

404. Takeichi, M. Multiple functions of α-catenin beyond cell adhesion regulation. *Curr. Opin. Cell Biol.* **54**, 24–29 (2018).

405. Stadler, M. *et al.* Exclusion from spheroid formation identifies loss of essential cell-cell adhesion molecules in colon cancer cells. *Sci. Rep.* **8**, 1–16 (2018).

406. Compton, C. C. Colorectal carcinoma: Diagnostic, prognostic, and molecular features. *Modern Pathology* vol. 16 376–388 (2003).

407. Ashley, N., Yeung, T. M. & Bodmer, W. F. Stem cell differentiation and lumen formation in colorectal cancer cell lines and primary tumors. *Cancer Res.* **73**, 5798–5809 (2013).

408. Okuyama, H. *et al.* Dynamic change of polarity in primary cultured spheroids of human colorectal adenocarcinoma and its role in metastasis. *Am. J. Pathol.* **186**, 899–911 (2016).

409. Shibata, H. *et al.* α-Catenin is essential in intestinal adenoma formation. *Proc. Natl. Acad. Sci. U. S. A.* **104**, 18199–18204 (2007).

410. March, H. N. *et al.* Insertional mutagenesis identifies multiple networks of cooperating genes driving intestinal tumorigenesis. *Nat. Genet.* **43**, 1202–1209 (2011).

411. Reina-Campos, M., Diaz-Meco, M. T. & Moscat, J. The Dual Roles of the Atypical Protein Kinase Cs in Cancer. *Cancer Cell* **36**, 218–235 (2019).

412. Vermeulen, S. J. *et al.* Transition from the Noninvasive to the Invasive Phenotype and Loss of α-Catenin in Human Colon Cancer Cells. *Cancer Res.* **55**, 4722–4728 (1995).

413. Raftopoulos, I., Davaris, P., Karatzas, G., Karayannacos, P. & Kouraklis, G. Level of α-catenin expression in colorectal cancer correlates with invasiveness, metastatic potential, and survival. *J. Surg. Oncol.* **68**, 92–99 (1998).

414. Benjamin, J. M. & Nelson, W. J. Bench to bedside and back again: Molecular mechanisms of-catenin function and roles in tumorigenesis. *Semin. Cancer Biol.* **18**, 53–64 (2008).